



**HAL**  
open science

# MICROSTRUCTURAL ANALYSIS OF THERMAL SPRAY COATINGS BY ELECTRON MICROSCOPY

Sophie Brossard

► **To cite this version:**

Sophie Brossard. MICROSTRUCTURAL ANALYSIS OF THERMAL SPRAY COATINGS BY ELECTRON MICROSCOPY. Mechanics [physics.med-ph]. University of New South Wales, 2010. English. NNT: . tel-00492966

**HAL Id: tel-00492966**

**<https://theses.hal.science/tel-00492966>**

Submitted on 17 Jun 2010

**HAL** is a multi-disciplinary open access archive for the deposit and dissemination of scientific research documents, whether they are published or not. The documents may come from teaching and research institutions in France or abroad, or from public or private research centers.

L'archive ouverte pluridisciplinaire **HAL**, est destinée au dépôt et à la diffusion de documents scientifiques de niveau recherche, publiés ou non, émanant des établissements d'enseignement et de recherche français ou étrangers, des laboratoires publics ou privés.

PLEASE TYPE

THE UNIVERSITY OF NEW SOUTH WALES  
Thesis/Dissertation Sheet

Surname or Family name: Brossard

First name: Sophie

Other name/s:

Abbreviation for degree as given in the University calendar: PhD

School: Materials Science & Engineering

Faculty: Science

Title: Microstructural Analysis of Thermal Spray Coatings by Electron Microscopy

Abstract 350 words maximum:

Plasma and High Velocity Oxy-Fuel (HVOF) spraying are two of the most common thermal spray processes. In both methods, heated particles are sprayed through a flame (either plasma or oxygen fuelled), before being projected at high velocity towards a substrate. Upon impact they flatten, forming splats, whose accumulation results in the formation of a coating. Such processes are used to achieve surface modification of substrates. However, understanding of the mechanisms of splat formation and the splat-substrate interactions is limited by the difficulty in performing high resolution analysis of the splat-substrate interface. This thesis has investigated NiCr splats thermally sprayed onto both aluminium and stainless steel substrates, where the substrates were subject to pre-treatments to vary surface chemistry and roughness. Features of interest include the grain structures of the splat and substrate, the presence, type and location of pores and oxides and the degree and type of contact between the splat and substrate. Localized substrate melting was observed, along with elemental interdiffusion between the splat and substrate. These observations led to the development of models describing splat formation. A range of substrate pre-treatments was used, such as etching, grinding, thermal or boiling treatments to create different substrate surface chemistry and roughness. The influence of substrate condition on splat characteristics was studied and their influence on splat formation was discussed. The substrate condition strongly influenced splat morphology. For example, boiling Al substrates prior to spraying promoted hydroxide formation, which inhibited splat adhesion. In contrast, heating the substrate during spraying significantly reduced splashing of the splats and promoted substrate melting. A high substrate surface roughness, induced by treatments such as grinding or grit blasting, strongly disrupted the spreading of the impacting particles, creating very irregularly-shaped splats with large pores. Spraying conditions also strongly influence splat formation: plasma sprayed splats are fully molten and characterized by frequent splashing and are strongly influenced by surface chemistry, while HVOF sprayed splats comprise partially molten particles that deform the substrate upon impact. These studies resulted in ten publications that constitute the submitted thesis.

Declaration relating to disposition of project thesis/dissertation

I hereby grant to the University of New South Wales or its agents the right to archive and to make available my thesis or dissertation in whole or in part in the University libraries in all forms of media, now or here after known, subject to the provisions of the Copyright Act 1968. I retain all property rights, such as patent rights. I also retain the right to use in future works (such as articles or books) all or part of this thesis or dissertation.

I also authorise University Microfilms to use the 350 words abstract of my thesis in Dissertation Abstracts International (this is applicable to doctoral theses only).

  
Signature

  
Witness

07.10.6.2010  
Date

The University recognises that there may be exceptional circumstances requiring restrictions on copying or conditions on use. Requests for restriction for a period of up to 2 years must be made in writing. Requests for a longer period of restriction may be considered in exceptional circumstances and require the approval of the Dean of Graduate Research.

FOR OFFICE USE ONLY

Date of completion of requirements for Award:

THIS SHEET IS TO BE GLUED TO THE INSIDE FRONT COVER OF THE THESIS



**COPYRIGHT STATEMENT**

'I hereby grant the University of New South Wales or its agents the right to archive and to make available my thesis or dissertation in whole or part in the University libraries in all forms of media, now or here after known, subject to the provisions of the Copyright Act 1968. I retain all proprietary rights, such as patent rights. I also retain the right to use in future works (such as articles or books) all or part of this thesis or dissertation.

I also authorise University Microfilms to use the 350 word abstract of my thesis in Dissertation Abstract International (this is applicable to doctoral theses only).

I have either used no substantial portions of copyright material in my thesis or I have obtained permission to use copyright material; where permission has not been granted I have applied/will apply for a partial restriction of the digital copy of my thesis or dissertation.'

Signed ..... *Biosciences* .....

Date ..... 07/06/2010 .....

**AUTHENTICITY STATEMENT**

'I certify that the Library deposit digital copy is a direct equivalent of the final officially approved version of my thesis. No emendation of content has occurred and if there are any minor variations in formatting, they are the result of the conversion to digital format.'

Signed ..... *Biosciences* .....

Date ..... 07/06/2010 .....



**ORIGINALITY STATEMENT**

'I hereby declare that this submission is my own work and to the best of my knowledge it contains no materials previously published or written by another person, or substantial proportions of material which have been accepted for the award of any other degree or diploma at UNSW or any other educational institution, except where due acknowledgement is made in the thesis. Any contribution made to the research by others, with whom I have worked at UNSW or elsewhere, is explicitly acknowledged in the thesis. I also declare that the intellectual content of this thesis is the product of my own work, except to the extent that assistance from others in the project's design and conception or in style, presentation and linguistic expression is acknowledged.'

Signed ..... B. Rossouw .....

Date ..... 07.10.6/2010 .....



**MICROSTRUCTURAL ANALYSIS OF  
THERMAL SPRAY COATINGS BY  
ELECTRON MICROSCOPY**

**Sophie Brossard**

**PhD Thesis**

**2010**

**School of Materials Science and Engineering, University of New South Wales**



## ABSTRACT

---

Plasma and High Velocity Oxy-Fuel (HVOF) spraying are two of the most common thermal spray processes. In both methods, heated particles are sprayed through a flame (either plasma or oxygen fuelled), before being projected at high velocity towards a substrate. Upon impact they flatten, forming splats, whose accumulation results in the formation of a coating. Such processes are used to achieve surface modification of substrates. However, understanding of the mechanisms of splat formation and the splat-substrate interactions is limited by the difficulty in performing high resolution analysis of the splat-substrate interface. This thesis has investigated NiCr splats thermally sprayed onto both aluminium and stainless steel substrates, where the substrates were subject to pre-treatments to vary surface chemistry and roughness. The aim of the work is to enhance knowledge of the formation of splats by studying and characterising in detail the morphology and microstructure of splats, along with the structures of the splat-substrate interfaces. Features of interest include the grain structures of the splat and substrate, the presence, type and location of pores and oxides and the degree and type of contact between the splat and substrate. Localized substrate melting was observed, along with elemental interdiffusion between the splat and substrate. These observations led to the development of models describing splat formation. A range of substrate pre-treatments were used, such as etching, grinding, thermal or boiling treatments to create different substrate surface chemistry and roughness. The influence of substrate condition on splat

characteristics was studied and their influence on splat formation was discussed. The substrate condition strongly influenced splat morphology. For example, boiling Al substrates prior to spraying promoted hydroxide formation, which inhibited splat adhesion. In contrast, heating the substrate during spraying significantly reduced splashing of the splats and promoted substrate melting. A high substrate surface roughness, induced by treatments such as grinding or grit blasting, strongly disrupted the spreading of the impacting particles, creating very irregularly-shaped splats with large pores. Spraying conditions also strongly influence splat formation: plasma sprayed splats are fully molten and characterized by frequent splashing and are strongly influenced by surface chemistry, while HVOF sprayed splats comprise partially molten particles that deform the substrate upon impact. These studies resulted in ten publications that constitute the submitted thesis.

## ACKNOWLEDGEMENTS

---

I would like to thank my supervisor, Paul R. Munroe, for his invaluable guidance and support during the past two and a half years. Thank you for providing me with the opportunity to complete my PhD, and for your unfaltering dedication in reviewing and perfecting my work. Thank you also for your patience in helping me to find solutions to problems. Your expertise has enabled me to further my skills in electron microscopy, researching, writing, and publishing. Thank you also for the trust that you have placed in me.

To my parents, Philippe and Marie-Paule, thank you for supporting me in accomplishing this achievement. You always made yourselves available to listen, provide advice, and provide support – even despite the distance.

Further, I would like to thank Margaret M. Hyland and Anh T. Tran for providing invaluable input into understanding my data and writing my papers. I would also like to thank you for providing me with the specimens that made this project possible.

I need to thank the staff of the Electron Microscopy Unit – particularly Katie, Sean, and Charlie – for their assistance with the microscope, and for their patience and for granting me additional time to complete my work.

I would like to thank the people in the School of Materials – notably, Chris Sorrel for helping me to successfully apply for a scholarship.

I would like to thank the many friends that I've made in Australia, at International House, NUTS, StudioFour, Comicide, ImproAustralia, etc. – you've also helped to make this PhD a reality.

Finally, I would like to acknowledge and thank the Australian Research Council for providing funding for this project.

## TABLE OF CONTENT

---

ABSTRACT.....	i
ACKNOWLEDGEMENTS.....	ii
TABLE OF CONTENT.....	v
<b>CHAPTER 1. Introduction.....</b>	<b>1</b>
<b>CHAPTER 2. Study of the Effects of Surface Chemistry on Splat Formation for Plasma Sprayed NiCr onto Stainless Steel Substrates.....</b>	<b>24</b>
<i>S. Brossard, P.R. Munroe, A.T. Tran, M.M. Hyland, Surface and Coatings Technology, 2010, 204 (9-10), p. 1599-1607.</i>	
<b>CHAPTER 3. Study of the Microstructure of NiCr Splats Plasma Sprayed on to Stainless Steel Substrates by TEM.....</b>	<b>58</b>
<i>S. Brossard, P.R. Munroe, A.T. Tran, M.M. Hyland, Surface and Coatings Technology, 2010, 204 (9-10), p.1608-1615.</i>	
<b>CHAPTER 4. Study of the effect of surface treatment on splat formation for plasma sprayed NiCr on aluminium substrates.....</b>	<b>85</b>
<i>S. Brossard, P.R. Munroe, A.T. Tran, M.M. Hyland, Surface and Coatings Technology, 2010, 204 (16), p. 2647-2656.</i>	

<b>CHAPTER 5. Study of the Splat-substrate Interface for a NiCr Coating Plasma Sprayed on to Polished Aluminium and Stainless Steel Substrates.....</b>	<b>116</b>
<i>S. Brossard, P.R. Munroe, A.T. Tran, M.M. Hyland, Journal of Thermal Spray Technology, 2010, 19 (1), p. 24-30.</i>	
<b>CHAPTER 6. Evidence of Substrate Melting of NiCr Particles on Stainless Steel Substrate by Experimental Observations and Simulations.....</b>	<b>135</b>
<i>A.T. Tran, S. Brossard, M.M. Hyland, B.J. James, P.R. Munroe, Plasma Chemistry and Plasma Processing, 2009, 29 (6), p.475-495.</i>	
<b>CHAPTER 7. Study of the effect of surface treatment on splat formation for HVOF sprayed NiCr on stainless steel substrates.....</b>	<b>170</b>
<i>S. Brossard, P.R. Munroe, M.M. Hyland, Journal of Thermal Spray Technology, 2010, DOI: 10.1007/s11666-010-9502-3</i>	
<b>CHAPTER 8. Study of the effect of surface treatment on splat formation for HVOF sprayed NiCr on aluminium substrates.....</b>	<b>203</b>
<i>S. Brossard, P.R. Munroe, M.M. Hyland, Journal of Thermal Spray Technology, 2010, DOI: 10.1007/s11666-010-9482-3.</i>	

<b>CHAPTER 9. Study of the splat microstructure and the effects of substrate heating on the splat formation for NiCr particles plasma sprayed on to stainless steel substrates.....</b>	<b>235</b>
<i>S. Brossard, P.R. Munroe, A.T. Tran, M.M. Hyland, Journal of Thermal Spray Technology, 2010 (in publication)</i>	
<b>CHAPTER 10. Examination of the splat microstructure, splat-substrate interface and the effects of substrate heating on the splat formation for Ni-Cr particles plasma sprayed on to aluminum substrates.....</b>	<b>274</b>
<i>S. Brossard, P.R. Munroe, A.T. Tran, M.M. Hyland, Journal of Thermal Spray Technology, 2010, DOI: 10.1007/s11666-010-9511-2</i>	
<b>CHAPTER 11. Effects of substrate roughness on splat formation for NiCr particles plasma sprayed on to aluminium substrates.....</b>	<b>318</b>
<i>S. Brossard, P.R. Munroe, A.T. Tran, M.M. Hyland, Journal of Thermal Spray Technology, 2010, DOI: 10.1007/s11666-010-9508-x</i>	
<b>CHAPTER 12. General discussion and summary.....</b>	<b>343</b>
<b>REFERENCES.....</b>	<b>358</b>



# CHAPTER 1

## INTRODUCTION

---

Thermal spray techniques are well established industrial methods used to deposit coatings on to substrates. The earliest record of thermal spray processing is from the beginning of the 1900s, when a Swiss engineer, M. U. Schoop, presented patents for a system where lead and tin were melted in a welding torch by the energy of an acetylene/oxygen flame. He modified the arrangement to be able to spray powdered materials, and then patented, in 1908, the wire-arc spraying process. In the 1970s there was an expansion of the thermal spray techniques, due to the development of plasmas. These techniques were able to satisfy the increasing demand for thermal barrier and wear resistant coating systems. More recently, most developments have focused upon increasing particle velocities, thus allowing a decrease in the temperature of the sprayed particles, obtaining coatings with high adhesion strength, high density and lower oxide content [1-3]. This led to the development of processes such as cold spraying, where the particles are sprayed in a solid state at very high velocity. Today, thermal spraying includes a wide range of processes where coating materials, in a wire or a powder form, are heated, with an electrical current, a plasma gas or a torch, and sprayed in particle form, which can be molten, partially molten or solid, with a carrier gas onto a substrate to form a coating. [1-3]

Coatings can be made from a wide range of materials (metals, ceramics or polymers) and be sprayed on to metal, as well as ceramic, substrates. The aim of the coating is

usually to improve engineering performances (for instance resistance to wear, corrosion or high temperature) and/or increase component life. The process may also be used to repair worn and damaged parts [4]. Applications of these coatings are widespread and can be found in aerospace, industrial gas turbines, the petrochemical, gas and automotive industries. Thermal spray methods offer a range of advantages over other coating techniques. Firstly, in addition to their versatility in terms of materials (coating and substrate), they usually operate at a relatively low cost. Another advantage is that the substrate does not usually melt during the formation of the coating (some melting can occur upon the impact of hot droplets, but this remains very shallow and localized), due to the moderate heat input by the thermal spray process. Therefore, the coating does not influence microstructural characteristics of the substrate, such as its chemical composition or its heat treatment conditions. Moreover, this limits the substrate distortion compared to, for instance, hard facing welding processes (arc, oxy-fuel, electron beam, laser). [1-3]

## **I. Description of the thermal spray processes**

Thermal spray coatings include, then, many different processes, for instance: the cold spray process, where the particles are sprayed using a very high velocity jet, but no flame; the HVOF and plasma spray processes, where a jet of comparatively lower velocity and a oxygen fuel/plasma flame is used to heat and melt the particle; the HVOF (High Velocity Air Fuel) process, similar to HVOF, but with an air-fuel flame; the flame spray process, one of the oldest spraying methods also uses an oxygen flame, but at relatively low velocities. Another method is the twin-wires arc process, which uses an electric arc created between the two feedstock wires to melt and spray

particles. For the present thesis, the two methods used, and thus those on which focus will be placed, are the plasma and HVOF processes.

### I.1. Description of the plasma spraying process

Plasma spraying is probably the most flexible and versatile of the thermal spray processes in terms not only of the materials that can be sprayed, but also the spray temperature and velocity and the particle size distribution (usually from 5 to 50  $\mu\text{m}$  for ceramics and from 20 to 120  $\mu\text{m}$  for metallic alloys). The most common plasma spray technique is Conventional Plasma Spraying (CPS), which is one of the atmospheric plasma spraying processes (where spraying is performed in air under atmospheric pressure). The design of a CPS gun is shown in Fig.1. The principle is as follows: an electric arc, formed between a tungsten electrode and an annular copper anode, heats and ionizes the introduced gases, usually argon, helium, nitrogen, hydrogen or a mixture of these, to create the plasma flame. When the gases pass through the arc they are heated, so they expand both axially and radially and accelerate through the exit nozzle. The energy is then released when electrons drop to a lower energy state and ions recombine. The released heat and associated radiation can generate a temperature in the core region of the plasma jet of up to 20 000°C. The powder is then injected in the plasma flame, where the particles are melted and sprayed onto the substrate, usually at velocities ranging from 80 to 400  $\text{m}\cdot\text{s}^{-1}$ . The spraying distance is typically around 100-150 mm.

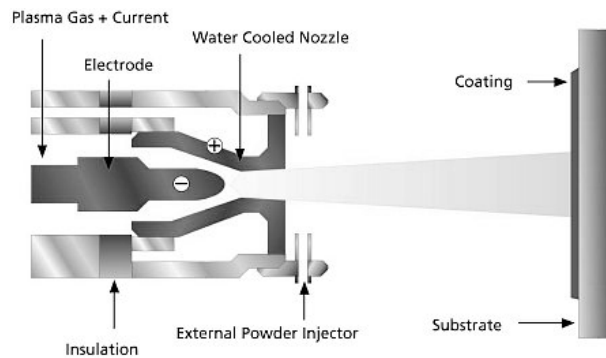


*Figure 1. Layout of a CPS gun [5]*

Other spray processes that use a plasma flame have been developed to produce coatings with particular characteristics. For instance, there is the Vacuum Plasma Spray process, where plasma spraying is performed under vacuum to prevent oxidation of the particles, and the Suspension Plasma Spray process, where a suspension of very fine particles is sprayed, allowing the production of coatings with a very fine microstructure.

## I.2. Description of the HVOF process

In the HVOF process, the flame is produced by the combustion of a mixture of oxygen and fuel gases (usually propane, propylene, hydrogen, heptane or kerosene). The layout of a HVOF gun is presented in Fig. 2. The combustion is confined to a chamber. The combustion gases then expand through a nozzle system, creating a jet with very high velocities. The flame temperature is typically around 3000°C. Then, the particles, once injected in the jet, melt or soften and are accelerated to usually around 400-800m.s<sup>-1</sup>. HVOF systems can vary in their design, but one feature that is typical for all such processes is the visible shock diamonds pattern, which can be observed in the free jet.

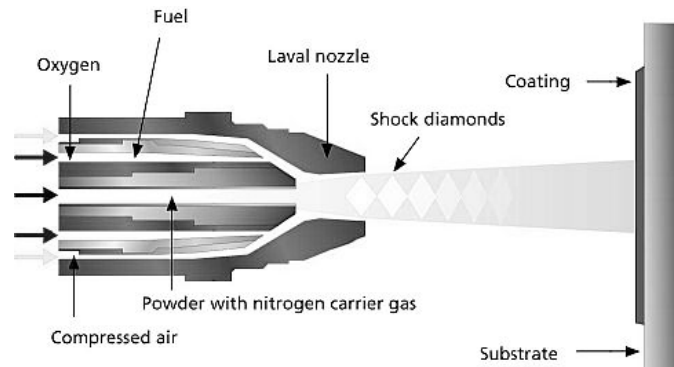


Figure 2. Layout of a HVOF gun [5]

Table 1 summarized the characteristics of both plasma and HVOF spraying processes. The differences in these characteristics then translate in differences in splat formation, morphology and microstructures, which are discussed in the next section.

**Table 1. Summary of the characteristics of plasma and HVOF spray**

	<b>Plasma Spray</b>	<b>HVOF spray</b>
Jet/Flame	Plasma jet	Oxygen Fuel flame
Temperature	In the jet: up to 20 000°C	In the flame: ~ 3000°C
Particles' velocity	80 to 400 m.s <sup>-1</sup>	400-800m.s <sup>-1</sup>
Particles' state	Mostly fully molten	Ranging from unmolten to fully molten

## II. Structure and formation of thermal sprayed coatings

In both the processes described above, the particles flatten upon impact with the substrate and form lamellae, which are often termed “splats”. The schematic in Fig. 3 shows for example the formation of a splat in the case of plasma spraying: the droplet

of NiCr, upon impact on the substrate, flattens in a more or less circular splat. Upon impact and spreading, several processes occur, such as the formation of pores (marked 1 on Fig. 3) or the interaction between splat and substrate that may result in substrate melting and mixing with the splat (marked 4 on Fig. 3), or also the occurrence of splashing, that can result in very irregularly shaped splats. Figure 4 displays examples of such resulting splats (more details on Figs. 3 and 4 may be found in the publication presented Chapter 2 and 8): splats such as the one Fig. 4a are often denominated as disk-shaped, and for Fig. 4b, as splashed.

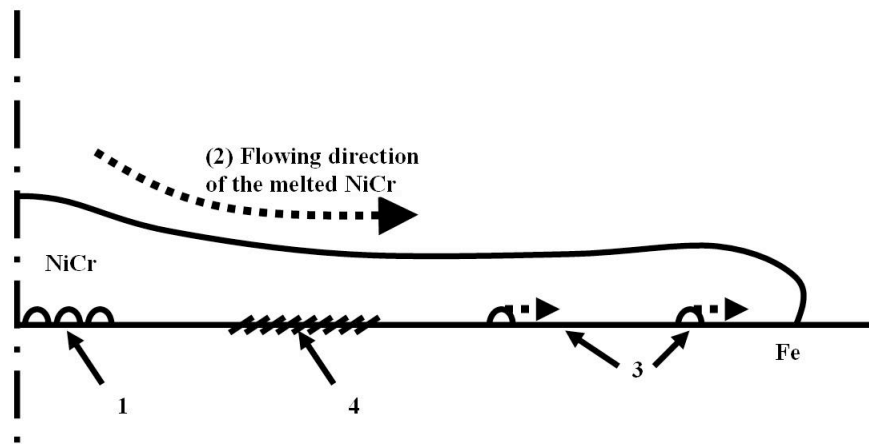


*Figure 3. Schematic representation of a NiCr droplet plasma sprayed and flattening on a stainless steel substrate, forming a splat*

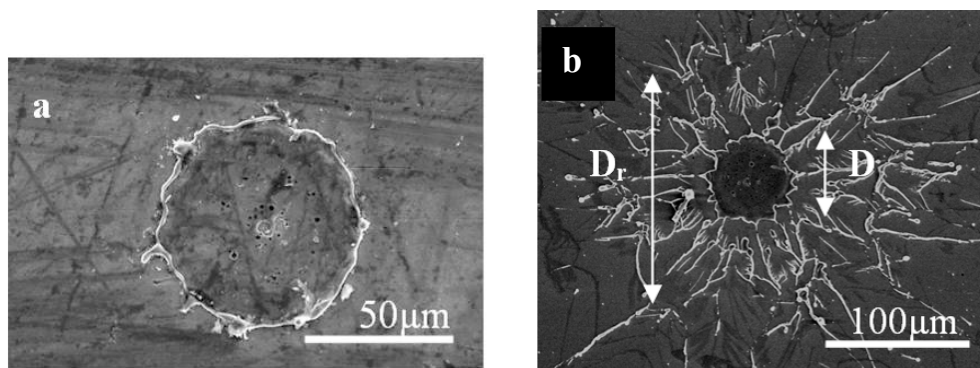


*Figure 4. SEM images of NiCr splats plasma sprayed on stainless steel substrates*

The accumulation of these splats upon the different passes of the spray gun results in a coating which, in the case of HVOF and plasma spraying, may be 50-250  $\mu\text{m}$  thick [1].

The microstructure of fully deposited coatings has usually been studied by the observation of cross-sections mainly at a macroscopic level (that is, structural features typically around 0.5  $\mu\text{m}$  or greater in size) or by the study of the exterior surface of the splat [6-9]. However, many features of note are either smaller than this order or buried underneath the splat surface. Many studies have also focused on the properties of such coatings (adhesion, strength, thermal and electrical conductivity, etc.). Both microstructure and properties of the splats have been shown to be strongly influenced by the spray conditions, such as temperature and velocity of the particles [2, 10]. However, a key step in understanding and improving thermal spray coatings is the study of the formation of the coatings, through the study of single splats, and their direct interaction with the substrate.

### II.1. Description of the plasma sprayed splats and coatings

In the case of plasma sprayed splats, where the particles impact the substrate in a fully molten state, several studies have investigated their formation *in-situ*, mainly with millimetre-sized droplets [11-15], the use of micron-sized droplets is possible, but more complicated to observe because of their smaller size [16]. Many models describing the impact of fully molten droplets on hard substrates have also been proposed, such as the ones suggested by Chandra *et al.* [13, 17, 18]. Several factors were found to have a significant impact on splat formation, and the occurrence of

splashing: specifically, the combination of materials used as substrate and feedstock powder [19, 20], the substrate surface topography (roughness being induced by oxidation or mechanical roughening) and substrate chemistry (notably the presence of oxide layers and/or adsorbates/condensates on the substrate surface) [2, 10, 11, 21-25]. An effect that was extensively studied was the temperature of the substrate during spraying [6, 19-21, 26-30]. Indeed, it was found that a temperature threshold exists for each substrate material above which splashing of the splats was significantly reduced; the majority of the splats exhibiting a disc-shaped morphology. Table 2 presents an example of such temperature, which is called the “transition temperature”, for a range of feedstock powder materials sprayed onto stainless steel.

**Table 2. Transition temperatures for various materials plasma sprayed onto stainless steel [6]**

Materials	Ni	Mo	Cu	Cr	Al <sub>2</sub> O <sub>3</sub>	TiO <sub>2</sub>	YSZ
Transition temperature (°C)	337	201	121	114	45	77	72

The transition temperature also depends on the substrate material and surface chemistry, for instance, when spraying Al<sub>2</sub>O<sub>3</sub> on to stainless steel, the observed transition temperature is around 45°C, but if the substrate is coated in gold (thus, with the same bulk thermal properties, but a different surface chemistry), the transition temperature is 150°C [31].

Several theories were proposed to explain such a phenomenon. One of the most widely recognized is the evaporation of adsorbates/condensates, present initially on

the substrate surface, due to the heat from the impact of the hot particle [6, 26, 31, 32]. The release of gas species upon heating from the spraying process creates a “gas cushion” causing instabilities before the splat spreading, and thus splashing. Heating the substrate during spraying allows such gas release to occur before the particles impact on the substrate, avoiding splashing. Instability leading to splashing may also be created by the early solidification of the bottom layer of the splat in contact with a cold substrate [20, 33, 34]. By heating the substrate, one can also delay solidification, so preventing splashing. This also may explain the variation of the transition temperature across the different feedstock materials. Finally, another explanation that has been given for the splashing phenomenon is the poor wetting of the liquid on the surface, which creates instabilities and removal of some of the melted which becomes material away. For ceramics sprayed onto metals, the wetting can be related to the free energy of formation of oxides of the substrate metal. More active metals, or those with higher thermal conductivity, have then a higher transition temperature [31, 33].

However, very little work has been published on the direct interaction between the coating and substrate by studying their interface at a microscopic or nano-scale level, possibly because it requires relatively complex equipment and methods of study. Kitahara *et al.*, studied the coating-substrate interface by spraying a range of materials including Ni and Cr, on to various substrates including mild steel and aluminium [35]. They observed, by X-ray diffraction, in most cases, the presence of an intermetallic layer at the interface, interpreted as evidence of localized substrate melting. For the case of Ni sprayed on to Al, for instance, such a layer was identified as being Al<sub>3</sub>Ni. However, for either Ni or Cr sprayed on to steel substrates, no intermetallic layers were observed, which was interpreted as an absence of substrate melting. On the other

hand, localized steel substrate melting was also observed by Zhang *et al.* [20] and by Li *et al.* [36], both when plasma spraying Mo. In this case, a Fe<sub>2</sub>Mo intermetallic phase was observed by transmission electron microscopy (TEM) at the interface. However, overall, observations of localized substrate melting are rare and such phenomena are usually not taken into account when modelling splat formation.

If substrate melting occurs, bonding between the coating and the substrate can be expected to be metallurgical. Otherwise, the adhesion would mostly occur by mechanical interlocking. Such interlocking, and consequently the adhesion strength of the coating, is often promoted by a rougher substrate surface, which is why substrates are frequently grit-blasted prior to spraying.

## II.2. Description of the HVOF sprayed splats and coatings

Depending on the materials used as feedstock powder (nature and size) and as the substrate (particularly its hardness), and on the spray conditions (notably particle temperature and velocity), particles may impact on the substrate in various states ranging from fully molten to solid. Moreover, some further melting of the particle may occur upon impact as the kinetic energy of the particle is transformed into a combination of mechanical deformation and thermal energy. Consequently, splats may form on the substrate either in a fully melted state, in a partially melted state or in a non-melted (i.e. solid) state [37, 38]. Trompetter *et al.* found, in the case of HVAF spraying (High Velocity Air-Fuel, a thermal spray process very similar to HVOF where the oxygen fuel gas is replaced by air), that the hardness of the substrate significantly influenced the proportion of molten splats, as for a harder substrate, less

kinetic energy will be put into substrate deformation and more into heating and melting of the impacting particle [39]. The study of the microstructure of fully deposited HVOF coatings has indeed showed that a bimodal structure may be found, with a mixture of melted and non-melted zones [40-42]. Substrate melting upon HVOF spraying was also observed by Guilemany *et al.*, when spraying WC-Co coatings onto polished and grit-blasted Cu substrates. They also found that melting was promoted by a higher substrate roughness [43].

However, it can be noted that studies of splat microstructure and the mechanisms of splat formation in the case of HVOF spraying are very limited. Nonetheless, parallels can be drawn with other thermal spray processes. When the particle impacts in a solid state, the situation may be compared with the cold spray process. In such cases, the interaction between the sprayed particle and the substrate depends heavily on the particle momentum, and the particle velocity has to be above a critical value for adhesion to occur, by mechanical interlocking and adiabatic shear instability (localized deformation at the particle-substrate interface) [44-46]. On the other hand, when the particle impacts on the substrate in a fully molten state, the case is similar to plasma spraying, which was described earlier.

### **III. Thesis objective**

As was noted above, a gap exists in the literature concerning the study of the splat microstructure and splat-substrate interface on a nano-scale level for both plasma and HVOF sprayed splats. Consequently, the aim of this thesis is to study such splats using a range of microscopy techniques. The study of the different types of splats that

have formed, their microstructure and their interface with the substrate will be discussed. On one hand, the process of splat formation will be discussed and, on the other hand, the influence of the substrate and spraying conditions on splat-substrate interactions will be described.

#### **IV. Description of the experimental methods used**

Several sets of thermally sprayed specimens were prepared, using various conditions of substrate pre-treatment (such as thermal/boiling treatments susceptible to modify the surface chemistry, or different roughness states) and spraying conditions (HVOF and plasma, with different particle velocity/temperature). This then allows the effect of substrate chemistry and roughness on splat morphology and splat-substrate interactions to be investigated. The different sets of specimens are summarized in Table 3.

More details on the preparation of the specimens and the spraying parameters are given in the corresponding chapters in this thesis.

**Table 3. Summary of the different specimens studied**

Set #	1	2	3
Spraying Conditions	Plasma spraying	HVOF spraying	Plasma spraying (Higher particle temperature/velocity)
Substrates	Steel/Al5052 <ul style="list-style-type: none"> <li>- As-polished</li> <li>- Thermally treated</li> <li>- Boiled</li> <li>- Boiled and thermally treated</li> </ul>	Steel/Al5052 <ul style="list-style-type: none"> <li>- As-polished</li> <li>- Thermally treated</li> <li>- Boiled</li> <li>- Boiled and thermally treated</li> </ul>	Steel/Al5052 <ul style="list-style-type: none"> <li>- As-polished</li> <li>- Thermally treated</li> <li>- Heated during spraying</li> </ul> Al1005 <ul style="list-style-type: none"> <li>- As-polished</li> <li>- Thermally treated</li> <li>- Roughened</li> <li>- Grit blasted</li> </ul> Al5052 <ul style="list-style-type: none"> <li>- Etched</li> <li>- Etched and thermally treated</li> </ul>

Several microscopy techniques were used in the study of the splats and the substrate, following the protocols described below:

- An AFM (Atomic Force Microscopy) Digital Instrument 3000 microscope and a profilometer Mitutoyo Surfpak-SV 600 were used to measure the roughness of the substrate. The AFM was used for the large majority of the substrate and

functions as follow: a tip scans the specimen surface and the variations in height are recorded, thus allowing a profile of the specimen surface to be generated. The roughness is calculated usually over  $5 \times 5 \mu\text{m}$  square located away from the splats or on unsprayed substrates. Three measurements are made for each substrates and the average is calculated. Figure 5 displays a image of the AFM and an example of a roughness profile that can be obtained.

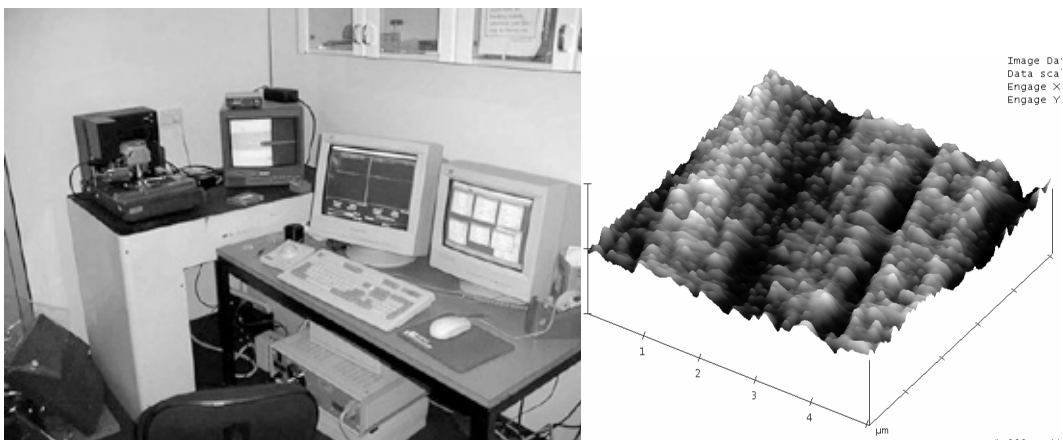


*Figure 5. AFM DI3000 and a typical AFM profile obtained on a polished Al substrate*

However for high roughness levels (more than  $\sim 3 \mu\text{m}$ ), the measurements can not be made with the AFM and the profilometer was used. It functions on a similar principle, except here the surface is scanned along a line.

- A scanning electron microscope (SEM) Hitachi S3400 allowed images of the exterior of the splats to be obtained to study their global morphology and, thus, classify them into different categories. Images of about 50 specimens were taken for each specimen. The proportion of each type of splat and their diameter,  $D$ , was measured, and the mean diameter  $D_m$  was calculated. These

measurements were made comparatively, to observe the frequency of a given category of splat or see if they may form for instance from the smaller or larger particles of the feedstock powder. Figure 6 displays an image of the microscope, an example of an SEM image of a splat and how the measurement of the diameter was performed.

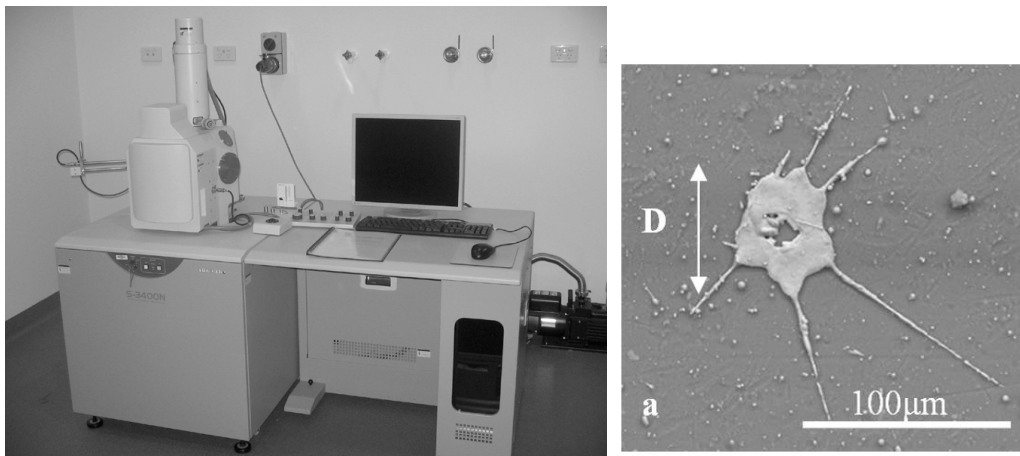


*Figure 6. Scanning Electron Microscope Hitachi S3400 and typical SEM image of a NiCr splat plasma sprayed on an Al polished substrate*

- A focused ion beam microscope (FIB) FEI XP200 (see Fig. 7) has a high energy gallium ions beam that is used to cut and image cross-sections through the splat-substrate interface. Cross-sections are made for each specimen and type of splats, at the different key locations of the splat (centre, periphery, splashed finger, etc.). This allows the preparation and examination of cross-sections showing features, such as the grain structure of the splat, the presence of pores at the interface or delamination. Oxide phases are observed, although their nature needs to be confirmed by TEM. Also, the grain structure of the splat and of the substrate under the splat can be observed.

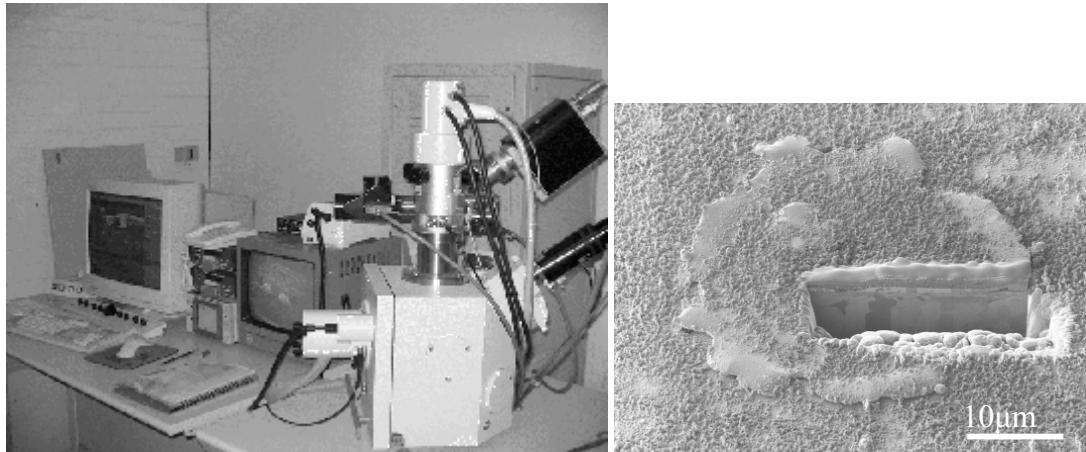


*Figure 7. FIB microscope FEI XP200 and FIB image of a cross-section made across a plasma sprayed splat found of a polished and thermally treated Al substrate*

- Transmission electron microscopy (TEM) is used to study electron transparent cross-sections prepared by FIB, allowing high resolution imaging as well as chemical analysis, and crystallographic analysis through electron diffraction. The fabrication of the TEM cross-sections is a relatively long and complex process that can be summarized as following: A dual beam microscope (which combines a FIB, for milling, and an electron beam, for imaging) xT Nova NanoLab 200 is used to cut out the section thanks to a partially automated program. Figure 8 displays an image of the Dual Beam microscope along a image of a prepared TEM section.

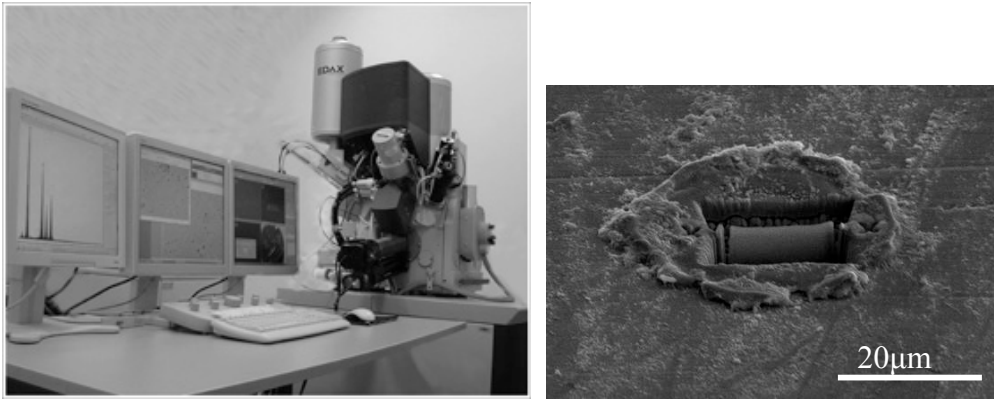


*Figure 8. Image of the Dual Beam and image of a TEM section cut across a plasma sprayed splat on a polished stainless steel substrate*

The second step is the lift-out of the TEM section and its relocation onto a copper grid covered with a polymer film transparent to the electrons. This is performed by picking the thinned section up with a glass needle, then moving it using a micro manipulator, and under an optical microscope. Figure 9 displays images of the micro-manipulator and a copper grid.

The copper grid can then be placed in the TEM microscope, a Philips CM200, for study of the cross-section. To this purpose, several tools can be used:

- Bright field images are taken to observe features such as the location of different phases, grain structure or the appearance of the interface. Indeed, contrast can come from the difference in absorption of the various materials (heavier elements tend to absorb more and then to appear darker), or from the grain orientation, and hence diffraction effects.

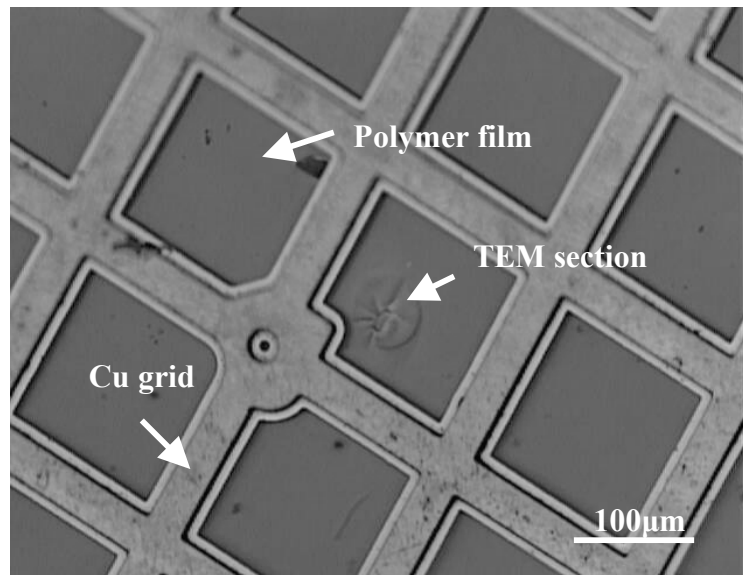
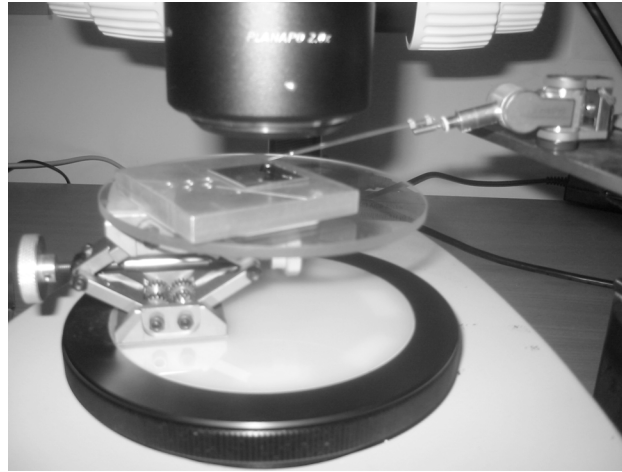


*Figure 9. Image of the micromanipulator and magnified image of the copper grid*

- EDS (Energy Dispersive Spectroscopy) gives an indication on the chemical elements present. Such chemical analysis can be done at a specific location, along a line or by mapping a local region of the structure. Maps are particularly useful as they give the location of the elements across a large area.
- The determination of the nature of a material has then to be proven by studying its diffraction pattern. After having orientated the crystal correctly using the Kikuchi maps, an image of the pattern is taken: the arrangement of the points of rings and their distance between themselves will identify

accurately the crystal structure of the material. The Kikuchi maps also give information of the crystal structure of the grain and its orientation.

Figure 10 displays an image of the TEM along with examples of a bright field image, an EDS map, an EDS map and a diffraction pattern.

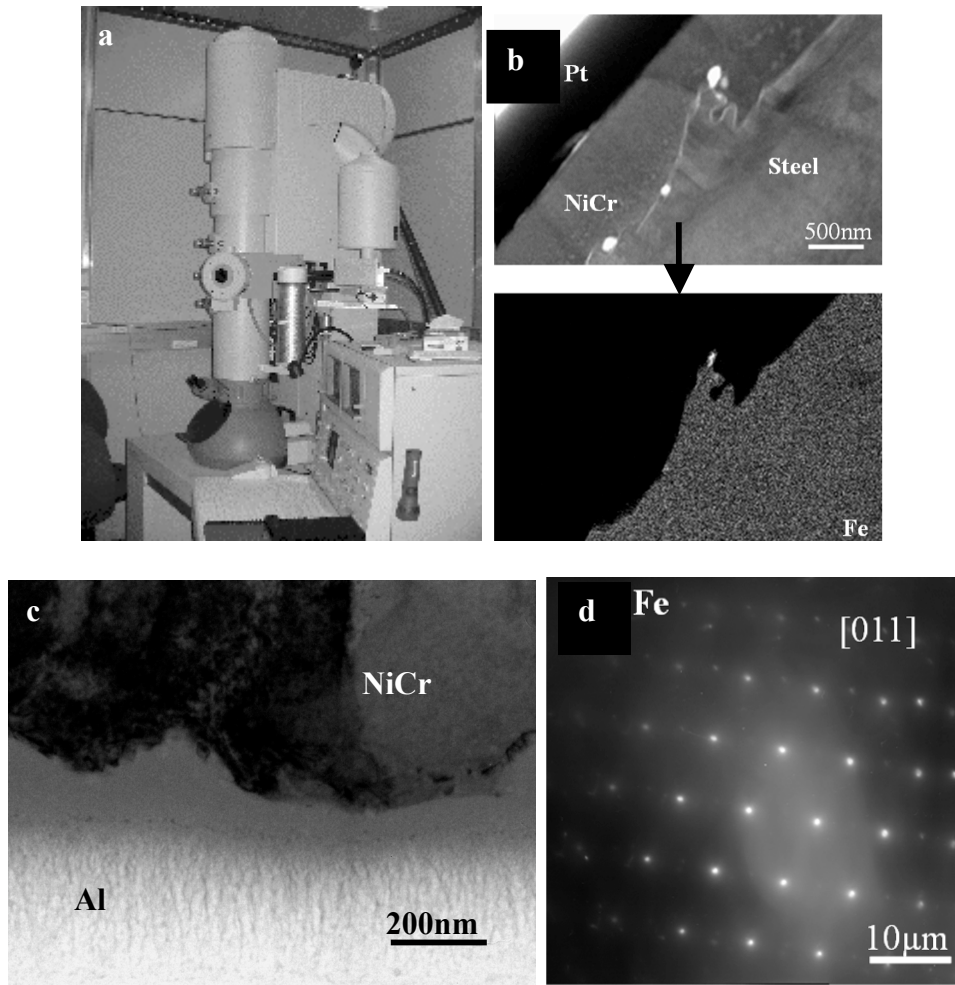


*Figure 10. (a) Image of the TEM CM200 microscope, (b) EDS map of Fe and the corresponding image of the section, (c) bright field image of the interface between NiCr and Al, (d) electron diffraction pattern for Fe*

## V. Thesis outline

These studies have resulted in several publications in journals, ten in total, and each constitutes a separate chapter of this thesis.

The first set of specimens was plasma sprayed at the Stony Brook University, New York, USA. This set constituted four stainless steel 304 and four aluminium 5052 polished substrates that had undergone several pre-treatments (as polished, heat-treated in air (350°C for 90 min), boiled in distilled water for 30 min, boiled and then heat-treated). Five papers were written from the study of this set of specimens.

The first and second publications, *Study of the Effects of Surface Chemistry on Splat Formation for Plasma Sprayed NiCr onto Stainless Steel Substrates* and *Study of the Microstructure of NiCr Splats Plasma Sprayed on to Stainless Steel Substrates by TEM*, presented in Chapters 2 and 3, have both been published in the journal ‘Surface and Coating Technology’. They focus on the behaviour of the steel substrates. The first paper examines the general morphology, splat-substrate interaction and the formation process of the splats, and how they are affected by the changes in the substrate surface chemistry induced by the various pre-treatments. The second paper provides support for the first paper and details the TEM observations, notably the identification of the various phases and microstructure.

The third paper, *Study of the effect of surface treatment on splat formation for plasma sprayed NiCr on to Al5052 substrates*, constitutes Chapter 4 and presents the observations made from the aluminium specimens: the different splat morphologies

and microstructures, how they may form and how they are affected by the various pre-treatments. It has been published in 'Surface and Coatings Technology'.

The paper in Chapter 5, *Study of the Splat-substrate Interface for a NiCr Coating Plasma Sprayed on to Polished Aluminium and Stainless Steel Substrates*, was written for the International Thermal Spray Conference in May 2009 in Las Vegas, where it was awarded the **Best Poster prize**. It was also subsequently published in a revised form in the Journal of Thermal Spray Technology. It compares the splat morphology, microstructure and interaction with the substrate between polished steel and aluminium substrates.

Finally, the fifth paper, *Evidence of Substrate Melting of NiCr Particles on Stainless Steel Substrate by Experimental Observations and Simulations* is presented in Chapter 6. The first author of this paper is A.T. Tran, from the University of Auckland in New Zealand. This paper was published in Plasma Chemistry and Plasma Processing. It proposes a model describing splat formation on polished steel substrates, from the electron microscope observations (SEM, FIB and TEM) provided by the candidate (who was the second author).

The second set of specimens constituted of 4 stainless steel substrates and 4 aluminium 5052 substrates that were HVOF sprayed at the University of Auckland. Prior to spraying the substrates were submitted to the same pre-treatments as the plasma sprayed specimens described above. This study resulted in two papers, *Study of the effect of surface treatment on splat formation for HVOF sprayed NiCr on stainless steel substrates* and *Study of the effect of surface treatment on splat*

*formation for HVOF sprayed NiCr on aluminium substrates*, both accepted for publication in the Journal of Thermal Spray Technology, and presented in Chapters 7 and 8. These papers detail the splat morphology, microstructure and the interaction with the substrate, and discuss the formation process and the potential effects of the pre-treatments, for each type of substrate material.

The third set of specimens was also plasma sprayed at Stony Brook University in December 2008. Compared to the first set, the gun used was more recent, of different manufacture and operated at a higher spraying temperature and velocities. Amongst the specimens were three stainless steel 304 substrates and three aluminium 5052 substrates, sprayed as-polished, after heat treatment (similar conditions as before) and heated during spraying. The Al 5052 alloy contains magnesium, which is suspected to influence substrate surface chemistry and, thus, splat formation. Consequently, two substrates made of Al 1005, an alloy with a minimum Mg content, and Al 5052 were sprayed, one as-polished and one after heat treatment. Finally, to investigate the effects of substrate roughness, several rough aluminium substrates were sprayed: after etching (by immersion in a HF solution), after etching and heat treating, after roughening by sand paper, and after grit-blasting.

Three different papers resulted from the observations of these specimens and were all accepted for publication in the Journal of Thermal Spray Technology. The first paper, *Study of the splat microstructure and the effects of substrate heating on the splat formation for NiCr particles plasma sprayed on to stainless steel substrates*, presented in Chapter 9, details the results of the three stainless steel specimens (splat microstructure and interaction with the substrates and the effects of heating before or

during spraying). The second paper, *Examination of the splat microstructure, splat-substrate interface and the effects of substrate heating on the splat formation for Ni-Cr particles plasma sprayed on to aluminum substrates*, presented in Chapter 10, details in a similar way the results on the three Al 5052 specimens, and includes the two Al 1005 substrates.

Finally, the rough specimens are studied in Chapter 11, *Effects of substrate roughness on splat formation for NiCr particles plasma sprayed on to aluminium substrates*, and compared with polished specimens, showing the strong influence of roughness levels on the splat formation and morphology.

Because these chapters are separate, and notionally stand-alone, journal publications, repetitions may inevitably be found, notably in the introduction and experimental methods sections.

Finally, Chapter 12 presents a general discussion and conclusion linking all the different findings with discussion of their relevance to the field of thermal spray coatings.

**CHAPTER 2**

**STUDY OF THE EFFECTS OF SURFACE CHEMISTRY ON  
SPLAT FORMATION FOR PLASMA SPRAYED NiCr ONTO  
STAINLESS STEEL SUBSTRATES**

---

*S. Brossard, P.R. Munroe, A.T.T Tran, M.M. Hyland, Surface and Coating  
Technology, 2010, 204 (9-10), p. 1599-1607*

**Abstract**

The plasma spray process involves the melting and spraying of a fine powder onto a substrate using a plasma jet. However, understanding of the processes of splat formation and bonding with the substrate is limited because of the difficulties in performing high resolution studies of the splat-substrate interface. In this study, a nickel-chromium powder was sprayed onto mirror polished stainless steel substrates that have undergone various thermal and boiling pre-treatments to modify their surface chemistry. Detailed microstructural characterization of the splats and their interfaces with the substrate was performed using several electron microscopy techniques. Splats' shapes, the nature of the splat-substrate interface and occurrence of substrate melting and chemical intermixing, along with the presence of various oxide phases (Ni, Fe and Cr oxides) were observed and discussed in relation to the

splat formation process. Such features were found to vary depending on the surface chemistry of the substrate.

## I. Introduction

Thermal spray processing is widely used in many industries (e.g. aerospace, gas turbine, petrochemical and gas generation, the automotive industry, etc.) to create coatings aimed at improving engineering performance and/or increasing component life. Thermally sprayed coatings have several advantages over other surface engineering techniques. In particular, when the coating is applied, the substrate undergoes either no, or minimal, melting, so it allows the substrate to retain its original characteristics, such as its chemistry, structure and properties. One consequence of this processing route, however, is that the bonding between the substrate and the particles (often termed splats) that form the coating tends to be mechanical [1]. That is, the heat and momentum of the particle promote plastic deformation of both the substrate and the impinging particle, which bond together by mechanical interlocking, rather than local melting and solidification at the splat-substrate interface. This limits the cohesive strength of the bond. However, if localized melting of the substrate occurs, strong metallurgical bonding may form between the particle and the substrate. This, however, is true only if there is not formation of an intermetallic phase that may be brittle and which may induce weakness of the interface. [4]

Plasma spraying is one of the most flexible and versatile of the thermal spray processes. Indeed, it can be configured to spray particles over a very wide range of

temperatures and velocities (the plasma temperature ranges typically from 8700 to 12,000°C, and the particles' velocity may vary between 80 and 400 m.s<sup>-1</sup>). As such, it allows melting and spraying of many different materials (if they exhibit a congruent melting behaviour) on to a wide range of substrates (metallic alloys, ceramics, polymers) and over a large range of particle size distribution (from 5 to 50 µm for ceramics, 20 to 120 µm for metallic alloys).

For plasma spray processing, particles are usually fully molten upon impact and are propelled at a velocity that is relatively low compared to other thermal spray processes [1]. In many cases, spraying is performed in air, which may lead to oxidation of metallic particles in flight. Oxides may also form around the splats, and the coatings formed usually contain porosity (usually 1 to 5vol.%). [1]

The structure of plasma sprayed coatings, as a result of the superimposition of spray beads resulting themselves from the stacking of splats on top of another, has been widely studied, and cross-sections of coatings have been obtained at a “macroscopic” level (i.e., resolution of about 0.5 µm) [6, 7]. It has been shown that splat morphology depends on both the materials involved (particles and substrates) and the spray conditions [19, 20]. Splat formation has often been investigated also through modelling since mechanisms occur in the matter of the microsecond and the micrometer [17, 18], and many studies can be found on the phenomenon of splashing (i.e., peripheral ejection of matter), particularly with the effects of adsorbates/condensates on the substrate surface [26, 32], solidification of the splat during flattening [20, 33], heating of the substrate [6, 20, 21, 26-28] and thermal contact resistance effects [28].

However, studies of the direct interaction between splats and the substrate, by observing their interface, and on the splat-substrate adhesion mechanisms are relatively limited due to the difficulties in preparing cross-sections and the ready observation of fine, nano-scale features at sufficient resolution.

Microstructural features of interest include the possible presence of voids, the occurrence, or not, of substrate melting and the extent of any intermixing between the coating and the substrate materials.

Zhang *et al.* sprayed molybdenum particles onto a steel substrate and found by transmission electron microscopy (TEM) a layer at the splat-substrate interface that they suggested as being intermetallic Fe<sub>2</sub>Mo, thus showing that substrate melting had occurred [20]. Their simulation also showed the possibility of substrate melting, which was consistent with the fragmented shapes of the splats (also induced by the surface tension effect [2]). Li *et al.* also found that substrate melting could occur, both experimentally and by simulation, when spraying Mo on to substrates of stainless steel, brass and aluminium. Moreover, they were able to estimate the depth of melting of the substrate under the splat (less than 0.5 µm for the steel and up to 3.5 µm for the aluminium) [36]. Finally, Kitahara *et al.* sprayed various materials (Ni, Cr, Ta, Mo, W) onto both Al and mild steel substrates. They also found that when localized melting of substrate occurred upon impact of the melted particle, in most cases intermetallic phases (identified by X-ray diffraction) were formed: that is, the bonding was metallurgical. In such a situation, it was then found that the adhesive strength of the interface was higher than the cohesive strength of the coating itself. However, in

the case of Ni and Cr sprayed onto mild steel no intermetallic phases were observed, which suggested that no, or very limited, substrate melting had occurred. Thus, there was no, or only partial, metallurgical bonding, and the adhesive strength was much lower [35].

Nickel-chromium coatings are often used as bond coats or for thermal insulation layer of steel, as diffusion or sacrificial barrier against corrosion, erosion, for example in boilers [1]. Sidhu *et al.* found that such coatings increase the degradation resistance of steel under hot corrosion conditions [47]. Similarly, Higuera *et al.* noted that plasma spraying of such a coating on steel provides a protective layer with very high adherence, although the presence of brittle oxides can adversely affect this property [48].

In this study, a NiCr powder was plasma sprayed on to 304L austenitic stainless steel substrates, which had undergone different pre-treatments, i.e. heat treatments in air and/or boiling in water, to vary surface chemistry mostly. The effects of such treatments on the surface were investigated in a previous study by X-ray Photoelectron Spectroscopy (XPS) [49]. The pre-treatments were found to produce oxide and hydroxide layers, thus varying the O, H, Fe and Cr contents of the surface. These effects are discussed more in detail in the results section. The roughness of the substrates was also evaluated before, and after, spraying as some variation may arise mainly from the oxidation of the surface during spraying.

The microstructure of single splats deposited on the substrate and their interface with the steel substrate were then investigated to study the influence of the surface

chemistry on the splat formation. For each substrate type, the splats were first categorized in terms of their shape and size; the microstructure of each type of splat (that is, features such as grain structure, phases, nature of the interface between the splat and substrate) was studied to determine the mechanisms of formation of the splat. The splat microstructure was then correlated to the surface condition of the substrate. In an associated paper [50], detailed descriptions of the microstructure of these systems, investigated by TEM, are given. These results are described briefly in this paper.

## II. Experimental procedure

Four different substrates were used; all made of 304L stainless steel. The substrates and their different treatments are listed in Table 1.

**Table 1. Substrate Nomenclature and Condition**

<b>Specimen</b>	<b>Substrate</b>	<b>Pre-treatment</b>
SS_P	Stainless steel	Polished (to a nano-scale smoothness)
SS_PT	Stainless steel	Polished and thermally treated
SS_B	Stainless steel	Boiled
SS_BT	Stainless steel	Boiled and thermally treated

Substrates were firstly mechanically ground and mirror polished with diamond paste, to a nano-scale roughness ( $R_a \sim 2\text{-}5$  nm). Specimen SS\_P was sprayed in the as-polished condition. The boiled substrates (SS\_B and SS\_BT) were placed into boiling distilled water for 30 min, while the thermally treated substrates (SS\_PT and SS\_BT)

were subsequently heated at 350°C for 90 minutes in air at atmospheric pressure. The objective of these treatments was to form surface oxides (or hydroxides for the boiled specimens) and/or to induce some modification in surface topology. Reference unsprayed specimens, having undergone the same pre-treatments, were studied in parallel in order to determine the effect of the treatment on the substrate surface state prior to spraying.

The sprayed material was a commercial NiCr alloy powder (Ni80-Cr20, Sulzer Metco 43 VF-NS, Wohlen, Switzerland, (-45+5)  $\mu\text{m}$ ). Plasma spraying was carried out with a Sulzer Metco (Wohlen, Switzerland) 7MB gun (with an 8-mm anode nozzle diameter), operated with an arc current intensity of 550 A and voltage of 74 V, at a spray distance of 80 mm. The feeding rate of the powder was of 1 g/min while the plasma gas was a mixture of nitrogen and hydrogen, with flow rates of 47.6 SLPM and 5.4 SLPM respectively. All specimens were sprayed with the substrates held at room temperature.

The specimens were then characterized using a range of analytical techniques. A Hitachi S3400 scanning electron microscope (SEM) was used to image the overall morphology of the splats and the substrates. The average surface roughness of the substrates was measured using a Digital Instruments DI3000 Atomic Force Microscope (AFM). A FEI xP200 Focused Ion Beam microscope (FIB) was used to mill cross-sections of the splats using an energetic gallium ion beam, and to image them using secondary electrons induced by the ion beam. Details of this protocol have been described elsewhere [51]. A FEI xT Nova Nanolab 200 dual beam microscope (that is a FIB and SEM combined into a single instrument) was used to prepare cross-

sections of splats (100-200 nm in thickness) suitable for TEM observation. These were prepared using the lift-out method as described elsewhere [51] and examined in a Philips CM200 transmission electron microscope (TEM) to which energy dispersive x-ray spectroscopy (EDS) facilities had been interfaced.

### III. Results

Experimental observations for both the sprayed and reference specimens are detailed in this section. First, the roughness of the various specimens was evaluated in order to obtain a relative indication of the condition of the surface. Next, the morphology and microstructure of the different types of splats are described following observations by SEM, FIB and TEM. Finally, splat morphology is related to the pre-treatment of the substrate.

For both the FIB and TEM observation representative cross-sections are presented. Only a relatively brief summary of the TEM results is given: as noted in the introduction a more detailed description of these results can be found elsewhere [50].

#### III.1. Estimation of the substrates' roughness measured by AFM

The roughness,  $R_a$ , was measured three times for each specimen on a 5x5  $\mu\text{m}$  square region by AFM, and results were averaged. This provided an indicative value of surface roughness of the specimen. For the sprayed specimens, the roughness was

measured towards the edge of the specimens, away from the presence of any splats. Results are presented in Table 2.

**Table 2. Average roughness measured for the different specimens using AFM**

<b>Specimen</b>	<b>Uns sprayed specimen</b>	<b>Sprayed specimen</b>
Polished	$[2.4 \pm 0.5]$ nm	$[5.4 \pm 2]$ nm
Polished and thermally treated	$[4.4 \pm 1]$ nm	$[69 \pm 20]$ nm
Boiled	$[4.2 \pm 1.5]$ nm	$[25 \pm 9]$ nm
Boiled and thermally treated	$[2.8 \pm 1.5]$ nm	$[24 \pm 10]$ nm

Despite the variations in these measurements, possibly due to the small size of the measured areas, (which is necessary to avoid the presence of any splats on the sprayed specimens), it can be observed that the heat treatment and the boiling treatment on their own both increase the roughness. However, boiling and heat treatment shows similar results as the boiling treatment alone (if one considers the level of experimental error in the roughness data), perhaps as after boiling the thermal treatment itself does not greatly increase the oxide thickness, but rather modifies its composition. Finally, the significant increase in roughness after spraying may be, in part, due to the oxidation by the hot gases resulting from the plasma flow, and, on the other hand, from the effects of splashing forming very thin (nanoscale) particles of NiCr on the surface. Indeed, observations of particle impact during plasma spraying showed the occurrence of, what these authors termed, impact splashing of very small droplets just after impact [12, 52]. Further, modelling experiments suggest that this is expected to occur even when disc-shaped splats are formed [53]). This may explain the much higher roughness found on the sprayed SS\_PT specimen. However, the

roughness of sprayed and unsprayed polished specimens is similar, possibly because the adhesion of the nano-droplets is limited on the polished specimen (on which the wetting of NiCr is quite poor, as will be detailed later).

Measurements of the roughness were made in order to give an indication on how the topography of the surface may be modified by the thermal and boiling treatment. From these results, it can be concluded that the changes are minimal compared to the modifications of the surface roughness attributed to material deposition.

### III.2. Description of the splats' morphologies and microstructures

#### III.2.a. *Study of the splats' size and morphology by SEM*

A large number of splats (about 50 per specimen) were observed using SEM, and their morphology qualified and diameter estimated (features such as splashed fingers were ignored when evaluating diameter, which was done by considering the smallest and largest diameter values measured from the splat, which is not perfectly circular, and calculating the average value). Images of typical splats are presented in Fig. 1.

The common splat morphologies were:

- Disc-shaped splats (Fig. 1a and 1b, with diameter,  $D \sim 35 \mu\text{m}$ ,  $20 < D < 60 \mu\text{m}$ ), with a distinct rim at the splat periphery. Some may exhibit sub-micron voids ( $D \leq 1 \mu\text{m}$ ) in the centre of the splat (Fig. 1a), whereas others display a large circular void ( $D \sim 5 \mu\text{m}$ ) in their centre (Fig. 1b).

- Flower-shaped splats (Fig. 1c,  $D \sim 30 \mu\text{m}$ ,  $15 < D < 45 \mu\text{m}$ ), which usually exhibit several, fine central voids ( $D \leq 1 \mu\text{m}$ ), which can often coalesce to form a single large void ( $D \sim 1\text{-}5 \mu\text{m}$ ).
- Fragmented splats (Fig. 1d,  $D \sim 22 \mu\text{m}$ ,  $10 < D < 30 \mu\text{m}$ ), in which it appears that molten NiCr has slid away from the central point of impact.
- Very fragmented splats (Fig. 1e,  $D \sim 15\text{-}25 \mu\text{m}$ ,  $8 < D < 45 \mu\text{m}$ ), which appear to be made up of several isolated fragments.

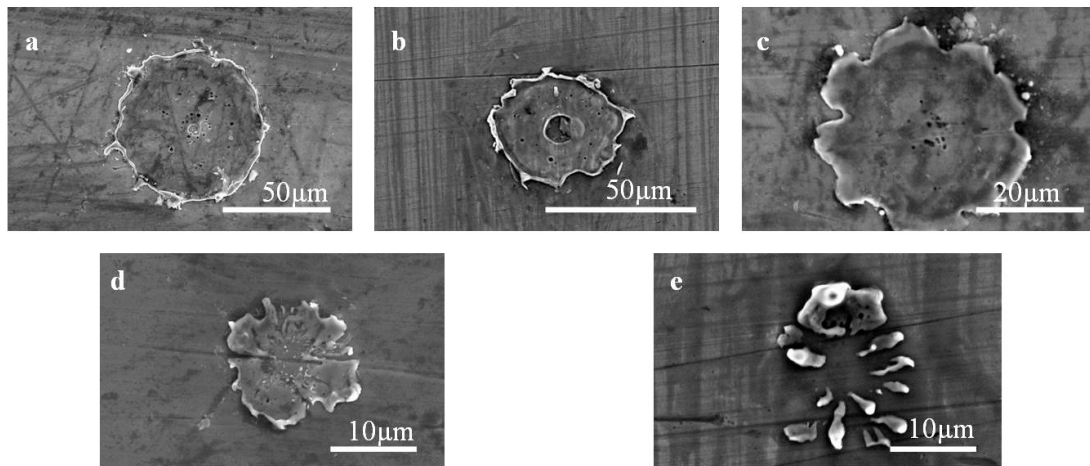


*Figure 1. SEM images of typical splats: (a) Disc splat showing a distinct rim and voids at the centre; (b) Disc splat with a central void and a distinct rim; (c) Flower-shaped splat; (d) Fragmented splat; (e) Very fragmented splat.*

### III.2.b. Study of the splats' microstructure by FIB cross-sectioning

Cross-sections of the different types of splats observed by SEM were prepared and examined using a FIB microscope for surface conditions. A significant number of cross-sections for each specimen were prepared and examined across the different splat types. In this paper, only the principal microstructural features observed in the

different splat cross-sections are described. The FIB cross-sectioning process requires the deposition of a strip of Pt on top of the section to protect the surface of the specimen from damage from the ion beam [51]. Such a layer is observed on all the cross-sections presented.

A cross-section taken across a disc-shaped splat (Fig. 2) shows that the splat is mainly composed of uniform, columnar grains ( $\leq 1 \mu\text{m}$  in diameter) (see region marked 1), which have grown normal to the substrate surface: the heat flux was extracted by conduction through the interface during solidification.

Moreover, despite the apparent good contact between the splat and the substrate, there are only a few regions where the grains boundaries of the splat and the substrate appear to be coincident across the splat-substrate interface, for example the region marked (2) in the centre of the splat, where a layer of smaller grains ( $D < 1 \mu\text{m}$ ) can be observed in the substrate. This alignment of grains suggests that melting of the substrate may have then occurred locally in this zone. Some voids can be observed at the splat-substrate interface (3) close to the central void and also at the rim of the splat (4). The latter seems to be associated with the curling up of the splat rim at its periphery, which occurs because of the surface tension effect during spreading, the poor adhesion of the splat under the rim and the shrinking of the splat to accommodate the stress arisen from the solidification and cooling down [2, 54]. In the region associated with the central void, a grey phase with no observable grain structure can be distinguished. This phase was identified to be NiO, as will be described later in the TEM section, (5).

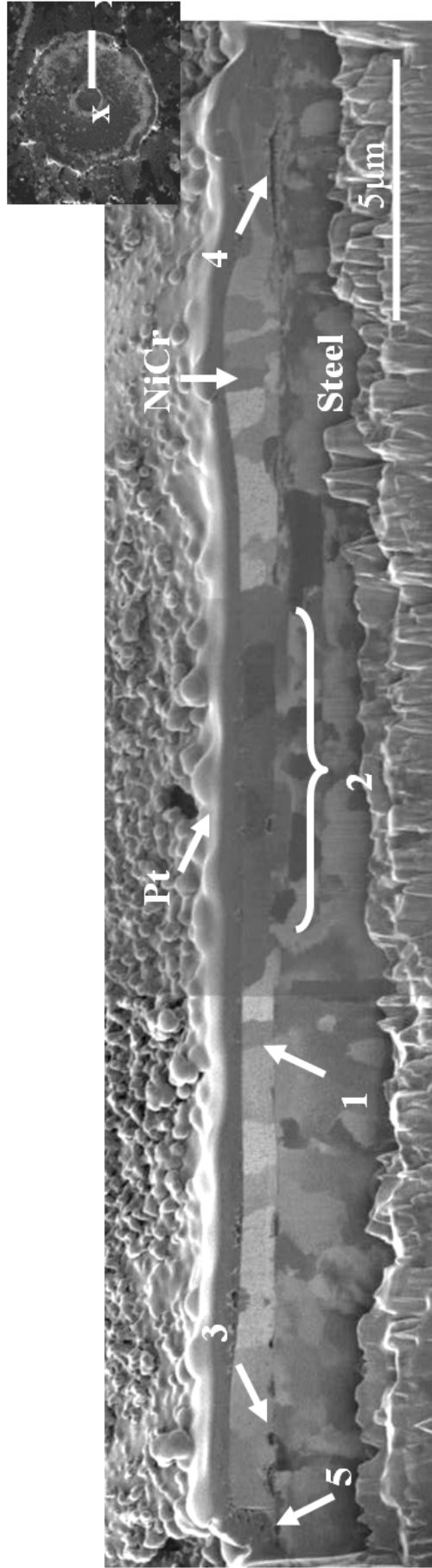
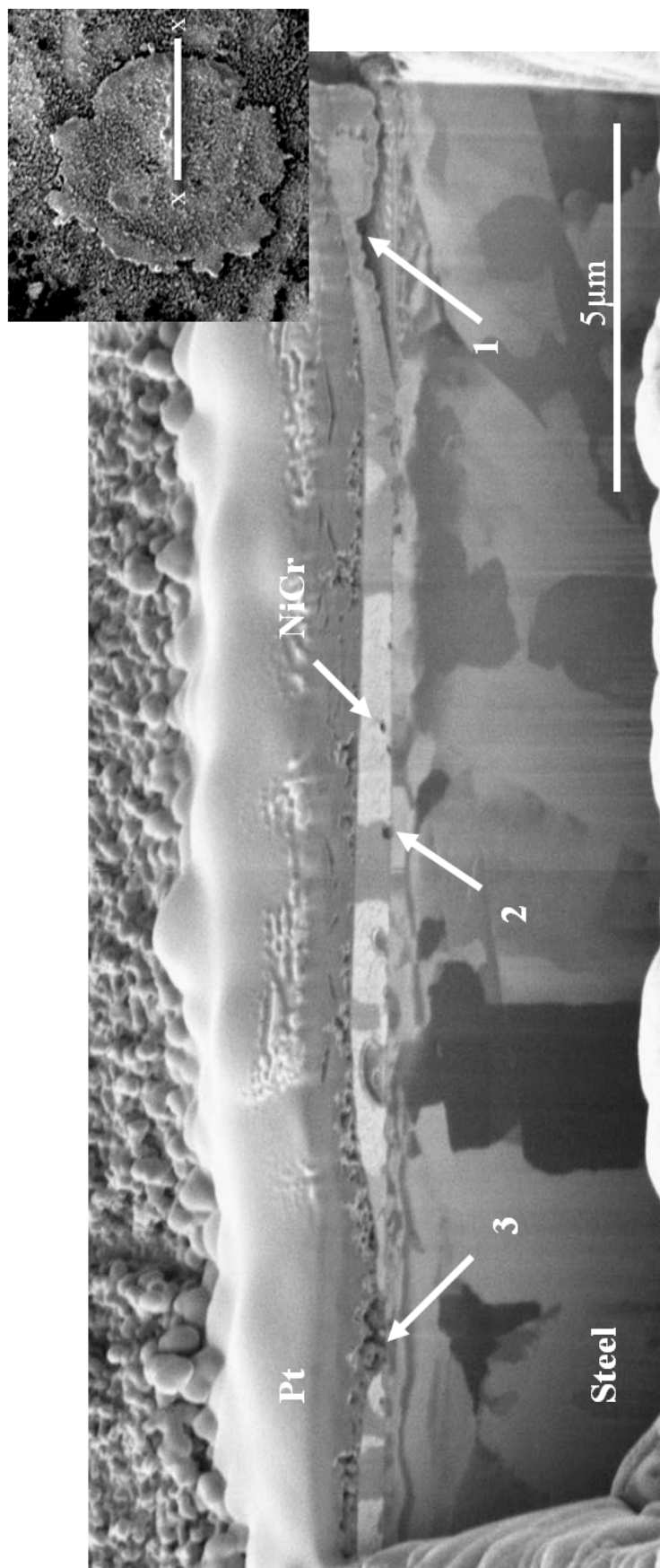


Figure 2. FIB cross-section of a disc-shaped splat (insert shows location of cross-section)

The cross-section of the flower-shaped splat (Fig. 3) shows that such a splat exhibits greater delamination away from the substrate, especially at its periphery (1). Some voids can be also observed at the interface with the substrate (2), but, in general, its structure is broadly similar to the disc-shaped splat. The grain structure of the substrate close to the interface with the splat is finer than that at a greater depth below the surface. This may arise from the surface treatment of the substrate or from a possible remelting of the substrate due to the splat impact and flattening followed by rapid solidification. Finally, it can be seen that the centre of the splat (3) is a very narrow layer of the NiCr splat, less than  $0.5\ \mu\text{m}$  in thickness.

Two cross-sections are presented through an irregularly-shaped splat (Figs. 4a and 4b).

The first section (Fig. 4a) is across a part of the splat that appears to have splashed away from the centre. It can be seen that the grains can be typified as large ( $\sim 2\text{-}4\ \mu\text{m}$ ) and normal to the substrate surface (1), suggesting solidification directed from the interface toward the top of the splat, at a slower rate than in other regions of the splat: this could be an indication of a higher thermal resistance at the splat / substrate interface. An oxide (probably NiO) region (2) adjacent to this region has no grain structure visible at this scale of observation, but contains what appear to be some isolated NiCr particles (3). Some voids are also found at the interface between the splat and the substrate (4).



*Figure 3. FIB cross-section of a flower-shaped splat*

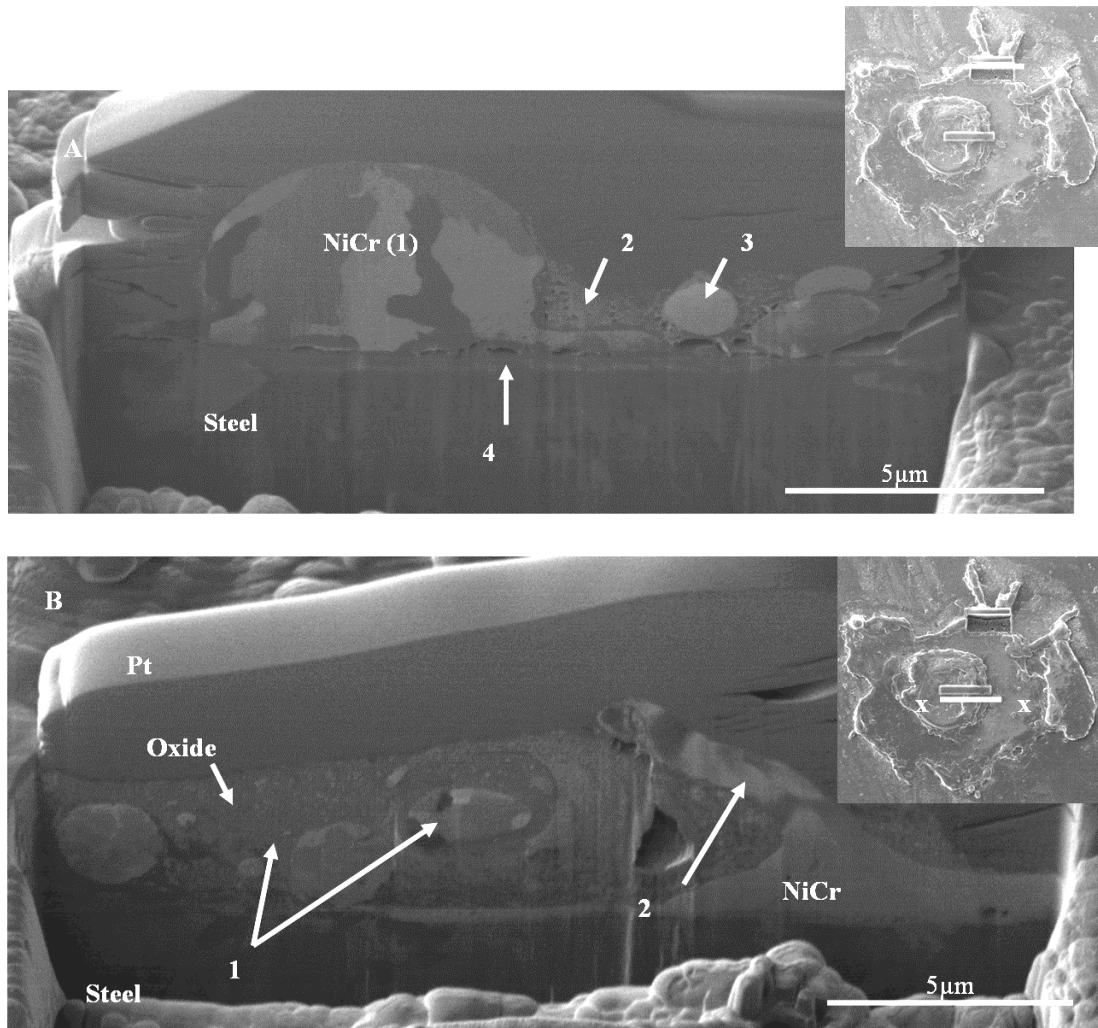


*Figure 4. FIB cross-sections of a splashed finger (a) at the periphery of an irregularly shaped splat, (b) across the central void of the splat*

The second cross-section, (Fig. 4b) shows the structure near the central void of the splat. This latter feature seems filled with a mixture of oxide and NiCr particles (1), and the shape of the actual NiCr splat (2) appears to suggest that the molten metal has been pushed upwards, away from the substrate. This effect might be associated with the gas released by the substrate heated from the molten splat or trapped during the impact. It then may have formed a bubble which may have become unstable. The oxide might then arise from the oxidation of the substrate or the splat due to the presence of both heat and oxygen. The embedded NiCr particles would also arise

from the instability of the gas evolution from the surface, which then acts to disperse the molten splat.

Finally, Fig. 5 depicts a cross-section that has been made across two splats that have clearly been deposited on top of each other. It is clear that the first deposited splat, at the splat-substrate interface, has been remelted due to the heat provided by the second splat, as the homo-epitaxial growth clearly indicates (see region marked 3). The melted NiCr has flowed from left to right during the flattening process. It seems that liquid material from both splats have spread, forming a thin layer (1), until the remnant heat generated was finally sufficient to remelt the first splat. At this point NiCr has accumulated, forming a thick layer (2). An unmelted region of the first splat can be observed (2), while on its outer surface some melting appears to have occurred: the new grains have coalesced on the pre-existing grains, as shown by the aligned grain boundaries (3). Finally, on the far right of the section, delamination between the first and second layer occurs due to the curling up of the top splat (4). Some oxide can also be observed in this region (5).

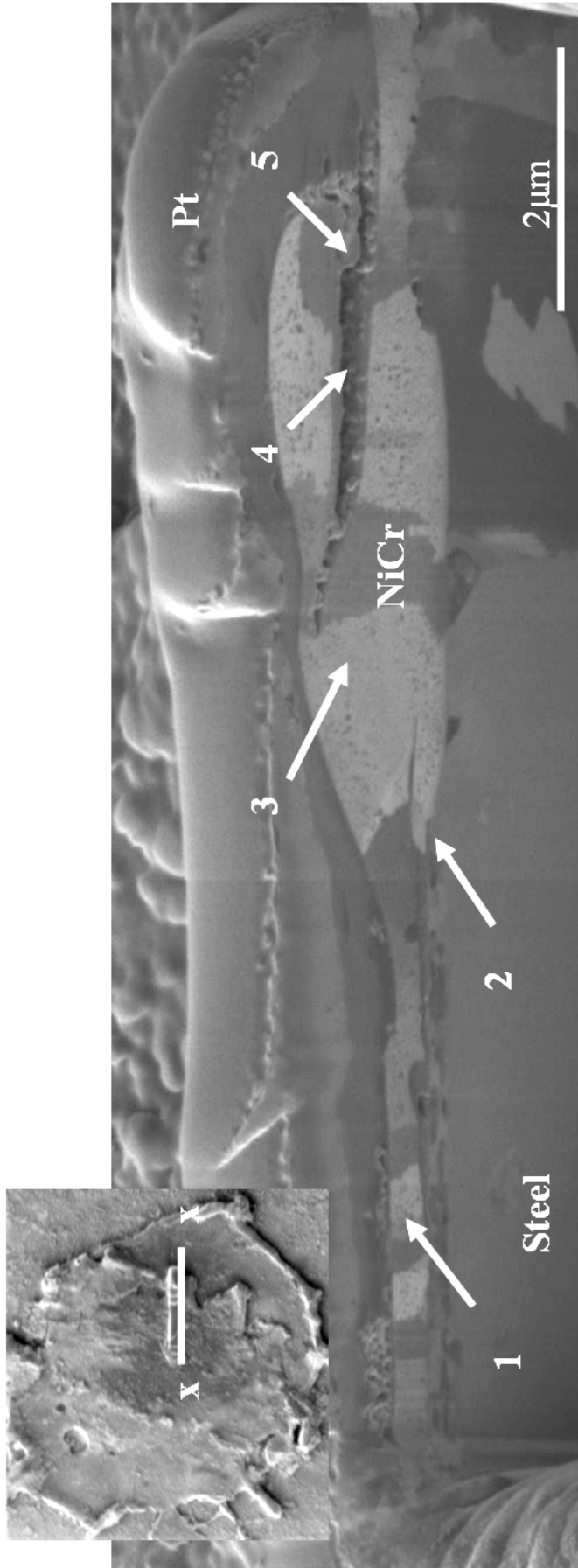


Figure 5. FIB cross-section of two splats on top of each other

### III.2.c. *Summary of the splats' characteristics observed by TEM*

Transmission electron microscopy allows very detailed studies of the interface between the splat and the substrate at high spatial resolution. This includes elemental maps and linescans across the interface, acquired using EDS, and crystallographic studies of the various phases associated with the splat-substrate microstructure. TEM specimens were made for each type of splat and each particular feature on each specimen. A range of microstructural features were observed and for reasons of brevity here, these are described in detail in another article [50]. (This associated paper provides detailed TEM studies including chemical and crystallographic evidence of the identity of the various phases that are present and crystallographic analysis of the splat-substrate interface.) A summary of these observations are presented in Table 2. The features described were found on all four substrates, but with different frequencies for each of the differing substrates. The principal observations here include the following:

- Evidence of chemical diffusion between the splat and substrate, together with localized substrate melting. Such phenomena were usually located neither in the centre nor the periphery of the splat, where the splat-substrate interface is usually distinct, but in the main body of the splat. Often the interface in this region is indistinct. EDS elemental linescans performed across such regions, show gradual variations in the concentrations of Ni and Fe, compared to much sharper elemental profiles when the interface is more distinct. This confirms that interdiffusion has occurred across this interface (Fig. 6). This is, however, insufficient evidence on its own to prove that substrate melting has occurred.

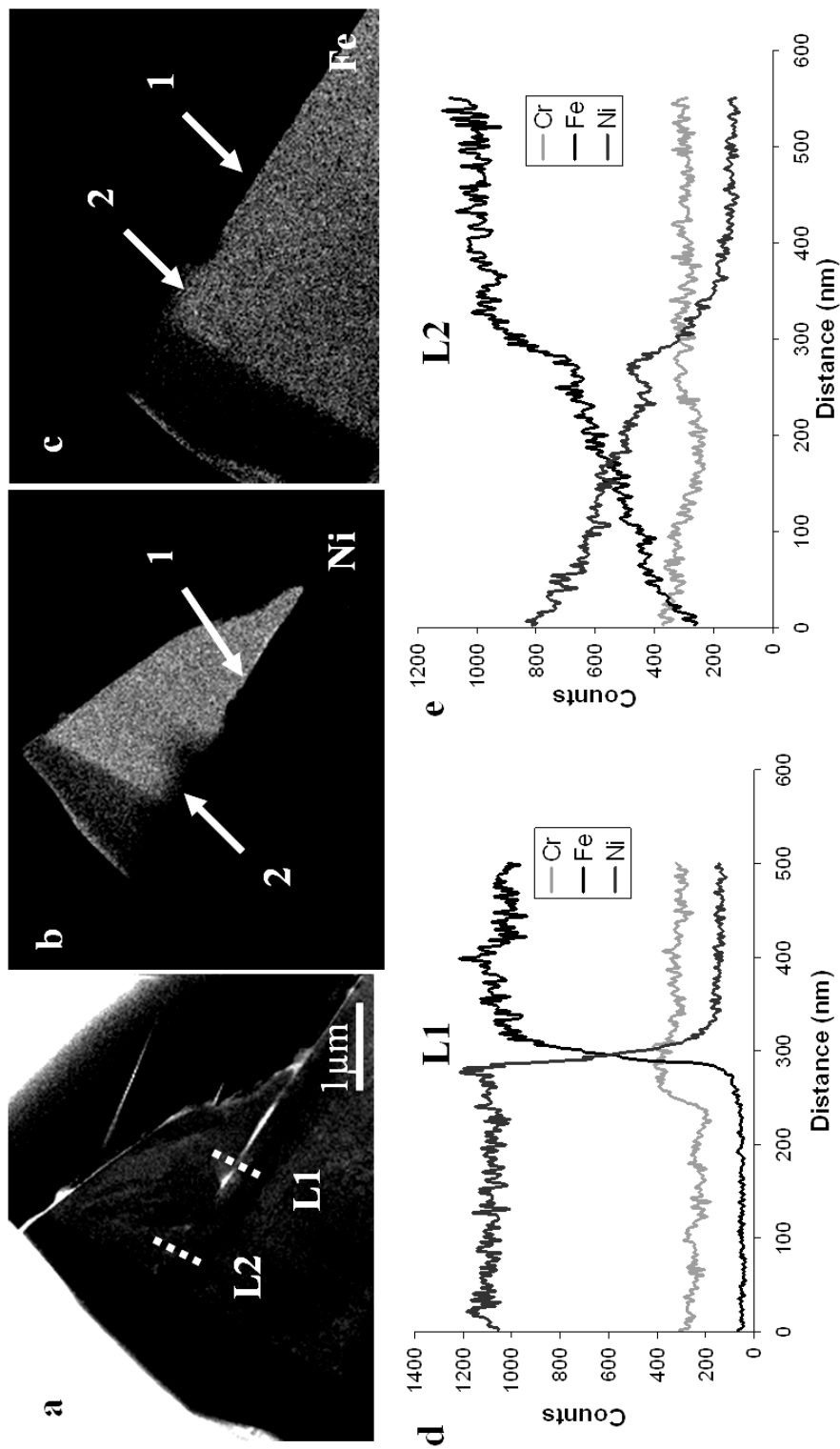
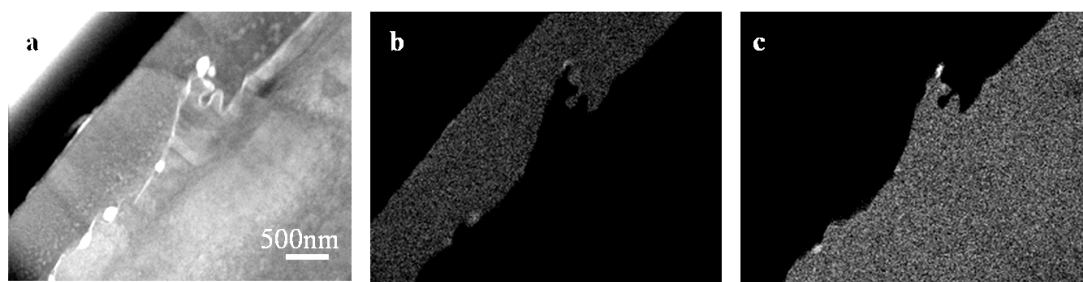


Figure 6. STEM image (a) and elemental mapping for Ni (b) and Fe(c); elemental line scan across the interface where the interface is clear (L1, d) and indistinct (L2, e).

- Besides, in a number of areas jetting of the substrate within the splat was observed. This is more strongly indicative of substrate melting: that is, the melted substrate may have splashed within the substrate, giving an irregular interface. If the solidification was too rapid for diffusion to take place the interface may remain chemically abrupt (Fig. 7). In this case, high angle boundaries between grains are present at the interface.



*Figure 7. STEM image (a) and elemental mapping for Ni (b) and Fe(c): irregular and clear interface*

For a number of other splats that were analysed in this way, interdiffusion of Ni and Fe occurred (on the scale of  $\sim 200$  nm) and the interface is indistinct (Fig. 8).

Finally, in some cases, grains which have grown across the splat-substrate interface were observed (Fig. 9).

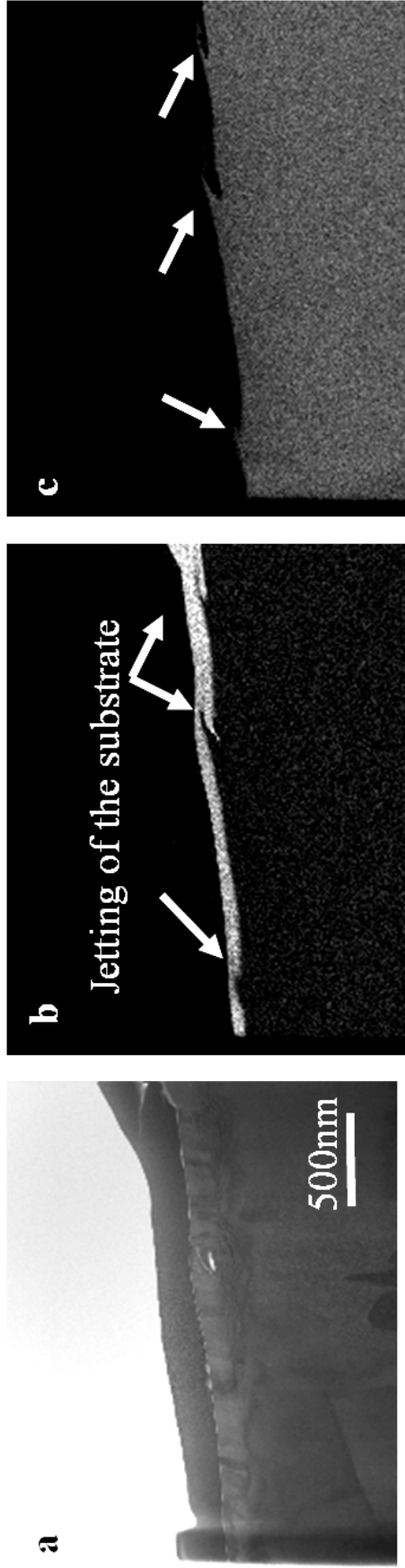


*Figure 8. STEM image (a) and elemental mapping for Ni (b) and Fe(c) phases: jetting of the substrate into the splat with an indistinct interface*

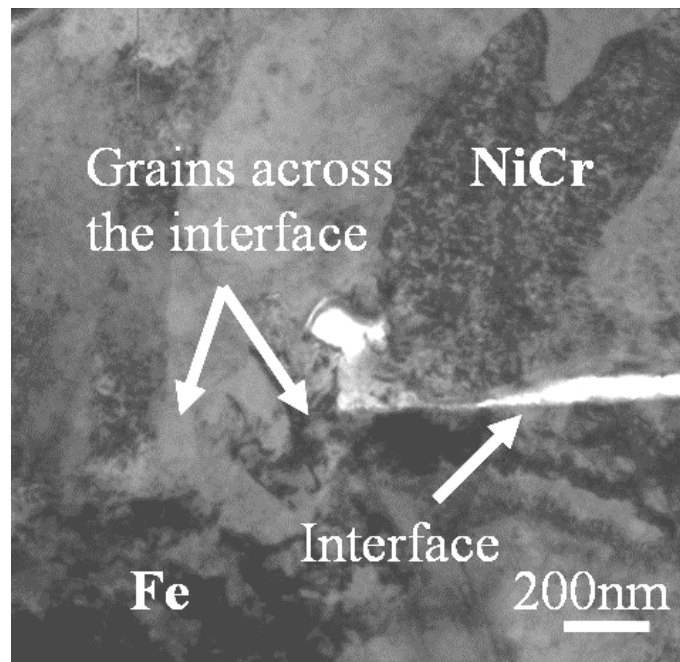


*Figure 9. Bright field TEM image of a splat substrate interface where a single grain bridges the interface*

- The presence of low angle boundaries; that is, the two grains across the interface are aligned in a similar orientation. This was observed even when there was evidence of no melting or diffusion. This may be because the melted NiCr nucleates and grows on the steel grains with a similar orientation, that is, it grows epitaxially.
- Various phases were identified using EDS and electron diffraction. Apart from NiCr and austenite (as expected), several oxides were found including FeO, NiO, NiCr<sub>2</sub>O<sub>4</sub>, Cr<sub>2</sub>O<sub>3</sub> and CrO<sub>3</sub>. These oxides were observed at different locations around and on top of the splats; the specific locations of these phases for particular splat types will be described in the following sections. Again, detailed descriptions of the characterization of these phases is provided in the associated paper [50].

Figure 10 presents a schematic representation of a disc-shaped splat summarizing the most common features described previously: shown in the schematic are the interface between the steel substrate (1) and the NiCr splat (2), which is distinct toward the centre and the periphery of the splat (3). However, in the region in between, substrate melting, local jetting and diffusion between splat and substrate may occur (4).  $\text{Cr}_2\text{O}_3$  or  $\text{CrO}_3$  were typically found as a thin layer on the outer surface of the splat (5), in some cases  $\text{FeO}$  was found at the periphery where the splat has curled up (6),  $\text{NiO}$  was found at the periphery (7) as well and in the central void (8). The  $\text{NiO}$  found in the central void was probably formed by the oxidizing gases released upon impact and spreading of the NiCr particle; it may then contain some NiCr particles (9).

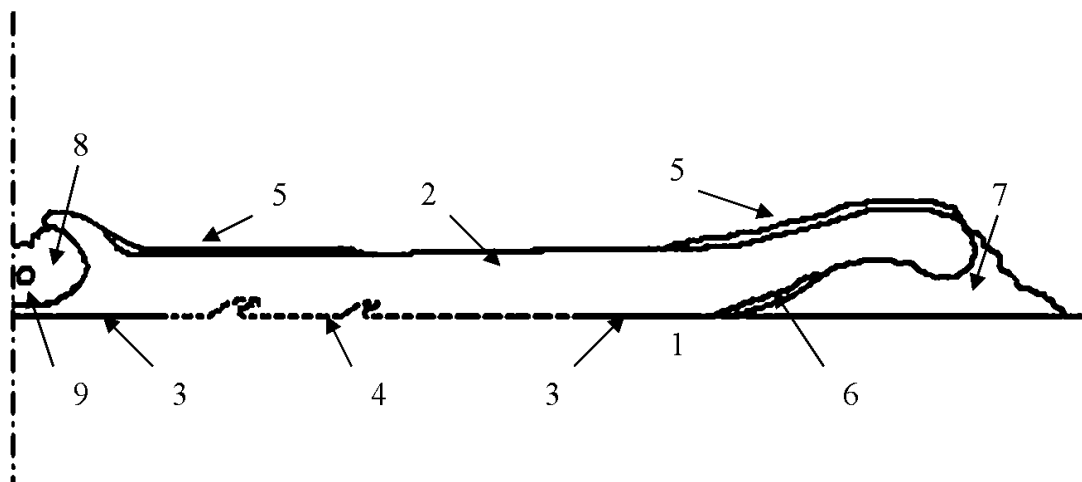


*Figure 10. Schematic representation of a typical disc-shaped splat*

### III.3. Description of the splats characteristics depending on the substrate pre-treatment

For each of the four surface conditions, images of about 50 splats were acquired for each specimen, in order to obtain an approximation of the statistical distribution of the

different types of splat morphologies present. The proportions of each type of splat observed by SEM on each specimen, along with the average diameter, were calculated. The frequency of the different features observed by FIB and TEM for the different specimens was also observed, although no value could be calculated considering the limited number of cross-sections that could be made and studied. All these results are summarized in Table 3.

**Table 3. Description of the different types of splat found on each specimen, their diameter, average population and particular characteristics**

	Type of splat	Diameter and population	SEM/FIB/TEM observations
SS_P	Disc-shaped with a central hole (Fig. 1b)	23% $D_m = 30\mu\text{m}$ $20 < D < 55\mu\text{m}$	Poor NiCr wetting Relatively thick splat (typically from 1 to $3\mu\text{m}$ )
	Fragmented (Fig. 1d)	<b>47%</b> <b><math>D_m = 20\mu\text{m}</math></b> <b><math>10 &lt; D &lt; 30\mu\text{m}</math></b>	Often coarse and irregular grain structure (up to $\sim 3\text{-}4\mu\text{m}$ in length). Substrate melting/interdiffusion frequent
	Very fragmented (Fig. 1e)	30% $D_m = 14\mu\text{m}$ $8 < D < 20\mu\text{m}$	Ni and Cr oxides frequent. No delamination or FeO Limited voids at interface
SS_PT	Disc-shaped with no central hole (Fig. 1a)	<b>80%</b> <b><math>D_m = 39\mu\text{m}</math></b> <b><math>20 &lt; D &lt; 60\mu\text{m}</math></b>	Good NiCr wetting Thin splats (less than $1\mu\text{m}$ ) Fine grain structure ( $\sim 1\mu\text{m}$ )
	Flower-shaped (Fig. 1c)	20% $D_m = 32\mu\text{m}$ $25 < D < 40\mu\text{m}$	Substrate melting/interdiffusion rare Ni oxide frequent, Cr oxide rare Delamination and FeO frequent Voids at interface
SS_B	Flower-shaped (Fig. 1c)	27% $D_m = 29\mu\text{m}$ $15 < D < 40\mu\text{m}$	Quite poor NiCr wetting. Quite thin splats ( $\sim 1\mu\text{m}$ ) Quite coarse grain structure (from 1 to $3\text{-}4\mu\text{m}$ in length), except for flower shaped (columnar)
	Fragmented (Fig. 1d)	27% $D_m = 25\mu\text{m}$ $15 < D < 30\mu\text{m}$	Substrate melting/interdiffusion common
	Very fragmented (Fig. 1e)	<b>46%</b> <b><math>D_m = 22\mu\text{m}</math></b> <b><math>10 &lt; D &lt; 40\mu\text{m}</math></b>	Ni and Cr oxide frequent Limited voids at interface Delamination or FeO rare

<b>SS_BT</b>	Disc-shaped with no central hole (Fig. 1a)	12% $D_m = 37 \mu\text{m}$ $20 < D < 50 \mu\text{m}$	Quite good NiCr wetting Thin splats (less than $1 \mu\text{m}$ ) Quite coarse grain structure (length of up to $4 \mu\text{m}$ ). Substrate melting/interdiffusion frequent Ni oxide frequent, some Cr oxide Limited voids at interface Delamination and some FeO
	Flower-shaped (Fig. 1c)	<b>78%</b> <b><math>D_m = 30 \mu\text{m}</math></b> <b><math>20 &lt; D &lt; 45 \mu\text{m}</math></b>	
	Very fragmented (Fig. 1e)	10% $D_m = 25 \mu\text{m}$ $15 < D < 45 \mu\text{m}$	

## IV. Discussion

### IV.1. Splat formation

From the experimental observations, the formation of a disc-shaped or almost disc-shaped splat could be summarized as described below.

When a NiCr particle impacts the stainless steel substrate (see schematic representation in Fig. 11), heat is transferred to the substrate by conduction, causing the desorption of adsorbates and condensates, such as the chemisorbed water from the surface. These released species may form one or, in some cases, several voids, in the centre of the flattened splat, leading to poor contact in this region (1). The void may reach a critical size, where it becomes unstable, creating a larger bubble-like void. Formation of such voids may also be due to the mechanics of the impact of the NiCr particle on the substrate: numerical simulations have shown that the pressure build-up at the point of impact causes a change in the curvature of the droplet, creating a central void [53, 55]. The presence of oxygen or water-rich gas trapped in this void(s) is presumably responsible for the formation of Ni oxide. This oxide is less stable than both  $\text{Cr}_2\text{O}_3$  and  $\text{CrO}_3$ , but its kinetics of formation is faster [56]. Meanwhile, the molten NiCr particle undergoes flattening across the substrate (2). It is possible that

species released from the surface are simultaneously covered by the flowing splat and may be pushed to the periphery because of the flow of melted metal (3). In this situation, good contact between NiCr and the steel substrate can be achieved. The heat from the molten splat is then sufficient to locally melt the steel substrate (4): the molten steel, pushed by the flowing splat, is then splashed within the splat, as observed by elemental mapping of the interface. Diffusion across the interface between the steel substrate and the splat can also occur in this zone. Such phenomena may occur due to the similar crystallographic structures of austenite and NiCr. Another factor may be a relatively slower cooling and solidification process, allowing diffusion to occur, rather than the formation of any intermetallic phase.

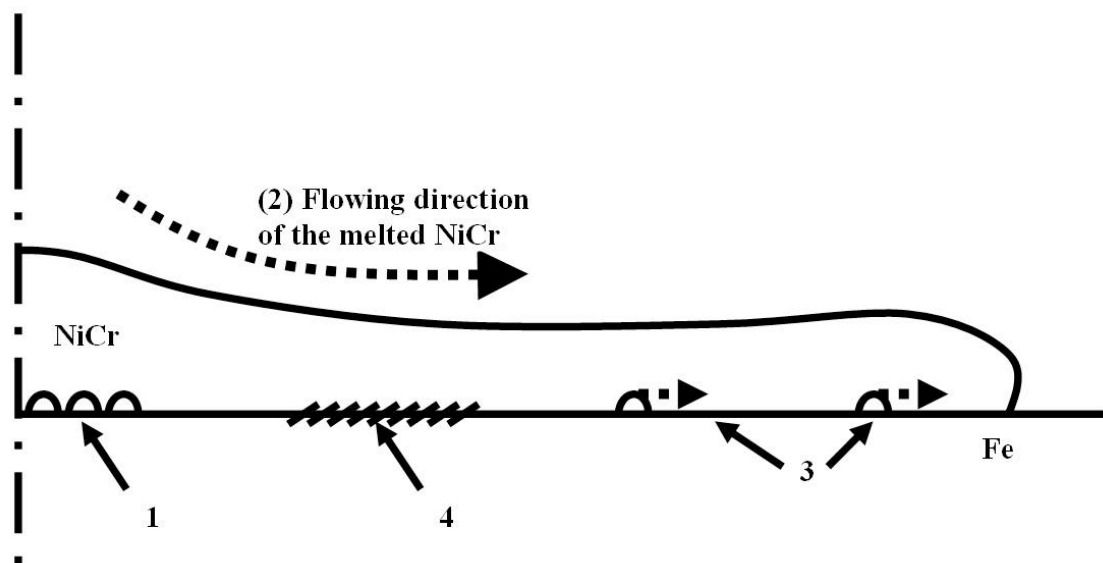


*Figure 11. Schematic representation of a splat undergoing flattening on a steel substrate*

Good contact and bonding is then achieved in the centre of the splat, but the contact is poor closer to the rim. It is possible that the species released from the substrate and driven outward by the flow of the splat inhibits good contact at the splat periphery.

In this instance, the periphery of the splat may curl up away from the substrate: it is known that curling up occurs where poor bonding is found at the periphery of the splat; when the splat solidifies and cools, the central part attached to the substrate cannot contract, but the upper surface shrinks so the edges of the splat curl up to accommodate the stress [54]. Chromium oxide also forms on the upper surface of the splat, although it cannot be deduced if this happens before, or after, complete solidification of the splat. Thicker splats are usually found to exhibit a higher concentration of this oxide, presumably because the heat necessary for its formation is present at the splat surface longer (a thicker splat exhibits relatively less surface for the heat to evacuate as compared to a thin splat, and thus cools down at a slower rate).

The splat solidification process is not fully understood and seems to be influenced by several factors. Many models disregard mechanisms such as melting of the substrate or poor contact between the splat and substrate [18, 57], which can not be modelled due to the lack of input data and the difficulty to address them. It is expected that the heat is principally removed by conduction through the interface with the substrate, whilst the radiative contribution is estimated to be in the order of 10% [2]. This would then lead to the assumption that solidification starts from the bottom of the splat as soon as the splat begins to flatten [2]. Here, electron diffraction studies [50] have revealed the crystallographic relationship across the interface in regions where good contact was found between the splat and substrate. In many instances low angle boundaries between the NiCr and steel grains were observed showing alignment of crystal planes across the interface. However, in these cases no substrate melting was noted. In such cases, NiCr may have solidified from the interface with the substrate

with the grains nucleating on the unmelted steel grains. This may be in agreement with previous modelling [2, 18, 57], nevertheless these models are unable to explain all the features found in the specimens studied here.

In most cases the splat-substrate contact at the interface seems good (no evidence of delamination nor voids at the considered resolution) and fine columnar grains ( $\sim 1 \mu\text{m}$ ) are observed (see Fig. 2 for instance). Sometimes for very thin splats, these grains tend to grow laterally (Fig. 3). Irregular splats exhibit quite coarse grains, which are often columnar, such as those shown in Fig. 4a, or more irregularly shaped grains. This may be explained by the relatively poor thermal contact and reduced spreading of the splat, meaning that NiCr remains molten for longer, leading to the formation of larger grains. These results are in agreement with studies by Bianchi *et al.*, who noted that with good contact at the interface, the heat can be mainly removed through the substrate [29]. This results in fine columnar grains, while if the contact is poor, the heat may be removed parallel to the interface, resulting in larger grains which tend to grow from the centre of the splat to the periphery [16]. Vardelle *et al.* also observed if the thermal conductivity of the substrate was low, then it may reach a high temperature and the heat may be removed from the splat by its outer surface [58]. This may be linked to the case of extended grains, laterally (for thin splats, Fig. 3) or vertically (for thick splashy splats, Fig. 4a).

However, the solidification process may be different where substrate melting occurs: Zhang *et al.*, who observed the occurrence of substrate melting when spraying Mo on steel, noted that splats may solidify on the molten substrate, where substrate melting may be limited by the fast cooling of the droplet [20]. The different structures found

here when melting of substrate occurred were described in the results section. However, no obvious solidification process can be concluded from these results, although they are consistent with the processes described by Zhang *et al.*

Kitahara *et al.* did not observe an intermetallic layer when spraying Ni and Cr on to on mild steel [35]. They interpreted this result as the sign that substrate melting had not occurred or was limited. However, the TEM study performed here clearly shows that melting has occurred, but did not produce an intermetallic layer. Moreover, spraying conditions have a significant influence on the occurrence of melting, as shown by the case of the SS\_PT specimen, where the splats were significantly thinner and substrate melting much less frequent. Thus, Kithara *et al.* may have used spraying conditions that did not favour melting.

#### IV.2. Effect of surface chemistry induced from the pre-treatment on the splat formation

TEM cross-sections of the unsprayed specimens did not show the presence of any particular surface oxide layer. That is, any phases present may be too thin to resolve in the TEM. Previous XPS studies of these specimens showed that Cr oxide and Fe oxide and iron hydroxide could be found on all the specimens, but that the heat and boiling treatments changed their relative proportions [49].

Grosvenor *et al.* examined splats on a number of iron substrates either heat treated at 150°C or following boiling for 2000 s. By XPS, it was found that on the heat treated specimens, a layer a few nm thick, comprising a mix of magnetite Fe<sub>3</sub>O<sub>4</sub> and

magnetite  $\gamma\text{-Fe}_2\text{O}_3$  was present [59]. For the boiled specimens, the surface layer was made of a mixture of  $\text{FeOOH}$ ,  $\text{Fe}_3\text{O}_4$  and  $\gamma\text{-Fe}_2\text{O}_3$  [60]. On the other hand, studies of the oxidation of stainless steel type 304 usually show that oxidation layers are made on the outer surface mainly of  $\text{Fe}_2\text{O}_3$ , and the inner layer made mainly of a mixture of Cr and Fe oxides ( $\text{Cr}_2\text{O}_3$ ,  $\text{Fe}_2\text{O}_3$ , spinel type  $\text{Fe}(\text{Fe}, \text{Cr})_2\text{O}_4$  or  $\text{Ni}_x\text{Fe}_{3-x}\text{O}_4$ ) [61], [62]. Furthermore, studies of corrosion have shown that  $\text{FeOOH}$  forms in presence of water and then transforms to  $\text{Fe}_3\text{O}_4$  [63]. Finally Cedelle *et al.* observed that pre-heating stainless steel substrates to  $400^\circ\text{C}$  may increase the thickness of the oxide layer, which would still be of the order of a few nm thick, without changing its composition [11].

Consequently, it is very probable that the heat treatment applied to the steel specimens increased the content of the various oxides and hydroxides on the surface, while boiling increases, principally, the hydroxide content. However, the complexity and fine scale of such layers make it difficult to identify with precision the exact concentration of the elements in these phases.

Other effects of the treatments concern the possibility of condensates and adsorbates, such as chemisorbed water, on the surface. Several studies on splashing phenomena and void formation in plasma spray concluded in the existence of a transition temperature ( $337^\circ\text{C}$  for Ni sprayed on stainless steel [6]). Specimens heated during, or just before, spraying above this temperature would see the proportion of splashed splats significantly reduced. One common explanation is that this temperature corresponds to one where condensates and adsorbates evaporate from the surface.

Thus, upon particle impact, much less gas is released from the substrate, inducing less splashing and porosity [21, 26, 32].

Comparing splat morphology between the polished and the polished and thermally treated specimens, it indeed appears that wetting of the NiCr has significantly been increased by thermal treatment, creating flatter and more disc-shaped splats. However, this can not be solely explained by the transition temperature phenomena, discussed earlier, as the heat treatment occurred prior to spraying. Cedelle *et al.*, when spraying nickel on non pre-heated and pre-heated at 400°C stainless steel substrates, found that the pre-treatment caused changes in the surface topography, resulting in a positive skewness (that is to say that the frequency of valleys is higher than the one of peaks), which accounted for the better wetting of the Ni splats and the shorter spreading time. (This was about twice as fast for heated substrates compared to the non pre-heated specimens) [11]. Another of the possible explanations may be that the changes induced by the heat treatment on the specimen surface include less condensates/adsorbates even days after the treatment: for example more FeOOH may have been converted to oxide, leading to less water release. Also, the oxidation of the surface can reduce the thermal contact between splat and substrate: McDonald *et al.* found that pre-heating, at 400°C, on an Inconel substrate resulted in a thermal contact resistance more than one order smaller than for the non-preheated substrate [28]. Then, less heating of the substrate occurs, leading to lesser melting of the steel, while the melted NiCr can spread over the substrate to form flatter and less fragmented splats. Finally, the wetting of the melted NiCr may be increased from a surface tension point perspective, due to the chemical interaction between the sprayed material and the surface oxides. It can also be noted that such flatter splats may cool

down more rapidly, which may explain why less Cr oxide is found on their outer surface.

When comparing splats between the polished and polished and boiled specimen, some increase in the irregularity of the shape of the splats can be noted. It is possible that the boiling treatment, by forming more hydroxide on the surface that may release water upon particle impact, increases the amount of gas released by the substrate thus decreasing the wetting of the melted NiCr.

Finally, heat treating after boiling still leads to flatter and more regular splats compared to boiling alone, but the splats observed on the specimen SS\_BT are mainly flower-shaped, with significant delamination under the rim, thus different to the splats observed on SS\_PT.

To summarize, the results obtained here show that the surface state has a significant influence on splat shape, microstructure and their interaction with the substrate. However, not all the microstructural features observed could be fully explained and further study is currently underway to improve the understanding of these effects.

## **V. Conclusion**

The plasma spraying of NiCr particles onto stainless steel substrates produced a diversity of splats ranging from disc-shaped to very fragmented. The observation of their microstructure and their interface with the substrate at a micro and nano-scale level, feasible through the application of various microscopy techniques, revealed the

presence of several forms of oxides, voids especially towards the centre of the splat, and also the occurrence of interdiffusion between the splat and substrate materials including jetting of the steel substrate within the splat. These latter observations indicate that localized substrate melting has occurred and this may also be indicative of good bonding between the substrate and the splat. The surface chemistry, in this instance associated with the presence of oxide and hydroxides induced by heat and boiling pre-treatment of the steel substrate, influences the splat formation and morphology. Possible factors include the extent of gas released from the substrate, which induces voids and oxidation of the splat, modifying the thermal contact resistance, thus the heat transfer from the splat to the substrate, and the wetting of the melted NiCr on the substrate. To further the explanation of these effects, further work on other different specimens, differences including other spraying conditions and substrate materials, is currently underway.

## CHAPTER 3

# STUDY OF THE MICROSTRUCTURE OF NiCr SPLATS PLASMA SPRAYED ON TO STAINLESS STEEL SUBSTRATES BY TEM

---

*S. Brossard, P.R. Munroe, A.T.T Tran, M.M. Hyland, Surface and Coating  
Technology, 2010, 204 (9-10), p. 1608-1615*

### Abstract

In the plasma spraying process fine particles are melted and sprayed onto a substrate using a plasma jet to form splats. However, the mechanisms of formation of these splats, and their dependency on the chemical state of the substrate, are not yet fully understood. Transmission electron microscopy was used here to study NiCr splats sprayed onto a stainless steel substrate in order to perform detailed microstructural characterization of the splat and the splat-substrate interface. These studies provided evidence of localized substrate melting, inter-diffusion and/or inter-mixing between the splat and the substrate. Furthermore, nickel, chromium and iron oxide phases were identified at various locations around the splat using a combination of energy dispersive spectroscopy and electron diffraction. Mechanisms of formation of the microstructural features observed are discussed.

## I. Introduction

Many properties, especially the mechanical behaviour, of thermal sprayed coatings are significantly influenced by the structure of the splats, and in particular, the nature of the coating-substrate interface. That is, the interactions between the substrate and the splats which are bonded to the substrate. This, in turn, will depend on a range of parameters including the surface condition of the substrate, as well as the particle characteristics (e.g. momentum, viscosity, etc.), which are influenced by the spray conditions. Features of importance include the splat morphology, the quality and nature of the bonding between the coating material and the substrate, including the presence of porosity and oxides. Such features can be studied by observing individual splats collected by spraying only a single pass on to the substrate. The characteristics of their interface with the substrate will contribute significantly to the eventual properties of the coating in service.

Transmission electron microscopy (TEM), which allows the observation of nano-sized features, has been previously used in the characterization of thermal spray coatings. For example, in case of nano-structured coatings [64], or for composite coatings, TEM can be used to identify the various phases and precipitates at the splat-substrate interface [65]. Sampath *et al.* studied the solidification of nickel coatings using TEM, where electron diffraction allowed identification of the orientation of the crystalline structure and therefore the presence of a preferred columnar oriented growth [66]. However, all these studies were performed on coatings, where spray processing had been continued to form a continuous coating. There have been very few TEM studies on single splats, as this requires the use of specialized characterization equipment, that is, a focused ion beam (FIB) microscope, which can

be used to prepare TEM cross-sections at precise locations, for example through isolated splats [51].

Furthermore, some of the previous TEM studies concluded that substrate melting occurred and metallurgical bonding was formed, since an intermetallic layer was detected at the splat-substrate interface. Zhang *et al.*, for Mo splats on mild steel, found an intermetallic layer which was suggested to be Fe<sub>2</sub>Mo. However, no detailed TEM observations, such as elemental spectroscopy or electron diffraction, were presented to support this hypothesis [20]. Kitahara *et al.* sprayed different materials (Ni, Cr, Ta, Mo, W) onto aluminium and mild steel substrates, and identified possible intermetallic layer not by TEM, but by using X-ray diffraction on cross-sections of the coatings [6]. Moreover, in the case of Ni and Cr splats on steel, no intermetallic layer was found thus suggesting that the degree of substrate melting was limited [35]. Chraska *et al.* studied TEM cross-sections of zirconia splats made on zirconia substrates that were polished, pre-heated or rough. However, due to the very high melting point of the ceramic substrates, no evidence of substrate melting was found [23]. Thus, detailed microstructural studies of the splat-substrate interface in thermal sprayed materials are very limited.

The results detailed in this article are part of a larger study aimed at observing the effects of substrate surface chemistry and roughness, induced by pre-treatments such as heating in air or boiling the specimens, in order to vary the amount and nature of oxides or hydroxides on the surfaces, on splat formation and splat-substrate interactions. The effects of the pre-treatment of the substrate on the splat morphology and interactions with the substrate are described in detail in another, related, study

[67]. The present study focuses on detailed microstructural characterization, mainly through TEM analysis, to investigate in detail the structure of disc-shaped NiCr splats sprayed onto steel substrates. The crystallographic relationships between the splats and the steel grains, evidence for the occurrence of substrate melting and the nature of splat-substrate chemical interactions, together with the presence, location and nature of oxide phases will be described. These observations have been used to support the observations and analysis in the related publication, where emphasis is placed on the effect of substrate conditions (surface chemistry and roughness) on the mechanism of splat formation and the development of splat morphology.

## II. Experimental procedure

The sprayed material was a commercial NiCr alloy powder (Ni80-Cr20, Sulzer Metco 43 VF-NS, Wohlen, Switzerland, (-45+5)  $\mu\text{m}$ ). The substrate was an austenitic stainless steel 304 (SS), polished to a nano-scale roughness ( $R_a \sim 2\text{-}5\text{ nm}$  and was evaluated by Atomic Force Microscopy; the results being presented elsewhere [67]). Four substrates with different pre-treatments were sprayed: polished (SS\_P); polished and thermally treated (SS\_PT); polished, boiled (SS\_B); polished, boiled and thermally treated (SS\_BT). Thermal treatment consisted of heating the substrate in air for 90 min at 350°C, and boiling was performed in distilled water for 30 min. The objective of these treatments was to modify the surface chemistry and roughness (found to vary from 2 to 25 nm); however their influence on splat formation will not be described in the present paper. Details of these pre-treatments, together with the study of their effects on the substrate surface topography and chemistry and on the

splat formation of the surfaces prior to plasma spray, have been provided in an associated article [67].

Plasma spraying was carried out with a Sulzer Metco (Switzerland) 7MB gun (with an 8-mm anode nozzle diameter), operating at an arc current intensity of 550 A and at an average arc voltage of 74V, with a spraying distance of 80 mm. The feeding rate of the powder was of 1 g/min while the plasma gas was a mixture of nitrogen and hydrogen, at a flow rate of 47.6 L/min and 5.4 L/min, respectively. All the substrates were held at room temperature during spraying.

An initial observation of the splats was performed using a Hitachi S3400 scanning electron microscope (SEM). Subsequently, TEM cross-sections (100-200 nm in thickness) were prepared by focused ion beam (FIB) microscopy using a Fei xT Nova Nanolab 200 dual beam microscope (that is, a FIB and SEM combined into a single instrument). These specimens were prepared using the lift-out method as described elsewhere [51] and examined in a Philips CM200 transmission electron microscope (TEM) to which energy dispersive spectroscopy (EDS) facilities have been interfaced. TEM cross-sections were observed through bright field images, Scanning TEM (STEM) images, EDS elemental maps and linescans and Kikuchi maps. Details on these various techniques can be found in the literature [68].

### **III. Results and Discussion**

Prior to TEM observation, the morphology of the splats collected on the stainless steel substrates was studied using SEM and different categories of splats were identified.

These different splat types were classified as either regular disk-shaped splats, flower-shaped splats, fragmented and very fragmented splats [67]. Examples of SEM images of typical splat morphologies for disk-shaped and flower-shaped splats are displayed in Fig. 1. Commonly observed features include either a single large pore (typically 5  $\mu\text{m}$  in diameter) or several smaller pores ( $\leq 1 \mu\text{m}$  in diameter) located in the centre of the splat. The formation of these pores may be attributed to the release of adsorbed species from the substrate, resulting from the heat released upon impact and flattening of the NiCr particle. Splats also often displayed a distinct rim, under which delamination may occur due to the accommodation of thermal stresses from the shrinking of the splat when undergoing directional solidification. Such delamination can be seen on the bright field TEM image of a splat cross-section shown in Fig. 2.

The various features described in the following sections were observed on a variety of splats made on the various substrate types described above: the features detailed here were found on all substrate types, but their frequency was found to vary depending on the pre-treatment of the substrate.

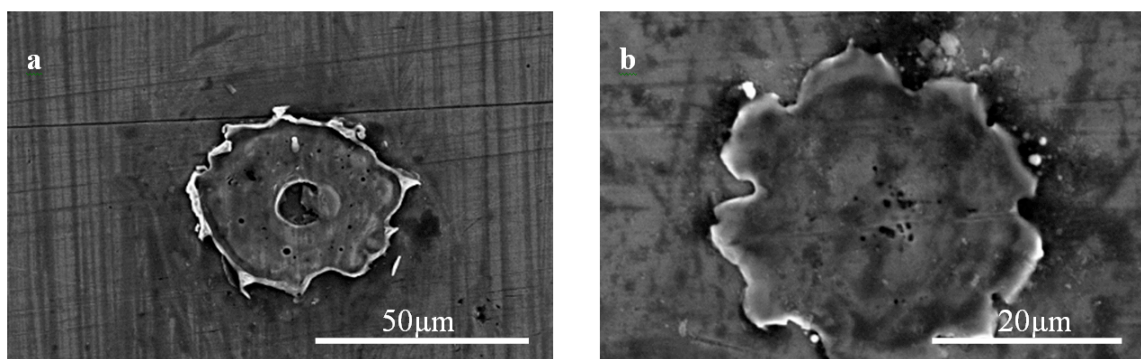


*Figure 1. SEM images of typical disc-shaped splats: (a) splat with a distinct rim, (b) flower-shaped splat*

### III.1. Identification of the various phases

Using energy dispersive spectroscopy (EDS) elemental mapping, a number of phases are readily apparent in TEM cross-sections. An example is displayed in Fig. 2. The steel substrate and the NiCr splat can easily be identified from the Fe and Ni maps, respectively. In addition, the presence of some oxide phases can also be seen, for example, the presence of chromium oxide, nickel oxide and iron oxide, can be deduced from these maps, by examination of the Cr, Ni, Fe and O elemental maps.

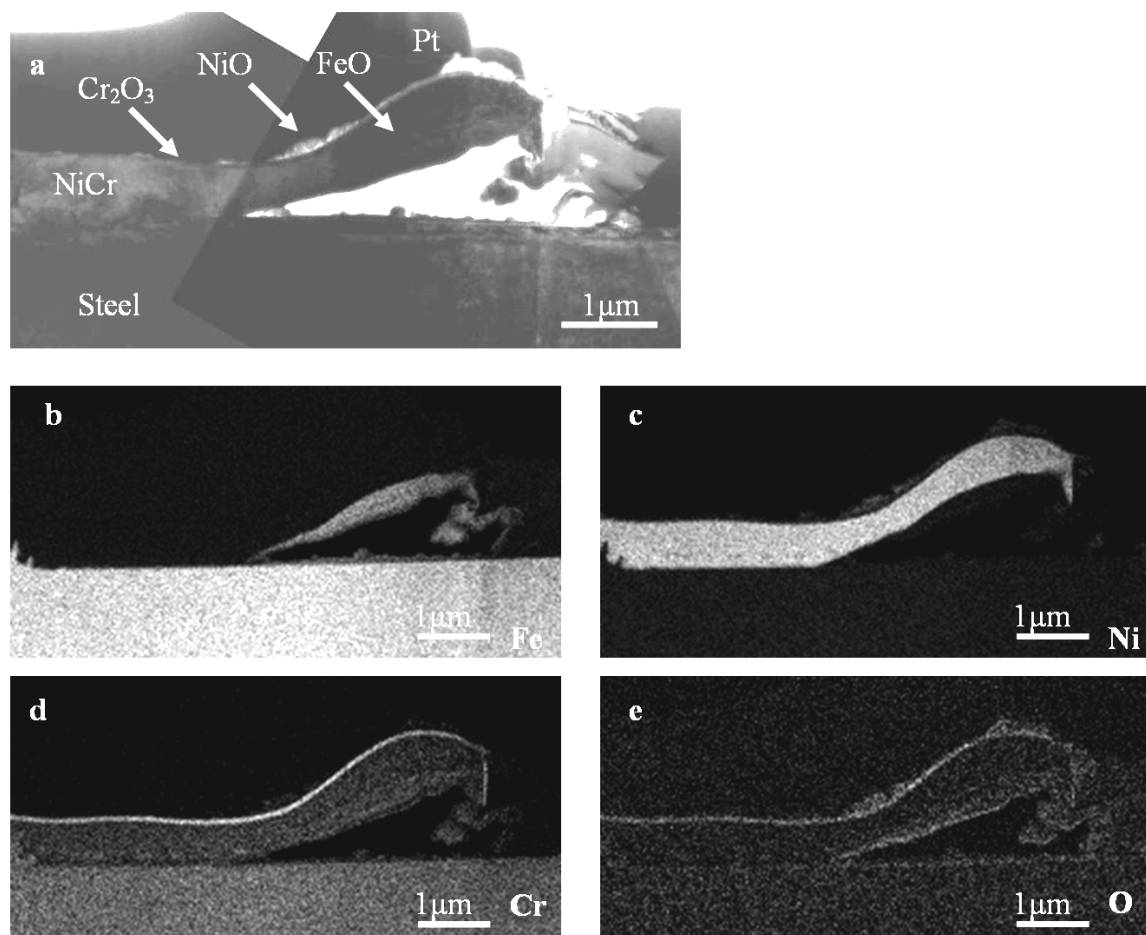
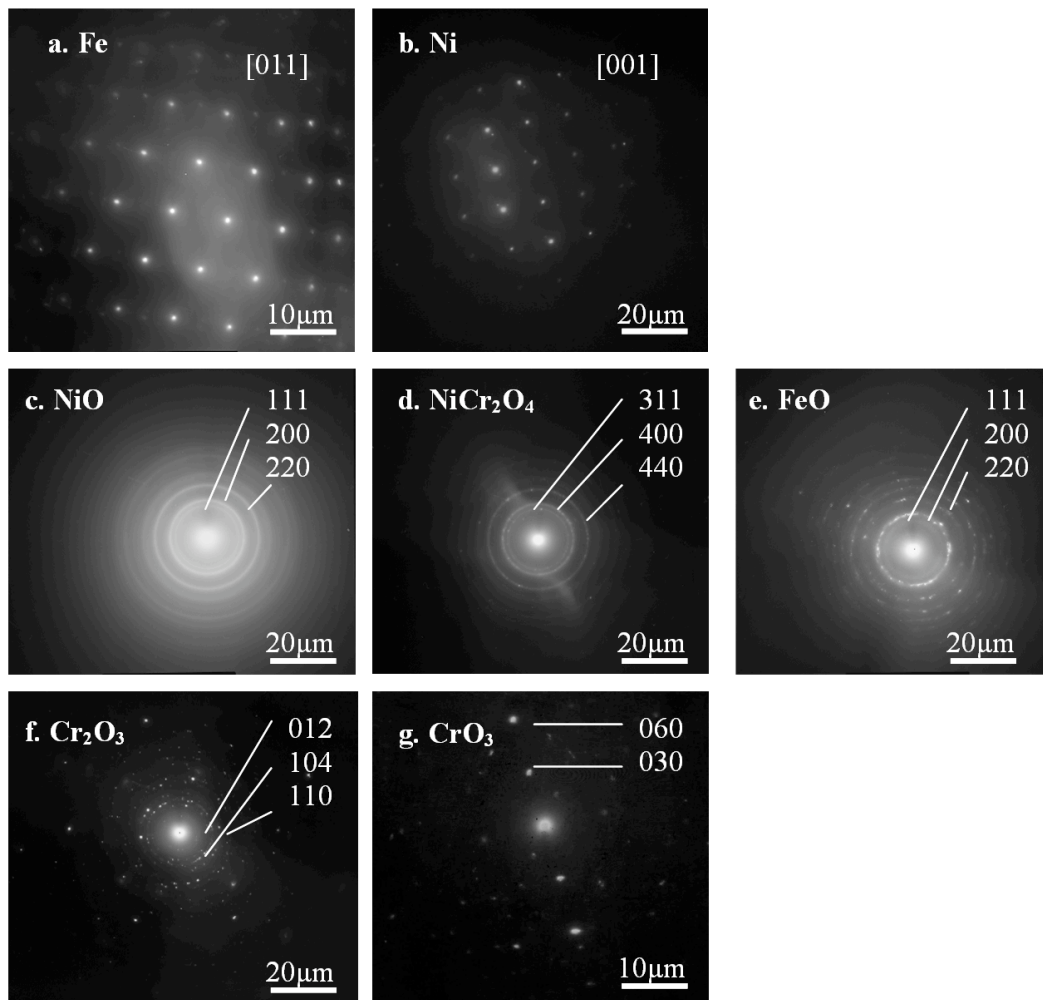


Figure 2. TEM cross-section of splat which has delaminated from the substrate: (a) bright field image, EDS elemental maps for (b) Fe, (c) Ni, (d) Cr, (e) O

However, this method alone has several limitations. First, characteristic peaks of different elements may overlap (for instance in this case, the K peak of oxygen overlaps with the L peak of chromium). Furthermore, the sensitivity of detection of light elements, such as carbon or oxygen is very limited [68]. Finally, such analysis only allows identification of elements, rather than compounds. For example, this type of analysis cannot readily differentiate between different forms of iron oxide, such as  $\text{Fe}_2\text{O}_3$  from  $\text{FeO}$ . Thus, electron diffraction was performed on all the various phases to permit the identification of each phase (typical patterns are presented Fig. 3).



*Figure 3. Examples of typical electron diffraction patterns of the various phases found: (a) Austenite, (b) Nickel, (c) NiO, (d) NiCr<sub>2</sub>O<sub>3</sub>, (e) FeO, (f) Cr<sub>2</sub>O<sub>3</sub>, (g) CrO<sub>3</sub>*

### III.1.a. *Identification of the metallic phases*

Austenitic stainless steel, which can be identified via the Fe map, has a face-centred cubic (f.c.c.) crystal structure with a lattice parameter of 0.352 nm. Figure 3a displays the pattern for austenite with a [011] zone axis. NiCr, identified through the Ni map, also has a f.c.c crystal structure with a lattice parameter of about 0.355 nm (the Ni lattice parameter is 0.352 nm, but the Cr in solid solution in the Ni matrix causes the slight expansion of the lattice, thus the lattice parameter is slightly larger [69]). Figure 3b presents the pattern for Ni with a [001] zone axis. The diffraction patterns of the two phases are then expected to be very similar, given the similarity of their crystal structures and lattice parameters, but depend on the orientation of each phase. It should also be noted that because both NiCr and stainless steel contain a significant concentration of chromium, the Cr elemental map cannot readily differentiate the location of each phase.

### III.1.b. *Identification of the oxides phases*

#### - *Nickel oxide*

Nickel oxide NiO may be difficult to observe using EDS mapping. Indeed it can be seen on the bright field image (Fig 4) that it appears highly electron transparent and porous and so emits a relatively weak X-ray signal, especially compared to the NiCr splate (for Ni mapping) or Cr oxide (for the O mapping) signals. However, it was found that nickel oxide exhibits a very recognizable structure (fine, nano-crystalline

grains) on bright field images and is generally found in pores present in the centre of the splat or at the splat-substrate interface, or at the periphery of the splat.

Diffraction studies confirms that this oxide is NiO, that is a face centred cubic phase (space group  $Fm\bar{3}m$ ) with a lattice parameter of 0.417 nm: the pattern for this phase (Fig. 3c) shows rings, as the grain structure is very fine ( $\sim 1$  nm or less) (Fig. 4); identification of the most intense rings can be found on the figure and to be consistent with the  $\{111\}$ ,  $\{200\}$  and  $\{220\}$  planes for NiO. In a few specimens, this fine, porous nano-crystalline phase was identified not as NiO, but a spinel,  $NiCr_2O_4$ . These phases can be discriminated through EDS elemental maps as the spinel also contains chromium, as can be observed Fig. 5. Its spinel structure (cubic  $Fd\bar{3}m$  with a lattice parameter of 0.832 nm) yields a diffraction pattern not dissimilar to NiO, but, from structure factor calculations the intensity of the 1<sup>st</sup> ring,  $\{311\}$  is expected to be more intense than the 2<sup>nd</sup> ring,  $\{400\}$ , while the ring intensity is the inverse for NiO (that is the  $\{200\}$  is brighter than  $\{111\}$ ). A comparison of the rings of the patterns in Figs. 3c and 3d illustrates this relative difference in intensity.

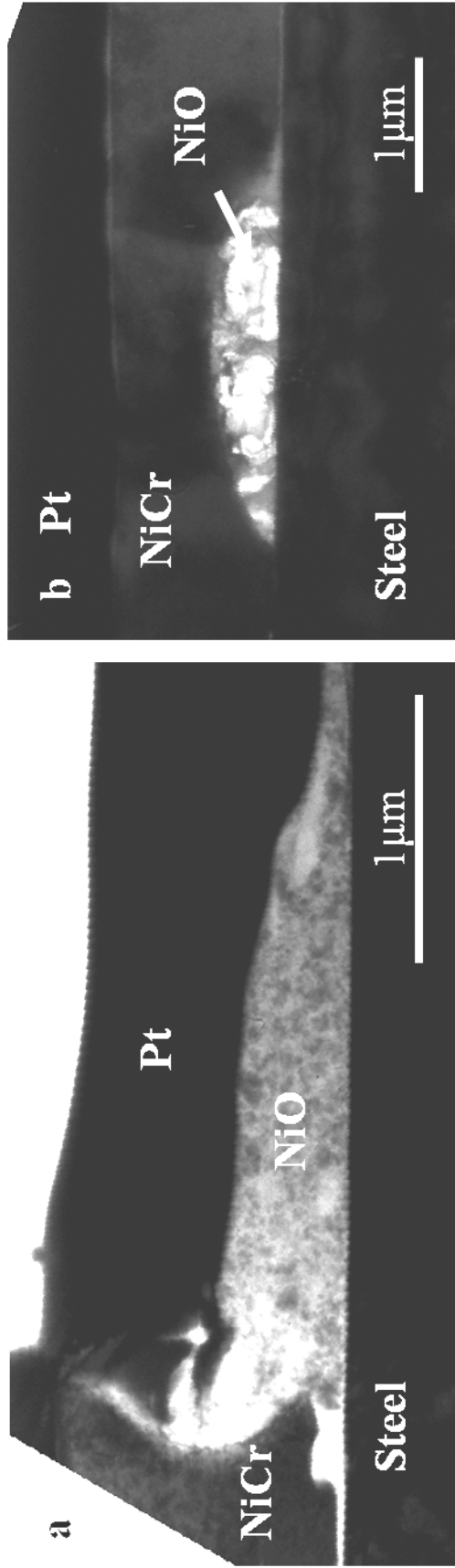


*Figure 4. TEM bright field images showing the presence of NiO: (a) at the periphery of a splat, (b) in a pore at the splat-substrate interface*

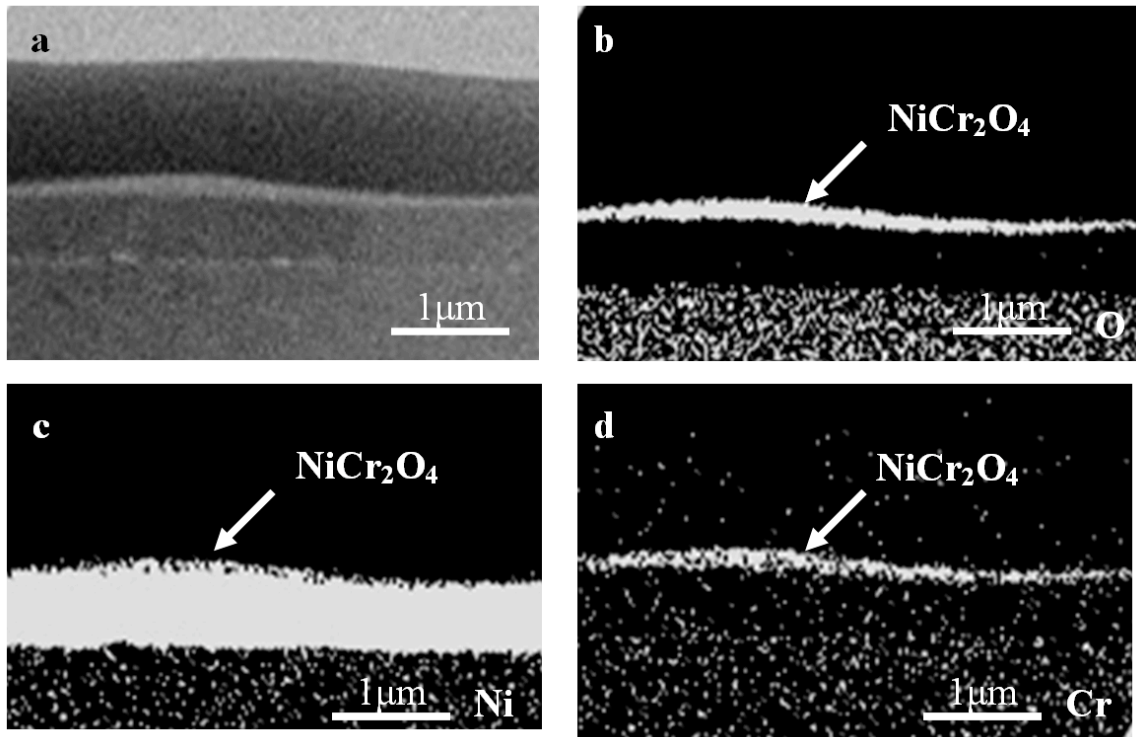


Figure 5. (a) STEM image showing a layer of  $\text{NiCr}_2\text{O}_4$  on top of the NiCr splat; EDS elemental maps for (b) O, (c) Ni, (d) Cr

The presence of NiO is important regarding the understanding of the formation of porosity at the centre of the splat and at the splat-substrate interface. Indeed, when the NiCr particle impacts on the steel substrate, it is believed that the heating of the substrate causes it to release gases, for example those arising from chemisorbed water. The nature and amount of released gases will depend on the chemical state of the substrate surface [49, 67]. Such a phenomenon could be responsible for the formation of pores in the centre of the splat and at the splat-substrate interface, where the presence of hot oxidizing and water-rich gas would promote also very likely the formation of oxides such as NiO.

- *Chromium oxide*

By studying the O and Cr elemental maps (Figs. 2d and 2e), a thin layer of chromium oxide can be observed on the outer surface of the splat. To identify the nature of this oxide (i.e. Cr<sub>2</sub>O<sub>3</sub> or CrO<sub>3</sub>), electron diffraction was used. The very limited thickness (i.e. ~ 10 nm) of the layer and the size of the grains (a few nm) inhibits, in some specimens, unambiguous identification of these oxides, but where identification was possible, both Cr<sub>2</sub>O<sub>3</sub> and CrO<sub>3</sub> were observed on different splats. However, there were no instances where these oxides were found to co-exist. Examples of patterns for these phases are displayed in Figs. 3f and 3g. Because of the small size of the grains, they display an indistinct arrangement of reflections which may form a poorly defined ring pattern, see Fig. 3f. Moreover, due to the small size of the Cr oxide layers, compared to the area analysed as defined by the selected area diffraction aperture, some information in the diffraction pattern may arise from nearby phases, such as the NiCr splat. Cr<sub>2</sub>O<sub>3</sub> has a rhombohedral crystalline structure (with a space group  $R\bar{3}c$ , with lattice parameters of  $a = 0.496$  nm and  $c = 1.359$  nm); the rings with the strongest intensities in this pattern were found to be consistent with the {012} and {104} and {110} planes of Cr<sub>2</sub>O<sub>3</sub>. CrO<sub>3</sub> has an orthorhombic structure (lattice parameters are  $a = 0.574$  nm,  $b = 0.856$  nm and  $c = 0.479$  nm); the most intense reflections in Fig. 3g were consistent with the (030) and (060) planes.

Cr<sub>2</sub>O<sub>3</sub>, CrO<sub>3</sub>, and also NiCr<sub>2</sub>O<sub>3</sub> form on outer surface of the splat. Their formation has been widely observed and described before in NiCr alloys [56, 70], as well as in plasma sprayed coatings [66]: Cr<sub>2</sub>O<sub>3</sub> is observed in most cases and is present as a thin

protective layer on the surface of NiCr alloys. In addition, spinel was occasionally observed at the outer surface of the splat.  $\text{CrO}_3$  is much less commonly observed. This may be because observations of  $\text{CrO}_3$  formation have been made following solid state oxidation reactions, rather than following plasma sprayed particles. Oxidation under plasma spray conditions also occurs under higher temperature and lower oxygen concentration (at least when oxidation takes place in the potential core of the plasma flow where the amount of oxygen, resulting mostly from the entrapment of the surrounding atmosphere, is still limited due to the high plasma flow viscosity). Moreover, Fukumoto *et al.* found both  $\text{Cr}_2\text{O}_3$  and  $\text{CrO}_3$  when studying in-flight oxidation of plasma sprayed NiCr particles [6]. In our case, any Cr oxide formed in-flight is likely apparent as fine particles in the vicinity of the splat-substrate interface. Indeed, as demonstrated by Syed *et al.* [71] on stainless steel particles, oxidation driven by convective motion within the molten particles due to Hill-type vortex is predominant in front of oxidation driven exclusively by diffusion at the molten particle surface. In this latter case, an oxide shell forms around the molten particles whereas in the first case, globular oxides are observed within the molten particles (since oxidation occurs by diffusion at the periphery of the particles, convective motion fragments then the oxide shell and fragments are entrained by the fluid motion within the molten particle).

- *Iron oxide*

For some splats, including the one presented Fig. 2, some iron oxide can be found under the rim of the splat. For example, on the Fe map, the phase containing Fe can be seen in addition to the presence of iron in the substrate. Diffraction studies allow the

identification of this oxide as FeO. Like NiO, this phase crystallizes in a cubic system (space group  $Fm\bar{3}m$ ) with a lattice parameter of 0.429 nm; this means that the patterns would be expected to be very similar to those from NiO. The diffraction pattern from this phase, displayed in Fig. 3e, again consists of rings due to the very fine grain structure. This FeO phase was only located under the rim of the splat, where delamination has occurred: this may be explained by the presence of hot oxidizing gases and the lift-up of the rim of the splat, due to the curling up; some Fe may become attached to the bottom surface of the splat after flattening, and become oxidized to form FeO. The formation of FeO, in competition with more oxygen-rich iron oxides, is probably due to the limited amount of oxygen present: as the oxidation occurs in some almost enclosed space (under the rim of the splat), most of oxygen available originates very likely from the gas released from the substrate and pushed at the periphery by the outward flow of the melted splat.

### III.2. Study of the splat-substrate interface

#### III.2.a. *Diffusion across the interface*

Through EDS mapping across the splat-substrate interface, the interface between nickel and iron appears in some regions to be sharp (region (1) on Fig. 6, showing a TEM cross-section across the rim of a central pore) and other regions to be indistinct (region (2) on Fig. 6).

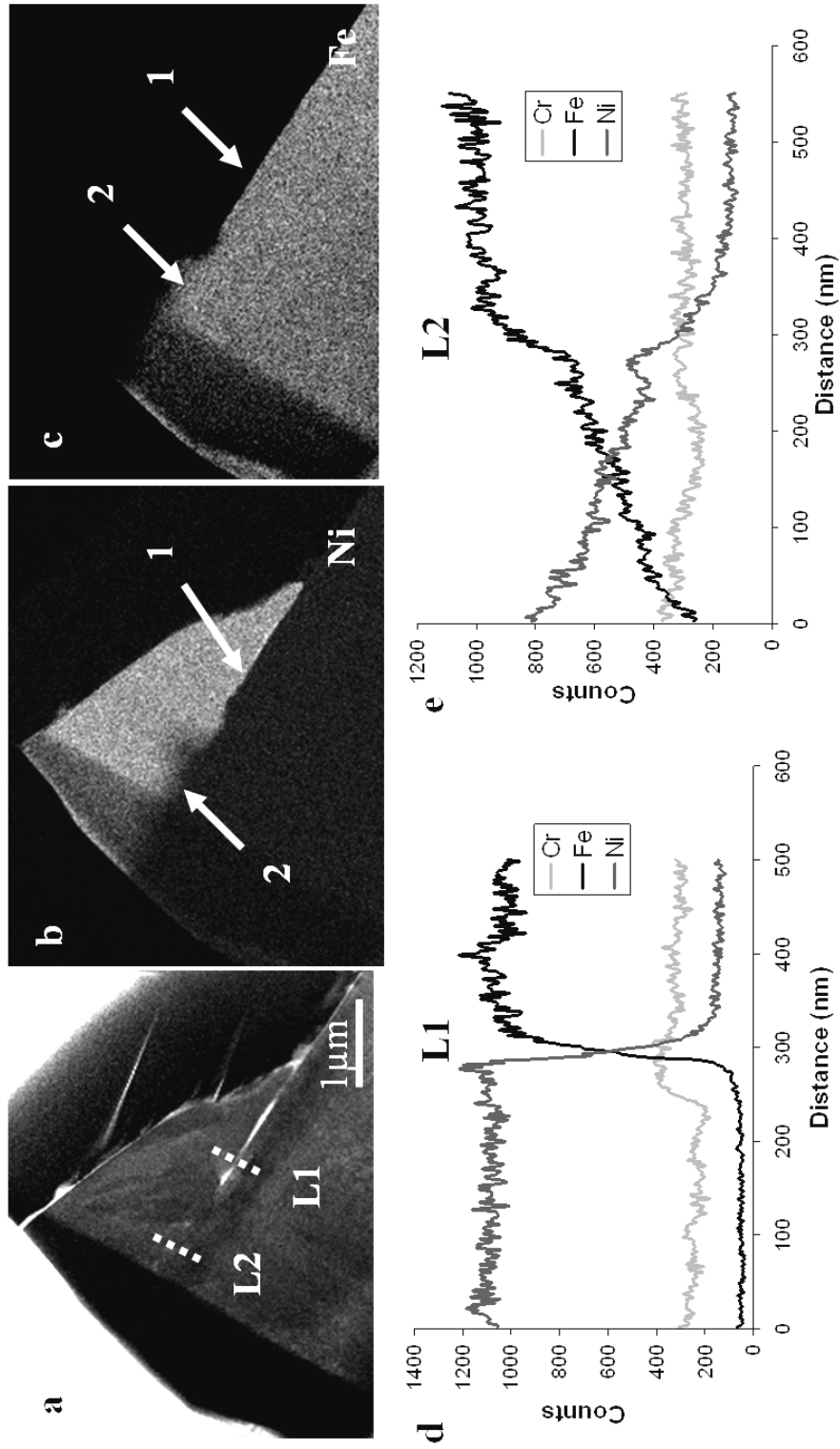


Figure 6. (a) STEM image showing part of a splat with zones where the interface is either locally clear or indistinct, EDS elemental maps for (b) Ni, (c) Fe, and elemental line scans across the interface where it is (d) clear (see zone marked 1), (e) indistinct (see 2)

Elemental linescans L1 and L2 were performed across these regions. For a sharp interface (Fig. 6d) the Ni and Fe concentrations vary abruptly. That is, there is a clear step function at the interface over a distance of a few nanometres. The finite width of this step probably associated with the diameter of the beam used (a few nm). Conversely, across the indistinct interface (Fig. 6e), the variation in elemental concentration is gradual. This indicates that diffusion of Ni and Fe has occurred across the interface over a distance of about 200 nm. One reason for such two distinctive interfaces could rely in variation in thermal resistance along the splat / substrate interface [2].

### III.2.b. *Substrate melting and splashing*

EDS mapping also revealed that in many of the TEM specimens observed, the interface is present as an irregular boundary, for example in Figs. 7 and 8. Such irregularities are evidence of localized substrate melting. That is, the steel substrate melts due to the heat released from the molten NiCr particle upon solidification and with the spreading of the molten splat, and local jetting of the melted substrate occurs within the splat.

The elemental maps presented in Fig. 7 show that jetting of the substrate into the splat has occurred, but the interface is clear and visible in both STEM image and elemental maps. This clearly indicates that no discernable diffusion has occurred. The solidification at this interface was probably very rapid, giving high angle boundaries

across the interface, as found by the observation of the orientation of each phase through Kikuchi maps.

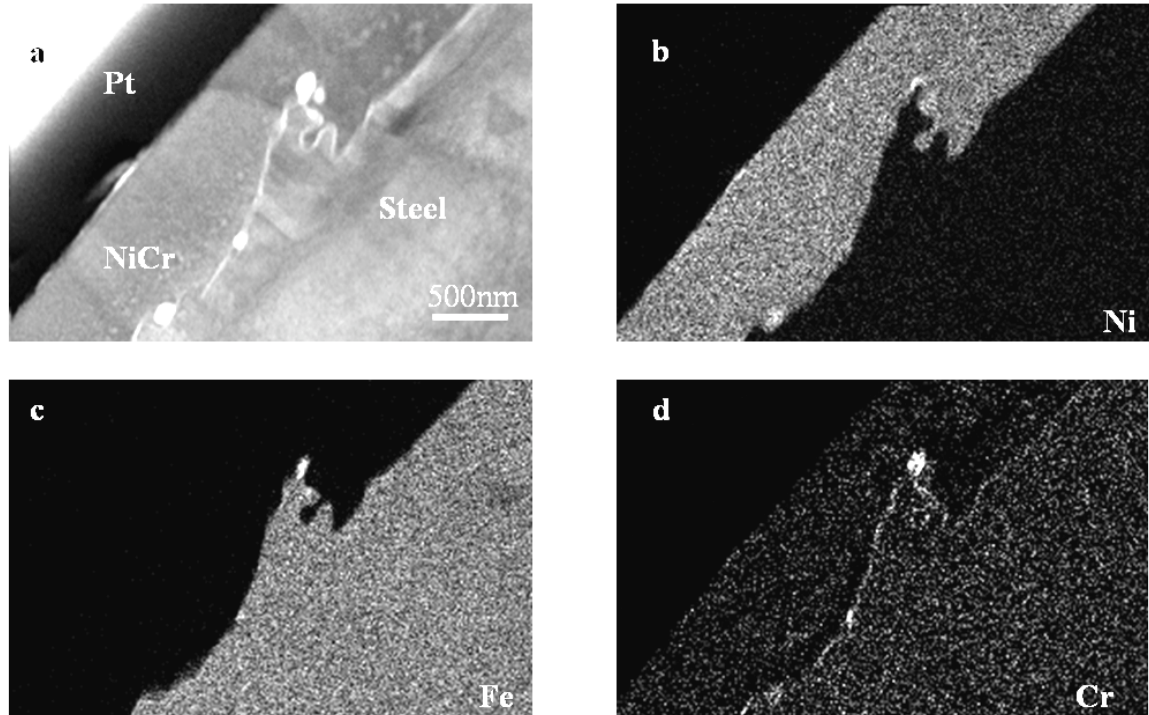


*Figure 7. (a) STEM image and EDS elemental maps for (b) Ni, (c) Fe, (d) Cr of a TEM cross-section where jetting of the substrate into the splat can be observed around a clear splat-substrate interface*

Solidification of the NiCr/steel interface into an irregular shape occurred too quickly for significant diffusion to occur, even if the steel substrate had melted.

In the case of the image shown in Fig. 8, the interface between the Ni and Fe phase is indistinct, an indication that diffusion across the interface has occurred in addition to substrate melting and splashing.

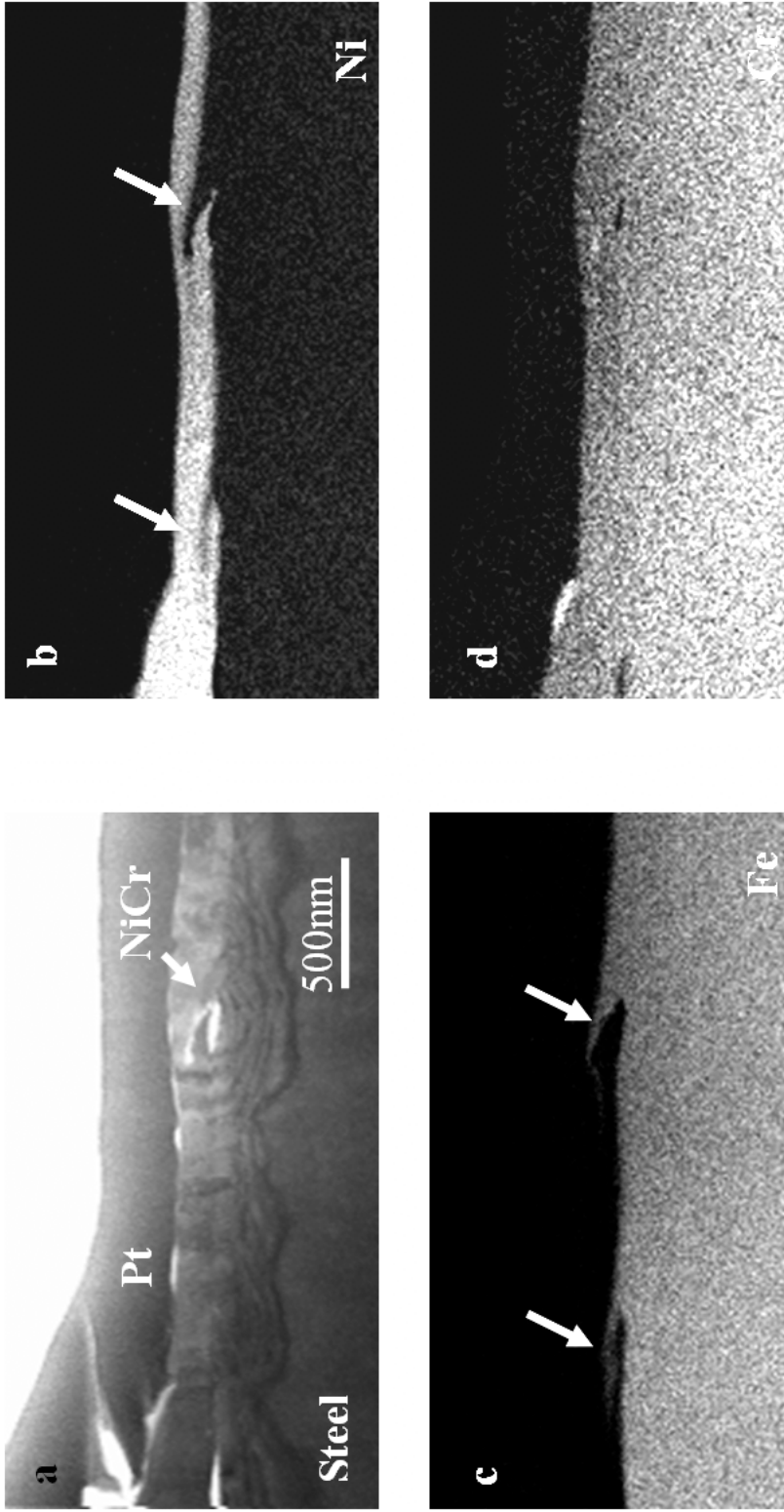


Figure 8. (a) STEM image and EDS elemental maps for (b) Ni, (c) Fe, (d) Cr of a TEM cross-section where jetting of the substrate into the splat can be observed for a more indistinct splat-substrate interface

In all cases, the direction of the jetting is the same as the direction of flow of the molten NiCr splat during impact.

### III.2.c. *Crystallographic relationship between splat and substrate*

Observations from both electron diffraction and EDS showed that the interface between the NiCr splat and steel substrate exhibited a range of possible microstructures.

On the bright field image shown in Fig. 9a, in the region marked (1), the interface is distinct and well-defined, showing no obvious interaction between the splat and substrate. Beside, in the region (2), the interface becomes sharp, and distinct grains can be observed to exist across the splat-substrate interface (3). In such cases, the EDS mapping suggests an indistinct interface at region 1, but a sharper interface at region 2 (Fig. 9b-c).

Another example of growth of grains across the interface is shown Fig. 10a: again grains having grown across the interface can be seen clearly (1), which on the EDS mapping (Fig. 10b-c) corresponds to the region where the splat-substrate interface becomes irregular and indistinct.

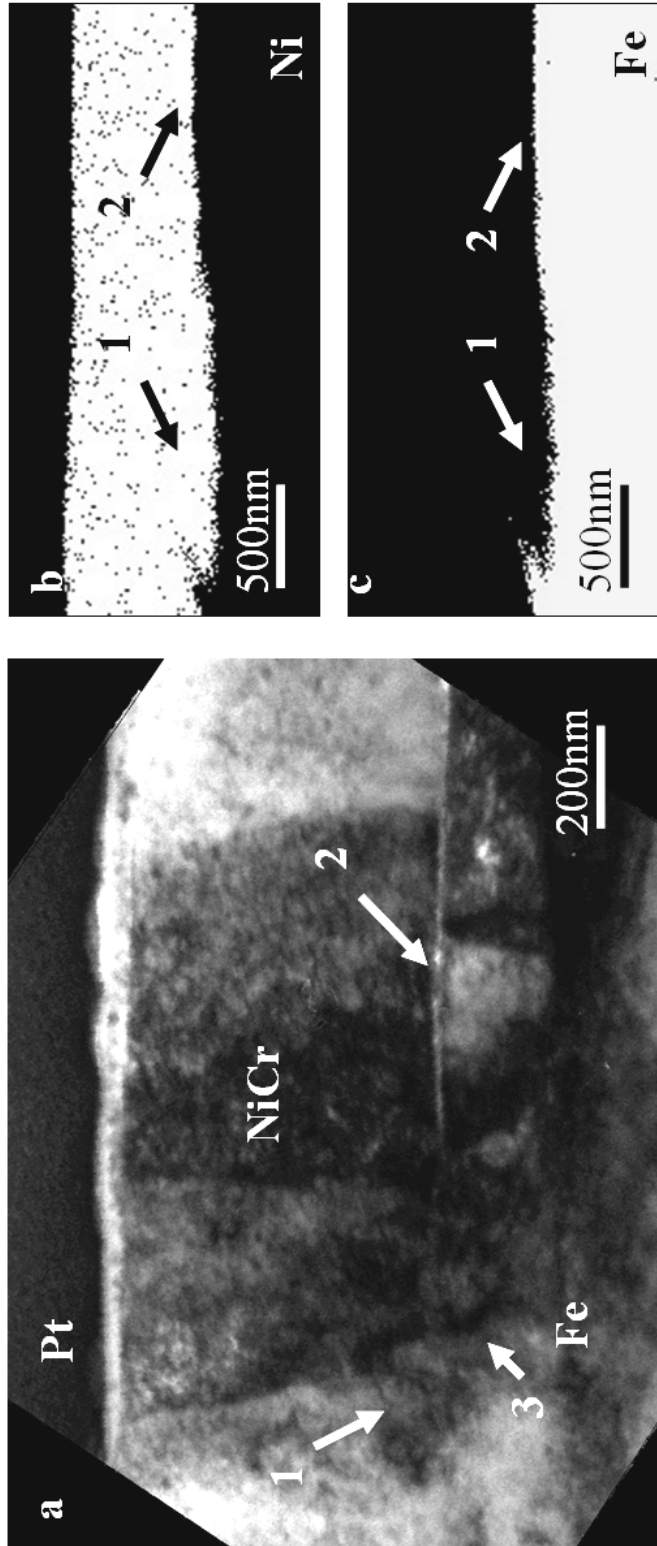


Figure 9. (a) TEM bright field image, EDS elemental maps for (b) Ni and (c) Fe, of a clear (1) and indistinct (2) interface and grain connections (3) between sputter and substrate

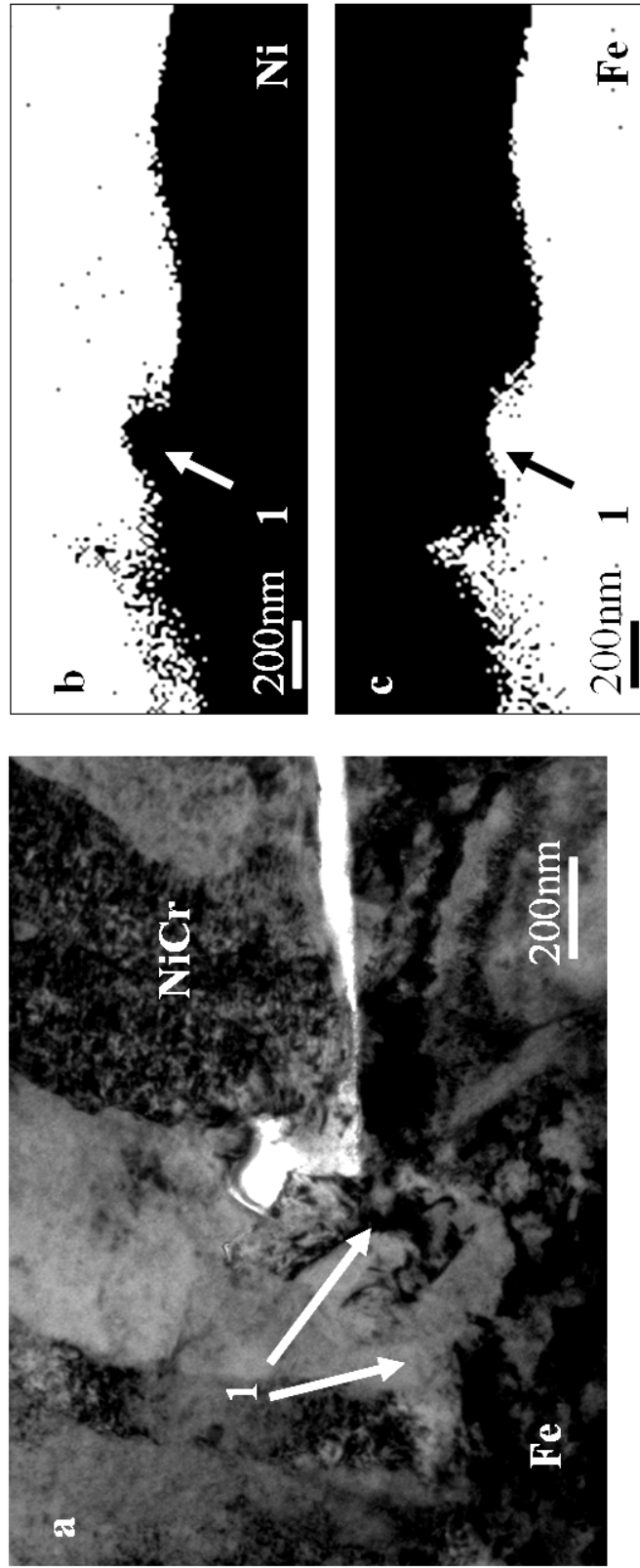


Figure 10. (a) TEM bright field image of a cross-section where grains extend across the splat-substrate interface (1) and EDS elemental maps of the corresponding region for (b) Ni, (c) Fe

As aforementioned, nickel and austenitic stainless steel are both face centred cubic with similar lattice parameters. This is consistent not only with the possibility of enhanced interdiffusion, but may lead to grains of the NiCr splat nucleating and growing with the same crystallographic orientation as the substrate (hetero-epitaxial growth). Electron diffraction was used to assess the crystallographic relationship between grains either side of the interface.

In many instances, observations from Kikuchi maps, when moving the electron beam across the interface, for example along the line L1 across the interface shown in Fig. 11, show no abrupt change in diffraction pattern, confirming that the crystallographic orientation either side of the splat-substrate interface is the same even though the phases are chemically distinct. Grain boundaries may also be coincident across the splat-substrate interface, as seen on Fig. 11 for the zones marked (1) (see also grains pictured on the associated schematic representation).

The observation of a similar crystallographic orientation across the interface may also occur in zones where the interface is straight and distinct, which is the case for the cross-section presented Fig. 11. This suggests that the nickel grain which has nucleated and grown on a steel grain has assumed the orientation of the steel grain, without any significant melting or interdiffusion occurring.

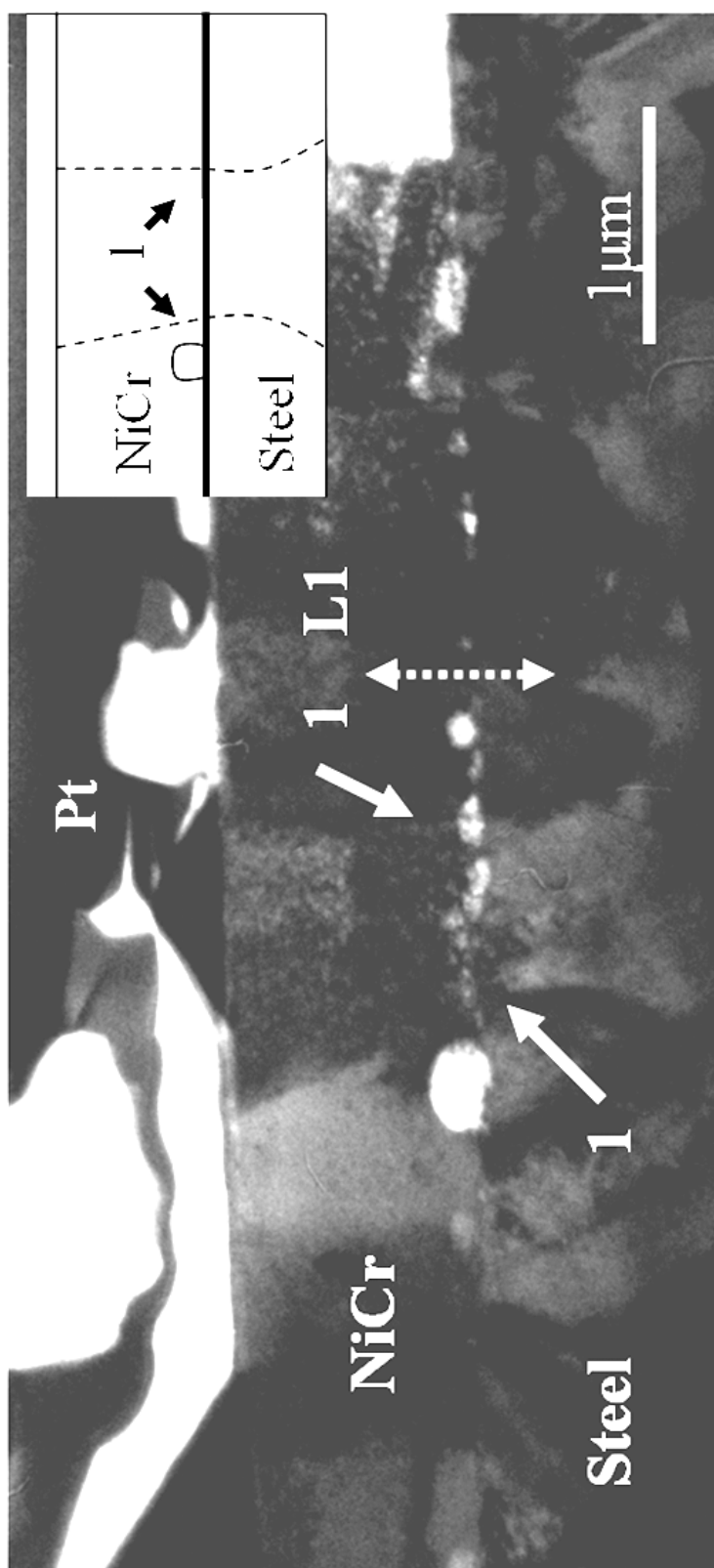
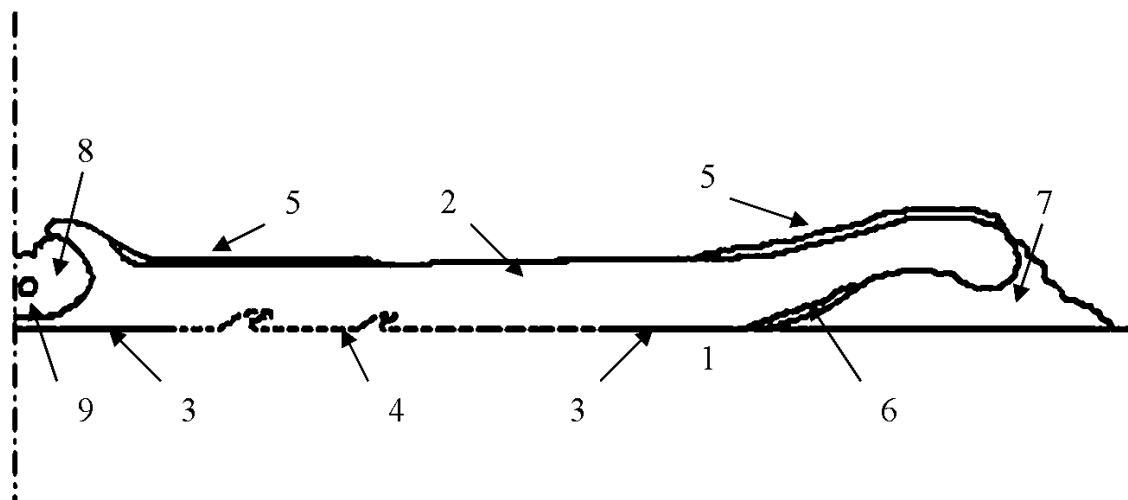


Figure 11. TEM bright field image showing a distinct splat-substrate interface across which some grain boundaries are coincident, the Kikuchi maps showing no change in the crystal orientation when moving the electron beam along the segment L1. The insert schematic representation shows the location of some coinciding grain boundaries

### III.3. Summary of the features observed

From the data described previously, it was possible to derive a schematic representation of a typical splat encompassing the features described through microstructural evaluation (Fig 12): the interface between the steel substrate (1) and the NiCr splat (2) is clear (no interdiffusion, then no substrate melting) toward the centre and the periphery of the splat (3). However, in the region in between, due to the substrate melting, the interface is indistinct and jetting can be found (4). Chromium oxide can be found on the outer surface of the splat (5), iron oxide at the periphery where the splat has curled up (6), nickel oxide at the periphery (7) as well and in the central pore (8). The latter feature, probably originating from the gas release upon impact and spreading of the NiCr particle, may also contain some NiCr particles (9).



*Figure 12. Schematic representation of a typical disc-shaped splat*

Clearly TEM, through FIB preparation of specimens, allows the observations of interfacial features that have not been observed previously. Some previous studies

have suggested the presence of an intermetallic layer between Mo splats and a mild steel substrate [20]. However, the results presented here clearly show that even with the occurrence of substrate melting and splat-substrate inter-diffusion and mixing, no intermetallic phase is present. This may be explained, in this study, by the close crystallographic structure between splat and substrate materials. This is also in agreement with the observations made by Kithara *et al.*, who could not identify an intermetallic layer when spraying Ni and Cr onto mild steel, compared to other material combinations [35]. However, they concluded that substrate melting must then have been either non-existent or limited, while here it has been unambiguously shown to occur. This paper shows that substrate melting and metallurgical bonding may exist without the presence of an intermetallic layer.

The identification at such a detailed scale of the various oxide phases formed along with the splat was never performed previously in thermal spray studies: indeed oxides have a significant influence on the properties of the coatings (mechanical, electrical and thermal properties, among others) and the knowledge of their nature, location and quantity may be critical to the behaviour of a sprayed component.

The observations made in the present paper provide then important information about the splat formation process and the development of the splat microstructure. Further discussion on the effect of surface roughness and chemistry on splat microstructure is discussed in the associate paper [8].

#### **IV. Conclusion**

Examination of the splat microstructure for NiCr splats plasma sprayed onto stainless steel substrates was performed at a nano-scale level using TEM techniques, such as bright field imaging, EDS elemental mapping and electron diffraction. This allowed the observation of particular features of the splat structure, such as the occurrence of substrate melting along with splat-substrate, inter-diffusion and inter-mixing and the identification of various phases, including both metallic phases (NiCr and steel) and oxides (NiO, FeO, NiCr<sub>2</sub>O<sub>4</sub>, Cr<sub>2</sub>O<sub>3</sub> and CrO<sub>3</sub>), along with identification of their typical locations. Importantly, it was found that metallurgical bonding between splat and substrate existed, but without the presence of an intermetallic phase. These results were then used in a larger study investigating the effects of surface chemistry on splat formation [67].

**CHAPTER 4**

**STUDY OF THE SPLAT FORMATION FOR PLASMA SPRAYED  
NiCr ON ALUMINUM SUBSTRATE AS A FUNCTION OF  
SUBSTRATE CONDITION**

---

*S. Brossard, P.R. Munroe, A.T.T Tran, M.M. Hyland, Surface and Coating  
Technology, 2010, 204 (16), p. 2647-2656*

**Abstract**

The study of splat formation, splat-substrate interactions and the influence of the substrate surface conditions on splat behaviour is a key step in understanding and improving the plasma spray process. In the present work, NiCr particles were plasma sprayed onto aluminium substrates to form single splats, and their microstructure, along with the splat-substrate interface, was studied using a range of microscopy techniques (SEM, FIB, TEM and AFM). From the observations made, a model summarizing the splat formation process has been proposed. Substrates with various surface conditions, induced by heating and/or boiling treatment prior to spraying, were used. It was observed that on the non-boiled specimens, the contact between splat and substrate was poor, possibly due to the desorption of adsorbates/condensates present on the substrate surface, and no splats were formed on the boiled specimens, due to the presence of a thick hydroxide layer.

## I. Introduction

Plasma spraying is a thermal spray process in which molten particles are propelled through a flow of plasma in order to be sprayed onto a substrate to form a coating resulting from the stacking of individual flattened particles, usually called lamellae or splats. Such coatings improve surface engineering performance and/or increase component life, while conserving most of the substrate's original characteristics (such as chemistry, structure and bulk properties). Thus, thermal spray processes, and particularly plasma spraying, are widely used in many industries (such as aerospace, gas turbines, petrochemical and automotive industry, etc.). One advantage of the plasma spray process is its flexibility and versatility, as it can be used to spray many different materials (metallic alloys, ceramic oxides and carbides, cermets, polymers etc) on to a wide range of substrates (metallic alloys, ceramics, polymers), over a large range of particle size distribution (from 5 to 50  $\mu\text{m}$  for ceramics, 20 to 120  $\mu\text{m}$  for metallic alloys), temperatures and velocities (temperatures in the plasma jet core may range from about 4000°C to 14,000°C, and the particles velocities from 80 to 300  $\text{m}\cdot\text{s}^{-1}$ ). Compared to other thermal spray processes, such as cold spray or High Velocity Oxy-Fuel spraying, most particles penetrating the plasma jet core are fully melted and impact the substrate at a relatively low velocity (impact velocities can be as high as 800  $\text{m}\cdot\text{s}^{-1}$  when considering High Velocity Oxy-Fuel spraying). Moreover, spraying is often performed in air thus particles may undergo in-flight oxidation. Other issues may include impact and flattening splashing and oxidation during splat formation and the presence of voids, cracks and delamination in the sprayed coatings

(total void content can evolve from less than 1% to about 30%, depending upon operating parameters, feedstock characteristics, etc.) [1, 4].

Furthermore, for effective performance of the coating, good adhesion between the substrate and the splats is required. Bonding between a splat and the substrate may be mechanical (the heat and kinetic energy from the impinging particle promoting deformation of both particle and substrate, and thus bonding occurs by mechanical interlocking; this may be especially common for rough surfaces) or metallurgical (localized melting of the substrate occurs, and the molten substrate may mix with the molten sprayed material, possibly forming intermetallic phases) [4].

However, very few studies of the direct interaction between splat and substrate and their interface at a microscopic level have been performed. Indeed, while the splat morphology (on which the materials involved, the substrate surface topology and spray conditions used have a strong influence [19, 20]) and the structure of coatings (through the superposition of layers of splats) have been widely studied, cross-sections have mostly been examined only on a macroscopic level ( $\sim$  micron scale). This is because the preparation and observation of cross-sections at a higher spatial resolution is relatively difficult and requires specific instrumentation [6, 7]. The mechanisms of splat formation have also been studied using modelling [13, 17, 18], by using *in-situ* experiments, mainly with millimetre-sized droplets [11-15], by observing the variations in splat morphology depending on the spray conditions [11, 19-25], or also by studying the solidification dynamics leading to the formation of notable microstructures within the splat [66, 72]. Nevertheless, the study of the

microstructure of the splats at a high-resolution level is an important step in understanding the mechanisms of coating formation.

In the present work, nickel-chromium particles were plasma sprayed on to an aluminium substrate. Ni-Cr is a commonly sprayed material, especially for bond coats or wear resistant coatings [1]. In a prior study, Kitahara et al., when spraying nickel (amongst other materials) onto polished aluminium and mild steel substrates, observed that, for Al, an intermetallic phase (identified by X-ray diffraction as  $\text{Al}_3\text{Ni}$ ) was present at the splat-substrate interface: intimate contact between coating and substrate and localized substrate melting had occurred [35]. Finally, the only other studies, to the authors' knowledge, of such plasma sprayed splats, and their interface with substrate, at a nano-scale level, that have been published were by the present authors, studying the splat microstructure and splat-substrate interactions for plasma sprayed Ni-Cr splats onto stainless steel substrates [50, 67].

Changes in the surface chemistry of the substrate have been shown to have a significant influence on splat formation: several studies have concluded that adsorbates/condensates present on the surface of the substrate may be desorbed due to heat released from the particle during the flattening stage, and this promotes splashing [6, 19, 32], while others have observed how splat formation may also be influenced by both the substrate surface roughness [73] and the thermal contact resistance between splat and substrate [27].

In this study, the surface chemistry of the aluminium substrates was varied by subjecting the substrates to various pre-treatments (heat treatment and/or boiling

treatments). Indeed, it has been shown that heating an alloy, such as 5052 Al, in air increases the thickness of the already present passivation layer of Al oxide ( $\gamma\text{-Al}_2\text{O}_3$ ) with, sometimes, the formation of an outer layer of MgO [74]. On the other hand, boiling aluminium in distilled water leads to the formation of an hydroxide layer, mainly boehmite ( $\text{AlOOH}$ ) [75]. The treatments applied are expected to influence splat formation, by varying the substrate surface chemistry characteristics. For example, both Tran *et al.* [55] and Trompetter *et al.* [76] have observed that the presence of a thick hydroxide layer, obtained by boiling the Al substrate, resulted in the non-adhesion of plasma sprayed and HVAF, respectively, sprayed NiCr particles.

Consequently, in this study single splats of NiCr were plasma sprayed onto aluminium substrate having undergone various pre-treatments and were studied using a range of microscopy techniques, focusing on their morphology, their microstructure, and the characteristics of the splat-substrate interface. The observed structures were interpreted in terms of both the spray method and substrate state.

## II. Experimental procedure

Four different substrate states were used; all prepared from a 5052 aluminium alloy. Their characteristics are listed in Table 1.

**Table 1. Substrate Nomenclature and Treatment Condition**

<b>Specimen</b>	<b>Substrate</b>	<b>Pre-treatment</b>
Al_P	Aluminium 5052	Polished (to a nano-scale smoothness)
Al_PT	Aluminium 5052	Polished and thermally treated
Al_B	Aluminium 5052	Boiled
Al_BT	Aluminium 5052	Boiled and thermally treated

All substrates were firstly mechanically ground and mirror polished with diamond paste until a mirror-like surface state was reached, corresponding to a nano-scale roughness. The boiled substrates were placed into boiling distilled water for 30 min, while the thermally treated substrates were heated at 350°C for 90 minutes in air at atmospheric pressure. The aim of these treatments is to form surface oxides for thermally treated substrates or hydroxides for the boiled specimens, and/or to induce surface roughness. Unsprayed substrates, having undergone the same pre-treatments, were studied to determine the effect of the treatment on the substrate surface state prior to spray processing.

The sprayed material was a commercial NiCr alloy powder (Ni80-Cr20, Sulzer Metco 43 VF-NS, Wholen, Switzerland, (-45 +5)  $\mu\text{m}$ ). Plasma spraying was carried out with a Sulzer Metco (Switzerland) 7MB gun (with an 8-mm anode nozzle diameter), operating at a current of 550 A and at a voltage of 74 V, with a spraying distance of 80 mm. The feeding rate of the powder was of 1 g/min while the plasma gas was a mixture of nitrogen and hydrogen, at a flow rate of 47.6 SLPM and 5.4 SLPM, respectively. Spraying was performed at room temperature.

The specimens were then characterized using several analytical techniques. A Hitachi S3400 scanning electron microscope (SEM) was used to image the overall morphology of the splats and the substrates. A FEI xP200 Focused Ion Beam microscope (FIB) was used to mill cross-sections of the splats using an energetic gallium ion beam, and to image them using secondary electrons induced by the ion beam. Details have been described in [51]. A FEI xT Nova Nanolab 200 dual beam microscope (that is a FIB and SEM combined into a single instrument) was used to prepare cross-sections of splats (100-200nm in thickness) suitable for TEM observation. These were prepared using the lift-out method as described in [51] and examined in a Philips CM200 transmission electron microscope (TEM) to which energy dispersive x-ray spectroscopy (EDS) facilities have been interfaced. Finally, the average surface roughness of the substrates was measured using a Digital Instruments DI3000 Atomic Force Microscope (AFM).

Several FIB and TEM cross-sections were prepared and studied for each particular feature and/or type of splat. However, for reasons of brevity only a small number of representative images will be presented here. The cross-section preparation process using FIB also involves the deposition of a layer of platinum on top of it prior to milling for protection purposes. This layer is visible on the FIB and TEM images presented.

### III. Results and discussion

#### III.1. Observation of the surface changes induced by the pre-treatment

##### III.1.a. *Effects of the heat treatment on the surface chemistry*

Aluminium naturally forms layers of protective oxide on its surface when in contact with air. Under normal atmospheric conditions, the film is composed of two layers. The inner oxide is a compact amorphous barrier determined solely by the temperature of the environment (it will be the same in either a dry or moist environment). Covering this inner layer is a thicker, more permeable outer layer of hydrated oxide [77, 78]. The total thickness at room temperature is typically 2-4nm, which means such layers may not be readily resolved by TEM using EDS elemental maps. When heating in air at atmospheric pressure an aluminium substrate at temperatures below 500°C the thickness of the oxide barrier increases linearly with temperature; heat treating at 350°C leads to an increase in the oxide thickness up to ~7 nm [78]. Furthermore, the outer layer of the oxide film is said to be hydrated, thus being susceptible to release chemisorbed water upon heating by the impact/flattening of a sprayed particle or by a heat treatment.

The surface chemistry of the different substrates prior spraying was investigated by x-ray photoelectron spectroscopy (XPS), as described in a previous study [49]. It was found that for Al\_P the surface consisted in a mixture of oxide (corundum  $\alpha$ -Al<sub>2</sub>O<sub>3</sub>), oxy-hydroxide and chemisorbed water; a similar surface chemistry was observed for the Al\_PT substrate, but with a lower concentration in oxy-hydroxide and chemisorbed water, as the heat treatment partially dehydrates the oxide layers.

SEM, FIB and TEM study of the polished substrate (AL\_P) did not reveal the presence of any particular layer on the substrate surface. The oxide layer may, indeed, be too thin to be readily resolved. Moreover, plan view imaging of the substrate surface showed that it was featureless with no particles present.

However, for the thermally treated Al\_PT specimen, the effects of oxidation can be readily observed as localized spots on the substrate surface. These localized regions are surrounded by a darker ring as it can be seen in the secondary electron SEM image shown in Fig. 1a (marked 1 on the image).

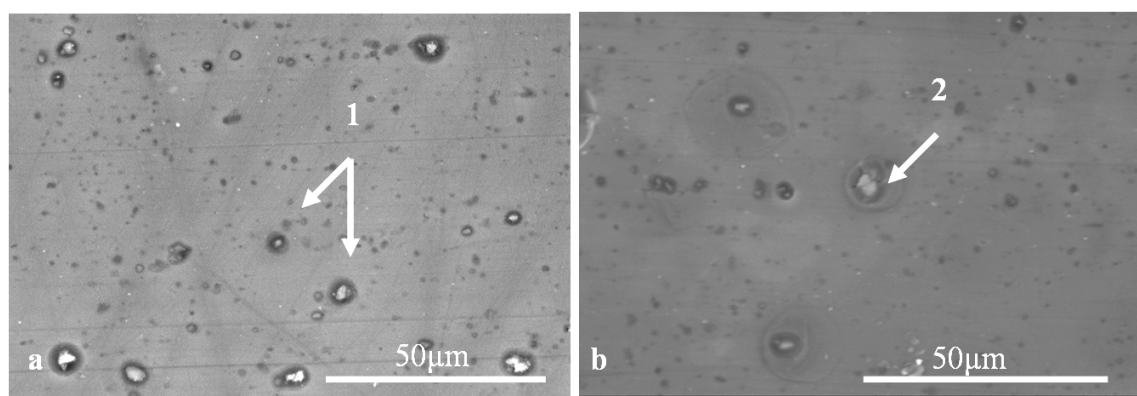


*Figure 1. Secondary electron image of the surface of (a) Al\_PT and (b) Al\_BT substrates prior to spraying*

The TEM cross-section prepared across such a particle, depicted in Fig. 2, shows that these regions are associated with the presence of iron-rich intermetallic particles (marked 1), which are commonly found in commercial Al alloys. The cross-sectional TEM images shows that these intermetallic particles are surrounded by aluminium oxide films (marked 2 in Fig. 2).

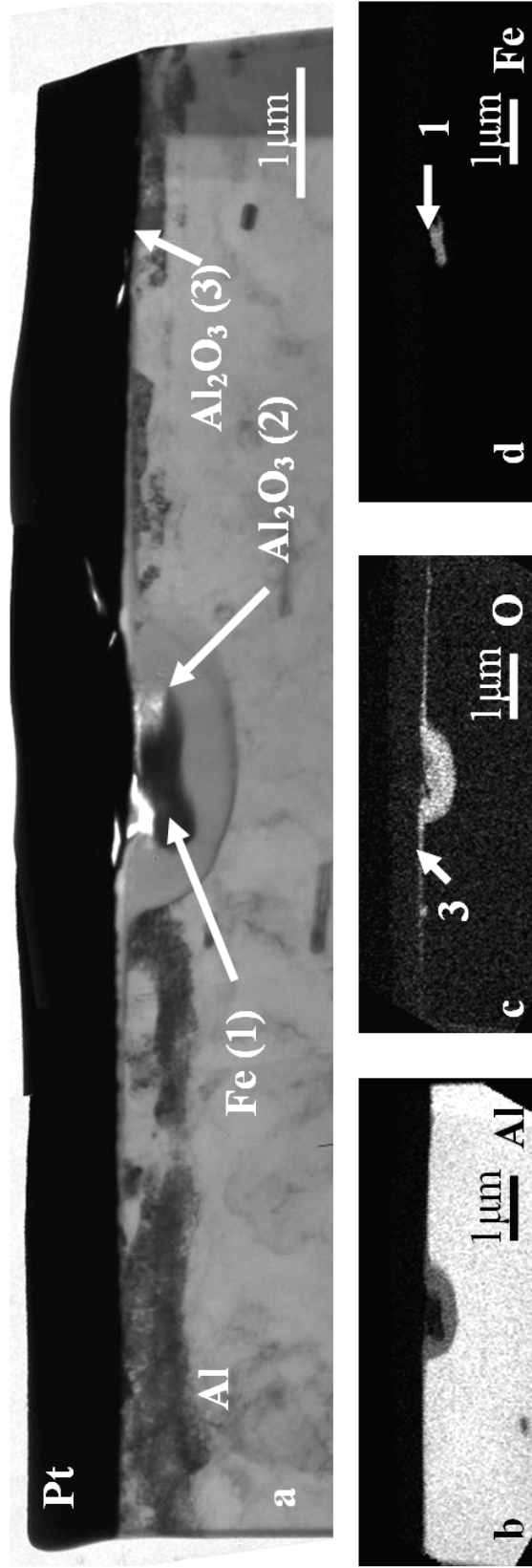
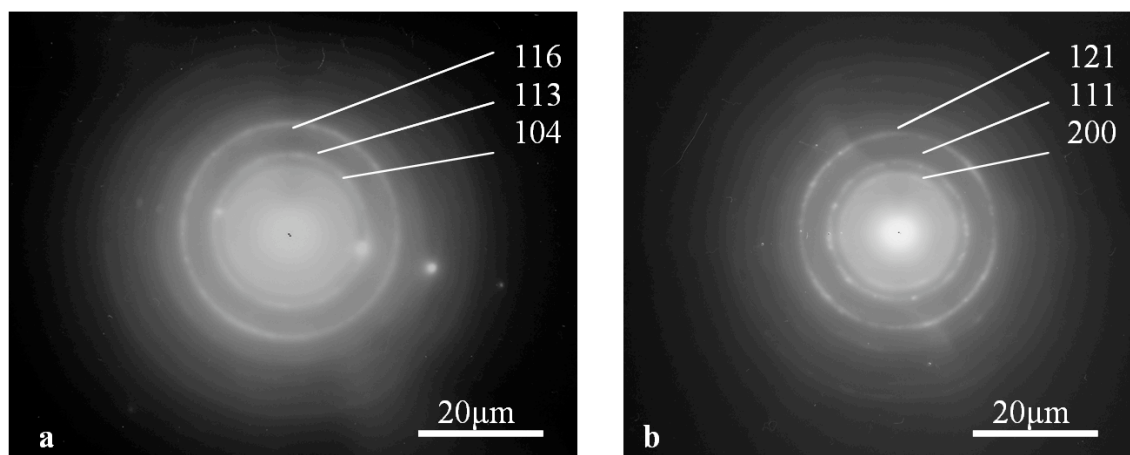


Figure 2. TEM cross-section prepared across a Fe intermetallic particle on Al<sub>2</sub>O<sub>3</sub> prior to spraying: (a) bright field image, EDS elemental maps for (b) Al, (c) O and (d) Fe.

The electron diffraction pattern from this region, as shown in Fig. 3a, was consistent with this phase being corundum  $\alpha$ - $\text{Al}_2\text{O}_3$ .



*Figure 3. Typical electron diffraction patterns from (a)  $\text{Al}_2\text{O}_3$  and (b)  $\text{AlOOH}$*

Away from these particles, a very thin layer of oxide (a few nanometres thick, the EDS mapping does not allow measurements of such a thickness with precision) formed on the surface of the substrate (marked 3 in Fig. 2). Electron diffraction could not be performed on this oxygen-rich layer to unambiguously identify this phase because of the thinness, but it is most probably  $\alpha$ - $\text{Al}_2\text{O}_3$ , as it is the oxide that was identified by XPS and that is expected to form [77, 78].

It should be noted that Mg is an alloy addition in the substrate material and may itself undergo oxidation: a layer of MgO might also form on the substrate surface [74]. However, this reaction normally occurs at temperatures greater than  $300^\circ\text{C}$ , and thus following heat treatment at  $350^\circ\text{C}$ , the presence of any such layer may be minimal and its presence was not resolved by elemental EDS mapping. However, the presence

of this oxide can be observed in other sections, for instance the Mg EDS elemental map in Fig. 4, a TEM cross-section prepared on the boiled and thermally treated specimen prior to spraying, shows a very thin layer of Mg at the surface of the Al substrate (marked 4 in Fig. 4). Oxidation of the substrate leading to the formation of an MgO layer may also occur from the heat provided by the spray process.

### III.1.b. *Effects of the boiling treatment on the surface chemistry*

Both boiled and boiled and thermally treated specimens present a similar surface morphology, such as shown in Fig. 1b. The same Fe-rich intermetallic particles as those observed for Al\_PT were present (marked 2 in Fig. 1b).

It is known that aluminium reacts with water. At temperatures less than 100°C bayerite,  $\alpha$ -Al(OH)<sub>3</sub>, is expected to form. At 100°C boehmite ( $\gamma$ -AlOOH) is the most probable hydroxide to form [75]. Examination of the boiled specimens prior to spraying by XPS in a previous study showed the presence of thick layers (>200 nm) of boehmite. For Al\_BT, XPS results suggested that the hydroxide layer may have been partially dehydrated by the heat-treatment [49], most probably on its outer surface and may form several transition aluminas ( $\gamma$ -Al<sub>2</sub>O<sub>3</sub>,  $\delta$ -Al<sub>2</sub>O<sub>3</sub>,  $\kappa$ -Al<sub>2</sub>O<sub>3</sub>) [75]. It can also be expected that such a partial dehydration may occur during plasma spraying.

A TEM cross-section of the surface of Al\_BT is presented in Fig. 4: a thick layer (marked 1) is found on the substrate (marked 2). This layer, whose thickness is usually around 200-300nm, is shown from the elemental mapping to be rich in Al and

O (3). The corresponding electron diffraction pattern is presented in Fig. 3b. Considering the poor accuracy in the measurement of radii of the diffraction rings, this pattern may be identified as being consistent with either alumina ( $\text{Al}_2\text{O}_3$ ) (see for comparison diffraction pattern shown in Fig 3a taken from the alumina phase in Fig. 2a) or boehmite  $\gamma\text{-AlOOH}$ . However, as explained above,  $\gamma\text{-AlOOH}$  is the expected phase following this boiling treatment as it results from the reaction of aluminium and water. Moreover, even if boehmite does transform into alumina, a complete transition would normally occur at a very high temperature ( $\sim 1200^\circ\text{C}$ ) [75], which is unlikely to occur even at  $350^\circ\text{C}$  or during the spraying process (which does not induce any melting of the substrate, the melting point of Al being at  $649^\circ\text{C}$ ). Thus, the phase observed on sprayed and unsprayed, boiled and thermally treated specimens is most likely to be hydroxide  $\gamma\text{-AlOOH}$ .

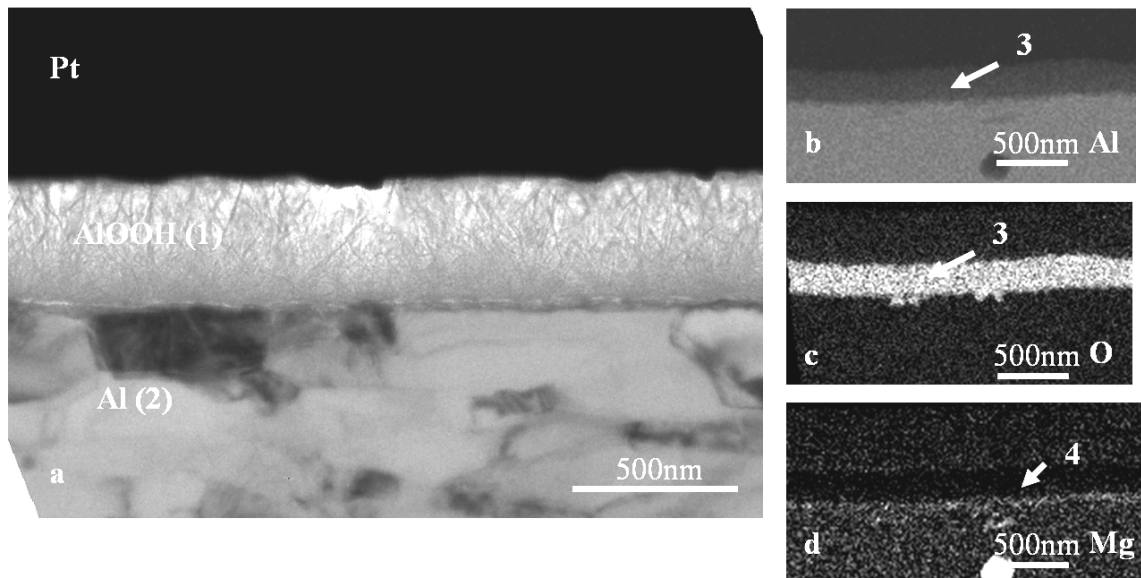


*Figure 4. TEM cross-section across the substrate Al\_BT prior to spraying: (a) bright field image, EDS elemental maps for (b) Al, (c) O and (d) Mg*

The Mg elemental EDS map also shows the presence of a thin layer rich in Mg, a few nm in width near the outer surface of the substrate (marked 4). As described previously, this is possibly MgO, formed from the oxidation of the Al alloy substrate.

### III.1.c. *Changes induced by the pre-treatments on the roughness*

The roughness,  $R_a$ , was measured three times for each specimen on a  $5 \times 5 \mu\text{m}^2$  randomly located square region by AFM; the average of those three measurements was calculated. This provided an indicative value of surface roughness of the specimen. Results are presented in Table 2. It can be seen from these results that both heat and boiling treatments increase the roughness of the substrate by, respectively, an average value of  $\sim 14\%$  and  $\sim 159\%$ . However, it overall remains on a nano-scale level.

**Table 2. Average roughness measured for the different specimens using AFM**

Specimen	Al_P	Al_PT	Al_B	Al_BT
Roughness (nm)	[ $7.3 \pm 2.3$ ]	[ $8.3 \pm 2.2$ ]	[ $18.9 \pm 3.8$ ]	[ $22.1 \pm 10.7$ ]

### III.2. Description of the splats found on the polished and polished and thermally treated specimens (Al\_P and Al\_PT)

Using SEM, images of about 50 randomly chosen splats were recorded for both substrates. Splats were identified as being in one of three categories for each substrate. Typical splat morphologies are depicted in Fig. 5 for each considered category, and they can be described as follows:

- Relatively irregularly shaped splats (Fig. 5a), with some splashed fingers up to 100  $\mu\text{m}$  in length. These were called “irregular splats”.
- Thin and fragmented splats (Fig. 5b), with a hollow splat centre. These were called “fragmented splats”.
- Very fragmented splats made of very irregular fragments (Fig. 5c). These were called “very fragmented splats”.

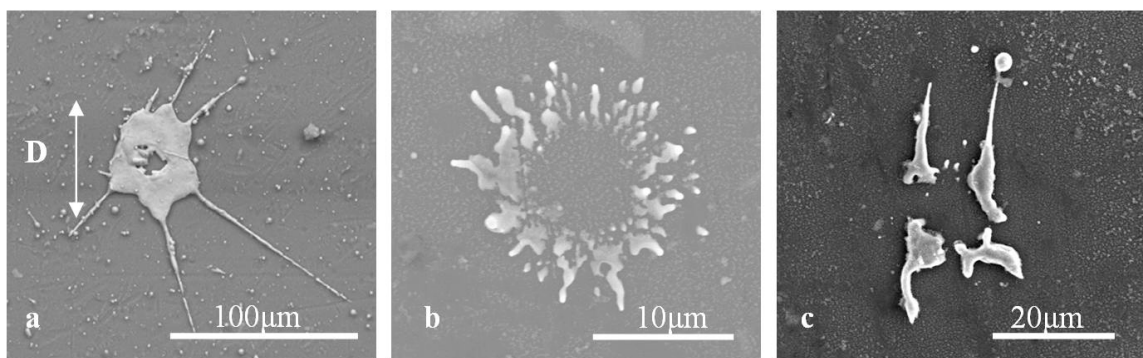


*Figure 5. SEM images of the different types of splats found on Al\_P and Al\_PT: (a) irregular splats, (b) thin fragmented splat, (c) very fragmented splat*

Diameters of the splats were evaluated, as well as the frequency of each category amongst the splat population of the specimen. Evaluation of the splat diameter was performed by considering the smallest and largest diameter value measured from the splat and calculating the average value; features such as splashed fingers were ignored (see for example Fig. 5a). Splats are not perfectly circular, but not highly elongated either, thus the smallest and longest diameters are of the same order of magnitude and this approach does not induce biases in the analysis of the standard deviation. The results are summarized in Table 3.

**Table 3. Proportion and average diameter of the different types of splats observed by SEM**

Specimen		Al_P	Al_PT
Type of splat	Irregular splat	$D_m = [29.0 \pm 10.4] \mu\text{m}$ 27%	$D_m = [34.5 \pm 10.3] \mu\text{m}$ 41%
	Thin, fragmented	$D_m = [26.4 \pm 13.6] \mu\text{m}$ 47%	$D_m = [16.7 \pm 4.7] \mu\text{m}$ 24%
	Very fragmented	$D_m = [22.3 \pm 7.5] \mu\text{m}$ 25%	$D_m = [19.7 \pm 6.0] \mu\text{m}$ 35%

From the values presented in Table 3, it can be noted that the splats deposited on the heat-treated specimen appears to be less fragmented, as the proportion of irregular splats is higher, and also the diameter of the fragmented splats is smaller, suggesting reduced break up of the impacting particle. The irregular splats also show a larger average diameter, suggesting that splats are flatter on the Al\_PT substrate. It is assumed that splats spread onto the surface irrespective of the substrate heat treatment and particle diameter.

Figures 6 and 7 show two FIB cross-sections of splats from the Al\_P substrate (similar cross-sections were seen for the Al\_PT substrate). Both cross-sections show poor contact (1) between the NiCr splat (2) and the Al substrate (3).

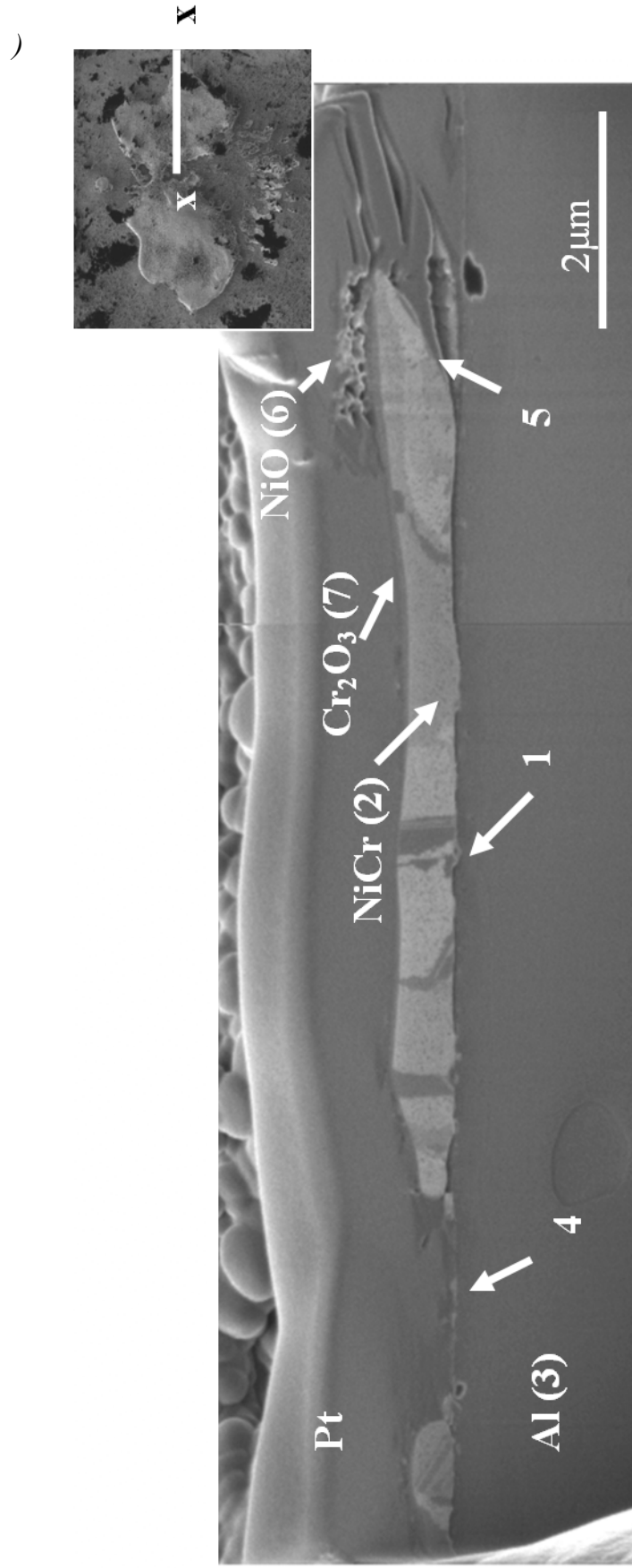
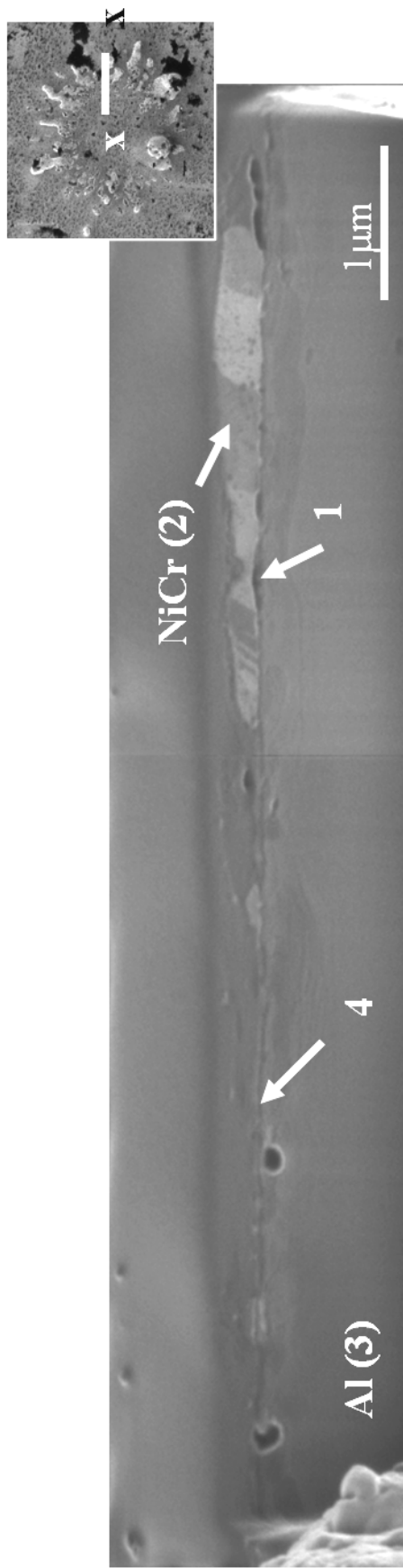


Figure 6. FIB cross-section of an irregular splat on Al<sub>P</sub> (see plan view image of splat in inset picture)



*Figure 7. FIB cross-section of a thin fragmented splat found on Al<sub>P</sub> (see plan view image of splat in inset picture)*

The cross-section shown in Fig. 6 shows the structure of an irregular splat: the grain structure (2) is quite coarse (about 1-2 $\mu$ m). It can be noted that NiCr is absent from the central void on the substrate (4) while some slight lift-up of the splat's rim has occurred at the periphery of the splat (5).

The cross-section shown in Fig. 7 was prepared across a very fragmented splat. It shows that such splats are quite thin (200-500 nm). No NiCr is detected in the centre of the splat (4), the thickness of the splat is not uniform while the grains' shape is slanted relative to the substrate surface (2). This reflects the movement of the outward flow of the molten NiCr during the splat spreading and solidification, suggesting that solidification started before the end of the spreading process.

Several types of oxides were also found around the splats (in voids, on top of the splats or at their periphery). They were identified by a combination of EDS and electron diffraction on TEM cross-sections, such as the images presented in Figs. 8 and 9. (In Fig. 8a the periphery of the NiCr splat (1) has been highlighted with a white line because of the lack of contrast between the splat periphery and the protective Pt strip):

- Nickel oxide, NiO, is often found filling voids at the splat-substrate interface (see for instance the void marked (1) in Fig. 9), in the central void, at the splat periphery and sometimes on the outer surface of the splat. This oxide has a very porous structure, as it can be seen on the FIB cross-section Fig. 6 (6) and the TEM cross-section Fig. 8 (2); spinel NiCr<sub>2</sub>O<sub>4</sub> was also observed to form on the outer surface of the splat, such as on the TEM cross-section presented in Fig. 9 (2). Both oxide species are expected to form on NiCr alloys [56, 70].

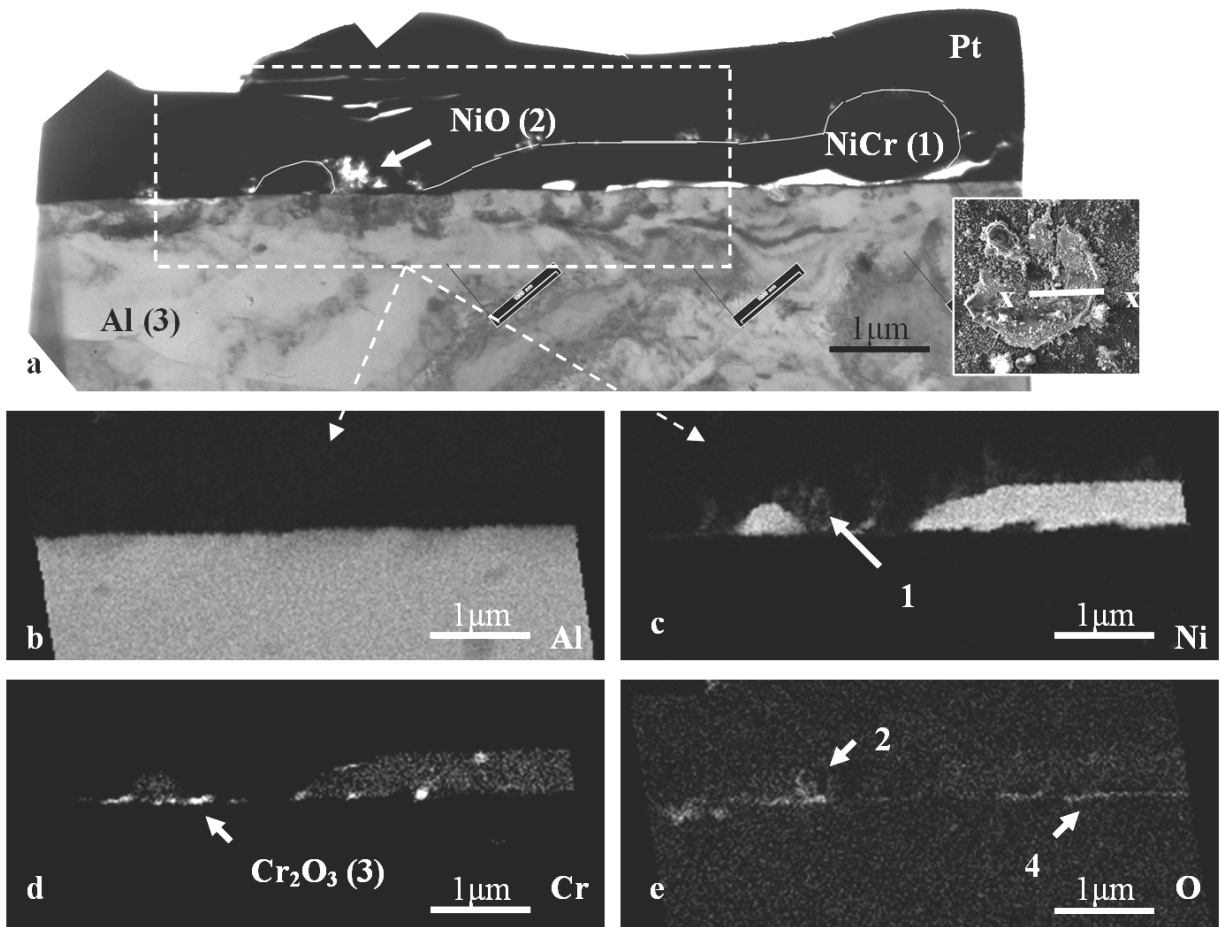


Figure 8. TEM cross-section of an irregular splat found on Al\_P (see inset image):

(a) bright field image, EDS elemental maps for (b) Al, (c) Ni, (d) Cr, (e) O

- $\text{Cr}_2\text{O}_3$ , as identified by electron diffraction, was found as a thin layer on the outer surface of the splat, in particular the more regularly-shaped splats, (for example Fig. 7 (7) and Fig. 9 (4)).  $\text{Cr}_2\text{O}_3$  was also found as small particles at the splat-surface interface, as seen on the TEM cross-section in Fig. 8 (3): in this case, it was most probably formed in-flight on the surface of the NiCr particle, and fractured upon impact of the particle on the substrate.

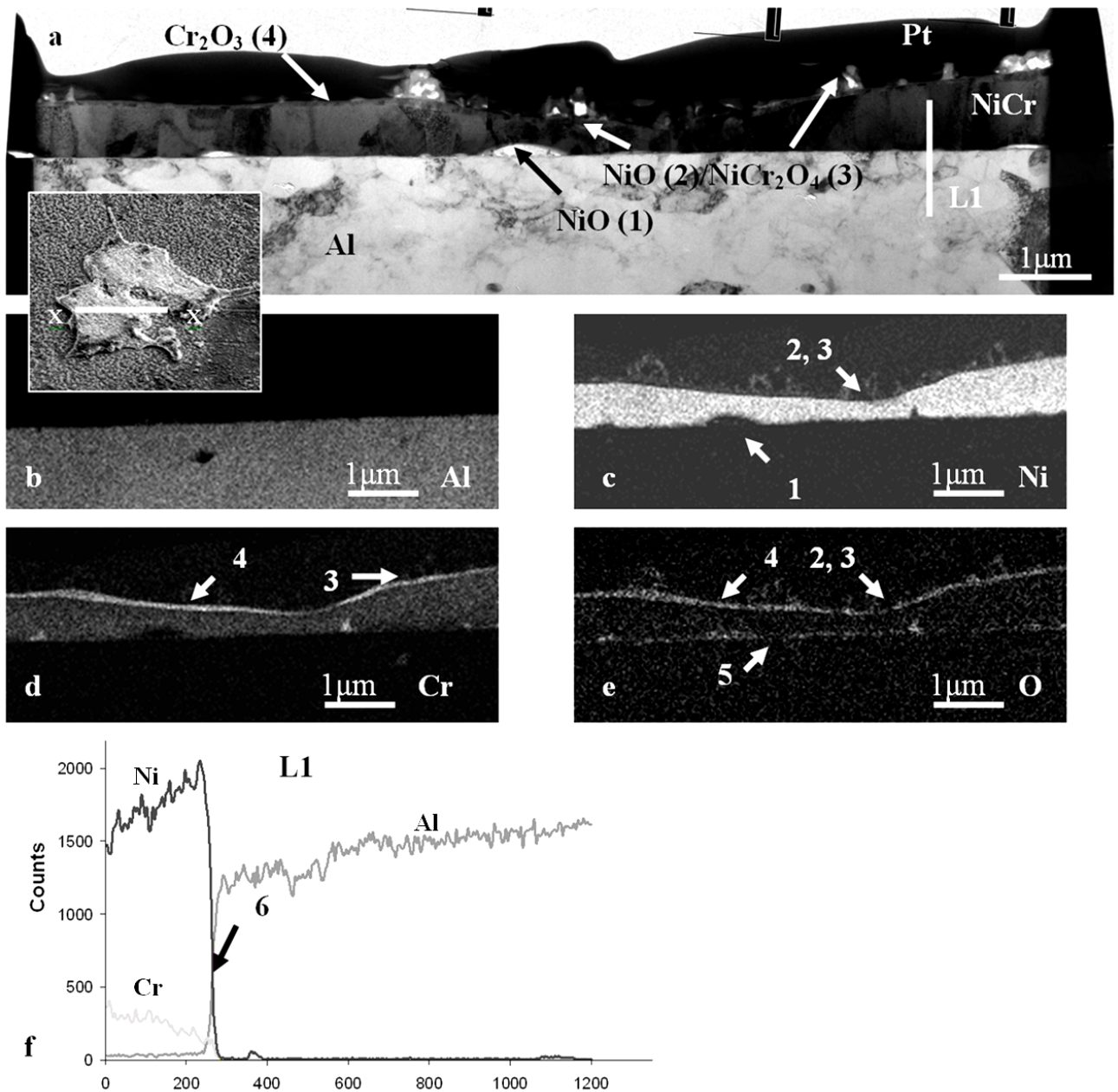


Figure 9. TEM cross-section of an irregular splat (see insert image) on an Al<sub>2</sub>O<sub>3</sub>/Pt substrate: (a) bright field image, EDS elemental maps for (b) Al, (c) Ni, (d) Cr and (e) O, (f) EDS elemental linescan performed across the interface along the line L1 on the bright field image

Unambiguous identification of CrO<sub>3</sub> and Cr<sub>2</sub>O<sub>3</sub> is sometimes difficult due to the very small size of the oxide layer or particle, as it prevents acquisition of unambiguously

clear diffraction patterns, but both phases have been often observed on NiCr alloys [56, 70]. Moreover, Fukumoto *et al.* found both Cr<sub>2</sub>O<sub>3</sub> and CrO<sub>3</sub> when studying in-flight oxidation of plasma sprayed NiCr particles [6].

- Al oxide was found, mostly on the surface of the substrate and at the splat-substrate interface (for instance it can be seen on the O map of the TEM cross-section Fig. 8e (4) and Fig. 9e (5)). This layer was too thin to allow unambiguous identification by electron diffraction, but it is expected to be corundum  $\alpha$ -Al<sub>2</sub>O<sub>3</sub>. Indeed, in the absence of water, this is the phase that forms upon oxidation of aluminium [74]. Moreover, this phase was found on both Al\_P and Al\_PT substrates.

More details on the identification of the different oxide species, notably by electron diffraction, can be found in a previous study by the same authors of NiCr splats plasma sprayed on stainless steel substrates [50]. The range and distribution of oxides described above was generally found on most of the splats examined on these substrates.

Finally, a linescan performed across the splat-substrate interface confirms that no elemental intermixing or interdiffusion between Ni and Al has occurred, as the concentration of Ni and Al varied sharply across the profile (Fig. 9f (6)).

### III.3. Formation of the splats on Al\_P and Al\_PT

#### III.3.a. *Irregular splats*

The NiCr sprayed particle impacts the surface in a fully molten state. Thus, no plastic deformation of the substrate is expected. The particle then flattens to form a splat. However, it was observed that the contact between splat and substrate was poor (as seen for instance in Figs. 6, 7 and 8a, and this was observed for most of the splats studied), no evidence of substrate melting was found and the grains cannot be typified as fine and columnar, but rather coarse and irregularly shaped. These observations suggest poor wetting of NiCr on the Al substrate. Indeed, the melting point of NiCr is significantly higher than Al (~1400°C compared to 649°C), and the NiCr particles impact the substrate in a fully melted state. Thus, if intimate contact between splat and substrate was achieved, substrate melting would have been expected. For example, Kitahara *et al.*, when spraying Ni on Al, found that substrate melting occurred, as an intermetallic layer ( $Al_3Ni$ ) was observed [35]. However, this was not observed here. Therefore, the poor contact between the splat and the substrate must induce a high contact thermal resistance. Heat of the splat is removed mainly by conduction through the interface with the substrate. Consequently, the supposedly high thermal resistance would lead to a much smaller cooling rate. Grains will then be coarser and equiaxed, as the temperature has time to homogenize across the splat (conversely, good contact between splat and substrate and thus good heat transfer through the interface leads to columnar grains). This is consistent with the observed shape of the grains of the splats (mainly coarse and not columnar).

Thus, the splat morphology and microstructure are highly influenced by the interaction of the molten NiCr particle with the substrate surface. In the case studied here, the contact is evidently inhibited by various phenomena. The main factor is the vaporization of adsorbates and condensates present on the substrate surface. Such a phenomenon has been widely investigated in the study of the splashing mechanisms: it was found that heating the substrate above a particular temperature, denoted the “transition temperature”, during spraying reduced significantly splashing of the splats, which were then more uniformly disc-shaped [6, 19, 32]. This was explained by the presence of adsorbates/condensates on the substrate surface that were released when the substrate was heated, either by the hot sprayed particle, creating a cushion of gas causing splashing of the flowing splat, or by the heating up of the substrate above the transition temperature, avoiding the splashing process. In the case studied here, splashing is relatively limited compared to the splat morphology observed in other studies and which was termed as “splasy” [6, 19, 32]. However, it is still probable that gases were indeed released from the substrate, which was sprayed at room temperature, creating a gas cushion limiting the contact and thus the heat transfer, between the molten splat and the substrate. Furthermore, the presence of voids at the splat-substrate together with the presence of oxides, such as NiO, and Al<sub>2</sub>O<sub>3</sub> at the interface (although the aluminium oxide layer was too thin to be readily detected by EDS mapping on the unsprayed specimens, it was clearly observed on the sprayed substrates, thus it has probably formed during spraying), strongly suggests the presence of hot oxidizing gases at the splat-substrate interface, notably H<sub>2</sub>O. The fact that the specimens were not degreased prior to spraying may have also added to the amount of adsorbates/condensates susceptible to vaporize. Consequently, the wetting of NiCr on the Al substrates may have been hindered by this gas release.

Most of the splats observed also displayed a large central void, in which phases such as NiO or NiCr<sub>2</sub>O<sub>4</sub> were often found. As explained before, the presence of oxides within the voids suggests that desorption of gases from the substrate upon impact/flattening of the NiCr certainly played a part in their formation. However, the size of this void is often large (1-2 μm in diameter), such that it may not be caused only by gases. Modelling of impact and flattening of molten particle has shown that a large central void can also be caused by the mechanics of the flowing molten material [15, 55]. It is probable that a combination of these two phenomena is responsible for the formation of the central void. However, the relative influence of these two factors in void formation is not known. Further study, especially modelling, is required in this instance. Another possible phenomenon may be the presence of an unmelted core within the impacting particle. However, this is unlikely as in plasma spraying it is expected that particles impact the substrate in a fully molten state [1, 4].

### III.3.b. *Thin fragmented and very fragmented splats*

For these fragmented splats (see Figs. 5b and 5c), it is quite probable that phenomena described above, such as poor wetting and gas released from the substrate, also occur. However, they are insufficient on their own to explain the significant fragmentation of the splat. Such a break up of the NiCr particle into several fragments is more likely to have occurred upon impact on the substrate. In plasma spraying, the particle velocity and temperature distribution are fairly large, thus it can be expected that some particles impact the substrate with a momentum great enough to lead to the explosion of the droplet and such fragmented shapes.

McDonald *et al.* modelled the impact of Mo particles on glass substrate after observing that the splats observed in such cases were very fragmented [79]. They found that fragmentation was promoted by a reduced cooling in the splat periphery due to a much higher thermal contact resistance (about two orders higher). In the case presented here, this could be linked to the gas release phenomenon which by creating a gas cushion hindered the contact between splat and substrate and causes a high thermal contact resistance, especially towards the periphery of the splat.

### III.3.c. *Influence of the heat treatment*

As described earlier, it is very probable that desorption of gases from the substrate upon impact has played a significant role in the splat formation. Yet such phenomenon must be then strongly influenced by the surface chemistry of the substrate.

This would mean that the heat-treated specimen would have, on one hand, a thicker oxide film compared to Al\_P, but on the other hand one may expect less gas to be released upon impact and flattening of a NiCr particle, thus a better wetting for molten NiCr and flatter splats would result. The splats observed on the Al\_PT specimen were indeed found to be less fragmented and flatter, as shown in the results presented in Table 3.

However, it can be concluded that the influence of such pre-treatment is relatively limited, especially when compared to the effects that were observed for heating during spraying (which was found to produce significantly flatter and more disc-

shaped splats [6, 19, 32]). This may possibly be due to the re-hydration of the outer oxide layer and/or re-contamination of the surface with adsorbates/condensates, in the time between the heat-treatment and the plasma spraying, when the substrate was left in air at room temperature.

#### III.4. Description of the boiled and boiled and thermally treated specimens (Al\_B and Al\_BT) post plasma spraying

No splats were found on either the Al\_B or Al\_BT substrates. However, some clustered particles, often 5-20  $\mu\text{m}$  in size, were found on the substrate surface. SEM images of typical particles are shown in Fig. 10.

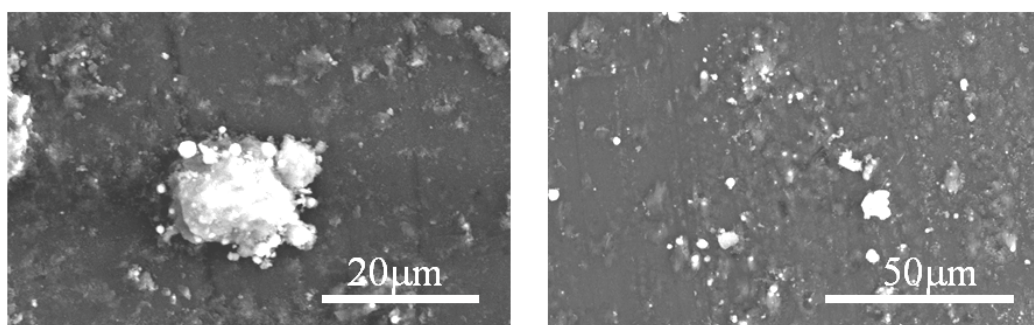


*Figure 10. SEM images of the clusters found on (a) Al\_B and (b) Al\_BT*

Figure 11 displays a bright field TEM image of cross-section of such a cluster present on Al\_BT. On the surface of the aluminium substrate (1), the Al hydroxide layer can be seen (2),  $\sim 300$  nm in thickness. Indeed, as it was discussed earlier, neither the heat treatment nor the spraying process is expected to produce enough heat to fully convert boehmite into alumina [75], however it may have been partially dehydrated, on its

surface, into transition alumina. Nevertheless, it was concluded that such layer would still be mainly hydroxide.

Within the substrate itself a Fe-rich intermetallic particle (3) was observed, surrounded by corundum  $\alpha$ -Al<sub>2</sub>O<sub>3</sub> (4), a structure similar to those described for the unsprayed specimens.

On top of the substrate, it was found that the clusters mainly consisted of nickel oxide NiO (5) and/or spinel NiCr<sub>2</sub>O<sub>4</sub> (6), together with some small NiCr particles (usually up to 2-3  $\mu$ m in diameter) (7). Some Al oxide or hydroxide phase can also be observed under the Ni-Cr-O cluster (8); it is up to 2-3  $\mu$ m in thickness and was observed to have formed directly above the Fe intermetallic particle. As noted earlier, identification of this aluminium and oxygen-rich phase is not straightforward, since EDS and electron diffraction do not allow simple differentiation between AlOOH and Al<sub>2</sub>O<sub>3</sub>. This phase appears to present a nano-crystalline equiaxed microstructure, as shown on the bright field image (Fig. 11a), clearly distinct from both the Al<sub>2</sub>O<sub>3</sub> and AlOOH phases observed on the unsprayed specimens (which appear respectively featureless and with needle-like nano-sized grains). It may be hypothesized that it is AlOOH: the fact that it is not in contact with the aluminium substrate could have then prevented the grains to have a uniform direction of growth, resulting in the equiaxed grain structure observed. This suggests that this phase was formed before spraying during the boiling process and was not observed on the unsprayed specimen possibly due to the lack of contrast with the rest of the specimen.

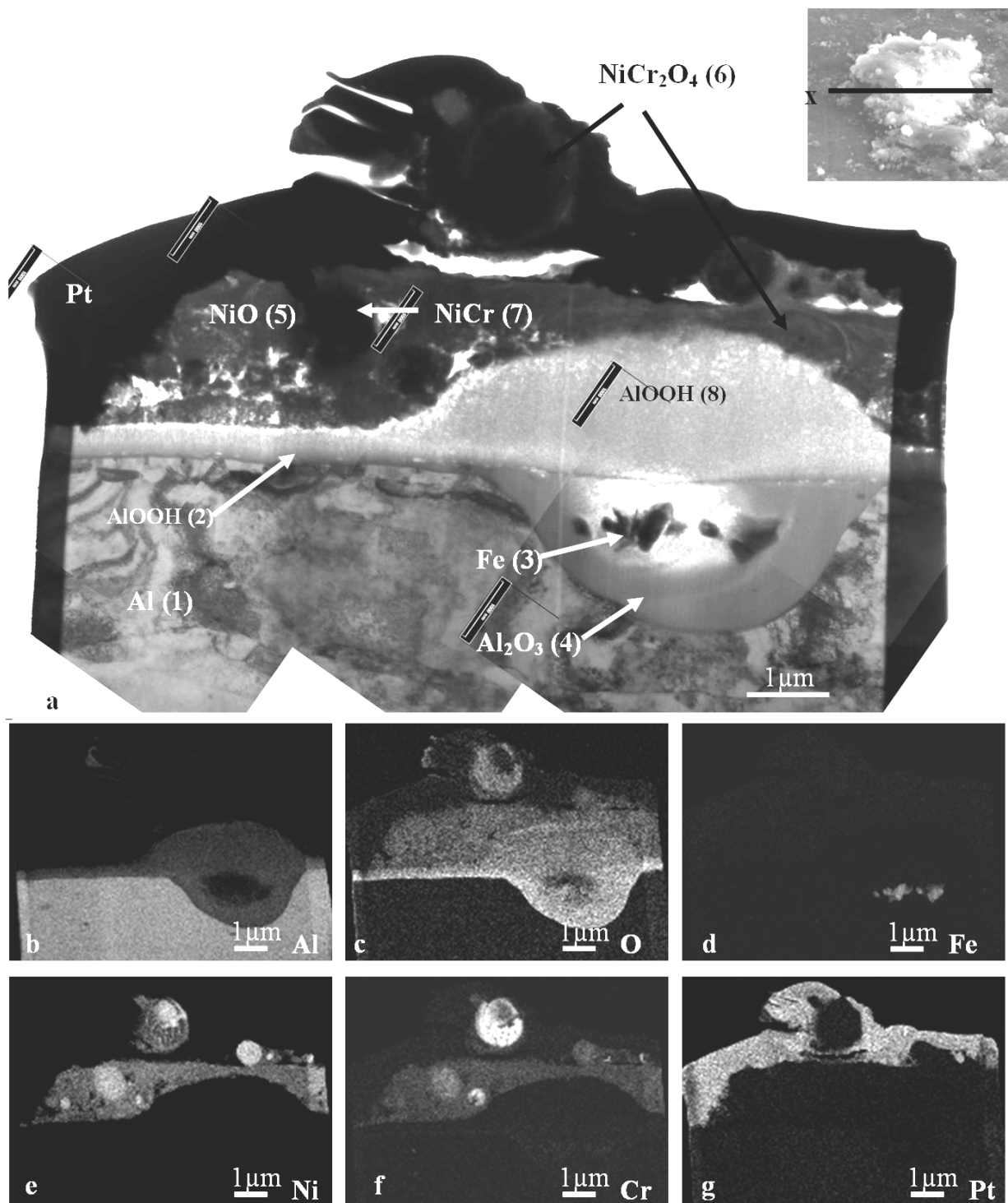


Figure 11. TEM cross-section of a cluster found on Al<sub>B</sub>(T) (see insert image): (a) bright field image, EDS elemental maps for (b) Al, (c) O, (d) Fe, (e) Ni, (f) Cr, and (g)

Pt

The absence of splats on the boiled specimens is in agreement with previous studies [55, 76], but is still not fully understood. It was hypothesized for Al\_P and Al\_PT that the release upon impact of a significant amount of gas from the substrate may cause fragmentation of the NiCr droplet. Extending this possibility to the boiled specimens could explain the absence of splats: upon impact from the sprayed particle, the partial dehydration of the hydroxide layer causes the release of sufficient gas that the particle cannot adhere to the substrate.

However, on these boiled substrates, clusters of oxide and of small NiCr particles that were usually a few microns in diameters, thus supposedly too fine to be from the original feedstock powder (whose diameter is comprised between 5 and 45  $\mu\text{m}$ ) were observed. Consequently, these particles presumably originated from the fragmentation of some of the sprayed particles upon impact. The heat from the plasma flow, along with the presence of oxidizing gases (spraying is performed in air in addition to the gases released from the substrate), may have caused oxidation leading to the formation of the clusters observed. Nevertheless, such clusters are insufficient to build a continuous thick coating. Consequently, it can be said that boiled aluminium substrates can not be thermally sprayed, principally due to the hydroxide layer that forms from the reaction with water. This shows the degree to which surface chemistry is a very important parameter in plasma spraying.

Conversely, the splats found on Al\_P and Al\_PT show that pre-heating the Al substrate prior to spraying has only limited influence on splat formation. Moreover, it was observed that the contact between splat and substrate is often poor, which suggest a poor overall adhesion of the coating. Further study is currently underway to

investigate the microstructure of splats sprayed under different conditions and how splat adhesion may be improved.

#### **IV. Conclusion**

To summarize, the study of Al substrates subjected to various pre-treatments and then plasma sprayed with NiCr particles lead to the following observations and conclusions:

- On the non-boiled specimens, the contact between splat and substrate was poor. Along with the different oxides formed and the presence of voids, this may be significantly detrimental to some coating properties (adhesion/strength, thermal/electrical conductivity, etc.). The formation of these different features was linked to, amongst other factors, the desorption of adsorbates/condensates from the substrate.
- On the boiled specimens, an absence of splats was noted, which was associated with the presence of a thick Al hydroxide layer causing the release of a significant amount of gas from the substrate and hindering splat adhesion.

Both set of observations confirmed the importance of the surface characteristics of the substrate. Studying the splat microstructure and the splat-substrate interface at such a high resolution proved to be an effective way of improving the present understanding of splat formation in the plasma spray process. Further work is currently underway to investigate, in a similar manner, the effects of different substrate conditions, surface roughness and spraying conditions.

## CHAPTER 5

# STUDY OF THE SPLAT-SUBSTRATE INTERFACE FOR A NiCr COATING PLASMA SPRAYED ON TO POLISHED ALUMINIUM AND STAINLESS STEEL SUBSTRATES

---

*S. Brossard, P.R. Munroe, A.T.T Tran, M.M. Hyland, Journal of Thermal Spray  
Technology, 2010, 19 (1), p. 24-30*

### Abstract

In the plasma spraying process, the mechanisms by which molten particles impact on and bond with the substrate are not fully understood. For this study a nickel-chromium powder was sprayed onto mirror polished aluminium 5052 and stainless steel 304 substrates to form single splats. The splats and their interface with the substrate were studied using detailed microstructural characterization with emphasis on the shape of the splats, the nature of the splat-substrate interface, including the degree of contact and the extent of melting of the substrate and mixing with the splat material, and the presence, either on or within the splats of phases such as oxides. It was shown that melting of the substrate, along with intermixing and diffusion between substrate and splat materials, occurred for the steel substrate, but not for the aluminium substrate. Oxides including nickel oxide, chromium oxide and aluminium

oxide were also observed, the type and distribution of these phases depended on the substrate type.

## I. Introduction

Thermal spraying processes, and plasma spraying in particular, permit the manufacture of coatings aiming at improving engineering performances and/or increasing component life without affecting the properties of the bulk substrate [4]. The mechanisms of adhesion between the sprayed coating and the substrate have a significant influence on the mechanical properties of the coating. Indeed, Kitahara *et al.* [80] found that when localized melting of substrate occurs upon impact of the molten particle, an intermetallic layer is usually formed and the bonding is regarded as metallurgical. In such a situation there, authors found that the adhesion strength at the splat-substrate interface was higher than the cohesive strength of the coating and failure tended to occur within the coating itself. If there is no, or only partial, metallurgical bonding, the adhesion strength is much lower. In the absence of substrate melting, adhesion between coating and substrate may occur by mechanical interlocking (especially in case of a substrate with a rough surface) and/or if diffusion occurs at the coating-substrate interface [81, 82]. This requires good contact between splat and substrate, and in that matter splashing of the splat on impact is ideally avoided [81]. Steffens *et al.* [82] showed that such contact occurred by diffusive contact zones, which were not present across the entire contact surface of the splat, but only in limited regions separated, usually, by pores at the splat-substrate interface. The degree of contact and interactions at these contact zones were improved by

increasing the contact temperature, which, in turn, depended on the properties of both the substrate and splat and the spray conditions.

Interfacial features, including the quality of contact between the splat and substrate, the possible occurrence of melting and the presence of pores and oxides were studied for NiCr particles plasma sprayed onto both stainless steel and aluminium polished substrates. Splat morphology and structure were also characterized. Comparison of the behaviour of the two substrates permits an understanding of the role of the nature of the substrate and its properties on splat formation and the interactions of the splat with the substrate. This paper is part of a larger study on splat formation for NiCr sprayed on aluminium and steel substrates depending on the surface chemistry, roughness and spraying method. This paper focuses, in particular, on the influence of the nature of the substrate on the splats' characteristics.

## **II. Experimental Conditions**

Stainless steel 304 and Aluminium 5052 were ground and mirror polished mechanically with diamond paste. The surface average roughness measured by Atomic Force Microscopy was between 5 and 10 nm. Substrates were then plasma sprayed at room temperature with a commercial NiCr alloy powder (Ni80-Cr20, Sulzer Metco 43VF-NF, Wohlen, Switzerland, 5-45 $\mu$ m), using a Sulzer Metco (Wohlen, Switzerland) 7MB gun operating at a current of 550A and a voltage of 74V. The spraying distance between the gun and the substrate was kept at 80 mm. The powder was injected at a feeding rate of 1 g/min. The plasma gas mixture was nitrogen and hydrogen, to limit to the maximum possible extent the oxidation of the

particles during flight. The spray conditions involved a flow rate of 47.6 SLPM (Standard Litres per Minute) and 5.4 SLPM, respectively. Only one pass was made in order to obtain single NiCr splats on the substrate surface.

Characterization of the specimens was carried out using a scanning electron microscope (SEM) (Hitachi S-3400X, Mito, Japan). Measurement of the surface roughness was performed using an atomic force microscope (AFM) (Digital Instrument 3000, Santa Barbara, USA). Cross-sections of the splats were prepared using a focused ion beam (FIB) microscope (FEI XP200, Hillsboro, USA). Transmission electron microscope (TEM) cross-sections were prepared using a dual beam high resolution focused ion beam instrument (FEI XT Nova Nanolab 200, Hillsboro, USA). They were then lifted out with a micro-manipulator and put on a carbon coated copper grid. TEM studies were performed using a Philips CM200 (Eindhoven, The Netherlands) to which an energy dispersive X-ray spectrometer was interfaced.

### **III. Experimental Results**

#### **III.1. Stainless Steel Specimen**

SEM images of about 50 single randomly chosen splats were taken and the splat morphology evaluated and the splat diameter,  $D$ , measured (features such as splashed fingers were ignored when evaluating diameter, which was done by taking the smallest and largest diameter value measured from the splat, which are not perfectly circular, and calculating the average value). The percentage of each splat type and the

median diameter,  $D_m$ , are seen to be indicative only, as the number of splats observed is insufficient to establish accurate statistical analysis. A more detailed analysis of splat size has been presented elsewhere [53]. According to their morphology, splats were classified in three categories:

- Disc-shaped splats (~23% of the analysed series) (Fig. 1a), with, usually, a large central pore (5-10  $\mu\text{m}$  in diameter) which appeared to originate from the release of gas by the substrate upon the impact of the particle. A very slight lip can also often be observed at the splat periphery. ( $20 < D < 55 \mu\text{m}$ ,  $D_m = 30 \mu\text{m}$ ).
- Near disc-shaped splats (47% of the analysed series) (Fig. 1b). A central pore still appears to be present despite the splashy appearance of the splats. ( $10 < D < 30 \mu\text{m}$ ,  $D_m = 20 \mu\text{m}$ )
- Fragmented splats (30% of the analysed series) (Fig. 1c). Despite the difference in shape with the previous splats, the centre of these splats is still NiCr-free. ( $8 < D < 20 \mu\text{m}$ ,  $D_m = 14 \mu\text{m}$ ).

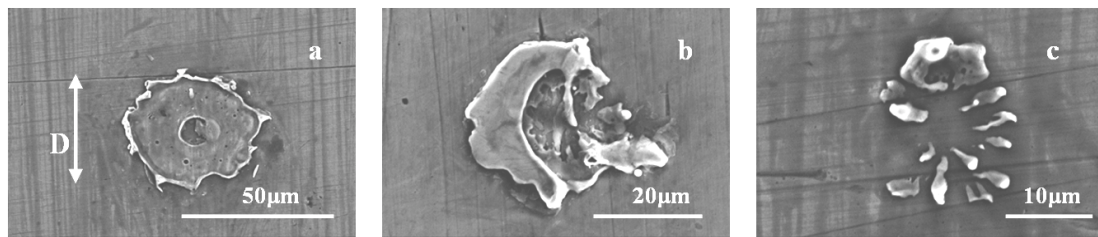


*Figure 1. SEM images of each type of splat found on the stainless steel substrate.*

For each category of splat, several FIB cross-sections were prepared and examined. A typical example for a near disc-shaped splat is shown Fig. 2. The inset image shows a SEM image of the splat prior to cross-sectioning. In the central pore of the splat (1) can be found a porous oxide phase, which will be shown later by TEM to be mainly NiO, along with some metallic NiCr particles (2). A thin layer of NiCr can be found at

the bottom of the pore (3), while the shape of the splat around the central hole shows a distinct rim (4): the NiCr seems to have been “pushed” upward on solidification, probably due to the instability of the gas released by the specimen upon impact (4). The large columnar grains ( $\sim 1\text{-}3\mu\text{m}$  in size) suggest a slow rate of solidification at the top surface of the splat (4). In certain zones, for example at the interface with the substrate, some small (sub-micron) grains, whose boundaries correspond with the ones of the grains of the splat, are apparent (5). This suggests melting of the substrate has occurred, followed by the simultaneous solidification of both phases. Finally, on the right hand side of the splat, what seems to be a thin layer of oxide can be observed at the periphery of the splat (6). From the FIB cross-sections, the aspect ratio, defined as being the diameter of the splat divided by its thickness, can be calculated. For this splat it has been found to be  $\zeta \sim 44$ . The thickness is measured on the flat portion of the splat between the central hole and the rim.

In summary, the structure of the central pore, as seen here, was commonly observed on other FIB cross-sections of this splat morphology. However, the contact at the splat-substrate interface in other splats was not always as good as in the cross-section shown: delamination can sometimes be found under the rim of the splats, as well as, occasionally, porosity. In contrast, cross-sections of splashed splats showed coarse grain structures along with NiO phases, and the contact at the interface was usually quite poor. However, cross-sections of regular disc-shaped splats showed that over their main flat part, between the central hole and the rim, grains were usually fine, contact between the splat and substrate was good, and as will be shown later, there is evidence of melting of the substrate, but limited oxide is present.

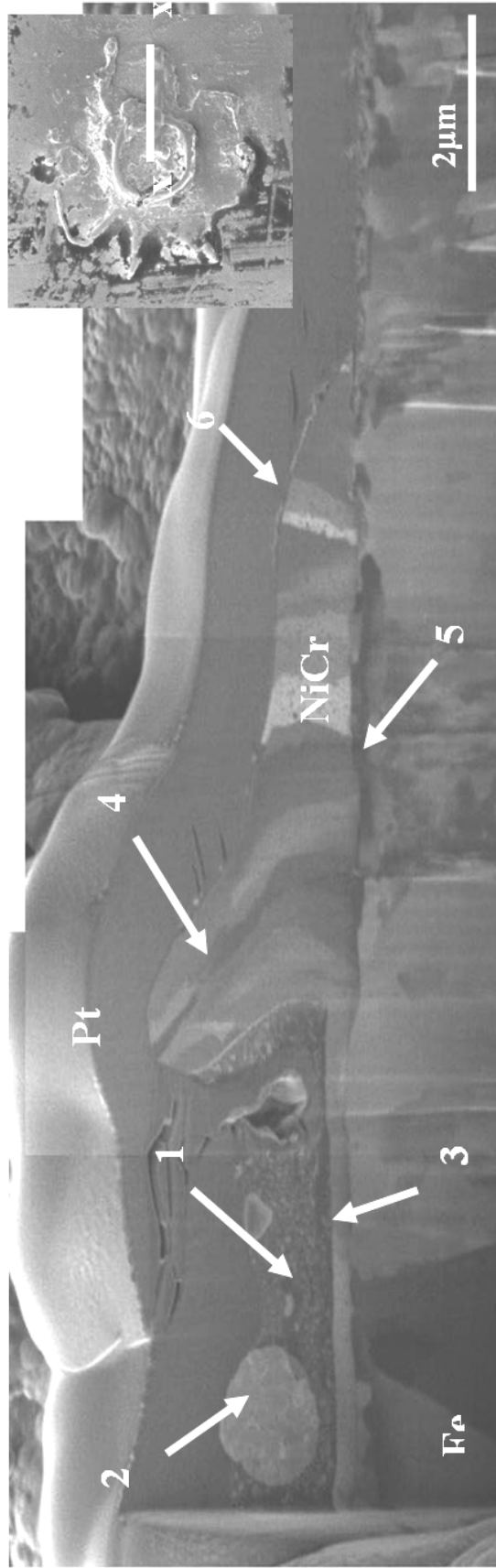


*Figure 2. FIB image of a cross-section of a near disc-shaped splat found on the stainless steel substrate*

Several TEM cross-sections were examined. For example, Fig. 3a shows a bright field image of a TEM cross-section made across the rim of a disc-shaped splat (see inset SEM image of the entire splat). This splat exhibits an accumulation of NiCr at the periphery (1), topped by a layer of CrO<sub>3</sub> (2), with also some delamination at the splat-substrate interface (3). Furthermore, through EDS elemental mapping (Fig. 3b and 3c), some chemical intermixing between the splat (Ni) and the substrate (Fe) can be seen (4): melting of the substrate has clearly occurred and it seems that the steel that has melted has flowed around the molten NiCr, and then gets folded into the splat. Study of this zone via electron diffraction, which allows study of the orientation of the grains, shows that the intermixed zone has a fine grain structure with high angle boundaries (4). EDS linescans across this zone (Fig. 3d) also shows that Fe and Ni interdiffusion across the splat-substrate interface has occurred (5). In contrast, the linescan made across a zone where the splat-substrate interface is clear (Fig. 3e) shows a sharp step-function at the interface.

Study of other TEM cross-sections reveals the presence of features such as thin layers of chromium oxide (either Cr<sub>2</sub>O<sub>3</sub> or CrO<sub>3</sub>) on the outer surface of some splats. NiO is present as a porous phase, not only around the central pores, but also in other pores at the interface or around the rim and splashed zones of splats. Melting of the substrate along with splat-substrate intermixing and diffusion is frequently observed, mostly at the interface in the main flat part of the splat.

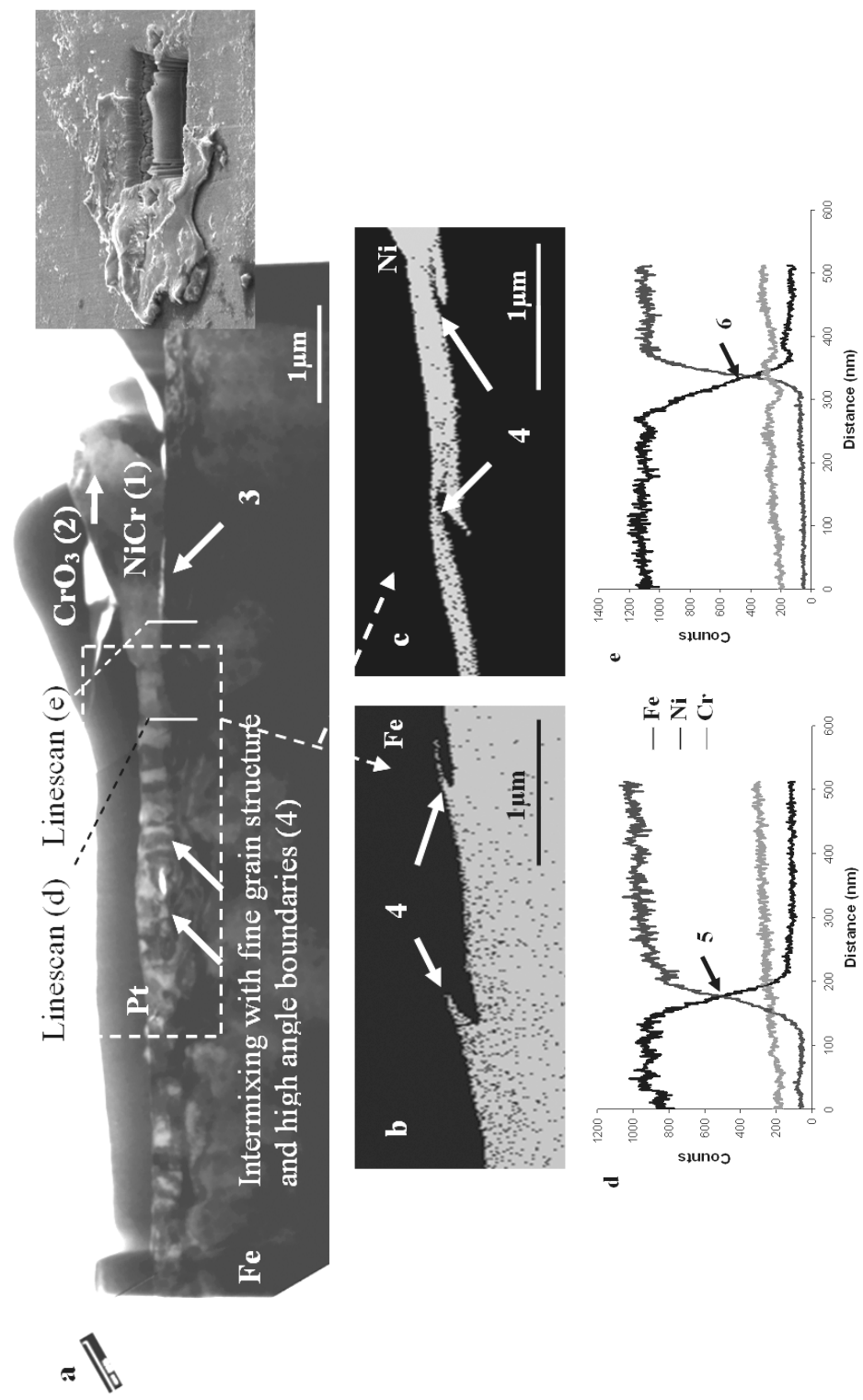
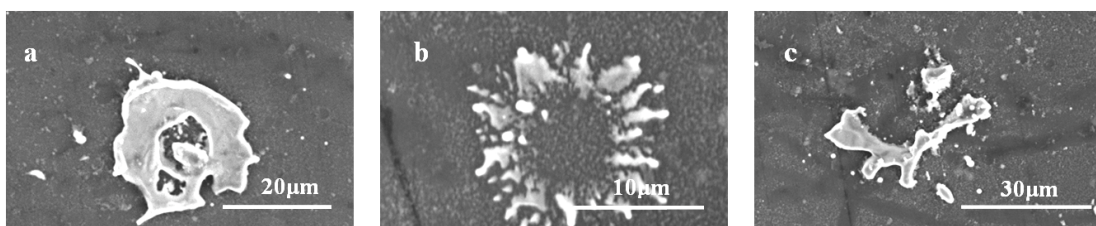


Figure 3. TEM cross-section of a disc-shaped splat from the stainless steel substrate: (a) bright field image, EDS elemental maps for (b) Fe and (c) Ni, (d-e) EDS linescans

### III.2. Aluminium Specimen

Observation of the SEM images, following the same method as for the steel specimen, showed that the morphology of the splats found on the aluminium specimen was quite different to the one for the steel specimen. In this case the splats were classified also in the three following categories:

- Thick and almost disc-shaped splats (Fig. 4a), often fragmented or with a large hole in the centre where the substrate was bare (~33% of the analysed series). ( $D_m = 28.3 \mu\text{m}$ ,  $20 < D < 43 \mu\text{m}$ ).
- Very fragmented and thin splats (Fig. 4b), with a circular shape (~49% of the analysed series). ( $D_m = 16.2 \mu\text{m}$ ,  $10 < D < 28 \mu\text{m}$ ).
- Very irregular splats (Fig. 4c) where it appears that the NiCr liquid has not spread across the substrate surface (~18% of the analysed series). ( $D_m = 17.9 \mu\text{m}$ ,  $10 < D < 25 \mu\text{m}$ ).



*Figure 4. SEM images of each type of splat found on the aluminium substrate.*

Several FIB cross-sections were performed on the different splat types found on the aluminium substrate. One section was made across a very fragmented and thin splat is shown in Fig. 5. It can be seen that the splat thickness increases from the centre (1) to the periphery (2). Moreover, from the shape of the grains (2), the NiCr liquid has been

ineffective in wetting the surface when impacting on the substrate and has slid away from the point of impact during flattening. Further, almost no material from the splat is found in a large central area (1). The splat-substrate interface is quite porous (3), and the contact between them is poor, and the grain structure irregular and coarse (2). Moreover, in the area marked (4) it appears that there is a part of the splat that suggests fragmentation of the splat droplet under impact. The splat is thin, with an aspect ratio estimated at  $\zeta \sim 80$ .

This poor contact between the splat and substrate was observed for every splat on the polished aluminium substrate, even for the almost disc-shaped splats. The latter are thicker ( $\zeta$  is usually around 40, compared to 80 for the splashed ones), with larger grains, but with poor contact. Further, very little oxide can be found even in the centre of the splats, which is usually free of NiCr. Finally, no evidence of substrate melting was found.

An example of a TEM cross-section is shown Fig. 6: This TEM cross-section was performed across a thick irregular splat. The bright field image (Fig. 6a) shows that the splat-substrate interface is clearly delineated and uniform (1). The contact between splat and substrate is poor: many large pores can be seen at the interface. Elemental mapping (Fig. 6b-f) reveals a layer of chromium oxide on the outer surface of the splat (2). This layer is too thin to get unambiguous electron diffraction data, but it is very probably either  $\text{CrO}_3$  or  $\text{Cr}_2\text{O}_3$ . There also a thin layer of oxide on top of the substrate, under the splat, which, on the basis of the EDS maps, is probably Al oxide (3). Furthermore, one can observe a significantly large intermetallic iron-rich particle within the substrate (4).

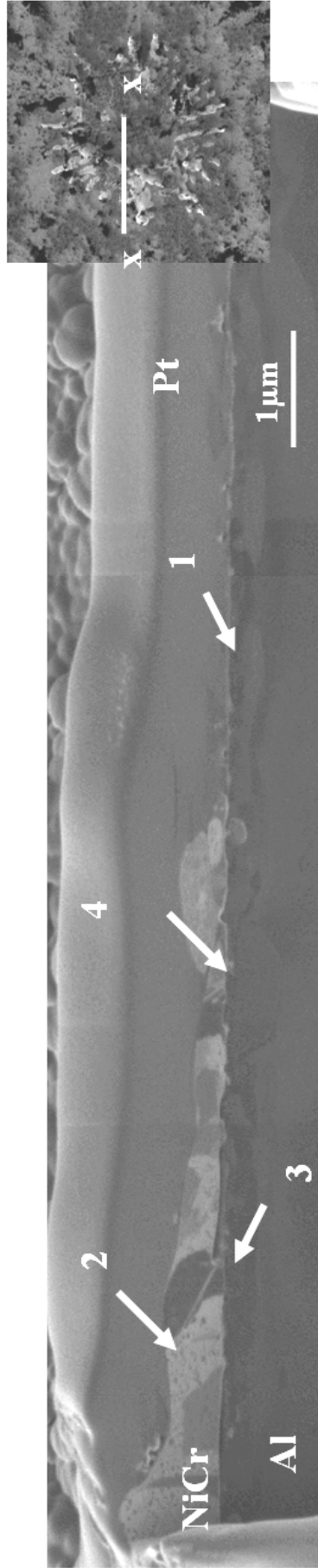


Figure 5. FIB image of a cross-section of a splashed splat found on the aluminum substrate.

The EDS linescan (Fig. 6g) performed across the splat-substrate interface confirms the absence of any mixing or diffusion between the aluminium and NiCr (5). On the other hand it shows a slightly higher concentration of Mg at the surface of the substrate (6). This was not evident on the mapping due to the lower spatial resolution of the maps. The Mg enrichment is attributable to effects from the heating in air of the substrate and the preferential oxidation of Mg, which segregates this element towards the surface [83].

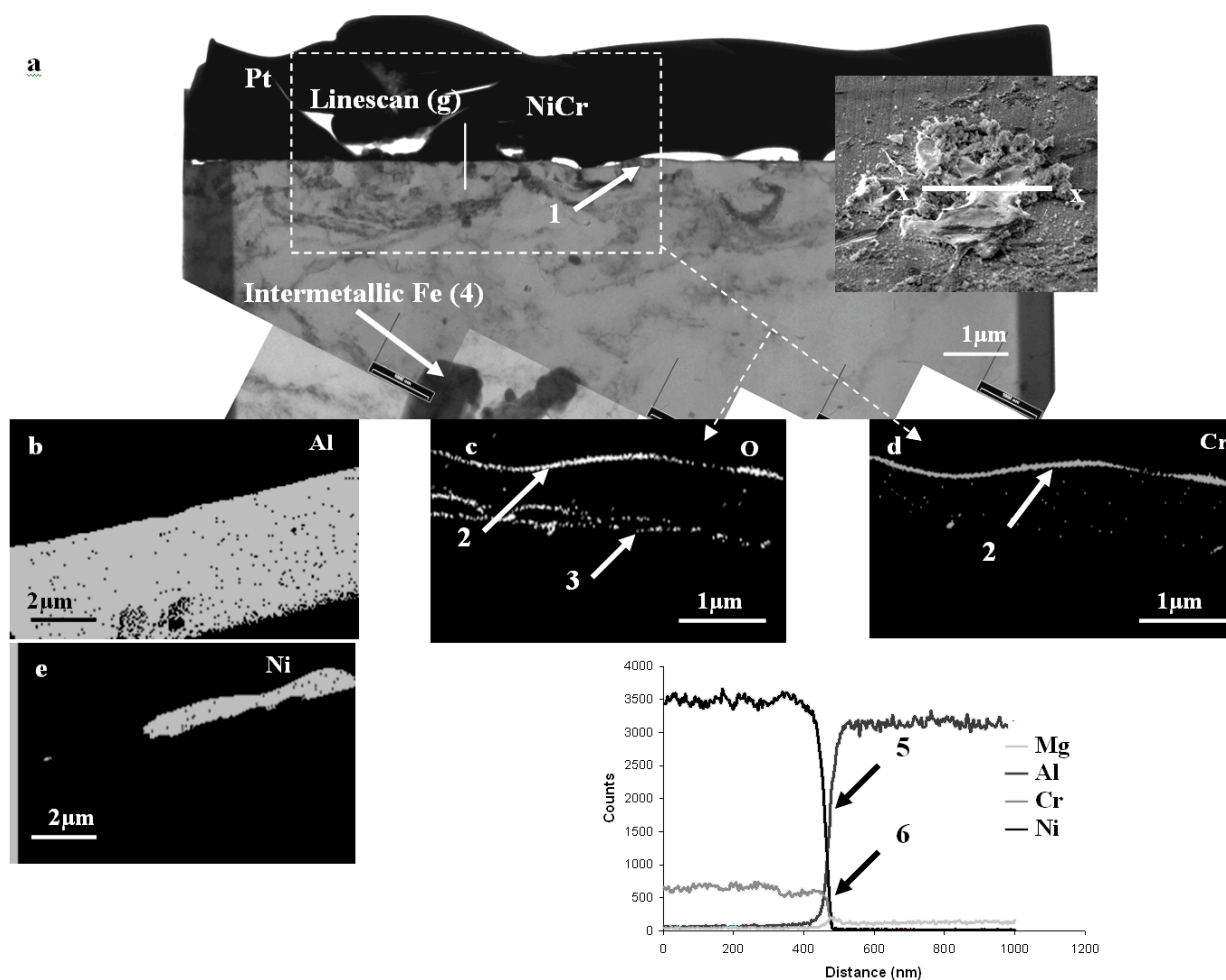


Figure 6. TEM cross-section of an almost disc shaped splat from the aluminium specimen: (a) Bright field image, EDS elemental maps for (b) Al, (c) O, (d) Cr, (e) Ni, (f) EDS linescan.

On all the TEM cross-sections examined on the different types of splats, no sign of chemical mixing between Al and NiCr could be found. The interface was always straight and clear and there were no structural features, such as the formation of additional phases or voids within the substrate. These observations suggest that no melting of the substrate has occurred. Moreover, the contact is mostly very poor with frequent evidence of porosity at the interface. Chromium oxide can be found sometimes either as a thin layer on top of the substrate or as small particle at the interface (in the first case it was probably formed after the flattening of the splat, while in the second case it was probably formed on the periphery of the melted particle before impact), nickel oxide can also be found as large porous clusters, especially on splashy splats. Mapping often reveals the presence of what is assumed to be a thin layer of Al oxide on top of the substrate. It is probably formed during spraying due to the heat of the plasma flame. Finally, intermetallic Fe and Mg-rich phases are frequently observed in the substrate.

#### **IV. Discussion**

One characteristic of the plasma spraying process is that almost all particles sprayed impact the substrate in a fully molten state. When the NiCr particles impact the stainless steel substrate (see Fig. 7), they heat up the substrate, causing the release of gas such as the chemisorbed water from the surface [49]. This released gas forms one of several pores in the centre of the flattened splat, causing a poor contact in this region (see 1 on Fig. 7). The pore may also reach a critical size where it becomes unstable, creating a

large bubble-like hole. The presence of oxygen and water-rich gas trapped into this pore(s) is probably responsible for the formation of Ni oxide. This oxide is less stable than both  $\text{Cr}_2\text{O}_3$  and  $\text{CrO}_3$ , but its kinetics of formation are faster [56]. Meanwhile, the molten NiCr particle undergoes flattening (see 2 on Fig. 7). It is possible that gas released from the surface is simultaneously covered by the flowing splat and may be pushed at the periphery because of the flow of melted metal (see 2 on Fig. 7). In this situation, good contact between NiCr and the steel substrate can be achieved. The heat from the molten splat is then sufficient to locally melt the steel substrate (modelling showed that temperature at the splat-substrate interface may reach  $1660^\circ\text{C}$ , the melting point of steel being  $1454^\circ\text{C}$  [55]) (4): the molten steel, pushed by the flowing splat, is then splashed within the splat, as observed by mapping of the interface (Fig. 3b/c). Diffusion across interface between the steel substrate and the splat can also occur in this zone. NiCr and austenitic stainless steel have the same crystal structure and similar lattice parameters, a (both face centred cubic, with lattice parameters of  $a = 0.352\text{nm}$  for the steel and  $0.355\text{nm}$  for NiCr). Grain growth between the two phases across the interface can therefore take place easily. Electron diffraction studies showed that NiCr and steel grains with the same orientation were found juxtaposed across the interface. Finally, the gas that has been pushed at the rim of the splats is probably the cause of the formation of NiO in this region. Moreover, the delamination under the rim is due to the curl up of the splat, occurring when the splat solidifies and cools down and the upper surface shrinks [54]. The formation of a thin layer of Cr oxide on the outer surface of the splat can be compared to the high temperature oxidation of NiCr alloys [70]. Some Cr oxide may also

originate from in-flight oxidation, especially small oxide particles found around the splat-substrate interface [6].

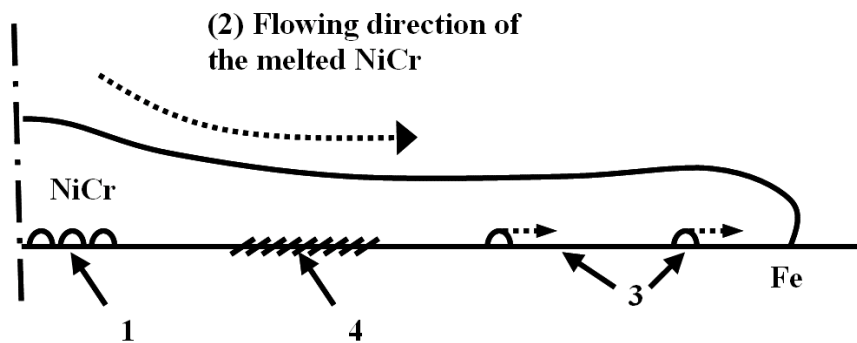


*Figure 7. Schematic representation demonstrating the process of molten NiCr splat spreading across a steel substrate*

The formation of the splat on the aluminium specimen is thought to be similar to that observed on the steel substrate in several areas. The gas release from the substrate upon impact and flattening is a key point, probably even more important for this substrate, as it seems that a gas cushion between the flattening splat and the substrate may form [49]. This could explain, on one hand, the porosity that can be found at the interface, and on the other hand, why many splats are very fragmented. That is, it appears as if the NiCr had slid away from the point of impact without adhering to the substrate. Ni and Cr oxides develop in a similar fashion as seen for the steel substrate: NiO can be found in pores, while Cr oxide is present in thin layers on top of some splats.

However, the main difference that has been observed between the splats on the stainless steel specimen and the aluminium specimen is the nature of the splat-substrate interface.

Indeed, the contact between the splats and the aluminium substrate is quite poor, and no sign of melting of the substrate, neither mixing or diffusion, has been observed. At first sight, this situation is quite unexpected, as the melting point of aluminium is much lower (649°C) than for steel (1454°C). For instance, *Li et al.* sprayed Mo on several substrates including steel and aluminium and found that melting of the substrate was more likely to occur with an aluminium substrate than with a steel substrate [36]. However, other parameters than the substrate melting point should be taken into account. Firstly, thermal diffusivity is important: at 25°C, the thermal diffusivity for stainless steel 304L is  $\sim 4 \times 10^{-5} \text{ m}^2 \cdot \text{s}^{-1}$  and  $\sim 58 \times 10^{-5} \text{ m}^2 \cdot \text{s}^{-1}$  for aluminium 5052 (calculated from [84]). This means that the heat brought to the substrate by the splat is more likely to be diffused into the bulk substrate for the aluminium, and the temperature at the surface is not elevated as for the steel substrate. Modelling of the splat formation described elsewhere in detail by *Tran et al.* showed that the thermal diffusivity had a strong influence on the degree of substrate melting [55].

Another factor is surface chemistry. XPS analysis suggests that compounds such as oxides and hydroxides may be present on both substrates' surface, mainly  $\text{Fe}_2\text{O}_3$  and  $\text{FeOOH}$  for steel,  $\text{Al}_2\text{O}_3$  and  $\text{AlOOH}$  for aluminium [49]. Upon heating hydroxides get dehydrated and transformed into oxide, which release water vapour. It is also suggested that the oxide/hydroxide layer may be slightly thicker on the aluminium surface (4.2 nm, against 3.5nm). Surface chemistry and its influence on splat formation is still not well understood, but if there is effectively more hydroxide on the Al specimen, or if it is more prone to release gas upon heating, then the degree of contact between splat and substrate

would be compromised, due, for instance, to the presence of an isolating gas cushion, and less heat would be transferred from the splat to the specimen. It is possible then that a combination of those two processes kept the aluminium substrate from reaching its melting point.

Such hypothesis could be studied on one hand using vacuum plasma spraying to spray NiCr on very “clean” Al and steel substrates, in order to limit to the maximum possible extent the influence of surface chemistry, or on the other hand by varying the surface chemistry and comparing splats between specimens made of the same materials. Research focused on investigating these issues is currently underway in a larger study investigating the splat microstructure and splat formation processes as a function of the substrate surface chemistry and roughness.

## **V. Conclusion**

Study of plasma sprayed single splats on aluminium and stainless steel substrates showed that the morphology and the characteristics of the splat-substrate interface were very different from one substrate to another. Splats found on the stainless steel specimen were more regular and disc shaped. But very importantly localized melting of the substrate and intermixing and diffusion were observed at the interface. Splats on the aluminium substrate were slightly more irregularly shaped. The contact at the splat-substrate interface was usually poor with a lot of porosity. For both type of splats, several oxide phases were observed. Their formation and the formation of the splats were discussed,

but further experiments will be needed to fully identify the origins of the differences observed between the steel and the aluminium specimens.

## CHAPTER 6

# EVIDENCE OF SUBSTRATE MELTING OF NiCr PARTICLES ON STAINLESS STEEL SUBSTRATE BY EXPERIMENTAL OBSERVATION AND SIMULATIONS

---

*A.T.T. Tran, S. Brossard, M.M. Hyland, B.J. James, P.R. Munroe, Plasma Chemistry and Plasma Processing, 2009, 29, p. 475-495*

### Abstract

Single NiCr splats were plasma-sprayed onto a polished stainless steel substrate held at room temperature. The splat-substrate interface was characterized by focused ion beam and transmission electron microscopy. The frequent observation of NiO particles, particularly in pores within the splat, and at the periphery of splat, suggests that the principal oxidation process occurs at the substrate surface, where the splats are exposed to a water vapour-rich environment. It was also observed that the splat adhered well in some locations where elemental-diffusion and jetting of the substrate occurred, suggestive of substrate melting. A three-dimensional numerical model was developed to simulate the impact of a splat onto a substrate. The simulation shows that the observation of the central pore in the splat and the phenomenon of substrate melting may occur.

Based on these results, the effect of water release on oxide formation and splat morphology can be explained.

### List of Symbols

B	Body force	t	Time
C <sub>p</sub>	Specific heat capacity	u	Velocity vector
f	Mass fraction	a	Thermal diffusivity
F	Volume of fraction of the droplet	q	Density
k	Thermal conductivity	l	Effective viscosity
L	Latent heat of fusion	l	Liquid phase
T	Temperature	s	Solid phase
T <sub>m</sub>	Equilibrium melting temperature	sub	Substrate
p	Pressure		

### I. Introduction

The nature of the splat-substrate interface in thermal spray coating is important in determining the mechanical, thermal and electrical properties of the coating. During impact of a molten droplet onto a substrate, local substrate melting may occur. The bonding between the splat and the substrate may improve with substrate melting. Nevertheless, substrate melting may cause substrate damage and alter its chemical properties. Hence, substrate melting has extensively been investigated. Kitahara *et al.* [35] reported that substrate melting occurred when nickel, chromium, molybdenum and

tungsten were plasma-sprayed onto aluminium and mild steel substrates. As a result, a layer of an intermetallic compound was formed at the substrate-coating interface [35]. Subsequently, Steffens *et al.* [82] indicated that substrate melting strongly depended on the droplet thermo physical properties, contact temperature and solidification time. Increasing the substrate or droplet temperature or spraying on a substrate with a low value of thermal conductivity (such as oxides) enhanced the degree of melting [82]. Zhang *et al.* [85] also detected an intermetallic layer between the molybdenum splat and the mild steel substrate and suggested that substrate melting occurred. Li *et al.* [36] have recently shown that the substrate melted and interacted with the spreading droplet. These experimental results confirmed that better bonding between the sprayed coating and the substrate could be achieved through the formation of intermetallic compounds as a result of substrate melting during droplet-substrate interaction [35, 36, 82, 86, 87].

Along with experimental studies, numerical simulations have also been conducted to predict the phenomenon of substrate melting under the impact of a molten droplet. Dallaire [88], Wang *et al.* [89] and Li *et al.* [36] studied splat solidification and substrate melting using a one-dimensional heat conduction. Li *et al.* [36] numerically and experimentally examined the phenomenon of substrate melting of different particle and substrate material combinations and suggested that both substrate and particle materials had an important role on the melting behaviour. They proposed a “temperature factor” which could be used to predict the potential for substrate melting. Based on this factor, substrate melting was not expected to occur for nickel and chromium on mild steel substrate [36]. However, these numerical simulations lacked precision because the kinetic

energy of the droplet and the free surface deformation were neglected in their models [36, 88, 89]. Subsequently, Zhang *et al.* [20] expanded the model to combine a two-dimensional free surface deformation model with a one-dimensional non-equilibrium rapid solidification model. Although the model could predict the solidification rate and splat morphology, the variation of the temperature inside the droplet and along the substrate-splat interface could not be obtained with a one-dimensional rapid solidification model. Ideally, the impact of a molten droplet must be modelled using three dimensions. Bussmann *et al.* [90, 91] developed a three-dimensional model using a volume tracking method to simulate water droplets falling with low velocity ( $\sim 1 \text{ m.s}^{-1}$ ) and to study the splash of a droplet on a solid surface. However, heat transfer and phase change during droplet impact were not considered in these models. Pasandideh *et al.* [18, 34] subsequently extended the model of Bussmann *et al.* [90, 91] to include heat transfer and solidification to simulate the droplet impact and solidification onto a flat surface. Since then, three dimensional numerical models have been extensively employed to study the splat spreading process and the splat shape [54, 79, 92, 93]. However, there have been only limited studies to consider the phenomenon of substrate melting during the flattening and solidification of the splat, in particular the temperature distribution of substrate surface as a function of time and locations. Thus, the aim of this study was to use a three-dimensional model to predict the splat shape formed and the phenomenon of substrate melting during the impact of molten nickel splat onto a polished stainless steel substrate. In addition, the cross-sections of the splat-substrate interface were experimentally examined using high resolution microscopy. Based on numerical analysis, the origins of the disk splat shape with a central pore, the effect of water release on oxide

formation, and substrate melting phenomena observed in the experiments were explained. The nucleation and growth of grains within the splat will be discussed in detail in a subsequent paper.

## II. Experimental Details

In this work, a 304 stainless steel substrate was mechanically polished to a mirror-like surface finish with the average roughness of 6.4 nm. A commercial NiCr alloy powder (Ni80-Cr20, Sulzer Metco 43VF-NS, Switzerland,  $-45+5\ \mu\text{m}$ ) was thermally sprayed onto the polished stainless steel substrate employing plasma spray technique at room temperature. Plasma spraying was carried out with a Sulzer Metco (Switzerland) 7 MB gun operating at a current of 550 A and a voltage of 74 V. The spraying distance between the gun and the substrate was kept at 80 mm. The powder was injected at a feeding rate of  $1\ \text{g}\cdot\text{min}^{-1}$ . The plasma gas mixture was nitrogen and hydrogen, at a flow rate of 47.6 SLPM and 5.4 SLPM, respectively. Collected splats on the (25 x 50 x 3 mm) substrate were characterised qualitatively and quantitatively using a Philips FEGXL30 scanning electron microscope (SEM) and ImageJ imaging software (National Institute of Health, Washington, DC). The splat-substrate interface was investigated using a focussed ion beam (FIB) microscope (FEI P200x). Samples were prepared for transmission electron microscopy (TEM) analysis (Phillips CM200) using a “dual beam” FIB (FEI Nova 200 Nanolab). The method of sample preparation for TEM analysis has been described elsewhere [94, 95]. Energy dispersive spectroscopy (EDS) was also conducted in the TEM.

The surface chemistry of the polished stainless steel substrate was examined using X-ray Photoelectron Spectroscopy (XPS—Kratos Axis Ultra DLD). The excitation source in use was Al Ka (1486.6 eV), along with pressure in the analysis chamber of  $10^{-8}$  Pa. “Wide” scans were collected from 1,100 to 0 eV. “Narrow” scans of Fe 2p, O 1 s and C 1 s with an energy of 20 eV were collected to examine the presence of oxide/oxyhydroxide species on the surface; the measured binding energies were referenced to C 1 s at 285.0 eV. The narrow scans were fitted using CasaXPS software with a mixture of Gaussian (G) and Lorentzian (L) for the peak shape. The fitting method was based on methods described in the literature [59, 60, 96].

### III. Numerical model

The impact of a molten droplet on the substrate was modelled using a free surface model in which the fluids (droplet and air) are separated by a distinct resolvable interface. At the interface between the droplet and surrounding air, the surface tension, which was based on the continuum surface force (CSF) model of Brackbill *et al.* [97], was modelled as a volume force concentrated at the interface. As a molten droplet impacts the colder substrate, the droplet temperature rapidly decreases. Once the droplet temperature reaches the melting temperature, the phase change from liquid to solid occurs. Because heat transfer due to convection and radiation are much smaller than through conduction they are not included in the model [34, 89]. Thus, the temperature distribution of substrate and droplet during droplet spreading and cooling is obtained using a transient heat conduction model. It has been reported that splat morphology is strongly dependent on the solid–

liquid contact angle which the interface made with the substrate surface through the droplet [97]. The contact angle, which is a constant or dependent on the contact line speed, was experimentally obtained through the enlarged photographs and measurements of each specific droplet on a substrate system. Thus, it is difficult to get the true value of contact angle. In this paper, dynamic contact angles were computed as part of the solution based on the volume of fraction (VOF) method [98]. The following assumptions were made to model the present problem mathematically:

- The liquid flow was incompressible and laminar.
- The effect of ambient air during droplet impact was negligible.
- The velocity of the solid phase is zero.
- Tangential stresses at the free surface, and gravitational force were neglected.
- No slip and no penetration boundary conditions were applied at the substrate surface.
- The energy source and the viscous dissipation were neglected.
- Thermal contact resistance and surface tension were constant.
- The physical properties of the substrate were constant.

Taking into account the above assumptions, the equations of mass, momentum, and energy conservation for the binary solid–liquid phase change system of an incompressible droplet are presented as below. Full details are described elsewhere [55, 98-100] and need not to be repeated here.

Mass conservation

$$\nabla \cdot u = 0 \quad (1)$$

Momentum conservation

$$\rho \frac{\partial u}{\partial t} + \rho \nabla \cdot (uu) = -\nabla p + \nabla \cdot \left( \mu_l \frac{\rho}{\rho_l} \nabla u \right) + \rho B \quad (2)$$

Energy conservation

$$\frac{\partial T}{\partial t} + \nabla \cdot (uT) = \alpha \nabla \cdot (\nabla T) + S_h \quad (3)$$

The relationship between droplet temperature and liquid mass fraction is given by:

$$f_l = \frac{C_{pl}}{L} (T - T_m) \quad (4)$$

The liquid and solid mass fraction is constrained to unity, that is:

$$f_l + f_s = 1 \quad (5)$$

The locations of contact lines, the interface between the droplet and air fluids, the shape and trajectory of the droplet were tracked using the ‘‘volume of fraction’’ method [98]. The volume of fraction of the droplet ( $F$ ) specifies the fraction of the volume of each computational cell in the grid occupied by the droplet and is defined to be unity for all the points inside the droplet and zero elsewhere. A value of  $F$  between 0 and 1 represents the interface between the droplet and air. The volume of fraction of droplet for a given flow is determined by the passive transport equation:

$$\frac{\partial F}{\partial t} + \nabla u F = 0 \quad (6)$$

Due to the small size of the droplet, gravitational forces were neglected in this study. Thus, surface tension is the dominant force contributing to body force governing the

droplet behaviour. The surface tension force per unit interface area given by CSF [97] model is:

$$F_{\alpha\beta} = -\sigma\kappa_{\alpha\beta}n_{\alpha\beta}\delta_{\alpha\beta} \quad (7)$$

The stress boundary condition at the free surface is [97]:

$$p_{\alpha} - p_{\beta} = -\sigma\kappa_{\alpha\beta} \quad (8)$$

where  $\alpha$  and  $\beta$  represent the droplet and air, respectively,  $\sigma$  is the surface tension coefficient,  $\kappa$  is the surface curvature, taken positive if the centre of curvature is in air,  $\delta_{\alpha\beta}$  is the interface normal vector pointing from the droplet to air which is calculated from the smoothed volume of fraction,  $dab$  is the interface delta function which is zero away from the interface to ensure that the surface tension force is only active near to the interface.

Heat transfer between the droplet and substrate was assumed to be due to heat conduction alone. A thermal contact resistance ( $R_c$ ) is used to account for discontinuity at the interface between the droplet and the substrate:

$$\frac{1}{R_c}(T - T_{sub}) = k \frac{\partial T}{\partial x} \quad (9)$$

where  $k_{sub}$  is the thermal conductivity of the substrate.

Since there is no flow inside a solid phase, the heat conduction equation through the substrate is written as:

$$\frac{\partial T_{sub}}{\partial t} = \alpha_{sub} \nabla^2 T_{sub} \quad (10)$$

In this study, the commercial finite element code CFD package Ansys CFX version 11 was used to model the solidification and spreading of droplet on the substrate. The governing equations are represented discretely in unstaggered, collocated grids and solved by

an algebraic multigrid solver for each control volume [101]. Further details about the numerical discretisation of the governing equations can be found in the Ansys manual [102]. However, the general solution algorithm for each time step is summarized as follows:

1. Determine the fluid topology by updating all the volume of fraction functions ( $F$ ). The volume of fraction of fluid is defined by solving Eq. 6 through the step function using VOF tracking method.
2. Interpolate to get the interface normal vectors and the surface curvature from the volume of fraction using the CSF model.
3. Obtain the body force from Eq. 7.
4. Solve the mass and momentum equations (Eqs. 1, 2) to get the coupled value of pressure and velocity field.
5. Solve implicit energy conservation for the droplet temperature (Eqs. 3, 4) with given liquid mass fraction ( $f_l$ ) and calculated velocity,
6. Update value of liquid mass fraction from Eq. 5
7. Update the liquid–solid boundary after a given time period based on liquid and solid mass fraction
8. Solve Eq. 9 for substrate surface temperature
9. Solve heat conduction Eq. 10 in substrate to get substrate temperature distribution.

A rectangular free surface domain for the droplet was made to be  $8r \times 8r \times 2.1r$  (where  $r$  is initial radius of droplet). The length of the substrate was chosen to ensure that the bottom

substrate temperature is constant at 25°C. Only a quarter of domains were modelled to reduce processing time. Symmetry boundary conditions were applied to two new boundaries. Adiabatic boundary conditions were used at the droplet-free surface (Fig. 1).

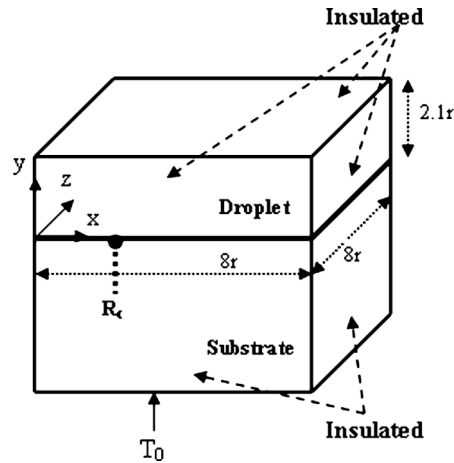


*Figure 1. Schematic of the droplet on substrate with thermal contact resistance ( $R_c$ ) at the droplet-substrate interface*

The physical properties of pure nickel droplet and stainless steel substrate are tabulated in Table 1. To improve the accuracy and stability of solution, a uniform of hexagonal mesh was used. The mesh size was set to 20 meshes for droplet radius. The same mesh size was applied for substrate domain. A very small time step of 0.5 ns was used in the model.

**Table 1. Physical properties of splat and substrate used in the simulation**

Physical properties	Ni [103, 104]	Stainless steel [103, 104]	Unit
Initial temperature	1,900	25	°C
Initial velocity	100		m.s <sup>-1</sup>
Melting point temperature	1,453	1,400-1,450	°C
Surface tension	1.78		N.m <sup>-1</sup>
Viscosity	3.3 x 10 <sup>-3</sup>		Pas
Latent heat of fusion	2.9 x 10 <sup>5</sup>		J.kg <sup>-1</sup>
Thermal conductivity of liquid	43		W.m <sup>-1</sup> .K
Thermal conductivity of solid	80	28	W.m <sup>-1</sup> .K
Specific heat capacity of liquid	620		J. m <sup>-1</sup> .K
Specific heat capacity of solid	595	690	J. m <sup>-1</sup> .K
Density of liquid	7,780		kg.m <sup>-3</sup>
Density of solid	8.450	7.854	kg.m <sup>-3</sup>

#### IV. Results

##### IV.1. XPS Results

The surface chemistry of polished stainless steel was studied using XPS. Wide scans and narrow scans were collected. Narrow scans of O 1 s, Fe 2p, and C 1 s were used to determine the oxidation state of each element. The O 1 s peak was analysed to determine

the presence of oxide and oxyhydroxide species. The O 1s peak was resolved into four different peaks representing the oxide ( $530 \pm 0.1$  eV), oxyhydroxide ( $531.3 \pm 0.1$  eV), adsorbed  $\text{OH}^\delta$  ( $532.1 \pm 0.1$  eV) and chemisorbed water ( $533.3 \pm 0.1$  eV) from lowest to highest binding energy, respectively (Fig. 2a) [59, 96]. The proportion of oxide, oxyhydroxide, adsorbed  $\text{OH}^\delta$  and chemisorbed water was estimated at about 49, 28, 18 and 5%, respectively. The presence of oxyhydroxide and chemisorbed water peaks in the polished stainless steel substrate suggested that the oxyhydroxide may be formed due to the hydration reaction of the native surface oxide with atmospheric moisture when it was exposed to the ambient condition. Under such moisture-promoting conditions, the formation of oxyhydroxide and adsorbed  $\text{OH}^\delta$  occurred through following reaction [105]:



In addition, the Fe  $2p_{3/2}$  envelopes were also fitted using Gupta-Sen multiplet peaks [59, 60, 96] to determine the presence of  $\text{Fe}^{2+}$  and  $\text{Fe}^{3+}$  in the oxide/oxyhydroxide species. They are metal peak and oxide multiple peaks which were further divided into two different peaks:  $\text{Fe}^{2+}$  and  $\text{Fe}^{3+}$  (Fig. 2b).

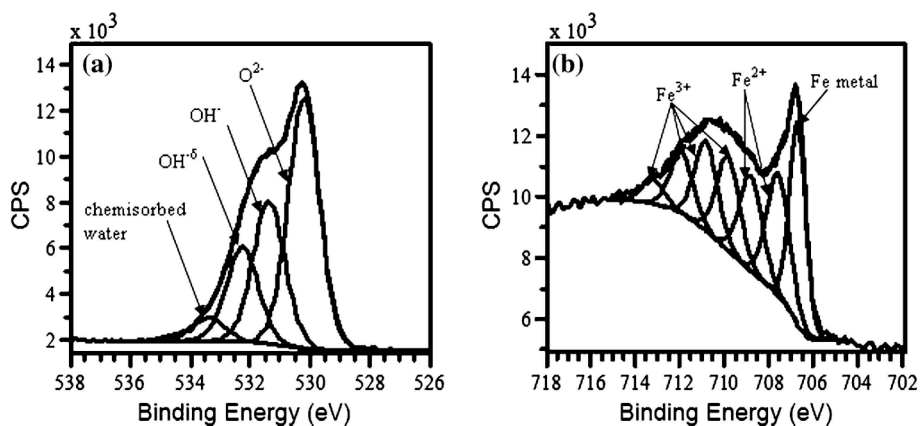


*Figure 2. Narrow scan of (a) O 1 s and (b) Fe 2p<sub>3/2</sub> photoelectron spectra of polished stainless steel substrate*

The oxide layer thickness was approximately 3.2 nm based on analytical equations in the literature [59]. It was reported that the oxide film formed when the stainless steel sample was exposed to atmosphere was oxyhydroxide at the outermost surface, together with a thin layer of Fe<sub>3</sub>O<sub>4</sub> [96, 106]. So, in summary, the outer surface film consisted of a very thin layer of FeOOH, followed by oxide layer with total thickness of 3.2 nm.

#### IV.2. Splat Characterisation

Collected splats on polished stainless steel substrates were examined in the SEM using secondary electron imaging. Five random areas with around 270 splats were analysed using ImageJ imaging software (National Institute of Health, Washington, DC) to obtain quantitative and qualitative information of splat morphologies. The obtained information included Feret diameter, area, circularity and perimeter of the individual splats. The Feret diameter is the longest distance between any two points on the boundary of the splat. Circularity is calculated by the formula  $4\pi(\text{Area})/(\text{perimeter})^2$ . A value of 1 represents to a perfect circle; the closer to zero, the more elongated the splat. A splat classification scheme was developed based on identification of splats as either ‘disk splats’ or ‘splash splats’ (Fig. 3). In addition, a central pore of various sizes was frequently observed in the disk splats. This allowed further characterisation of disk splats into two sub-categories: (a) round disk splats (Fig. 3a) and (b) doughnut disk splats (Fig. 3b). Round disk splats

are here defined as splats whose central pore diameter was smaller than 4  $\mu\text{m}$  (termed a micro-pore). Doughnut disk splats are defined as a round disk splat with a central pore larger than 4  $\mu\text{m}$  in diameter (termed a macro-pore). The image analysis results show that there were about 10.8, 34.7 and 54.5% of round disk splats, doughnut disk splats and splash splats, respectively. The round disk splats had an average diameter with standard deviation of  $\sim 40.7 \pm 10.5 \mu\text{m}$  and a circularity of  $0.69 \pm 0.11$ . Doughnut disk splats had a similar diameter and circularity compared to round disk splats, with an average diameter of  $\sim 41.5 \pm 14.2 \mu\text{m}$  and a circularity of  $0.67 \pm 0.2$ .

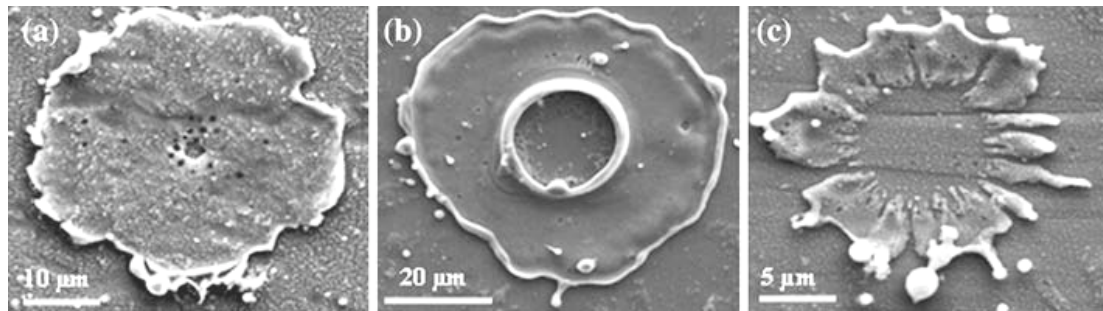


*Figure 3. SEM images of the two sub-categories of disk splat: (a) round disk splat, (b) doughnut disk splat, and (c) splash splat*

The microstructure of the splat-substrate interface was further characterised using FIB and SEM. Several FIB cross sections were made and studied for each category of splat. A typical FIB cross section of a round disk splat is presented in Figs. 4a/b. The inset image on the top right in Fig. 4a shows that FIB cross-sections were prepared at two locations: near the central pore (A) and across the rim at the periphery of the splat (B). The darker area on the top of the splat surface was the deposited platinum strip used to protect the specimen surface against the beam damage during milling. Some porous oxide can also

be observed

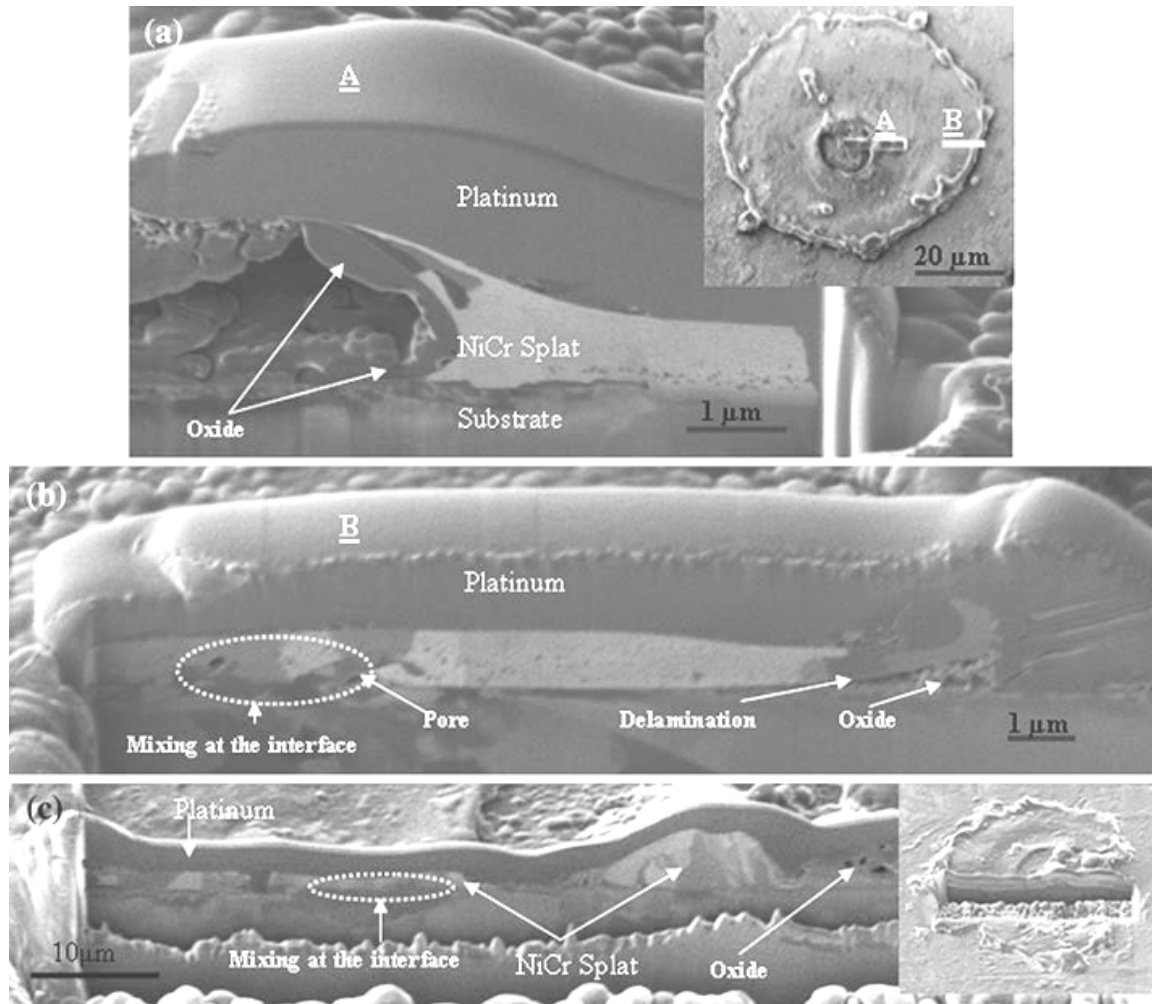


Figure 4. Cross-sectional FIB of disk splat at two locations of interest: (a) near the centre pore (A) and (b) across the splat rim (B), (c) cross-sectional FIB image of a doughnut disk splat.

The inset image on the bottom left of image shows the entire section surface of splat on the wall of the cavity near the central pore. The degree of contact between the splat and

the substrate was very high at this location (Fig. 4a). In contrast, there were some fine pores and a high degree of delamination away from the substrate at the splat periphery (Fig. 4b). The delamination at the splat periphery is probably due to the splat lifting off the substrate due to contact during solidification. The average splat thickness ranged from 1 to 3  $\mu\text{m}$ . It was also observed that oxide was formed along the periphery of the splat (Fig. 4b). The splat consisted of columnar coarse grains. More importantly, the FIB image (Fig. 4b) also indicates a local area at the splat-substrate interface where there is apparent inter-mixing of the splat and the substrate. This will be presented in more detail in the section describing the TEM data.

Another FIB image of the splat-substrate cross section was made across a doughnut disk splat (Fig. 4c). The darker area on the top of splat surface was the deposited platinum strip. The inset image on the right shows the top surface of the splat. It was evident that the splat is in good contact with the substrate. Aside from the central macro-pore, no pores were found at the splat-substrate interface. However, there are significant differences in the grain size and the grain shape of the splat along the interface. A fine-grained microstructure with a grain size of  $\sim 1 \mu\text{m}$  and columnar-oriented growth is observed for the splat towards the splat periphery. In contrast, the grains become larger and more irregular towards the centre of the splat where a porous oxide phase was also observed. Again, in local areas there is evidence of inter-mixing between the splat and substrate, indicative of substrate melting, as described in detail in the TEM section.

### IV.3. TEM Results

The very high temperature used in the plasma spray process can lead to oxidation of the splat and melting of the stainless steel substrate during impact of the NiCr splat. Detailed microstructural characterisation was performed using TEM analysis at various locations around the splat-substrate interface. Elemental mapping and line scans were also performed, using EDS, at locations of interest to investigate the elemental distribution at the interface.

The layer of platinum was deposited on the top of splat surface used to protect the specimen surface against beam damage during preparation. A range of features was clearly observed at the splat-substrate interface. On the one hand, there was a region of distinct interface between the splat and the substrate with a high degree of delamination towards the periphery of the splat (marked 1). Alternatively, there was excellent contact between the substrate and the splat near the centre of the splat (marked 2). The interface in this location appeared indistinct and blurry. The elemental line scan across the interface at the location indicated in Fig. 5b shows that the concentration of chromium across the interface region was uniform (Fig. 6). However, the more gradual change of nickel and iron curves at the splat-substrate interface suggested that there was diffusion of Ni and Fe across the interface over the distance of 100 nm approximately. Both indistinct interface and line scan results suggested that substrate melting may occur in this location. In addition, in order to locate the phases at the splat-substrate interface, EDS elemental mapping was used. Through elemental mapping around location A, as shown in Fig. 5b, it is clear that the splat-substrate interface was irregularly shaped with

the evidence of jetting of the substrate within the splat. The elemental maps of Ni and Fe show that iron from the substrate has jetted into the NiCr splat. More importantly, the diffusion of this element was in the direction of the droplet's flow and deformation along the radial direction. Furthermore, electron diffraction was also used in this zone to study the grain orientation.

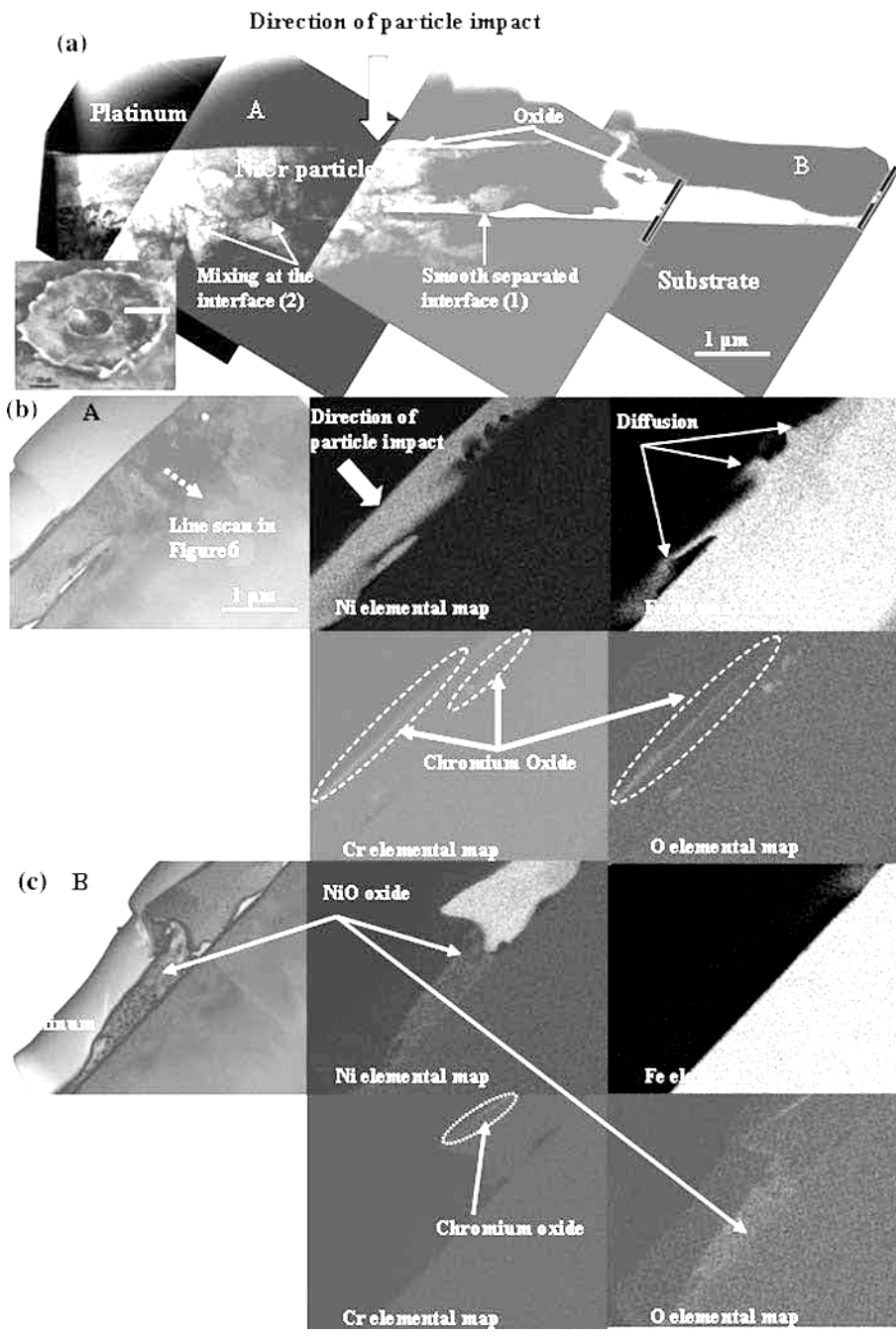


*Figure 5. (a) A bright-field cross-sectional TEM image of a NiCr disk splat with diameter of ~ 52  $\mu\text{m}$  (inset image of the disk splat at the bottom left), elemental maps of (b) region A and (c) region B*

Nickel and stainless steel have the similar lattice parameters and crystal structures, resulting in grain growth between two phases across the interface. The studies, not shown here [107], found that NiCr and stainless steel grains were juxtaposed with the same orientation across the interface. Thus, all these studies, with evidence of diffusion and jetting, suggested that substrate melting has occurred. It was also observed that oxide regions were found to accumulate at the periphery of the splat or to form as a thin layer at the outer surface of the splat (Fig. 5a). Through the elemental mapping shown in Fig. 5b/c, the identity of the oxide at the interface was clearly determined. It was suggested that a high concentration of nickel oxide accumulated at the periphery of the splat and under/around the pore and the central pore, while a very thin layer of chromium oxide has formed at the outer surface of the splat.

Extensive TEM analysis was also performed through the central pore of the splat and through various types of splats. From analysis of a range of splats sprayed on to a polished stainless steel substrate, it was found that substrate melting with diffusion and jetting between the splat and the substrate repeatedly occurred at precise locations near the centre of the splat. Nickel oxide and small amount of chromium oxide were commonly found at the centre pore, at the micro pore and at the periphery of the splat. A trace of iron oxide and chromium oxide was observed at the splat-substrate interface

where substrate melting occurred. Selected area diffraction patterns were also used in this study (not shown here) [107], to determine the structure of the oxide. Through a range of diffraction analysis, a number of oxides including NiO, Cr<sub>2</sub>O<sub>3</sub> or CrO<sub>3</sub> and FeO were observed.

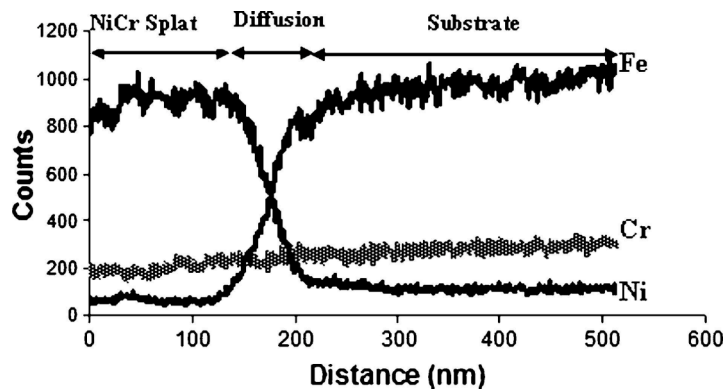


Figure 6. EDS elemental line scan across the splat-substrate interface in region A indicated in Fig. 4b

Taking into account the FIB and TEM analysis of the splat shape, pore formation at the splat-substrate interface and oxides formation at various locations, a schematic diagram of a cross section of half of a typical disk-like splat is shown in Fig. 7.

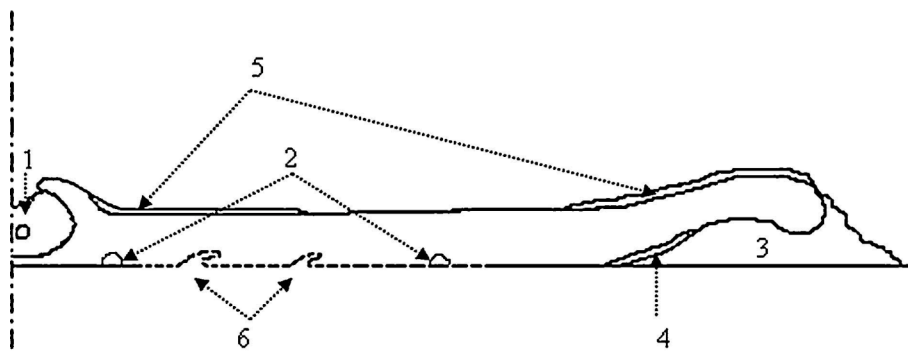


Fig. 7 Schematic of a half cross-section of a disk-like splat

The disk-like splat has a central pore and curls away from the interface at the periphery. NiO particles are present within pore at the splat-substrate interface (2), centre pore (1), and at the periphery of the splat (3). A thin layer of chromium oxide is shown at the outer surface of the splat (5). A trace of a chromium-rich phase was also found in the centre pore (1). Inter-diffusion between splat and substrate occurs in localised regions (6). In addition, trace of FeO was formed in the enclosed pores (2) and at the periphery of the splat (4).

#### IV.4. Numerical Modelling

The powder used in this study was NiCr alloy with 20% of chromium. However, due to the lack of available data for the physical properties of NiCr alloy, the properties of pure nickel were used for the model. The impact of a nickel splat on a stainless steel substrate was simulated using a free surface model with heat transfer and solidification. The solidification and the spreading process of molten splat depended strongly on the thermal contact resistance between the splat and the substrate surface [10, 13, 28]. It is well-known that thermal contact is a complex function of variety parameters, e.g. substrate surface properties, spraying conditions, the extent of contact at the substrate-splat interface. In addition, thermal contact resistance varies with time and position along the interface. Thus, to measure a real value of thermal contact resistance is impossible. Instead, a constant value of thermal contact resistance was mostly used in numerical modelling of splat solidification and spreading process. Reported values of thermal

contact resistance range widely from  $10^{-9}$  to  $10^{-5}$   $\text{m}^2\cdot\text{K}\cdot\text{W}^{-1}$  for different cases from good to poor contact between the splat and the substrate [10, 28, 34, 108].

The high proportion of disk-shaped splats collected on polished stainless steel substrates along with the occurrence of substrate melting suggests there is very good contact between the splat and the substrate. Thus, a low value of thermal contact resistance of  $10^{-8}$   $\text{m}^2\cdot\text{K}\cdot\text{W}^{-1}$  between the splat and substrate was used in the numerical model to examine the splat morphology, the splat-substrate interface and the extent of substrate melting phenomena. The splat morphology as a function of thermal contact resistance will be discussed in details in subsequent paper. The initial temperature of the droplet was chosen to ensure that the maximum temperature on the stainless steel substrate surface was higher than its melting point. However, melting and re-solidification of the substrate have been neglected in the model.

The sequence of the numerical simulation of a 20  $\mu\text{m}$  diameter nickel splat with the initial temperature of 2,400°C and velocity of 100  $\text{m}\cdot\text{s}^{-1}$  onto a stainless steel substrate held under ambient condition is shown in Fig. 8. The time measured from the moment of impact is indicated next to each frame. When a molten droplet strikes the solid substrate, the droplet velocity rapidly decreases which causes a pressure build-up at the droplet-substrate interface (Fig. 9a). The pressure at the contact point increases to a very high value (170 MPa) in a very short period of time (0.01  $\mu\text{s}$ ). Due to the very high pressure inside the droplet, the droplet deforms and spreads outwards in a radial direction to form a splat. As the droplet spreads on the substrate, the pressure is rapidly decreased. With

time, the pressure all over the splat reduces to ambient pressure.

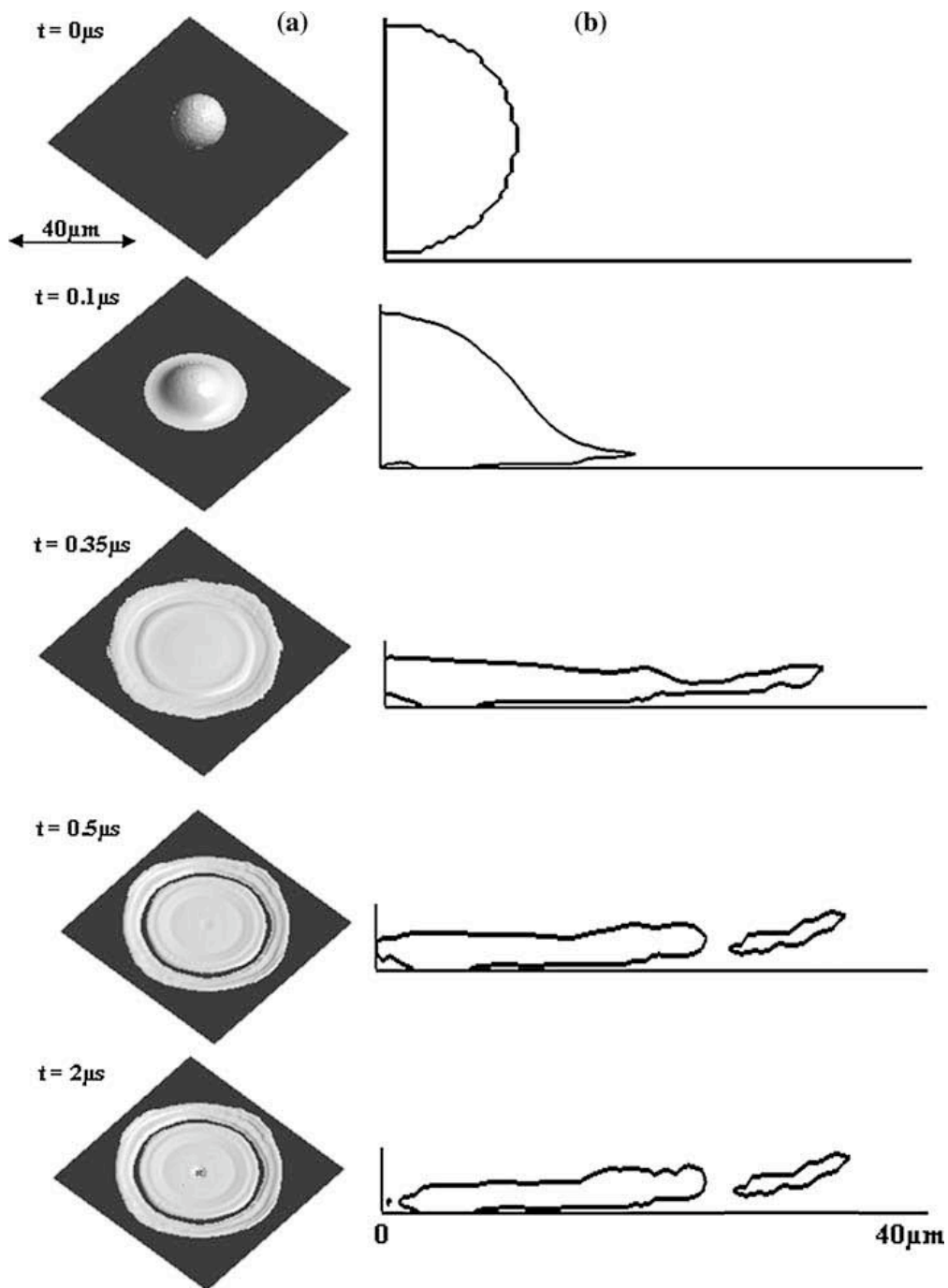


Figure 8. (a) The sequence of the numerical simulation of a  $20 \mu\text{m}$  diameter nickel splat at  $2,400^\circ\text{C}$  with a velocity of  $100 \text{ m}\cdot\text{s}^{-1}$  onto a stainless steel substrate held at  $25^\circ\text{C}$ , (b) a schematic diagram of a half cross-section of a splat

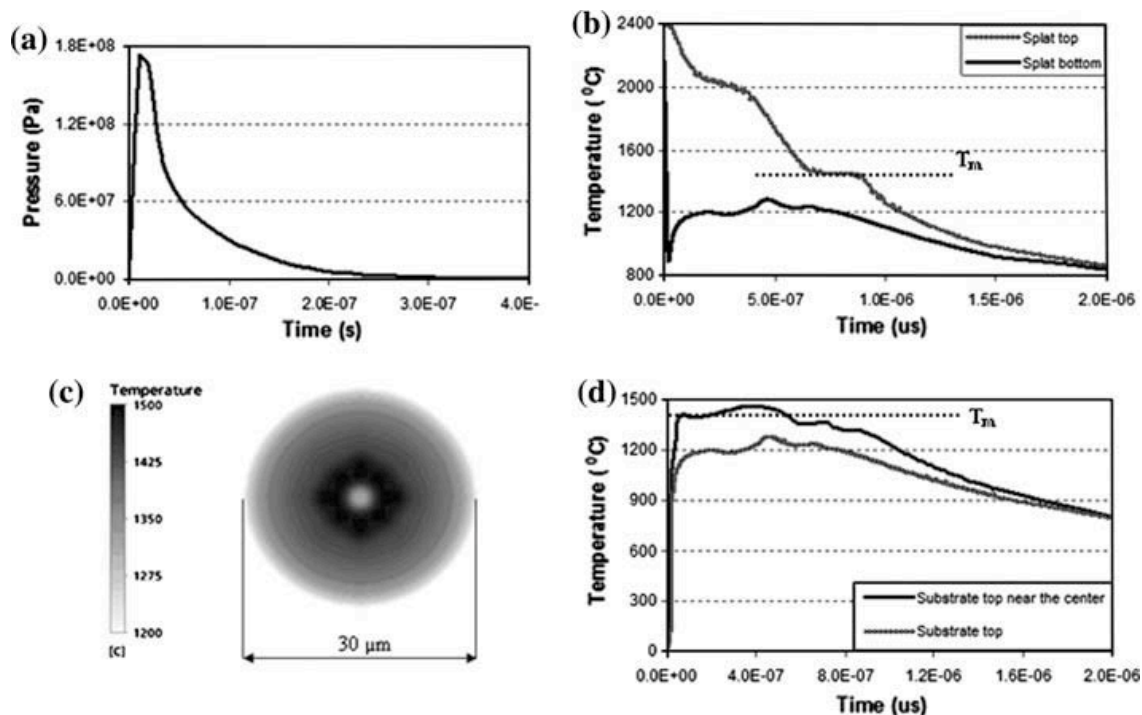
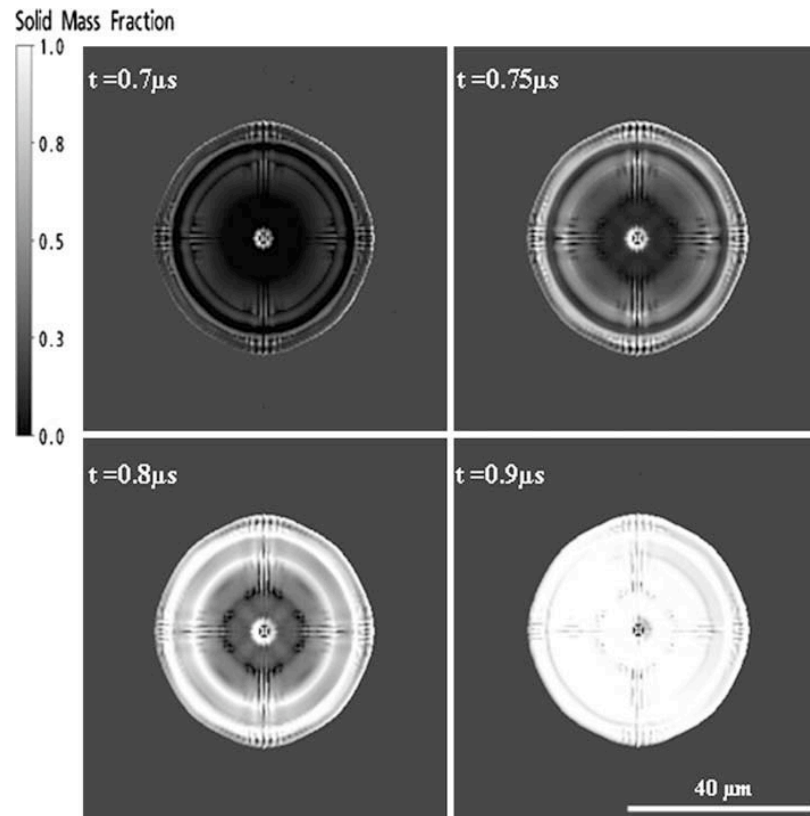


Figure 9. (a) Pressure distribution at the contact point, (b) temperature distribution of splat top and splat bottom, (c) temperature distribution of substrate surface within a radius of  $15 \mu\text{m}$  from the centre of the impact at  $t = 0.35 \mu\text{s}$ , (d) temperature distribution of substrate surface at centre and at location of  $5 \mu\text{m}$  from the centre of the impact

It was observed that immediately after impact, the temperature of the underside of the splat decreased to below the melting point of nickel (Fig. 9b). A thin layer of liquid becomes solidified at the splat underside. The upper liquid portion continues to deform and to flow over the solidified layer and spread out to a maximum diameter of  $70 \mu\text{m}$  at a time of  $\sim 0.35 \mu\text{s}$ . Because the liquid and solid portions of the splat move at differing velocities, the liquid portion of the splat detaches to form a ring (Fig. 8). Finally, the splat jets out to form a round disk-shaped splat with a diameter of  $\sim 44 \mu\text{m}$ . It is also observed

that the solidification process starts from the periphery and moves toward the centre of the splat as shown in Fig. 10. The rapid solidification at the periphery of the splat leads to the obstruction of splat flow, causing the thicker part at the edge (Fig. 8).



*Fig. 10 Solidification front advancing of splat with time*

It was observed from the half cross-section of the splat (Fig. 8b) that a central pore was formed in the early stages of the splat spreading. The formation of this central pore is expected due to the change of the surface curvature of the droplet. When the droplet hits the substrate, a high pressure builds at the point of contact. Thus, the normal pressure gradient from the contact point towards the free surface of droplet was positive, resulting in a concave curvature (Eq. 8). A centre micro-pore with a diameter of 1.5 μm

approximately was also observed. A gas cavity was also formed between the splat and the substrate within 8  $\mu\text{m}$  distance from the centre of the splat.

Curling up at the edge of the splat was observed with a curl angle of  $\sim 8 \pm 1^\circ$  (Fig. 8b). Splat curling at the periphery is frequently observed in the previous experimental part. The phenomenon can be explained by the stress generated by thermal expansion mismatch at the splat-substrate interface, or from the surface tension of the splat droplet. Thermal stress was not included in the model, but nevertheless, curling is still predicted. Thus the splat curling up in Fig. 8b can be explained solely on the basis of surface tension which was assumed to be the dominant factor.

It was found from the modelling that, the contact pressure rapidly decreased during the droplet spreading. Particularly, the contact pressure at the periphery (0.1 MPa at 0.01  $\mu\text{s}$ ) was significantly smaller than that at the central splat (170 MPa approximately). Thus, the impact pressure at the periphery of the splat is not enough to overcome the capillary pressure required to force liquid into the surface crevices where it would otherwise solidify and bond to the substrate. Without this bond, the splat edge could not be kept in place against the surface tension which pulls the splat edge inwards. The direction of the surface tension force vector in this model is consistent with previous work [109], resulting in the curling up of the splat at its perimeter.

The temperature distribution through the splat cross-section is shown in Fig. 9b. The bottom surface of the splat is located at the centre of the impact at the splat-substrate

interface. The top surface of the splat is located 1  $\mu\text{m}$  above the centre of impact. It was observed that when the splat interacted with the colder substrate surface, the temperature of the bottom of the splat quickly dropped below the melting point of 1,453°C and so a thin layer of solid was formed. However, due to the high temperature of the top of the splat, the temperature of the bottom of the splat then increased through thermal conduction, but remained below the melting point. Heat then transferred from the hot splat to the colder substrate. The temperature of the top surface of the splat rapidly decreased to the melting point after 0.7  $\mu\text{s}$ . The cooling rate is highest at this time. The top of the splat then started to solidify. During the solidification process, its temperature was unchanged and the solidification process completed after 0.9  $\mu\text{s}$  approximately. The solidified splat continued to cool for a further 2  $\mu\text{s}$ . The average cooling rate was estimated from the temperature history to be  $\sim 8 \times 10^8 \text{ }^\circ\text{C}\cdot\text{s}^{-1}$ .

Because stainless steel has a very low value of thermal diffusivity ( $5 \times 10^{-6} \text{ m}^2\cdot\text{s}^{-1}$ ), most of the heat is retained at the surface: this retards the conduction of the heat front to the bulk. The substrate surface was heated from the impacting splat to a sufficiently high temperature for sufficient time, resulting in substrate melting phenomena, where its temperature reaches the equilibrium melting temperature of the stainless steel. Once the substrate melts, a thin layer of liquid substrate was pushed ahead of the interface toward the NiCr splat in order to establish an equal distribution of internal energy [110]. More importantly, due to the formation of the central pore, the splat-substrate interface changes from one in contact to one in non-contact. As a result, the temperature at the centre of the splat is no longer highest. The distribution of temperature of the substrate surface is

shown in Figs. 9c/d. Thus, the simulation confirmed that the substrate melting was restricted to the locations near the centre of the splat.

## V. Discussion

To predict the possibility of substrate melting when molten droplets impact the substrate, Li *et al.* [36] developed a one-dimensional numerical model and proposed a “temperature factor” as an index for substrate melting. This factor was a function of droplet and substrate temperature and their thermal properties. Based on this suggestion, the interface temperature between the stainless steel substrate and nickel splat, in our case, was  $\sim 1,300^{\circ}\text{C}$ . Thus, substrate melting was not expected to occur for nickel chromium on a stainless steel substrate. However, our three-dimensional numerical model shows that the interface temperature increased to  $1,465^{\circ}\text{C}$  shortly after contact was made, which was higher than substrate melting point. As a result, substrate melting occurred. The disagreements between Li *et al.* [36] and our results may be due to the lack of convective heat transfer due to impact and the over-simplifications of uniform splat thickness in the one-dimensional model which leads to an under-prediction in the interface temperature. Thus, to examine splat morphology and the potential of substrate melting, a full three-dimensional numerical model with heat transfer and solidification is more accurate and more applicable.

In this study, splats with central pore of various sizes were frequently observed. This structural feature was characterised for the typical disk splat shape when NiCr particles

were plasma-sprayed onto a polished stainless steel substrate. Splats with a central pore have been occasionally observed during thermal spray processing [18, 111-113]. Li *et al.* [112] suggested that the central pore formation was due to either the rebound of the solid core of a partially melted powder particle or due to moisture release at the splat-substrate interface. Mehdi-Nejad *et al.* [92] modelled the motion of molten nickel on a flat surface and observed the formation of central pore. However, the simulation was incomplete due to the lack of the heat transfer between the splat and substrate. From our simulation, it was predicted that immediately after impact, the pressure at the contact point increased to a very high value which induced a concave curvature towards the free surface of the droplet. A bubble then rises up through the liquid film and then breaks through the free surface to form the micro-pore at the centre of the splat. Based on this mechanism, a central micro-pore with a diameter of  $\sim 1.5 \mu\text{m}$  is predicted.

Experimentally, however, both micro-and macro-pores were observed. While the micro-pore formation can be explained by pressure-induced concave curvature of the droplet, an additional mechanism is needed to explain the formation of the larger pores observed in doughnut splats. Experimental evidence, outlined below, suggest that the release of water vapour from the surface of the substrate plays an important role.

The surface layer of polished stainless steel is partially composed of physisorbed water and oxyhydroxides [113]. Oxyhydroxides on the substrate surface readily dehydrate, releasing water vapour as a product, and converting to oxide when the substrate surface temperature rises above  $300^\circ\text{C}$ . The simulations show that when the molten droplet

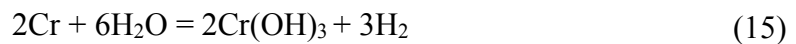
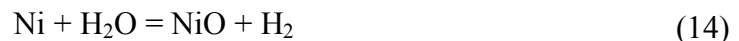
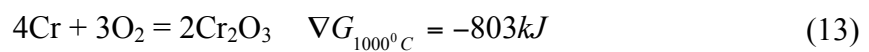
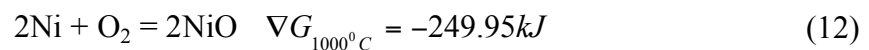
impacted on the substrate, the substrate temperature rapidly increased to temperatures significantly higher than 300°C (Fig. 9) in the initial period of impact. As a result, the dehydration of oxyhydroxide layer on the substrate surface can occur, releasing water vapour in the process. The water release will generate a gas layer between the substrate and the droplet, which would probably increase the thermal contact resistance. However, how the contribution of the water layer on the thermal contact resistance and on the splat morphology were not considered in this paper. During micro-pore formation due to high contact pressure, the released water vapour may either fill the enclosed pores or escape at the periphery of the droplet. The accumulation of water vapour released was highest at the centre of the splat and expanded the micro-pore which finally exploded to form a centre bubble-like pore which was characteristic of doughnut disk splats. Thus, it was suggested that the micro-pores and macro-pores were formed due to, respectively, the pressure build-up at the splat-substrate interface and the water release at the substrate surface.

The doughnut disk splat is characteristic of the impact of the droplet on the substrate with water release. In contrast, the micro-pores at the centre of splat are characteristic of clean substrate surface. Those findings are also consistent with our previous experimental results that the percentage of round disk splats on a substrate significantly increased with a decrease of oxyhydroxide proportion. For example, on polished stainless steel substrate with a high proportion of oxyhydroxide, about 45.5% of disk splats were collected [49] whereas 97.4% of disk splats were collected on polished and preheated substrate with a significantly lower proportion of oxyhydroxide on the outermost substrate surface.

Although the effect of the flow of the water vapour was not considered in this paper, it is likely to affect the spreading ability of the liquid splat and to distort splat morphology. It was experimentally observed that doughnut disk splats had a larger diameter and less regular shapes than disk splats.

The high temperature of plasma spray can promote oxidation of the droplet. It was reported that the formation of oxide during plasma spraying can take place either in flight or after impact during splat cooling [66, 114]. When the NiCr particle is oxidised,  $\text{Cr}_2\text{O}_3$  formation is thermodynamically more stable than NiO (Eqs. 12, 13). In contrast, the rate of the  $\text{Cr}_2\text{O}_3$  formation is smaller than that of the NiO formation by nearly three orders of magnitude. Thus, NiO formation is kinetically more favourable than  $\text{Cr}_2\text{O}_3$  formation. It was confirmed that kinetics are a dominant factor contributing to the oxidation of NiCr alloy [115-118]. Thus, a continuous layer of NiO was expected to form at the outermost surface if the particle was oxidised. In the case of in-flight oxidation in plasma spraying, several groups [66, 114, 117, 119, 120] have presented evidence of the oxide segregation towards the front surface of the particles to form an oxide shell for different plasma sprayed materials such as nickel, steel and iron. The accumulation of oxide at the front surface was attributed to the difference in viscosity between liquid metal and its oxide. With respect to the formation of oxide shell at the front surface of the droplet during flight, when the oxidised molten droplet strikes the substrate, the continuous layer of NiO spreads underneath the metal splat along the radial direction. Thus, it was expected that a thin layer of NiO was formed at the interface and accumulated at the periphery of the

splat. However, the observation of a thin layer of chromium oxide at the outermost surface of the splats and a significant amount of NiO found in specific locations: such as in enclosed pores, at the centre bubble-like holes and at the periphery of splats implied that the principal oxidation process occurs at the substrate surface. It was expected that the water vapour released from the dehydration of oxyhydroxide on the substrate surface was either trapped in enclosed pores at the splat-substrate interface or flowed in radial direction toward the periphery of the droplet. Thus, these special locations contained species such as H<sub>2</sub> and H<sub>2</sub>O in an oxidizing atmosphere which sets up a redox system to transfer oxygen across pores. With the presence of this redox system, the oxidation reaction rate of Ni to form NiO noticeably increased [115] (Eq. 14). In addition, the presence of chromium oxide in insignificant amounts in those specific locations was due to the formation of hydrated species which easily vaporized [115] (Eq. 15). The formation of thin layers of chromium oxide on the outer surface of the solidifying splat was due to the diffusion of chromium from the splat to form the most thermodynamically stable oxide with a passage of time.



The temperature distribution of the substrate confirmed that substrate melting phenomena can occur in the case of good contact between the droplet and the substrate. However,

due to the formation of the central pore, the highest temperature was at the locations between the central pore and the periphery of the splat. Thus, substrate melting was supposed to occur at those locations. When the substrate melting occurred, the liquid substrate was pushed up towards the splat to form the interlocked structure shown in Figs. 4 and 5. The diffusion of atoms from the substrate into the splat significantly improved the bonding.

## **VI. Conclusion**

The impact of NiCr particles onto polished stainless steel substrate during plasma spraying has been studied experimentally and numerically. A disk splat shape with a central pore of various size is characteristic of these spray conditions. The formation of chromium oxide at the outermost surface and the frequency of nickel oxide formation, particularly in enclosed pores, at the centre bubble pore and at the periphery of splat, suggest that the principal oxidation process occur at the substrate surface where the splats are exposed to the water vapour-rich environment due to the conversion of oxyhydroxide to oxide on the substrate surface. It was also observed that the substrate is melted and locally diffuses into the splat at certain regions to form interlocking features. The formation of iron oxide along with nickel oxide in enclosed pores and at the periphery suggests that the substrate melting may occur, which enhances the bonding between splat and substrate. The occurrence of substrate melting along with diffusion and jetting of the substrate contributes to the bonding mechanism for NiCr alloy particles plasma-sprayed onto stainless steel substrate.

A three-dimensional numerical model with free surface deformation and heat transfer has been developed using couple-solvers (Ansys CFX packages) to simulate the impact of nickel splat onto stainless steel substrate during plasma spray. A low value of thermal contact resistance was used to study the splat shape and the possibility of substrate melting. The obtained temperature distribution of substrate as a function of time and locations was more accurate and more applicable than one-dimensional model [36]. The simulation results illustrate good agreement with the experimental observations. Particularly, the simulation can explain the formation of the central pore and the locations of substrate melting. With substantial information from the simulation, the mechanisms of the pore formation can be clarified.

## CHAPTER 7

# STUDY OF THE SPLAT FORMATION FOR HVOF SPRAYED NiCr ON STAINLESS STEEL SUBSTRATES AND THE EFFECTS OF HEATING AND BOILING PRE-TREATMENTS

---

*S. Brossard, P.R. Munroe, M.M. Hyland, Journal of Thermal Spray Technology (in publication), 2010*

### Abstract

The HVOF process is a widely applied thermal spray technique used to form dense coatings with high bond strength. However, little is known about the mechanisms by which the coating forms and adheres to the substrate. The present study investigates the splat formation process by examining the morphology and microstructure of NiCr single splats sprayed on to stainless steel, using a range of electron microscopy techniques. Notable features include evidence of the deformation of the steel substrate by the impacting particle, the presence of porosity towards the centre of the splat, and under the rim due to the curling-up of the splat, and the identification of several oxide phases, including  $\text{Cr}_2\text{O}_3$ , FeO and NiO. From these observations, a description of the splat formation process is proposed. Effects of the substrate surface chemistry were studied by

comparing the morphology of the splats on several substrates having undergone various pre-treatments.

## **I. Introduction**

The High Velocity Oxy-Fuel (HVOF) spray process allows the manufacturing of coatings of a very wide range of materials (ceramics, metallic alloys, polymers) on a range of substrates, by spraying a fine powder through a mixed oxygen/fuel gas (hydrogen, heptane, kerosene, etc.) flame. The coatings produced, typically, have high bond strength and a dense microstructure in comparison to other thermal spray processes for which particles may be sprayed at higher temperature and lower velocities. Other advantages include higher coating thickness capacity, a smoother surface finish, lower porosity content and a lower concentration of oxides in the coating. [1, 4]

Many properties (mechanical, thermal, dielectric, resistance to corrosion, etc.) of the finished coating depend significantly on its microstructure and its interaction with the substrate. Microstructures of thick HVOF coatings have been widely studied [40-42] and it has been shown that they depend on several factors, such as the feedstock powder and spray conditions [37, 38]. The mechanisms of coating formation are, however, not fully understood. Studying single splats, specifically their formation and their interaction with the substrate, is essential in obtaining a more complete understanding of coating formation to allow optimization of spray conditions.

One notable characteristic of the HVOF process is that, depending on the materials used as feedstock powder (nature and size), the substrate (particularly its hardness) and on the spray conditions (which influence particle temperature and velocity/momentum), splats may form on the substrate either in a fully melted state, in a partially melted state or in a non-melted (i.e. solid) state [37, 38]. These three different states may then be found to be present together within a single coating, giving the coating a bimodal microstructure with a mixture of melted and non-melted zones [40-42].

Splat formation, in circumstances where the particle impacts on the substrate in a non-melted state, may be compared with the cold spray process. That is, the interaction between substrate and particle upon impact depends significantly on the particle velocity or momentum; if the particle velocity is above a critical value, the particle and/or substrate will undergo plastic deformation as the kinetic energy of the particle is transformed into mechanical deformation and thermal energy. Adhesion of the particle on to the substrate may include the phenomena of mechanical interlocking and adiabatic shear instability (that is, there is localized deformation at the particle-substrate interface) [44-46].

Conversely, the situation where the particles impact the substrate in a fully melted state may be more readily compared to the plasma spray process. Splat formation for this process has been more widely studied through modelling, studies of splat splashing, and investigations of the possibility of substrate melting [2, 20, 35, 36, 50, 67].

However, studies on the splat formation specifically associated with the HVOF process, in particular where the particles impact the substrate in a semi-melted state, are relatively limited. Trompetter *et al.*, who HVAF sprayed NiCr particles on to a range of substrates with differing hardnesses, observed three distinct types of splats, ranging to fully melted to non-melted, and that their proportion was influenced by the substrate hardness. However, they did not investigate, in detail, either the splat microstructure or the splat-substrate interface [39]. Another study performed by Guilemany *et al.* examined the substrate-coating interface for a fully deposited WC-Co coating HVOF sprayed on both a polished and a grit-blasted Cu substrate. They found that at the coating-substrate interface a layer of very fine grains. The layer thickness was thinner for the smooth substrate, and somewhat thicker for the grit-blasted substrate. This was interpreted as evidence of substrate melting upon impact of the WC-Co particles [43]. Lastly, a model proposed by Sobolev *et al.* studied the effect of in-flight oxidation of the particle on the splat formation during the HVOF process, leading to the conclusion that this oxidation leads to an increase in splat thickness, with a decrease in both the splat radius and in the pressure developed upon impact. As a result, the splat and substrate made less contact and consequently a decrease in the adhesion and increase in porosity was observed. However, this effect was noted to be in competition with an increase in the wetting of the splat on the substrate due to the oxygen dissolved in the particle [121].

This study was motivated by the current lack of understanding concerning the splat formation in the HVOF process and the influence of surface chemistry on this process. In this study, NiCr (an alloy often used in thermal sprayed coatings as bond coat or for

protection of steel against heat, corrosion [122], erosion, for example in boilers [1]) was HVOF sprayed on to stainless steel substrates. These substrates underwent various pre-treatment, such as polishing, heat treating and/or boiling in distilled water. The aim of these pre-treatments was to create different substrate surface conditions, in terms of chemistry and roughness. This, then, allowed an investigation of how the substrate conditions may affect splat morphology and the mechanisms of splat formation. The splat microstructure and its interface with the substrate were investigated using a range of microscopy techniques and related to both the spray conditions and substrate chemistry.

## II. Experimental procedure

Four different substrates were used; all prepared from 304 L stainless steel. These are listed in Table 1.

**Table 1. Substrate Nomenclature and Condition**

<b>Specimen</b>	<b>Substrate</b>	<b>Pre-treatment</b>
SS_P	Stainless steel 304	Polished (to a nano-scale smoothness)
SS_PT	Stainless steel 304	Polished and thermally treated
SS_B	Stainless steel 304	Boiled
SS_BT	Stainless steel 304	Boiled and thermally treated

All substrates were firstly mechanically ground and mirror polished with diamond paste, to a nano-scale roughness. The boiled substrates were placed into boiling distilled water for 30 min, while the thermally treated substrates were heated at 350°C for 90 minutes in

air. The aim of these treatments is to form surface oxides (or hydroxides for the boiled specimens) and/or to induce some level of surface roughness. All treatments were performed at least several hours before spraying.

The sprayed material was a commercial NiCr alloy powder (Ni80-Cr20, Sulzer Metco 43 VF-NS, Switzerland, (+45, -5  $\mu\text{m}$ )). HVOF spraying was carried out with a Sulzer Metco (Switzerland) Diamond jet (DJ-2600) gun, fuelled with air at 160 psi and propylene at 110 psi. The feeding rate of the powder was of 26g/min, the carrier gas being nitrogen at 140 psi. A single swipe pass was made, at the velocity of  $0.4 \text{ m}\cdot\text{s}^{-1}$ , and at a spray distance of 266mm.

The specimens were then characterized using a range of analytical techniques. A Hitachi S3400 scanning electron microscope (SEM) was used to image the overall morphology of the splats and the substrates. A FEI xP200 Focused Ion Beam microscope (FIB) was used to mill cross-sections of the splats using an energetic gallium ion beam, and to image them using secondary electrons induced by the ion beam. Details have been described elsewhere [51]. A FEI xT Nova Nanolab 200 dual beam microscope (that is a FIB and SEM combined into a single instrument) was used to prepare cross-sections of splats (100-200nm in thickness) suitable for TEM observation. These were prepared using the lift out method as described elsewhere [51] and examined in a Philips CM200 transmission electron microscope (TEM) to which energy dispersive x-ray spectroscopy (EDS) facilities have been interfaced.

A number of FIB and TEM cross-sections were made and studied, at least one for each particular feature and/or type of splat, but only a small number of representative images will be presented here. The preparation of cross-section involves the deposition of a layer of platinum on top of the area of interest prior to milling for protection purposes. This layer is then present in the images shown here.

### III. Results and discussion

#### III.1. Description of the different types of splats observed by SEM

SEM images of 50-60 splats were observed for each specimen. From these observations it was noted that the majority of the splats observed, for the all four substrates, appeared to be formed from fully melted NiCr and presented a mainly disc-shaped morphology. Figure 1 presents typical SEM images of the different splats found for the various substrates. Amongst these splats, two types can be seen: large fully melted splats (diameter between 30 and 200  $\mu\text{m}$ , see Figs. 1a to 1d), with a shallow depression in their centre (marked 1 on Fig. 1b), and small fully melted splats (diameter usually between 10 and 30  $\mu\text{m}$ , see Fig. 1e), with no depression observed. Evaluating the diameter  $D$  was performed by taking the smallest and largest diameter value measured from the splat, which is not perfectly circular, and calculating the average value; features such as splashed fingers were ignored (see for example Fig. 1d). The large fully melted splats shown were found to present differences principally in the morphology of their rim, which may be either significantly irregular, with a granular or dendritic aspect (Fig. 1a), or quite smooth with thin splashed fingers (Fig.1b), or smooth with a surface that has

become irregular and undulating (Fig. 1c) or finally very irregular with some radial cracks (Fig. 1d).

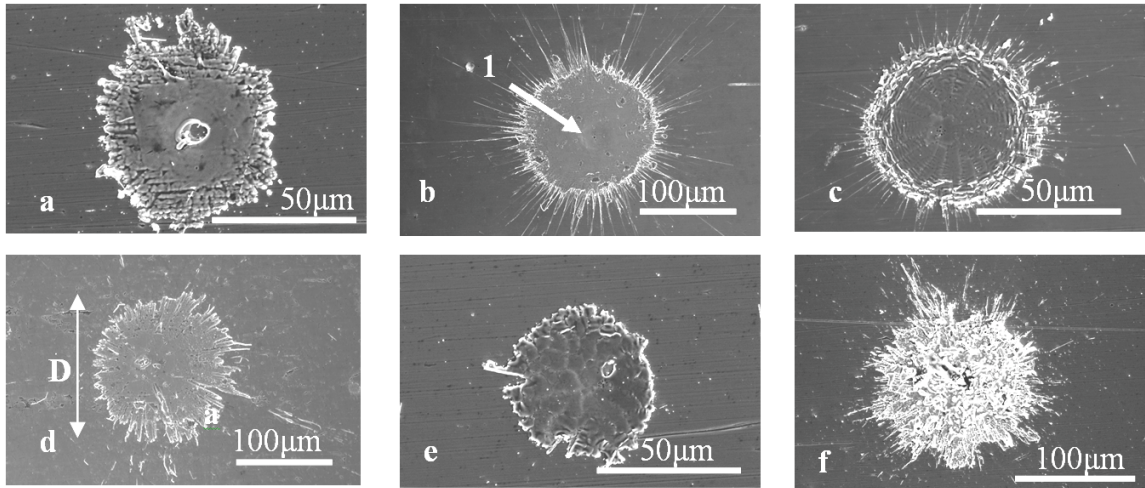


*Figure 1. SEM images of the different types of splats: large fully melted splat (a) with a irregular dendritic/granular rim, (b) with a smooth rim and thin splashed fingers, (c) with a rim displaying an undulating surface, (d) with an irregular rim with radial cracks, (e) small circular splat, (f) partially melted splat*

For the all four substrate conditions, a small number of splats (~ 8%) appeared to have formed from a partially melted particle. Figure 1f displays a SEM image of such a splat. These are usually disc-shaped; such splats apparently consist of a mixture of non-melted fragments within a melted matrix. Their diameter ranged from ~70 to ~210  $\mu\text{m}$ .

### III.2. Structure and formation of the large fully melted splats

#### III.2.a. *Description of their microstructure as observed by FIB and TEM*

For these large fully melted splats, a number of characteristic features were observed which were noted for all four substrates.

Firstly, the substrate at the centre of these splats always exhibited a depression, or shallow crater. For example on the FIB cross-section presented Fig. 2, towards the centre of the splat it can be noted that the splat-substrate interface is curved (marked 1). Also, porosity is almost always found towards the centre of the splats, near the splat-substrate interface. For the cross-section in Fig. 2, at the centre of the splat, a large single pore (marked 2), together with a number of some smaller pores (marked 3), can be observed. Large pores were not always present. Instead, some smaller pores may be observed, such as for the splat whose TEM cross-section is displayed in Fig. 3 (marked 1).

Another important feature is the splat-substrate interface. In the large fully melted splats, the contact between splat and substrate was usually very good, such as for example Fig. 2 (marked 4), at least away from the rim of the splat. TEM study of the splat-substrate interface, for example Fig. 3, shows that the interface appears quite distinct in the bright field TEM images (marked 2). However, the elemental linescan performed across the same interface showed the presence of an interdiffusion zone between Ni and Fe over distances of up to 200nm, depending on the exact location of the linescan. In most cases, the interdiffusion is significant where the interface becomes slanted towards the

periphery of the crater (marked 3 on Fig. 3, 150nm), while there is no, or limited, interdiffusion, observed at both the centre of the splat or closer to the splat rim.

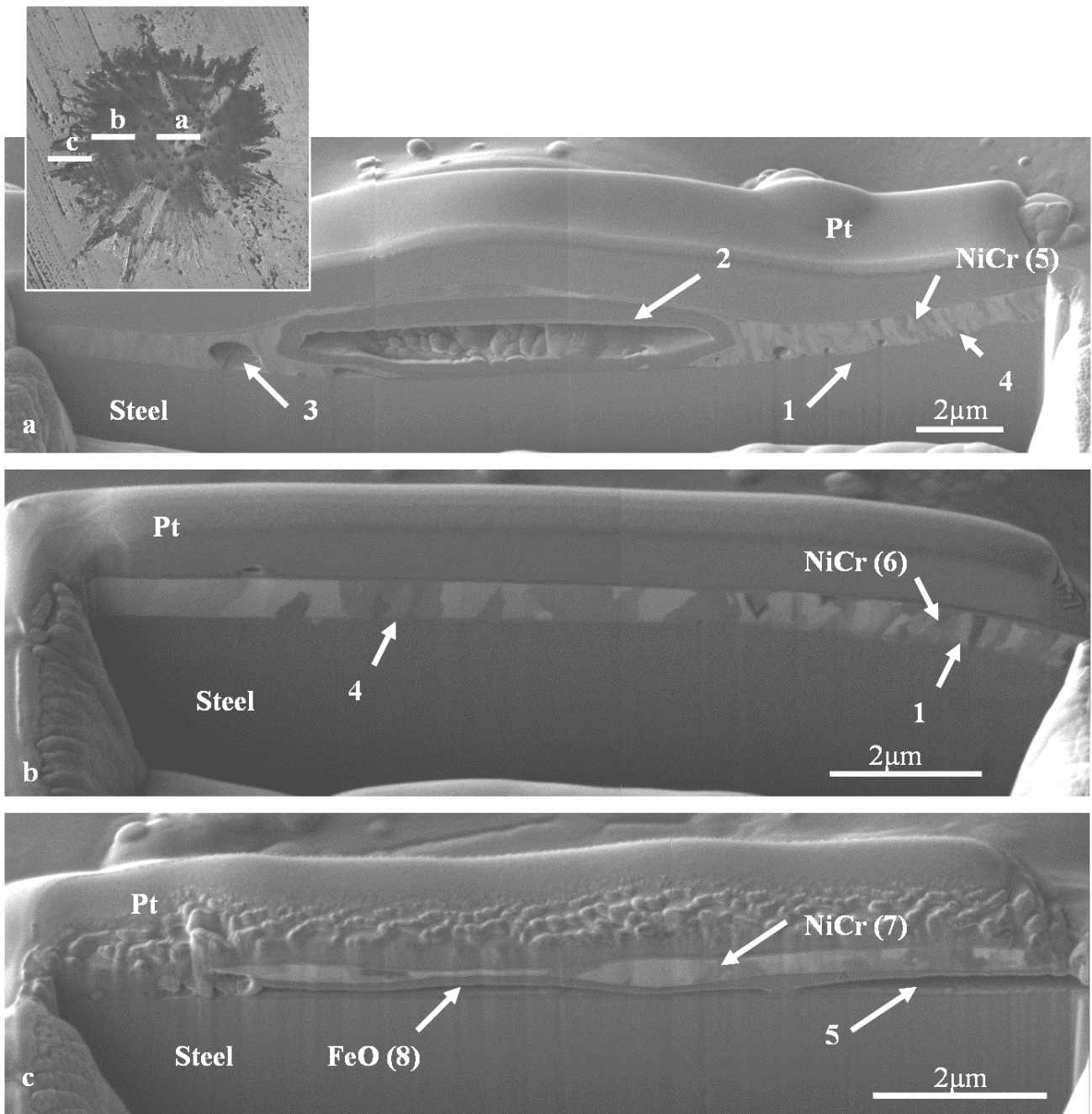


*Figure 2. FIB cross-sections on a fully melted splat with an irregular rim (the insert image shows an image of the splat in plan view before sectioning) found on SS\_P, (a) across the centre, (b) across the rim of the crater and (c) across the rim of the splat*

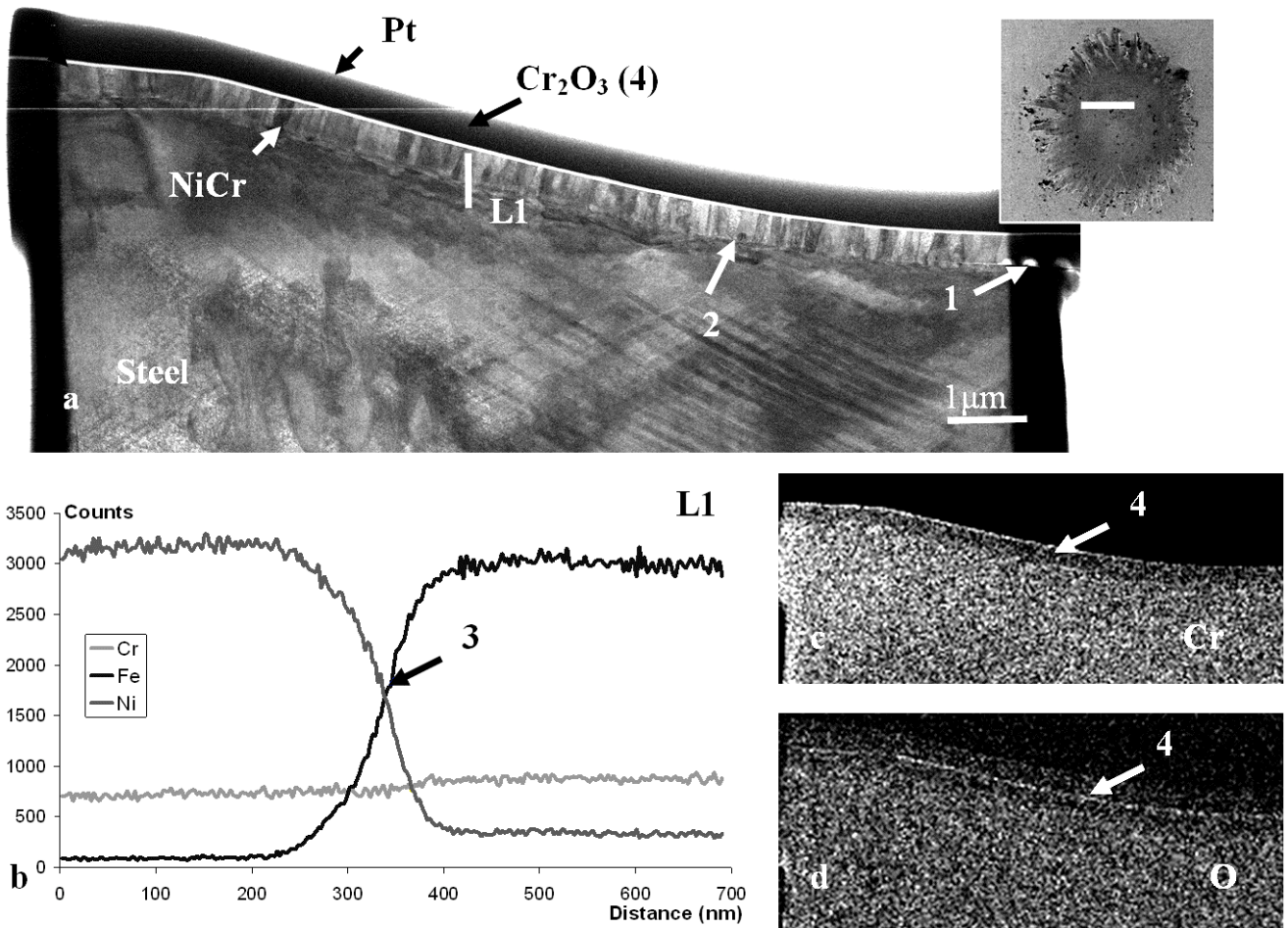
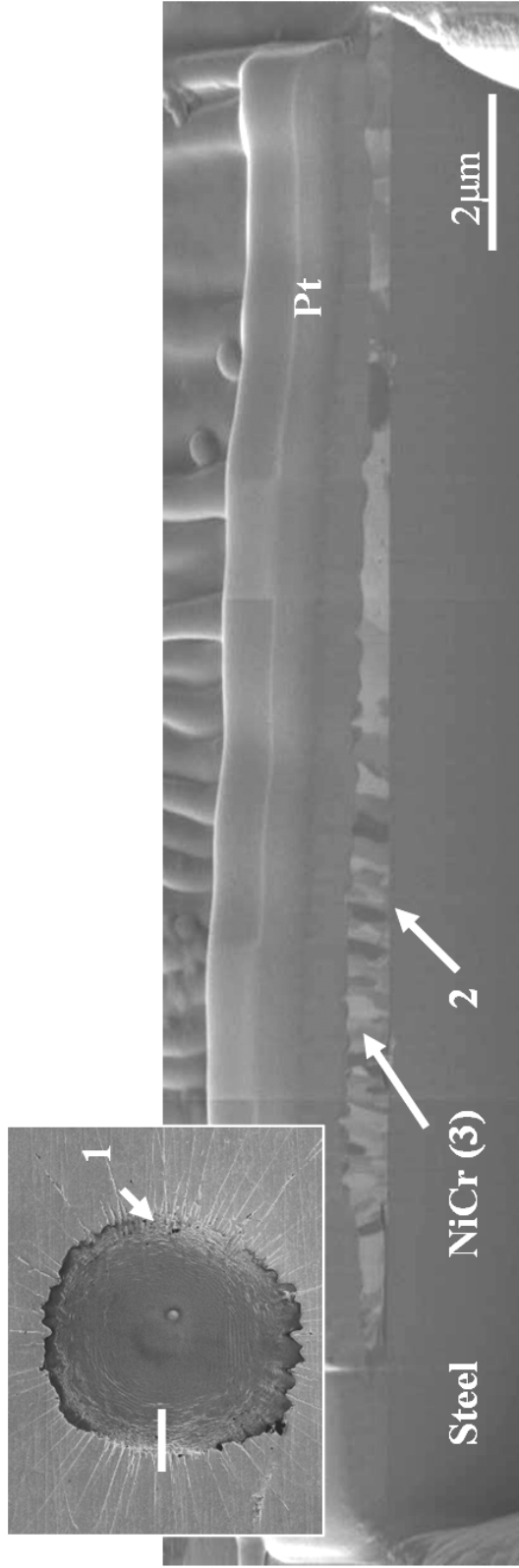


Figure 3. TEM cross-section across the centre of a fully melted splat found on SS\_P (see inset image): (a) bright field image, (b) elemental linescan across the splat-substrate interface at the region L1, elemental maps for (c) Cr and (d) O

The splats' rims, as noted in the SEM images, may differ from splat to splat. On Fig. 2c, one can observe the structure under an irregular rim, where delamination has clearly occurred (marked 5). On the other hand, figure 4 displays a FIB cross-section of the rim of a splat showing an undulating outer surface towards the splat periphery (marked 1). Here, the contact between substrate and splat is good (marked 2).



*Figure 4. FIB cross-section across the rim of a splat found on SS\_PT and presenting a undulating outer surface close to the splat periphery (see insert image)*

Observation of the grain structure is consistent with the previous comments. For example in Fig. 2, inside the crater the grain structure is fine and columnar (marked 6), which is consistent with the good contact between splat and substrate, since this is an indication of rapid solidification and effective removal of the heat through the substrate. Towards the periphery, however, the grain structure becomes coarser and more equiaxed (marked 7): the solidification rate in this region must have been lower and, correspondingly, the contact between splat and substrate is poorer (marked 5), preventing efficient heat removal through the substrate. On Fig. 4 however, the contact is better at the periphery, thus the grain structure is much finer (marked 3).

Several oxide phases were identified in characteristic locations around the splat. First, nickel and iron oxides were found to often form in the pores found at the centre of the splats. In large pores, a thick and dense layer was often observed to cover the walls of the pores, such as that seen on Fig. 2 (marked 2), but also visible on Fig. 5 (marked 1).

Such a layer was identified using TEM as being FeO: the EDS elemental maps (see Fig. 5d and e) show that Fe is present in the layer (O is present as well, but EDS is less sensitive to the presence of oxygen), and the electron diffraction pattern obtained from this region is consistent with FeO (see diffraction pattern Fig. 6a).

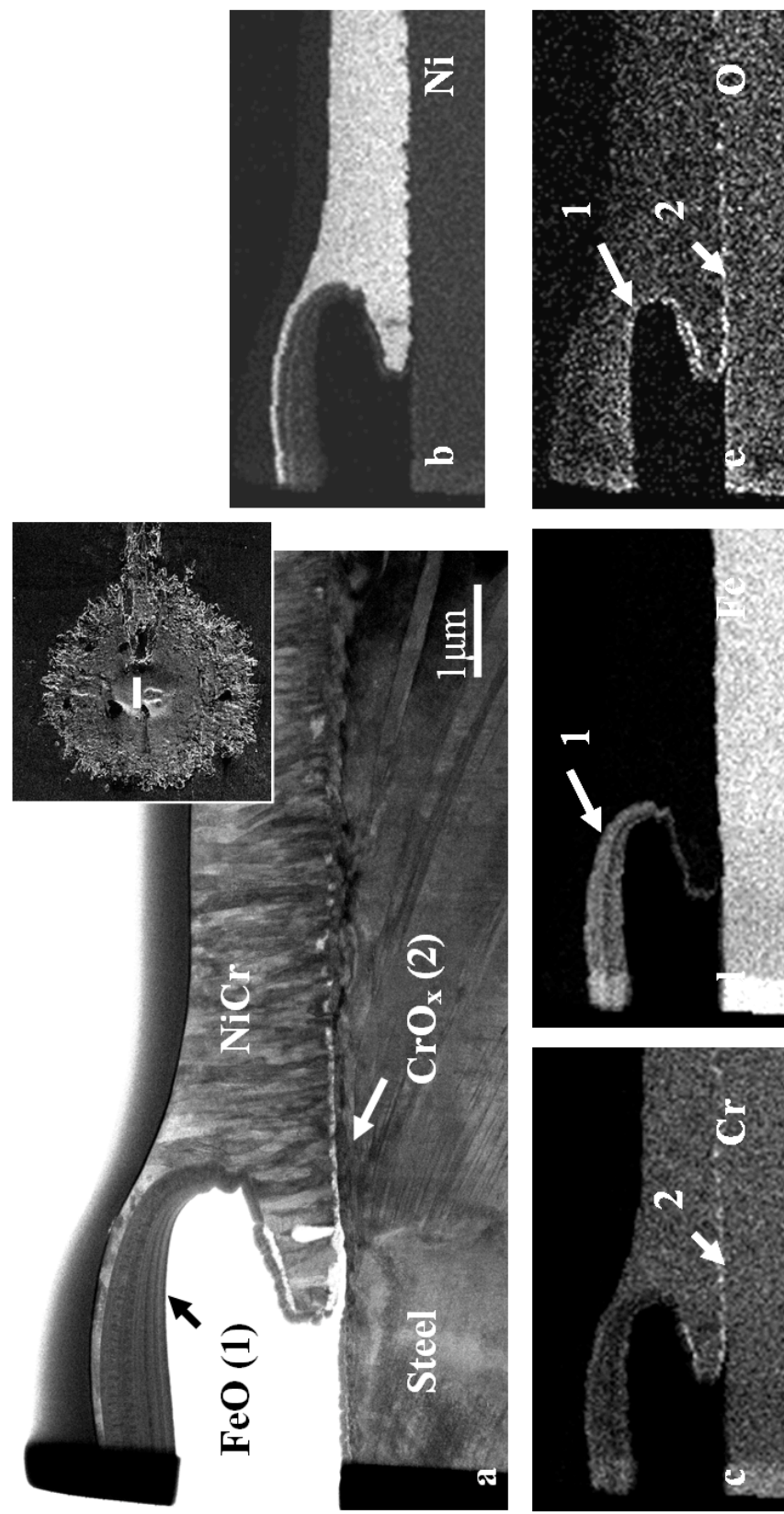
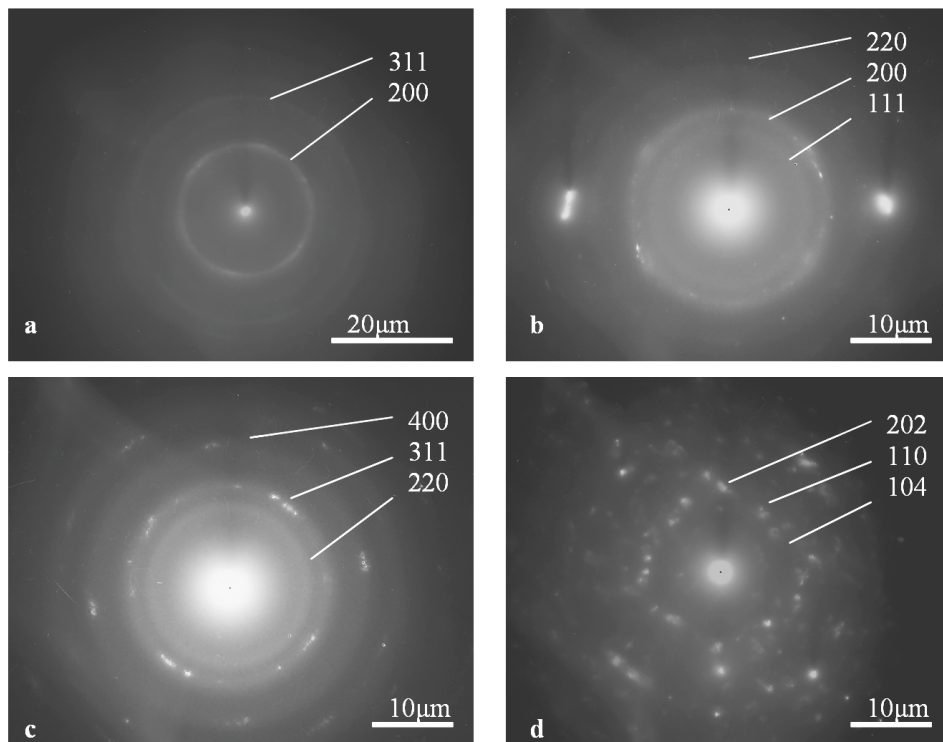


Figure 5. TEM cross-section across the centre of a fully melted splat found on SS\_P (see inset image) and presenting a large central pore: (a) bright field image and elemental maps of (b) Ni, (c) Cr, (d) Fe and (e) O

NiO was found to be more prone to form in the smaller pores, for example on the TEM cross-section shown in Fig. 7 (marked 1).  $\text{NiCr}_2\text{O}_4$  spinel was also found in similar locations in other, similar splats. Both types of oxides were identified using EDS, together with electron diffraction methods (see their diffraction patterns shown in Fig. 6b and c). More detail on the identification of oxide phases in NiCr splats on steel substrates using TEM can be found elsewhere [50].



*Figure 6. Diffraction patterns of the different oxides found: (a) FeO, (b) NiO, (c)  $\text{NiCr}_2\text{O}_4$ , (d)  $\text{Cr}_2\text{O}_3$*

Furthermore, at the periphery of splats where delamination is observed, a layer of oxide was often seen on the lower surface of the splat, such as on Fig. 2 (marked 8). Identification by TEM-EDS and electron diffraction showed that this phase was FeO.

Finally, it was often found that a thin layer of Cr oxide is present on the outer surface of the splats (marked 4 on Fig. 3 and (2) on Fig. 7). When this layer was thick enough for an electron diffraction pattern to be readily obtained, it was identified as Cr<sub>2</sub>O<sub>3</sub> (see diffraction pattern Fig 6d), which is, indeed, the Cr oxide phase most likely to be formed on these splats [56, 70].

In some cases, the layer of Cr<sub>2</sub>O<sub>3</sub> was notably thicker and, appears to have cracked upon cooling and solidification due to thermal expansion mismatch (chromium oxide coefficient of thermal expansion is  $\sim 7 \mu\text{m}/\text{m}\cdot^\circ\text{C}$  [123], in comparison to  $\sim 16 \mu\text{m}/\text{m}\cdot^\circ\text{C}$  for NiCr [84]), as it can be observed on the TEM cross-section displayed in Fig. 8 (marked 1), made on a small fully melted splat (a similar structure was found on some large fully melted splats). This phenomenon creates the patterns of cracks that can be observed on the outer surface of some splats (marked 2 on the inset SEM image in Fig. 8). Chromium oxide was also observed by EDS mapping at the splat-substrate interface, for instance in Fig. 5 (marked 2), but in such cases it could not be unambiguously identified by electron diffraction. This oxide may arise from either the oxidation of the steel substrate [61, 62], or the oxidation of the splat.

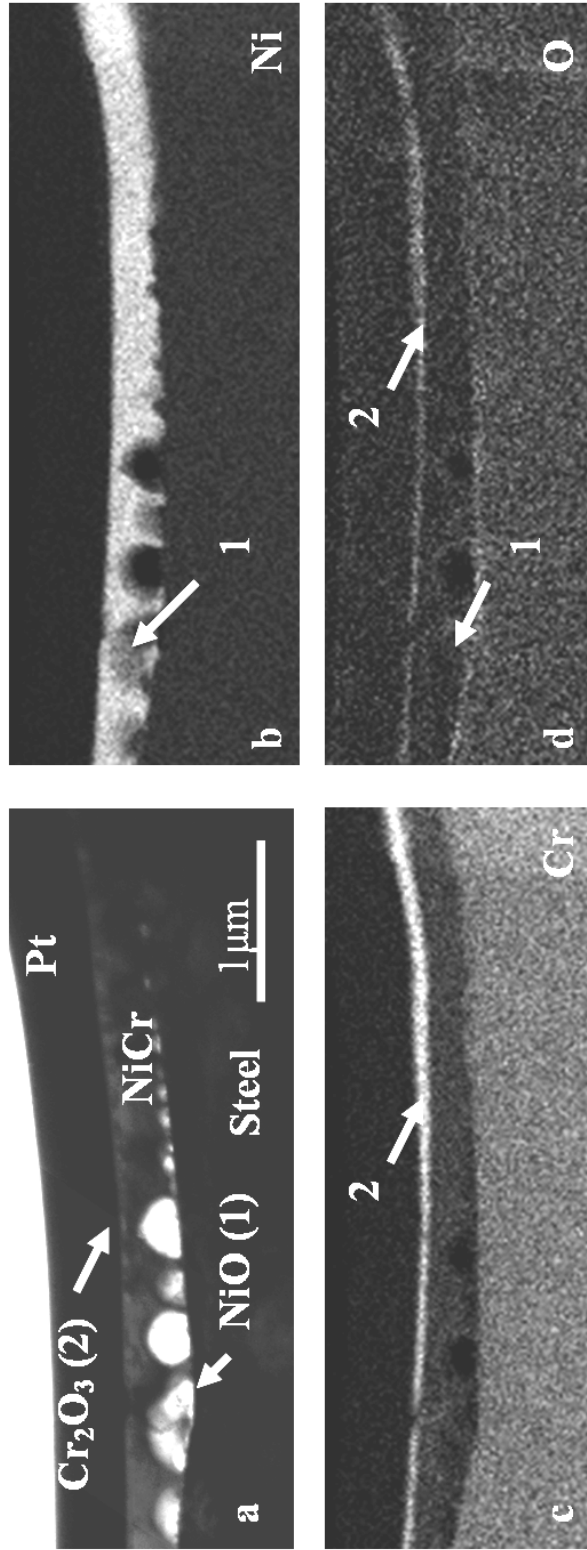


Figure 7. TEM cross-section across the centre of a fully melted splat found on SS\_BT presenting small pores at the splat-substrate interface with NiO: (a) bright-field image, EDS elemental maps of (b) Ni, (c) Cr, (d) O

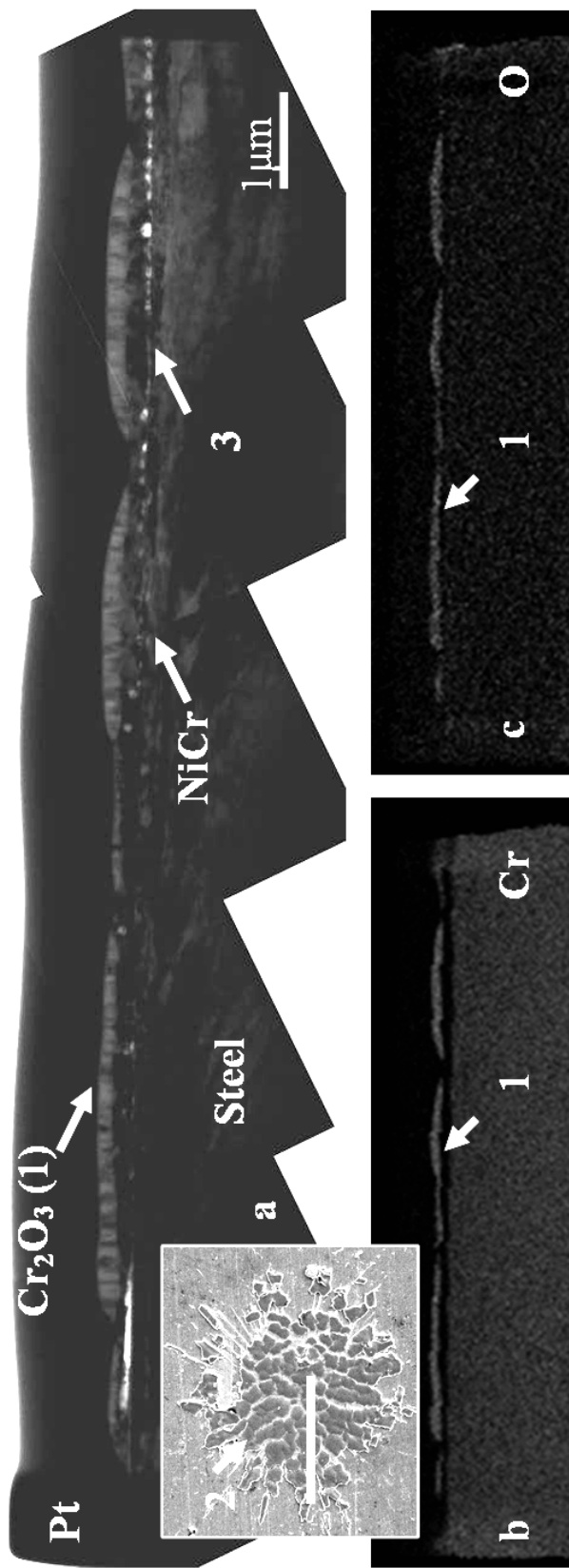


Figure 8. TEM cross-section of a small fully melted splat (see insert image) from the SS\_BT specimen:

(a) bright field image and elemental maps for (b) Cr and (c) O

### III.2.b. *Description of the splat formation process*

FIB and TEM cross-sections of these splats did not reveal the presence of any non-melted remnants from the original sprayed particle. However, this may not mean that the sprayed particle was completely molten when it impacted on the substrate. Indeed, analysis of similar fully melted splats prepared by plasma spray processes [67], showed that in this case the substrate shows no evidence of deformation. However, in this study the observation of a shallow crater indicates that the substrate must have been deformed by the impinging particle. Substrate deformation, observed usually for the cold spray process where the particles impact the substrate in a solid state, has also been observed to varying degrees for HVOF in a number of previous studies and, therefore, is not unexpected [39, 124, 125]. The deformation of the substrate is attributed to the “peening effect”, is said to lead to an increased adhesion of the coating by inducing a high level of compressive residual stress in the coating [124-126].

Zhang *et al.* noted, for HVOF sprayed particles in a partially melted state, that they were comprised of a non-melted core surrounded by a layer of melted material [127]. Based on the hypothesis that the NiCr particles impacted the steel substrate in such a state, the non-melted core could then have been responsible for the substrate deformation observed. This brings the question of the behaviour of the non-melted components following impact.

Previous studies have shown that further melting may have occurred upon impact from the transformation of the kinetic energy of the particle in heat and plastic deformation [39]. However, this may account for only a limited volume of material. Diameters of the largest splats are around 200  $\mu\text{m}$ , and examination of the FIB and TEM cross-sections showed that the thickness of the splats may be up to 2  $\mu\text{m}$ . An estimate of splat volume would, therefore, correspond to the volume of a sphere of diameter of around 24  $\mu\text{m}$ . This is far less than the maximum diameter of the feedstock powder (45  $\mu\text{m}$ ).

A possible explanation may be that the non-melted core may have rebounded from the substrate upon impact. Study of the cold spray process showed, indeed, that for a solid Ni particle to adhere on steel, it must impact the substrate with a velocity superior to a critical velocity of 640  $\text{m}\cdot\text{s}^{-1}$  [128]. Considering the range of impact velocity that is typical for HVOF (400-800  $\text{m}\cdot\text{s}^{-1}$  [4]) , this velocity may not be achieved on primary impact of the particle, and is certainly unlikely to be achieved on secondary impact after a rebound. Thus, the solid core, if it has rebounded away the substrate, does not subsequently adhere to the substrate.

One may note though that the splats are fully contiguous: there is not evident sign of the rebound of a solid core. Another possibility would be then to consider the fact that smaller particles impact on the substrate in a more molten state compared to larger ones [37]. The largest particles could then have simply not adhered to the substrate because they impacted in a mostly solid state. However this would lead to the presence of many impact marks on the substrate, while only very few of these were observed. Consequently

the hypothesis of the rebound of a solid core is more plausible, and the absence of evidence of rebound in the shape of the splat may be explained by the solidification rate of the splats which may have been slow enough to allow the molten NiCr splat to smoothen.

It was observed that some splats displayed a large central pore, for example as seen in Figs. 2 and 5. Porosity at the splat-substrate interface is often found in the case of plasma sprayed specimens: it was then hypothesized that such pores may partly form due to gas release from the substrate particle impact and flattening due to desorption of adsorbates/condensates present on the surface of the substrate [2, 67, 129]. A similar phenomenon was also studied by Sobolev *et al.* in the case of HVOF sprayed coatings [130]. Gases may also be entrapped under the impacting droplet [92], or be released after having been dissolved within the liquid droplet [129]. However, the amount of these gases is limited and some pores observed here are significantly large (a few  $\mu\text{m}$  in diameter). Modelling of splat formation in plasma spraying has also shown that due to the mechanics of flow of the melted particle (change of curvature in the droplet) a large open central pore was found to form [15, 55]. This may be applicable to the HVOF study here, with the difference being that the pore remains closed, possibly due to the lower temperature of the splat and the better contact between splat and substrate leading to a faster solidification, which would not leave sufficient time for the pore to become unstable and burst open.

Some other splats display some fine porosity in their centre near the splat-substrate interface, for example in Fig. 7. In such cases, gas release is most probably the cause of their formation. The presence of oxides, such as NiO, within these pores supports this hypothesis, as it shows that hot oxidizing gases must have been present within these pores. Moreover, if gas release indeed occurs, this should take place all along the splat-substrate interface. However, porosity is only observed at either the centre of the splat or towards its periphery. The gas released must then be pushed in direction of the periphery of the splat by the flowing melted NiCr during splat flattening. This would cause the presence of hot oxidizing gases at the splat-substrate interface under the rim of the splat. At this location delamination of the splat is often observed and a layer of FeO on the bottom surface of the splat: possibly when the flattened splat solidifies and cools down, curling up of the rim occurs to accommodate the thermal stress rising from the decrease in temperature, leading to the lift-up of the rim of the splat [54, 130]. On the bottom surface of the splat being lifted up, some Fe must have deposited from the steel substrate, which then is oxidized by the hot gases from the gas release described previously.

Finally, a common feature of the splats observed was the interdiffusion of NiCr and steel across the splat-substrate interface, even though the images showed that the interface appeared straight and distinct in structure. Diffusion across the interface may not be indicative of substrate melting. Indeed, if localized melting of the substrate had taken place, variations in the splat-substrate interface would likely have been observed [50], which was not the case here. Thus, the diffusion observed must arise from the very good contact between splat and substrate and the diffusion of the heat from the melted NiCr

into the substrate. This is also consistent with the observation that the degree of interdiffusion observed (usually around 200nm) is quite limited. It should also be noted that diffusion is maximum on the slanted walls of the crater, while it does not occur at the centre of the splat or at the periphery. At these locations, the contact between splat and substrate is poor possibly because of the porosity formation for the centre of the splat, and the decrease of the pressure applied by the impacting and flowing particle on the substrate towards the periphery. Consequently, it is expected that no, or limited, diffusion occurred there.

Figure 9 displays a schematic representation summarizing the splat formation process: upon impact the substrate gets deformed by the non-melted core (1), while the melted NiCr starts spreading to form a splat (2), then the non-melted core rebounds (3). In the centre a large pore may form (or alternatively a number of smaller pores) (4), while the melted NiCr spreads, pushing outwards gas that may be released from the substrate (5), and interdiffusion across the splat substrate interface takes place (6). In the end, curl-up of the splat occurs at its periphery (7) and oxides (FeO, NiO...) may form in the central pore and/or under the rim of the splat (8). Cr oxide was also found to form as a thin layer on the outer surface of the splat (9).

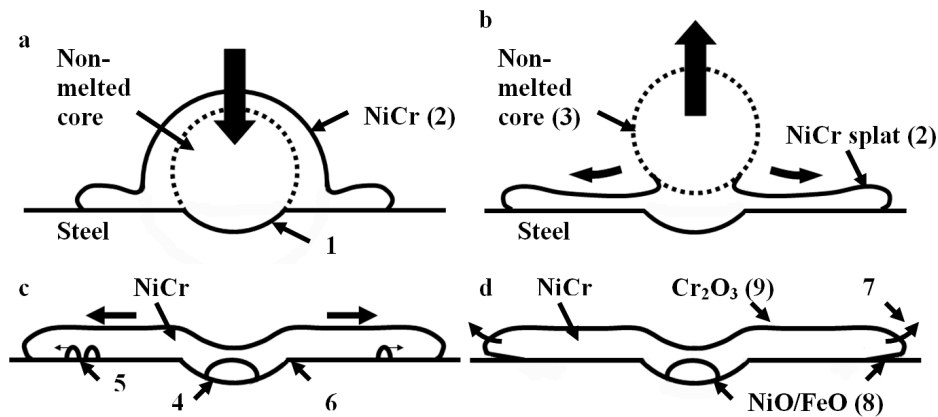


Figure 9. Schematic representation of (a) a Ni-Cr particle impacting on the steel substrate and (b) the non-melted core rebounding from the substrate, then (c) the splat flattening and (d) solidifying and cooling down

### III.3. Structure and formation of the small fully melted splats

Such splats have typically a diameter  $\sim 30 \mu\text{m}$  and a thickness of  $\sim 0.5 \mu\text{m}$ . The volume of these splats corresponds to an initial spherical particle of diameter of  $\sim 9 \mu\text{m}$ . They would then most probably originate from the smallest particles of the feedstock powder.

For these splats, their structure is quite similar to that of the larger fully melted splats, in terms of grain structure, porosity and oxide phases. However, some noticeable differences were found: firstly, as it can be seen in Fig.8a (marked 3), no crater or evidence of substrate deformation was observed. Consequently, unlike the large splats described in the previous section, it is probable that the NiCr particle was fully melted when impacting the substrate, which is consistent with the observation that smaller particles undergo further melting than the larger ones. Also, no interdiffusion was

detected across the splat-substrate interface (marked 3 on Fig. 8a). This could be linked to the thinness of the splats leading to rapid solidification, hindering the occurrence of interdiffusion, the small size of the particles meaning a lower momentum upon impact, and also to the absence of substrate deformation, which shows the pressure applied by the impacting particle on the substrate was limited.

#### III.4. Structure and formation of the partially melted splats

FIB cross-sections of a partially melted splat, similar to that shown in Fig. 1f, confirmed the assumption that they comprise a mixture of non-melted fragments in a matrix of NiCr that had melted. Figure 10 presents two cross-sections on such a splat. A mix of fine grains (marked 1,  $d < 1 \mu\text{m}$ , from the phase that was fully melted) and very large grains (marked 2,  $d \sim 2\text{-}10 \mu\text{m}$ , probably originating from the non-melted particle) can be observed. The melted phase allows the splat here to have a good contact with the substrate (marked 3). However, some pores were observed close to the splat periphery, possibly due to a lack of melted material to fill them (marked 4). On some other splats the voids were found to be significantly large ( $<10\mu\text{m}$ ) and towards the centre of the splat. When examining the splat-substrate interface, especially towards the centre of the splat, one can note that it is slightly curved (marked 5). This is due to the deformation of the substrate by the impact from the particle, forming a shallow crater.

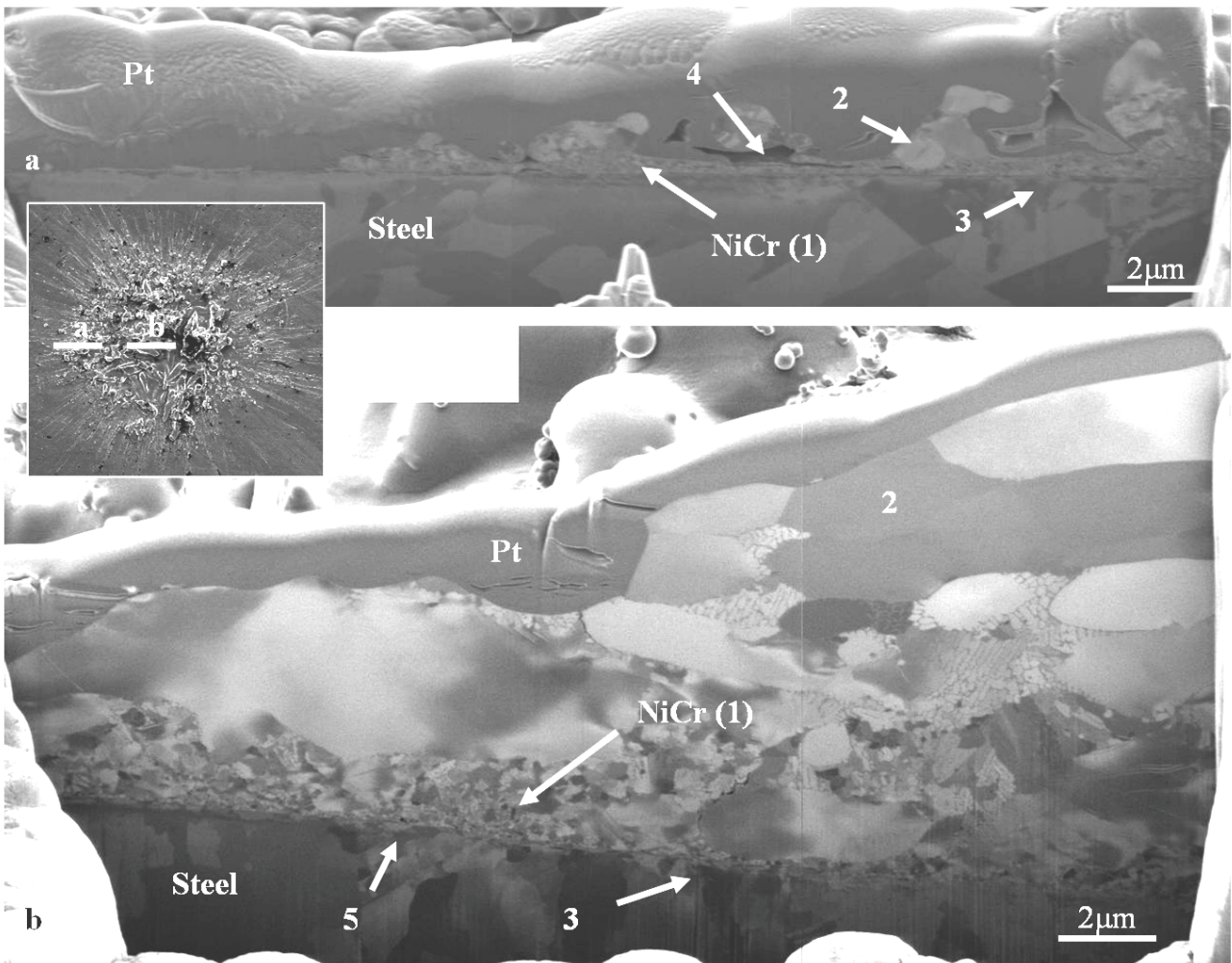


*Figure 10. FIB cross-sections of a partially melted splat (see insert image), found on SS\_B, (a) across the periphery and (b) towards the centre of the splat*

Chemical analysis using EDS in the TEM did not show the presence any particular oxide phase. One may expect some of the oxides that have been observed on the fully melted splats, such as NiO, FeO or NiCr<sub>2</sub>O<sub>4</sub>; presumably these oxides, if present, were in such small amounts that they were not detected using TEM.

Such splats, compared to the large fully melted splats, display a shallow central crater as well, showing that deformation has also occurred. However, the partially melted splats are much thicker and display large non-melted fragments embedded in a fine grained matrix that appears to have been fully melted upon splat formation. Consequently, it seems that such splats were formed from the impact of a partially melted particle, the non-melted core causing the deformation of the substrate, in the same way as the fully melted splats, except such a core may break up upon impact, the fragments being then embedded within the melted NiCr. This large thickness, however, inhibits the preparation of TEM specimens that allows ready observation of any oxide phase or interdiffusion across the splat-substrate interface.

### III.5. Effects of the pre-treatments on the splat morphology and formation

Stainless steel exhibits on its surface very thin layers of oxide comprising an outer layer of mainly of  $\text{Fe}_2\text{O}_3$ , and an inner layer of mainly of a mixture of Cr and Fe oxides ( $\text{Cr}_2\text{O}_3$ ,  $\text{Fe}_2\text{O}_3$ , spinel type  $\text{Fe}(\text{Fe},\text{Cr})_2\text{O}_4$  or  $\text{Ni}_x\text{Fe}_{3-x}\text{O}_4$ ) [61, 62] ). X-ray photoelectron spectroscopy (XPS) studies also showed that some hydroxide may be present on the surface [49]. Previous studies for plasma sprayed NiCr showed that heat treatment of a steel substrate may result in increasing the oxide content, converting, for example, the hydroxide into oxide, and/or thickness of this oxide layer [67]. Cedelle *et al.* found that substrate heat treatment also resulted in a positive skewness, which accounted for the better wetting of the plasma sprayed Ni splats and a shorter spreading time [11]. On the other hand, boiling stainless steel is expected to increase the hydroxide content ( $\text{FeOOH}$ )

of the oxide layer. In any case, the oxide/hydroxide layers before spraying are very thin (less than a few nanometres) [67]. The heat and boiling treatments were also found to slightly increase the nano-scale roughness of the steel specimens [67].

For each specimen, SEM images of 50-60 splats were taken and for each type of splat the average diameter and their relative proportions were evaluated. Examination of the splat population for each of the different substrates conditions showed that the relative proportion of the partially melted splats was consistent (~8%). For the small fully melted splats, their proportion is more variable, usually between 10 and 20% of the splats observed. However, both categories did not present significant variations between the various substrates.

Conversely, the fully melted splats were found to differ between the different specimens, but only by the morphology of their rims. The central part of the splat was always broadly similar. This suggests that formation of this central portion is mainly governed by the mechanics of the melted (or partially melted) NiCr impacting with a high kinetic energy on the substrate, thus, with building up of a high pressure at the interface with the substrate, undermining the possible effects of the surface chemistry. However, towards the periphery of the splat, where the pressure applied by the melted NiCr on the substrate becomes minimal, surface chemistry may influence the wetting of NiCr, thus the manner in which the splat spreads and in the differences in rim morphology.

Table 2 summarizes the different rim morphologies that were observed along with the approximate mean diameter of the splats, along with the standard deviation of the diameters. Despite the uncertainties, some trends can be observed. When observing plasma sprayed splats on similarly treated steel substrates, it was found that the heat-treatment improved the wetting of NiCr on steel, giving flatter splats [11, 67]. It seems here that the heat-treatment may have had a similar action: by improving the wetting of NiCr on steel, the splats were flatter, thus with a larger diameter, and with a better contact with the substrate towards the periphery, thus being less prone to delamination and the formation of cracks during cooling. The undulations observed on the surface at the rim also indicate wetting and contact: it seems that the flow of molten NiCr becomes retarded and stopped by the friction from the intimate contact with the substrate. This is possibly due to the fact that the increase in the oxide content and nano-scale roughness/skewness of the surface produced by the heat-treatment [11, 67] improves the wetting of NiCr on steel and also decreases the amount of adsorbates/condensates on the substrate, thus less gas is released from the substrate upon splat formation and the contact between the splat and the substrate is improved (more details on the effects of heat-treating on the surface chemistry may be found in a previous work by the same authors [67]). The splashed fingers may also be caused by the increased nano-scale surface roughness.

**Table 2. Various splat morphologies and corresponding average diameters for the splats found on the different specimens.**

<b>Specimen</b>	<b>Description of the large fully melted splats</b>	<b>Average diameter</b>
SS_P	Irregular dendritic/granular rim (Fig. 1a)	[65 ± 21] μm
SS_PT	Rim ranging from smooth with thin splashed fingers to circular with an undulating surface (Fig. 1b/c)	[86 ± 38] μm
SS_B	Irregular rim with radial cracks (Fig. 1d)	[83 ± 41] μm
SS_BT	Rim ranging from irregular with radial cracks to circular with an undulating surface (Fig. 1c/d)	[91 ± 32] μm

The boiling treatment also appears to significantly increase the splat diameter, but splats tend to display an irregular rim prone to delamination and radial cracks. Such cracks may be linked to this increase in diameter: the splats would be indeed much thinner, including regions towards the splat periphery, and thus more prone to cracking.

However, the manner in which boiling the substrate creates the morphologies observed is not clear. Possibly, the increase in the FeOOH content of the steel surface causes on one hand a slight increase in nano-scale roughness/skewness, which may improve the wetting of NiCr, but on the other hand, due to the dehydration of the hydroxide upon splat formation, more gas may be released from the substrate upon splat formation, hindering the contact between splat and substrate and causing the irregular morphology of the rim.

In summary, pre-treatments influence splat formation and morphology through modifying the surface chemistry and roughness, but this affects splat morphology mainly towards

their periphery. No significant effect on the oxide content and the porosity formed towards the centre of the splat was found. On the other hand, it is possible that porosity formed due to the delamination under the rim may be affected by the pre-treatments. Porosity, along with the oxide content, are known to be significant features which influence the properties of the fully deposited coating, such as thermal and dielectric conductivity or resistance to corrosion [38, 122, 127]. However, as the effects of the pre-treatments on porosity and oxide is limited, such pre-treatments of the substrate may not be very influential factors on the final properties of the HVOF sprayed coatings, especially compared to other spray conditions factors such as the temperature and velocity of the particles.

When comparing with plasma sprayed NiCr splats on similar substrates [67], HVOF splats can be noted to present interesting points of difference. For example, in HVOF the amount of oxide is reduced. Regarding the porosity, the amount of small pores ( $< 1 \mu\text{m}$ ) is significantly reduced for the HVOF splats, but the central pores are larger than the ones usually observed for the plasma splats. This may be explained by a stronger influence, in their formation process, of the mechanics of the flow of the liquid splat, compared to the gas release phenomenon. Further, despite the absence of evidence of substrate melting, as found for plasma sprayed splats, the contact between splat and substrate is usually better. In HVOF the splat shapes are also more uniform and regular, as plasma sprayed splats in most cases tend to be more fragmented and splashy. Finally, the depression from the impact of the particle and the formation of very large central pores are characteristic of HVOF splats, as there is no deformation of the substrate in the case of plasma spray and

the pores found in the centre of the splats are much smaller and caused mainly by the presence of gas. It is consequently logical that HVOF coatings are often found to be denser and with lesser oxide content compared to plasma coatings [1].

#### **IV. Conclusion**

In conclusion, the study of HVOF sprayed NiCr single splats on stainless steel, and the comparison of their morphology depending on the pre-treatment of the steel substrate, lead to the following observations:

- The sprayed particle impacts the substrate in a partially molten state, and its solid core caused the deformation of the substrate, thus the formation of a shallow crater.
- In the case of the fully melted splats, the solid part of the sprayed particle rebounds from the substrate. In the case of the partially melted splats, some non-melted fragments remain embedded in a matrix of melted NiCr. In both cases, only a fraction of the initial particle adheres to the substrate.
- Splats usually display some porosity at the splat-substrate interface in their centre, and also at the periphery where delamination may have occurred. Elsewhere, the contact between splat and substrate is good, and the interdiffusion between Ni and Fe across the interface shows that metallurgical bonding may have taken place.
- Some  $\text{Cr}_2\text{O}_3$  may form as a thin layer on the outer surface of the splat, while NiO and FeO may be found where porosity has formed.

- Changes in surface conditions induced by the heat and boiling pre-treatments may influence splat formation through the way melted NiCr wets on the substrate and the amount of adsorbates/condensate that may get desorbed from the substrate. However, their effect is quite limited.

To apply high resolution microscopy techniques to the study of single splats is a novel way of studying thermal spray coatings and has shown to bring a new insight in the splat microstructure and how splats interact with the substrate.

**CHAPTER 8**

**MICROSTRUCTURAL STUDY OF SPLAT FORMATION FOR  
HVOF SPRAYED NiCr ON PRE-TREATED ALUMINIUM  
SUBSTRATES**

---

*S. Brossard, P.R. Munroe, M.M. Hyland, Journal of Thermal Spray Technology, 2010,  
DOI: 10.1007/s11666-010-9482-3*

**Abstract**

In this study, the mechanisms of splat formation and the influence of substrate surface conditions were studied for NiCr splats HVOF sprayed on to Al. The specimens, having undergone various substrate pre-treatments, were observed at high resolution using various electron microscopy techniques with emphasis on the splat microstructure and the splat-substrate interface. From the observations made here, a model for splat formation is proposed, whilst the effects of surface chemistry on this process were investigated. It was found that that due to the deformation of the substrate on impact of the partially molten particle, effective contact may be achieved between the substrate and the splat. However, in many cases much of the initial projected particle did not adhere to the substrate after

impact. The presence of oxide or hydroxide layers on the surface of the substrate was influential on the adhesion of the NiCr splat

## **I. Introduction**

Understanding of splat formation in the High Velocity Oxy-Fuel (HVOF) spraying process is a key step in the design of coatings with improved properties and performance.

The HVOF spray process is a relatively recent development compared to many other spray processes and the characteristics of the coatings produced by this method, such as high bond strength and thickness capacity, relatively low porosity and oxide contents, etc., make it a competitive alternative for the production of coatings in many industries (aerospace, industrial gas turbine, petrochemical/gas industries, automotive industry, etc.).

The HVOF system operates through the injection of a powder in a stream of combusted gases, a mixture of oxygen and a fuel gas (hydrogen, heptane, kerosene, etc.). Depending on the powder feedstock (material type and powder size) and the spray conditions (temperature of the flame and velocity of the carrier gas), the sprayed particles may impact the substrate with a range of velocities (usually 400-800 m.s<sup>-1</sup>) and variable state (from completely solid to fully melted) [1, 4]. This may create a variety of splat types (solid, partially melted or fully melted). The splat morphology will also depend on the properties of substrate, such as its hardness and roughness [39]. Depending on the spray

conditions it is possible to create coatings with a bimodal structure, consisting of a mixture of melted and non-melted zones [40-42].

Although the microstructure of fully prepared coatings has been widely studied [40-42], little work has been performed regarding the microstructure and formation of single splats prepared by the HVOF spray process.

However, some parallels may be drawn between the HVOF process and other spray processes. The formation of fully melted splats may be compared to the splat formation in the plasma spray process, which has been more widely studied and modelled [2]. Similarly, the situation where the particles impact the substrate in a non-melted state can be linked to the cold spray process, where there have also been a significant number of studies performed [44-46]. However, often in HVOF, sprayed particles may impact the substrate in a partially melted state. For example, Trompetter *et al.* observed the occurrence of the different types of splats and the influence of substrate hardness by spraying NiCr on to a range of substrates. It was found that increasing the substrate hardness increased the proportion of melted splats, as the kinetic energy is dissipated upon impact less in the deformation of the substrate and more in heating and deformation of the sprayed particle. However, the microstructure of such splats at its interface with the substrate was not described in detail [39]. The coating-substrate interface, however, was examined for a WC-Co coating HVOF sprayed on to a Cu substrate by Guilemany *et al.* They observed a thin layer of fine-grained materials at the interface with the substrate, which they interpreted as evidence of substrate melting [43]. However, this study

concerned a relatively thick coating and not single splats. Finally, Sobolev *et al.* studied the effect of oxidation of the particle on the splat formation: they showed that effects may include thicker and smaller splats having less effective contact with the substrate due to a decrease in the build-up in pressure upon impact, although dissolution of oxygen within the splat was thought to increase its wetting on the substrate [121].

The present study also aims to investigate the influence of pre-treatments (such as heat-treating and boiling), inducing differences in the surface conditions (via variations in surface chemistry and roughness), on the splat morphology and the interaction with the substrate. Indeed, for the case of plasma spray, surface chemistry and roughness have been shown to have a significant influence on the splat formation. For example, for oxidized steel substrates Cedelle *et al.* found that plasma sprayed nickel particle had a better wetting and smaller spreading time, giving flatter splats, compared to non-oxidized steel substrates [11]. For Al, previous studies in the case of plasma sprayed NiCr showed that preheating the aluminium substrate resulted in slightly flatter and less fragmented splats; it was also observed that on boiled substrates, on which a thick (a few hundred of nm) hydroxide layer is formed, no splats would adhere [55, 131]. This was also observed by Trompetter *et al.* when HVOF spraying NiCr particle on to Al, along with the observation that the presence of a thick (~ 650 nm) oxide layer did not hinder splat formation, but may increase the proportion of fully melted splats [76]. Explanations for these various effects included the occurrence of gas release from the substrate, notably water from the (partial) dehydration of the Al hydroxide, which could hinder the splat

adhesion, and this study intends to enquire on such effects for the case of HVOF spraying.

In this study, a NiCr powder was sprayed by HVOF on to aluminium substrates that, prior to spraying, were subjected to different pre-treatments: polishing, heat-treating and/or boiling. A range of microscopy techniques were used to observe the splat morphology, microstructure and the nature of the interface with the substrate for four Al specimens with different surface pre-treatments, to investigate how the surface chemistry may affect the splat formation in the case of the HVOF spraying process.

## II. Experimental procedure

Four different substrates were used; all prepared from a 5052 aluminium alloy. These are listed in Table 1.

**Table 1. Substrate Nomenclature and Condition**

<b>Specimen</b>	<b>Substrate</b>	<b>Pre-treatment</b>
Al_P	Aluminium 5052	Polished (to nano-scale smoothness)
Al_PT	Aluminium 5052	Polished and thermally treated
Al_B	Aluminium 5052	Boiled
Al_BT	Aluminium 5052	Boiled and thermally treated

All substrates were firstly mechanically ground and mirror polished with diamond paste, to a nano-scale roughness (measurement of the roughness were made for similar

substrates for another study by the same authors and details can be found in the relevant publication [131]) were made. The boiled substrates were placed into boiling distilled water for 30 min, while the thermally treated substrates were heated at 350°C for 90 minutes in air. The aim of these treatments is to form surface oxides (or hydroxides for the boiled specimens) and/or to induce some level of surface roughness.

The sprayed material was a commercial NiCr alloy powder (Ni80-Cr20, (-45 +5)  $\mu\text{m}$ ) (Sulzer Metco 43 VF-NS, Wohlen, Switzerland). HVOF spraying was carried out with a Sulzer Metco (Wohlen, Switzerland) Diamond jet (DJ-2600) gun, fuelled with air at 160 psi, oxygen and propylene at 110 psi, the flow rates being 744, 419 and 128 SCFH respectively. The feeding rate of the powder was of 26g/min, the carrier gas being nitrogen at 140 psi. Five swipe passes were made, at the velocity of 0.4  $\text{m}\cdot\text{s}^{-1}$ , and at a spraying distance of 266mm. HVOF spraying was performed at room temperature.

The specimens were then characterized using a range of analytical techniques. A scanning electron microscope (SEM) (Hitachi, S3400-X, Mito, Japan) was used to image the overall morphology of the splats and the substrates. A focused ion beam microscope (FIB) (FEI, xP200, Hillsboro, USA) was used to mill cross-sections of the splats using an energetic gallium ion beam, and to image them using secondary electrons induced by the ion beam. Details have been described elsewhere [51]. A dual beam microscope (that is a FIB and SEM combined into a single instrument) (FEI, xT Nova Nanolab 200, Hillsboro, USA) was used to prepare cross-sections of splats (100-200nm in thickness) suitable for transmission electron microscope (TEM) observation. These were prepared using the lift-

out method as described elsewhere [51] and examined in a TEM (Philips, CM200, Eindhoven, The Netherlands) to which energy dispersive x-ray spectroscopy (EDS) facilities have been interfaced.

Several FIB and TEM cross-sections were made and studied, at least one for each particular feature and/or type of splat, but for the sake of brevity only representative images will be presented here. The process of cross-section preparation also involves the *in-situ* deposition of a layer of platinum on top of the splat prior to milling to protect the outer surface of the splat from ion beam damage. This layer is then present, and labeled, on the images obtained.

### III. Results and discussion

#### III.1. Description of the splats observed on the polished and polished and thermally treated specimens

Figure 1 displays SEM images of the different types of splats found on the polished (Al\_P) and polished and thermally treated (Al\_PT) substrates. When the NiCr particles impact on the Al substrate, they create a crater in the substrate that can be observed on all the splat-substrate cross-sections examined. Figure 1a shows such a crater where the NiCr has not adhered to the substrate. The uneven surface of the crater, relative to the surrounding substrate, is clearly visible.

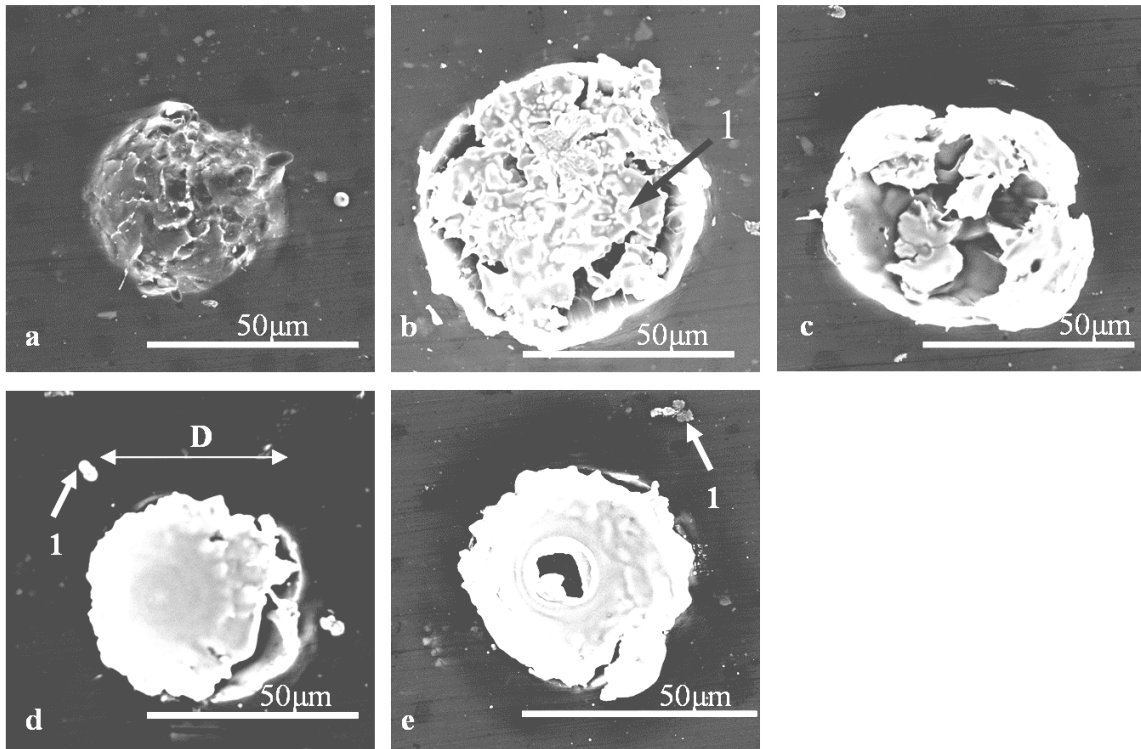


*Figure 1. SEM images of (a) a substrate crater, and different types of splats found on Al\_P and Al\_PT: (b) partially melted splat, (c) fragmented fully melted splat, (d) non-fragmented fully melted splat, (e) non fragmented fully melted splat with a central pore*

The splats observed on Al\_P and Al\_PT substrates were, generally, similar and exhibited the following characteristics:

- Some splats were formed from NiCr that was only partially melted. Figure 1b shows an example of such splat: it appears to be composed of unmelted fragments (marked 1 on Fig. 1b) within a melted matrix. These splats will be denoted as “partially molten splats”.
- Other splats were formed from NiCr particles that were fully melted, as shown by the less granular structure compared with the previous type of splat (Fig 1b). Two types of these splats can be distinguished: on one hand splats which appear to

have broken into several fragments, such as the splat shown in Fig. 1c. Other splats appear to have fractured less and adhered to the impact crater, see Fig. 1d, such that it forms almost a fully disc-shaped splat. A central pore may be present in some splats, such as the one shown in Fig. 1e. All of these splats will be denoted here as “fully molten splats”.

### III.1.a. *Structure and formation of the fully melted splats*

#### - *Observation of FIB and TEM cross-sections of the splats*

Figure 2, a FIB cross-section made across a fully melted fragmented splat, similar to the one shown in Fig. 1c, is presented. The cross-section of the crater from the impact of the NiCr can be clearly seen and is about 4  $\mu\text{m}$  in depth (marked 1). The splat-substrate interface is irregular in shape (1), and one can note that the Al substrate has been lifted-up above the initial substrate surface at the periphery of the crater (2). This suggests that the aluminium substrate had undergone some localized melting in addition to being deformed.

Moreover, zones that are bare of NiCr (3) were found between NiCr fragments, which display a quite irregular and coarse grain structure (4). On top of the NiCr region, a thin layer ( $\sim 50\text{-}100$  nm) was observed (5). This layer was identified by TEM as being a chromium oxide (see description of the TEM cross-section presented in Fig. 4).

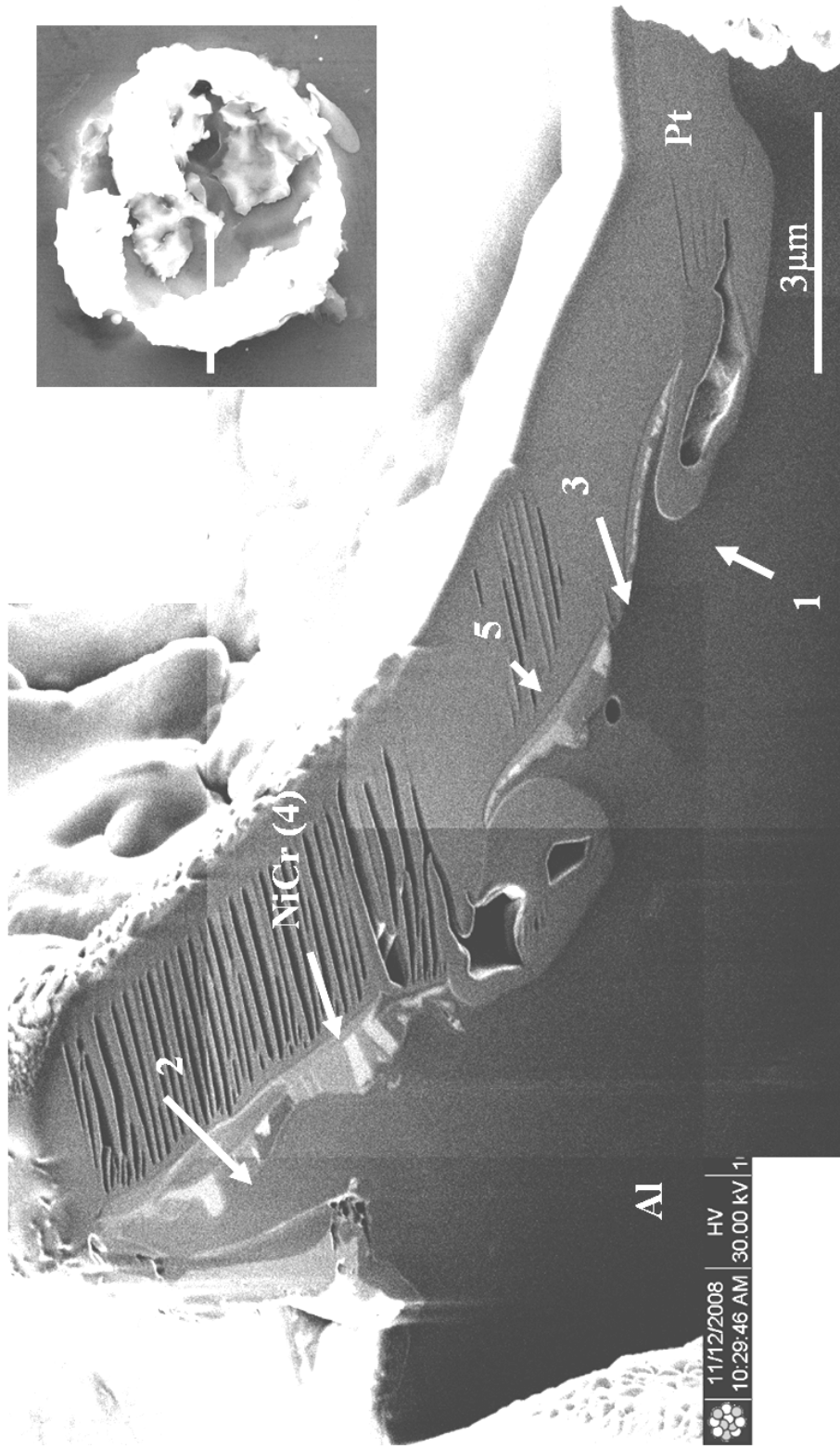


Figure 2. FIB cross-section of a fragmented and fully melted splat (the insert image shows an image of the splat in plan view before sectioning) from Al\_PT

Figure 3 shows a FIB cross-section of a non-fragmented fully melted splat, similar to the splat shown Fig. 1d. The splat-substrate interface is still irregularly shaped (1), but to a lesser degree compared to the fragmented splat shown in Fig. 2. The contact between splat and substrate is also good, except in the centre of the splat (2) where some delamination seems to have occurred. Furthermore, the grain structure of the splat is very fine ( $d < 0.5 \mu\text{m}$ ) and columnar (3).

Finally, figure 4 presents a TEM cross-section of a fully melted splat. Again the splat-substrate interface is very irregular (1), with the Al substrate being lifted-up at the periphery of the crater (2), but in some areas the splat-substrate interface is also quite indistinct (1): an EDS linescan performed across the interface (marked L1, Fig. 4f) shows that Ni has diffused into the substrate to a depth of about 150nm (3). This confirms the occurrence of substrate melting. On closer inspection of the interface, a fine grained structure was observed within the substrate (4): NiCr appears to have intermixed with the molten Al substrate, which was jetted within the splat, but as the solid solubility of Ni in Al is extremely limited [132] it may have frozen in the fine grained microstructure observed. The fact that the variation of Al and Ni concentrations, as measured by the linescan across the splat-substrate interface, is gradual suggests that this is not a stoichiometric intermetallic phase.



Figure 3. FIB cross-section of a fully melted splat (see insert image) on Al\_PT

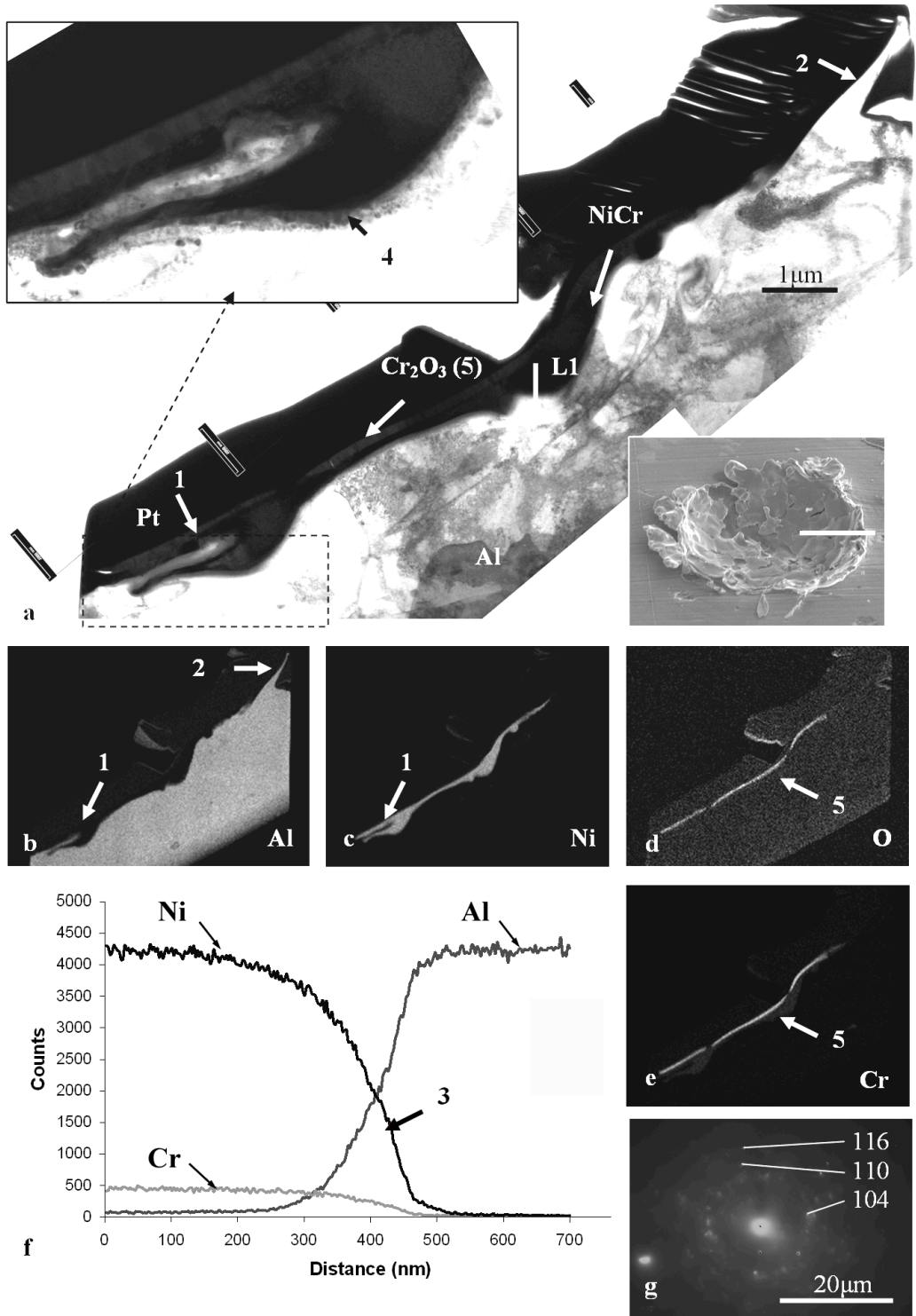


Figure 4. TEM cross-section of a fully melted splat (see insert image) from the Al\_PT specimen: (a) bright field image, (b) elemental EDS maps for Al, (c) Ni, (d) O, (e) Cr, (f) linescan across the splat-substrate interface, (g) diffraction pattern of Cr<sub>2</sub>O<sub>3</sub>

This is contrary to observations, for example, by Kitahara *et al.* for plasma spray of Ni onto Al substrates [35]. Moreover, diffraction patterns taken from this phase exhibited reflections which prevented unambiguous identification. Consequently, the structure observed may more likely be a very fine grained metastable mixture of a non-equilibrium Ni-Al phase formed due to the rapid solidification of the aluminium substrate into which some Ni has dissolved. Finally, on the outer surface of the splat, the layer observed (5) was identified by both EDS mapping (see Fig. 4d and e) and electron diffraction as Cr<sub>2</sub>O<sub>3</sub> (see diffraction pattern Fig. 4g).

From other TEM cross-sections made on similar splats, it was found that other oxide phases can also be present, such as NiO and NiCr<sub>2</sub>O<sub>4</sub>. These are both usually located not only on the outer surface of the splat, but also at the periphery of the splat or in pores at the interface. Al<sub>2</sub>O<sub>3</sub> was also observed, mostly in pores at the splat-substrate interface.

One can note that for all these cross-sections it appears that the splat only partially fills the crater, which itself is smaller in diameter than the initial sprayed particle. For example, for the splat presented in Fig. 3: by measuring the radius  $R_c$  of the crater and the depth  $h_c$ , and approximating this as a fraction of a sphere, the volume  $V_c$  of the

corresponding sphere can be calculated by the expression  $V_c = \frac{4}{3}\pi\left(\frac{R_c^2 + h_c^2}{2h_c}\right)^3$ . The

initial sprayed particle is expected to be at least equal to  $V_c$ , thus here at least  $164 \times 10^3 \mu\text{m}^3$ . However, the volume of the deposited splat  $V_s$ , calculated by measuring its radius  $R_s$  and thickness  $h_s$ , can be calculated by  $V_s = \pi R_s^2 h_s$ , and is evaluated here to be around

$2.5 \times 10^3 \mu\text{m}^3$ , thus only  $\sim 1.5\%$  of the initial particle volume. This consequently shows very low deposition efficiency, at least with respect to the deposition of the first layer of splats (values are usually expected to range from 30 up to 90% [133, 134]). Nevertheless, it is possible that for additional layers of splats, which will then deposit on NiCr and not on aluminium, the deposition efficiency may be higher.

- *Description of the formation process*

In the plasma spray process, particles impact on the substrate in a fully melted state and no deformation of the substrate is observed. Here, for the HVOF process, FIB and TEM cross-sections have shown that the splats characterized by the presence of a deep semi-spherical crater, due to the deformation of the substrate upon impact of the sprayed NiCr particle. This suggests that the particles were, therefore, not fully molten upon impact.

Zhang et al., when HVOF spraying Inconel powder, explained the bimodal structure of the coating, comprising a mixture of melted and non-melted zones, by considering that the sprayed particle was partially melted and comprised a solid core surrounded by molten material [127].

Figure 5 presents a schematic representation of the formation of a fully melted splat: upon impact, the substrate is deformed by the solid core of the partially melted NiCr particle (Fig. 5a).

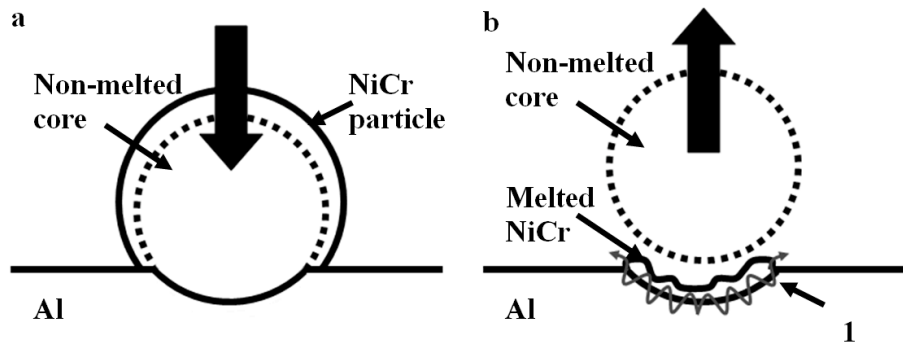


*Figure 5. Schematic representation of (a) a Ni-Cr particle impacting on the aluminium substrate and (b) the formation of a fully melted splat*

From the FIB and TEM cross-sections, it appears that only a limited amount of the NiCr particle has adhered to the substrate. This leads to the conclusion that the non-melted core of the particle has most probably rebounded from the substrate after impact, while some of the melted particle has adhered to the substrate. This is shown in Fig. 5b. Melted segments of the particle may also be splashed away from the splat during formation. Such fragments may either fall away from the substrate (which is sprayed whilst held in a vertical position), or fall back on the substrate and form very small splats (see for example the particles marked 1 on Figs. 1d and e). Such splashing phenomena is consistent with what is often observed for plasma spray [135, 136].

FIB and TEM cross-sections also showed signs of localized substrate melting: that is, irregular splat-substrates interface (see Fig. 2 (1) and Fig. 4 (1)), jetting of Al at the periphery of the crater (see Fig. 2 (2) and Fig.4 (2)), and mixing of Ni and Al at the interface (see Fig. 4 L1), forming a very finely grained non-equilibrium structure. Such melting may be expected as the melting point of NiCr ( $\sim 1400^{\circ}\text{C}$ ) is significantly higher

than that of Al (~649°C). The manner in which the particle impacts on the substrate, that is involving a high kinetic energy, and deformation of the substrate, ensures very good contact between the particle and the substrate. Structural features that may usually limit such contact, such as the presence of an oxide layer or the desorption of adsorbates/condensates from the substrate surface which cause the release of gases upon impact [2, 32, 131], are here of lesser importance because of the high pressure applied by the impacting particle on the substrate.

Subsequently, the Al substrate is locally melted at the splat-substrate interface in the crater, due to the flowing movement of the melted splat. The Al substrate may also get jetted within the splat and/or on the sides of the crater (see (1) on Fig. 5b). Such jetting was observed in other cases where the impacting particle is, for the most part, solid upon impact, such as in cold spray [45] or, in certain conditions, HVOF [137]. However, jetting occurs here more frequently and at a significantly greater scale.

Finally, various oxides may form due to the presence of hot gases, possibly from the HVOF flame, such as  $\text{Cr}_2\text{O}_3$  which is found as a thin layer on the outer surface of the splat, or NiO and  $\text{NiCr}_2\text{O}_4$  when they are found on the outer surface of the splat as well. Oxides found in pores at the splat-substrate interface such as NiO and  $\text{Al}_2\text{O}_3$ , may form, however, due to the presence of gas released from the substrate upon heating by the spraying process. Such phenomenon of desorption of adsorbates/condensates has been studied in more detail in plasma spray studies [50, 67, 107, 131].

### III.1.b. *Structure and formation of the non-melted/partially melted splats*

#### - *FIB and TEM observations*

Figure 6 shows a cross-section prepared by FIB across a partially melted splat, similar to the splat shown in Fig. 1b. A mix of non-melted particles, which exhibit a coarse grain structure (with a diameter,  $D$ ,  $\sim 1$  to several  $\mu\text{m}$  in diameter) (1) and fully melted zone, with a finer grain structure ( $d < 0.5 \mu\text{m}$ ) (2), can be observed. Large pores are present (3), formed from the cavity between the non-melted particles, that is a region not fully filled by the melted NiCr. However, where some NiCr has melted, the contact between splat and substrate is good (4). Furthermore, a crater made by the deformation of the substrate upon impact can be seen to be around  $3 \mu\text{m}$  in depth (4). Also, as seen for the fully melted splats, comparing the volume of the NiCr splat with the size of the crater, which indicates the initial size of the NiCr particle, suggests that the splat only represents a fraction of the initial NiCr particle. Indeed, from the FIB image, the NiCr particle creating such crater of depth of about  $7 \mu\text{m}$  and diameter of about  $22 \mu\text{m}$  should have a volume of at least  $231 \times 10^3 \mu\text{m}^3$ , while the volume of the splat itself is estimated to be around  $2 \times 10^3 \mu\text{m}^3$ , which thus represents only about 0.8% of the initial particle. This means that a large fraction of this particle must have rebounded away from the substrate.

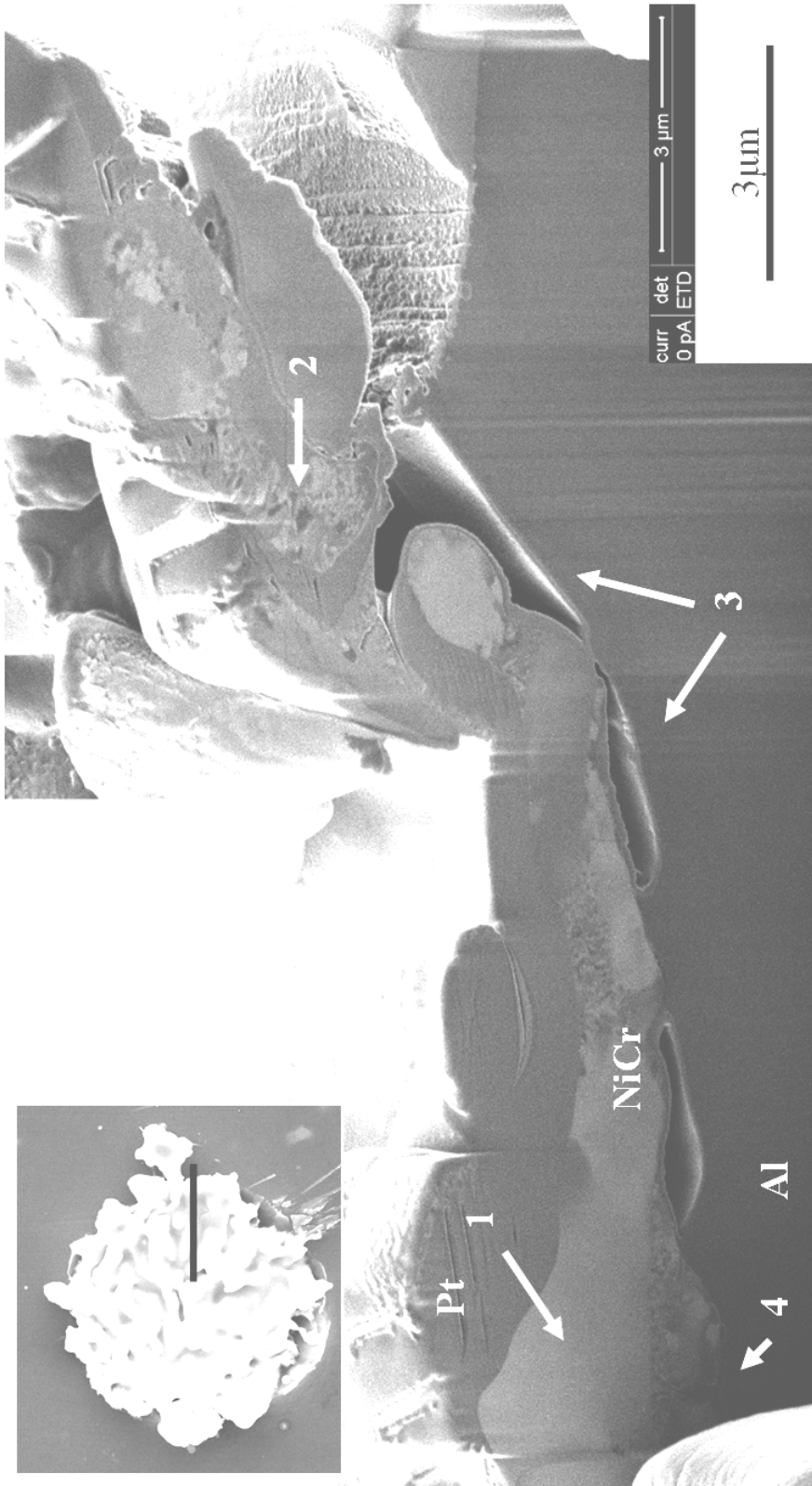


Figure 6. FIB cross-section of a partially melted splat (see insert image) on Al/Pt

TEM studies of these splats, although somewhat difficult to prepare due to the larger thickness of the splats and the greater depth of the crater, showed that from the non-melted zones, no oxide phases or substrate melting were evident. However, for the locally melted zones, the features found were similar to the ones observed for the fully melted splats, which are described below.

- *Description of the formation process*

The crater observed for the fully melted splat is present as well for the partially melted splats, suggesting that the formation process starts similarly as for the fully melted splats: the NiCr particle impacting the substrate in a partially melted state, with a solid core responsible for the deformation of the substrate (Fig. 5a). The non-melted fragments may then be from this non-melted core, which may have fragmented upon impact. It is also very possible that some parts (melted or non-melted) rebound from the substrate. Indeed, for most of these partially melted splats, the NiCr phase barely fills the crater in the substrate, and the original sprayed particle must have been significantly larger than the crater created.

III.1.c. *Effects of the substrate surface heat treatment*

For both Al\_P and Al\_PT specimens, SEM images of 50-60 splats were recorded, and for each type of splat described above, the average value  $D_m$  of their diameter  $D$  and the

relative population were evaluated. Evaluating the diameter was performed by taking the smallest and largest diameter value measured from the splat, which is not perfectly circular, and calculating the average value; features such as splashed fingers were ignored (see for example Fig. 1d). Results are summarized in Table 2. It should be noted that these values are broadly indicative as the number of splats studied is insufficient to calculate precise statistics of splat morphology. The impact craters with no NiCr present were not included in this analysis due to their relatively low frequency. Results for the boiled specimens were not included either, as the splats formed on those substrates are significantly different and will be discussed later.

**Table 2. Relative proportions and average diameters of the different types of splats found on the Al\_P and Al\_PT specimens**

		Specimens	
		Al_P	Al_PT
Type of splat	Unmelted/partially melted splat (Fig 1b)	19% $D_m = [56.4 \pm 14.9] \mu\text{m}$	17% $D_m = [54.4 \pm 10.9] \mu\text{m}$
	Fully melted splat, fragmented (Fig 1c)	68% $D_m = [44.4 \pm 10.5] \mu\text{m}$	64% $D_m = [42.7 \pm 12.3] \mu\text{m}$
	Fully melted splat, non fragmented (Fig. 1d/e)	13% $D_m = [48.5 \pm 21.3] \mu\text{m}$	19% $D_m = [48.8 \pm 12.6] \mu\text{m}$

Considering the relative imprecision of the values, it can be noted that the different types of splats, on one hand, have similar mean diameter, which is the diameter of the crater,

and, on the other hand, are present on both specimens in approximately the same proportions.

Protective oxide layers naturally form on aluminium: an inner compact and amorphous oxide layer, covered with a more permeable layer of hydrated oxide [77, 78], reaching at room temperature a total thickness of 2-4nm. The heat treatment applied (350°C, 90 min in air) is expected to increase the oxide layer thickness up to about 7 nm, and may also cause dehydration of the outer oxide layer, possibly converting some of the hydroxide into oxide [49].

However, these changes in the surface chemistry of the substrate do not seem to have a significant influence on the splat shapes and, thus, the splat formation. This is a substantial difference compared to plasma spraying, where similar heat treatments of the substrate before spraying were found to make the splats flatter and less fragmented, possibly by improving the wetting of the NiCr on the Al [131]. This difference may be explained by the different temperature and velocity with which the particle impacts on the substrate: In the plasma process the particle velocity is lower and its temperature higher, thus the particle is fully melted upon impact and the surface state may have a significant influence on the spreading of the melted NiCr. In the HVOF process, on the other hand, the higher velocity and lower temperature possibly means that, firstly, the substrate gets deformed, which may fragment or disrupt the oxide layers, and secondly the pressure applied by the particle on the substrate upon splat formation is higher, thus the way the melted NiCr wets the substrate surface is not as influential.

### III.2. Description of the splats found on the boiled and boiled and thermally treated specimens

#### III.2.a. *Description of the splats morphology and microstructure*

In previous studies of boiled Al specimens, it was shown that the boiling treatment produces a thick hydroxide layer (boehmite,  $\text{AlOOH}$ , about 300nm in thickness) on the surface of the substrate [55, 131]. Indeed, aluminium reacts with water in the following way: under 100°C bayerite  $\alpha\text{-Al(OH)}_3$  is expected to form, then from 100°C boehmite  $\gamma\text{-AlOOH}$  is the most likely hydroxide to form [75]. Such a layer, present on both Al\_B and Al\_BT, is apparent as a dense homogenous dark layer on FIB cross-sections, and was found to partially dehydrate upon heating, releasing water vapour. More details on these layers can be found in a study by the same authors [131].

Splats on both boiled and boiled and thermally treated specimens were overall similar in morphology and examples are displayed in Fig. 7. In the crater shown in Fig. 7a, a structure is seen that is similar to the non-boiled specimens. However, some fragmented parts of melted NiCr can be found, arranged in an approximate circle. The difference between the splats observed here, and those on the polished substrates, is the amount of NiCr that has adhered in the crater, ranging from a thin ring (Fig. 7a) to the crater being almost completely covered with NiCr (Fig. 7b and c).

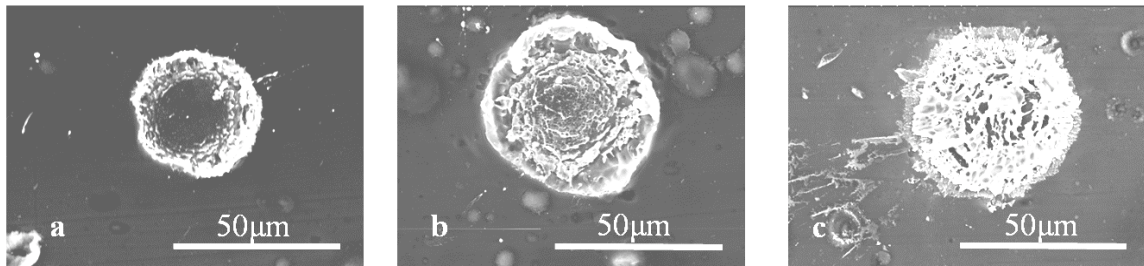


*Figure 7. SEM images of typical splats found on (a, b) Al\_B and (a, b, c) Al\_BT*

Splats on Al\_BT indicate more NiCr adhered to the crater than for Al\_B, and thicker splats, such as the one shown in Fig 7c, which were only found on Al\_BT. No partially melted splats, as seen for Al\_P and Al\_PT, were found.

Figure 8 shows a FIB cross-section of a typical splat. The crater here is about 5 μm deep (1), but compared to splats present on the non-boiled specimens, less NiCr has adhered to the substrate (2). Furthermore, the shape of the NiCr fragments and also the shape of their grains are quite irregular. Some lift-up of the Al substrate at the periphery of the crater can also be observed (3). The hydroxide layer produced by the boiling treatment, which exhibits a dark contrast on the FIB cross-section can be observed here just outside the crater (4), and some thinner remnants of this layer can also be seen in the crater (5).

TEM examination of the splats, for example the cross-section presented Fig. 9, confirms the presence of Al hydroxide: on one hand EDS elemental maps (see Fig. 9b and d) confirm the presence of a layer rich in Al and O on top of the Al substrate; on the other hand the electron diffraction pattern (see Fig. 9f) obtained from this layer presents rings that are consistent with boehmite  $\gamma$ -AlOOH (as described in a previous study [131]).

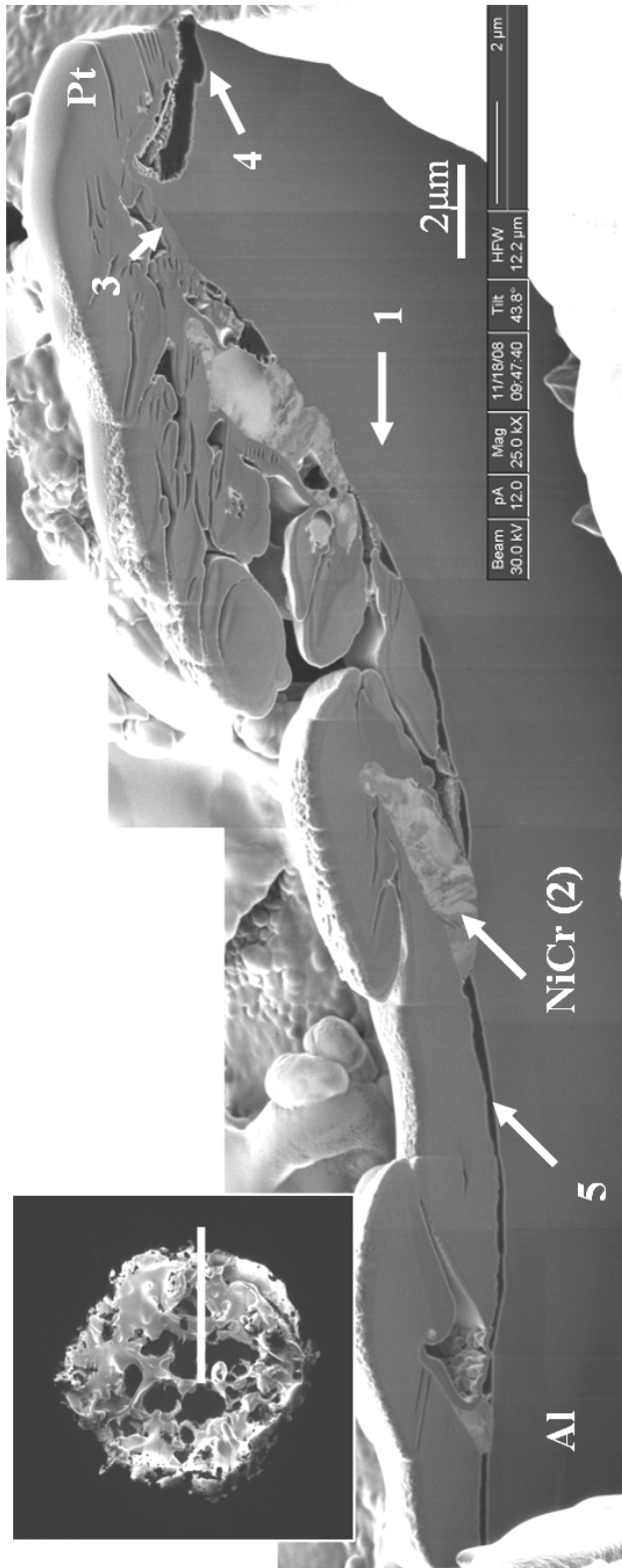


Figure 8. FIB cross-section of a fully melted splat (see insert image) on Al\_BT

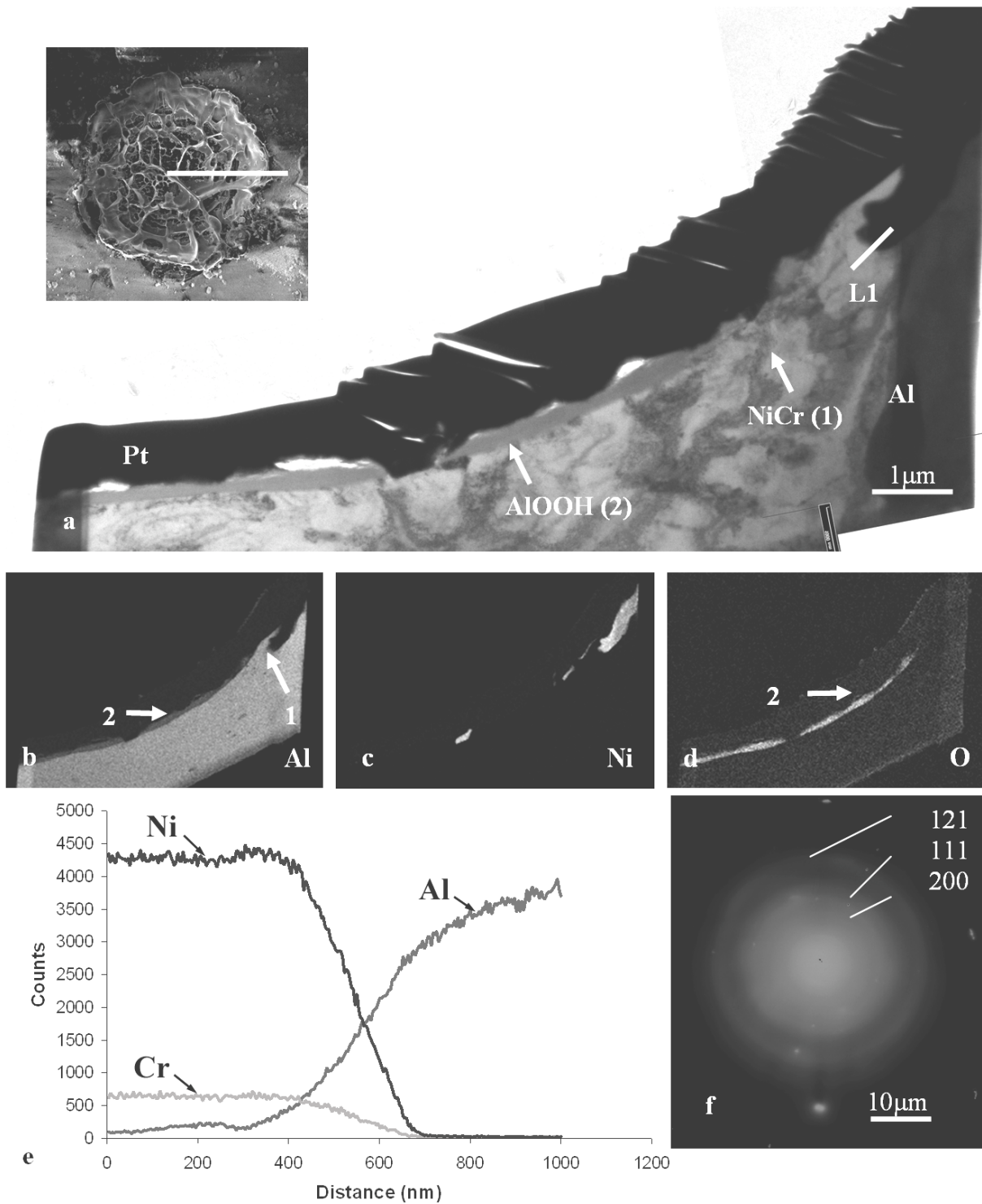


Figure 9. TEM cross-section of a typical splat (see insert image) found on Al<sub>2</sub>O<sub>3</sub>/BT: (a) bright field image, EDS elemental maps for (b) Al, (c) Ni and (d) O, (e) elemental linescan made across the splat-substrate interface, (f) diffraction pattern of AlOOH

It should be noted that corundum  $\text{Al}_2\text{O}_3$  presents a similar ring pattern to boehmite and the two phases are not readily distinguished using electron diffraction. However, x-ray photoelectron spectroscopy (XPS) data suggested that the phase most likely to be present is  $\gamma\text{-AlOOH}$  [49]. Furthermore, it can be noted that no NiCr is present on top of the Al hydroxide phase: the fragments of NiCr that have adhered to the substrate are directly in contact with the aluminium. In these regions, the contact between the splat and substrate is good and the splat-substrate interface irregular. The elemental EDS linescan performed across the interface is that area shows that, similarly to the Al\_P and Al\_PT substrates, Ni has diffused into the substrate to a depth of about 150nm.

### III.2.b. *Splat formation and effects of the boiling treatment*

It has been observed that on both boiled and boiled and thermally treated aluminium specimens, before spraying, a relatively thick ( $\sim 300$  nm) layer of hydroxide was present on the substrate surface. Such layer was also found to inhibit adhesion of splats in the case of plasma spraying, possibly due to the dehydration of the hydroxide layer from the heat from the spray process, causing the release of a significantly large amount of gas that hinder the contact between NiCr and the Al substrate [131].

Here, FIB and TEM cross-sections showed that the splat microstructure is similar to the one of the splats found on Al\_P and Al\_PT in several places, suggesting similarities in the splat formation process. The crater shows that the sprayed particle impacted in a

partially melted state, and the solid core deformed the Al substrate, causing the crater observed. A limited amount of NiCr was also found to have adhered to the substrate. This was probably made possible by the partial destruction of the hydroxide layer by the NiCr particle impacting on the substrate with a high momentum. Indeed, such a layer was found to be much thinner and not uniform inside the craters. Moreover, no NiCr could be found where the hydroxide layer was present. It should be noted, however, that much less NiCr constitutes the splats on the boiled specimens compared to the non-boiled ones: even if it gets partially destroyed, the hydroxide layer does completely limit the adhesion of NiCr onto the substrate.

Where the hydroxide layer has been removed, similar to the case of the fully melted splats on Al\_P and Al\_PT, the high pressure build up from the impact of the high momentum particle along with the relatively high temperature of the melted NiCr allows very good contact between NiCr and Al and sometimes the localized melting of the substrate, which may then be jetted by the flowing movement of the splat, and mixed with the NiCr phase.

An important point of difference between boiled and non-boiled specimens is the absence of partially melted splats on the boiled specimens. However, it is expected that the breaking up of the solid core, which led on the polished substrates to the formation of partially melted splats, may also occur for the boiled substrates, and possibly with the same frequency. A possible explanation may be that the breaking up of the solid core upon impact means that the pressure applied by the particle on the substrate is not as

high, thus the hydroxide layer remains and hinders splat adhesion. However, on Al\_P and Al\_PT it was seen that the crater for the partially melted splats was usually around the same dimension as the one for the fully melted splat: if deformation of the substrate occurs in the same way, this means that the pressure applied should be similar and disruption to the hydroxide layer should similarly occur. Another hypothesis may be that only the non-melted fragments did not adhere to the substrate and rebound like the solid core for the fully melted splats. This is in agreement with the observation that much less NiCr can be found in the splats on the boiled specimens compared to the non-boiled ones. Thus, insufficient melted NiCr is present to form the matrix in which the non-melted fragments may become embedded.

Finally, comparing splats between Al\_B and Al\_BT showed that on Al\_BT the splats contained a higher volume fraction of NiCr (for example Fig. 7c). This may be explained by the heat treatment of Al\_BT, which may have allowed a partial dehydration of the hydroxide layer, thus less gas would be released upon splat formation, and NiCr could have a better adhesion on the substrate. It is also possible that the heat treatment caused the hydroxide layer to be more brittle, leading to more damage upon impact by the sprayed particle.

In conclusion, while the thermal treatment at 350°C was observed to have a limited effect on splat formation, the boiling treatment had a strong influence on the adhesion of the splats.

### III.3. Comparison between HVOF and plasma sprayed splats

When comparing the results obtained in the present study with the plasma spraying of NiCr particles onto similar substrates, which were studied previously by the same authors [131], it can be noted that the splats formed are significantly different in morphology. On one hand, in the case of plasma spraying there were no signs of substrate deformation or melting, with usually quite a poor contact between splat and substrate. However, some authors have found that substrate melting could occur, when plasma spraying Ni and Cr onto Al substrates, for instance Kitahara *et al.*[35], or when plasma spraying NiCr on stainless steel [50]. On the other hand, there was no sign for plasma sprayed splats that most of the sprayed particle would rebound for the substrate, as seen for HVOF. Nevertheless, upon subsequent spraying passes, it is expected that rebound of the NiCr particle would cease, as NiCr coatings are often sprayed onto Al by HVOF [1].

Concerning the effects of surface chemistry, in the case of plasma spraying, heat treating the Al substrate slightly increased the wetting of NiCr, giving splats a more circular and flatter morphology, and boiling completely prevented any splat to adhere on the substrate [131]. For the HVOF process it can be noted that the effects of the pre-treatments, and, thus, the changes in the surface chemistry they create, are weaker. A possible explanation is that due to the lower temperature and higher velocity of the sprayed particles, and the partially melted state in which they impact on the substrate, the influence of elements such as wetting and gas desorption is hindered by the fact that the particle impacts the substrate with a high momentum, therefore applying a high pressure to it. Moreover, from

the deformation of the substrate, the layers formed by the pre-treatments tend to be altered, thus NiCr may interact more directly with the Al substrate, without the presence of oxides or hydroxides. Work is currently being performed on splats sprayed in different conditions to bring further insight into these hypotheses.

#### **IV. Conclusion**

In summary, NiCr was HVOF sprayed on to Al substrates having undergone various pre-treatments (boiling and heating) which modified their surface chemistry. The following observations were made:

- For all specimens, the NiCr particles impacted the substrate in a partially molten state. The solid core deformed the substrate, creating a crater in which only a small portion of NiCr particle adhered to the substrate. Where effective contact between molten NiCr and Al was achieved, substrate melting often occurred: the molten aluminium may then be jetted within the splat and/or lifted-up at the periphery of the crater, and at the splat substrate interface, the mixing of both phases may lead to particular very finely grained microstructure made of a mixture of Ni and Al grains.  $\text{Cr}_2\text{O}_3$  was found to form as a thin layer on the outer surface of the splats, and in some pores at the splat-substrate interface NiO or  $\text{NiCr}_2\text{O}_4$  may form as well. Some splats were also found to be made of a mixture of non-melted fragments in a melted matrix of NiCr, but they were absent from the boiled specimens.

- The thermal treatment is expected to increase the thickness of the  $\text{Al}_2\text{O}_3$  layer present on top of the substrate, and was found to increase the amount of molten NiCr that adheres to the substrate.
- The boiling treatment created a thick and dense boehmite layer on top of the Al substrate, which significantly limited the amount of NiCr adhering on the substrate.

Consequently, using electron microscopy to study the splat microstructure at a nano-scale level allowed a new insight on the mechanisms of splat formation, while it was shown that substrate surface conditions can be a significantly important parameter regarding the influence on splat formation and thus the performances of the fully deposited coating.

## CHAPTER 9

# STUDY OF THE SPLAT MICROSTRUCTURE AND THE EFFECTS OF SUBSTRATE HEATING ON THE SPLAT FORMATION FOR NiCr PARTICLES PLASMA SPRAYED ON TO STAINLESS STEEL SUBSTRATES

---

*S. Brossard, P.R. Munroe, A.T.T Tran, M.M. Hyland, Journal of thermal Spray  
Technology, 2010, (in publication)*

### Abstract

The plasma spraying process is still poorly understood in term of the processes by which the coating is built up, especially coating interactions with the substrate. This present study enhances this understanding by studying, through a range of electron microscopy techniques, single NiCr splats plasma sprayed onto stainless steel substrates, which were first exposed to different heat treatments. The microstructure of the splats, particularly the splat-substrate interface, was characterized, and the formation of the observed features is discussed. Evidence of localized substrate melting and inter-mixing with the splat material was found, showing metallurgical bonding. The structures observed were also correlated to the treatment of the substrate, demonstrating how such treatments can

influence the properties of the fully deposited coating by modifying the splat formation process. Most notably, heating the substrate during spraying was found to significantly modify splat formation by reducing splashing and increasing the extent of substrate melting.

## **I. Introduction**

Conventional plasma spraying is one of the most commonly used thermal spray processes due to its flexibility and versatility, allowing the manufacturing of coatings made of almost any material with a congruent melting point on to a wide range of ceramic, metallic or polymer substrates. Such a process permits the substrates to retain their original characteristics (chemistry, structure and properties), as they undergo no or minimal melting. Further, it avoids the use of potentially polluting chemical solutions. However, understanding of the mechanisms of interaction between substrate and coating and the nature of their interface is limited for many thermal spray processes. [1, 4]

Coatings are made through the accumulation of the sprayed molten particles which flatten upon impact to form lamella, often termed splats. The microstructure of fully deposited coatings has been studied through the observation of cross-sections at both a macroscopic and microscopic level [6-9]. However, for a more detailed insight of the coating formation process and the nature of the splat interaction with the substrate, study of single splats is necessary and a number of prior studies have been performed which have investigated these features. Morphology of the splats has also often been observed at both

a macroscopic level (with millimetre size droplets, allowing *in-situ* study of their formation [11-15]) and microscopic level (with micron size droplets) [16], to understand the influence of factors such as the spray conditions, the combination of materials used as substrate and feedstock powder [19, 20], the temperature of the substrate during spraying [6, 20, 21, 26-29] or the substrate surface topography and chemistry [11, 21-25]. For example, it was observed that substrate temperature during spraying was a key parameter for the control of splashing of the splats. Specifically, for substrates heated above a particular temperature, termed the “transition temperature”, disc-shaped splats were obtained, instead of very irregularly shaped splats [6, 20, 21, 26-28]. Possible explanations for such phenomenon include desorption upon heating of adsorbates/condensates that were initially present on the substrate surface, and the solidification of the splat starting during flattening.

There have been relatively fewer published studies that have focused on the coating-substrate interface. Kitahara *et al.*, studied the coating-substrate interface by spraying a range of materials including Ni and Cr, on to various substrates including mild steel [35]. They observed, by X-ray diffraction, in most cases, the presence of an intermetallic layer at the interface, interpreted as evidence of localized substrate melting. However, such interactions were not observed for the case of either Ni or Cr sprayed on to steel substrates. Localized steel substrate melting was also observed by Zhang *et al.* [20] and by Li *et al.* [36], both when plasma spraying Mo. In this case, a Fe<sub>2</sub>Mo intermetallic phase was observed by transmission electron microscopy (TEM) at the interface. In such cases, bonding between the coating and substrate is said to be metallurgical. Elsewhere,

the adhesion of the coating is expected to occur by mechanical interlocking [1], as substrate melting has either not been investigated or directly observed [23, 25, 82, 138, 139].

Modelling has also been widely used to describe the splat formation process [13, 17, 18]. However, such models cannot explain all the features observed, such as localized substrate melting, possibly due to the lack of precise input data and the difficulty of modelling discontinuous, non-averaged, heat transfer resistance across the interface.

Indeed, very little work on splat microstructure and the splat-substrate interface at high resolution has been performed. In the present study, particles of NiCr, a material often used in thermal sprayed coatings as bond coat or for protection of steel against heat, corrosion [122], erosion, for example in boilers [1], were plasma sprayed to form single splats. The substrates used were 304 stainless steel and subjected to different heat treatments, i.e. sprayed at room temperature as-polished, sprayed at room temperature after being heat-treated and heated during spraying. Such treatments are expected to vary the substrate's surface chemistry, which may in turn influence the splat formation process and their final morphology. Indeed, as noted earlier, heating the substrate during spraying may significantly reduce splashing upon splat formation [6, 20, 21, 26-28]. Furthermore, NiCr or Ni splats formed on pre-heat treated steel specimens were found to be much flatter, with a larger diameter [11, 67]. Cedelle *et al.* suggested this was possibly due to a better wetting from the Ni splat, supposedly from the positive skewness resulting from the heat treatment [11], which increases the oxide content of the substrate surface [49].

Previous studies, by the same authors as this present publication, have described the microstructure of plasma sprayed NiCr splats on steel substrates which had first undergone various pre-treatments (as-polished, thermally treated, boiled, boiled and thermally treated etc) [50, 67]. Evidence of localized substrate melting was observed, as well as an increase in splat diameter for both heated and boiled specimens. It was also noted that pre-heating the substrate prior to spraying significantly reduced the occurrence of substrate melting, possibly because the splats were also noted to be thinner. However, compared to the work presented here, spraying conditions were significantly different (that is, both the velocity and temperature of the sprayed particles were notably lower). As a result, the morphologies of the splats in this study were significantly less splashy than the splats analysed here.

The NiCr single splats formed on the steel substrates (sprayed as-polished, after thermal treatment or heated during spraying) were studied using a range of electron microscopy techniques, to investigate their microstructure and their interaction with the substrate. Observations were then used to discuss the effects of substrate surface chemistry induced by heat treatments and the splat formation process.

## **II. Experimental procedure**

Three different substrates were used; all prepared from stainless steel 304. These are listed in Table 1.

**Table 1. Substrate Nomenclature and Conditions**

<b>Specimen</b>	<b>Substrate</b>	<b>Pre-treatment</b>
SS_P	Stainless steel	Polished (to a nano-scale smoothness)
SS_PT	Stainless steel	Polished and thermally treated prior to spraying
SS_PH	Stainless steel	Polished and heated during spraying

All substrates were firstly mechanically ground and mirror polished with diamond paste, to a nano-scale roughness. The thermally treated substrate was heated at 350°C for 90 minutes in air. Such a treatment is expected to increase the oxide content of the substrate surface, partially dehydrate the oxide layers, and/or to induce some level of surface roughness. One substrate was also heated to a temperature of 350°C 30 min before spraying and held at that temperature during spraying, which is above the expected transition temperature at which adsorbates/condensates species, such as water, present on the substrate surface may be released [49].

The sprayed material was a commercial NiCr alloy powder (Ni80-Cr20, Sulzer Metco 43 VF-NS, Switzerland, (-106+45)  $\mu\text{m}$ ). Plasma spraying was carried out with a Sulzer Metco (Switzerland) 7MB gun (with a nozzle diameter of 8 mm), operating at a current of 550A and at a voltage of 62V, with a spraying distance of 100mm. The feeding rate of the powder was of 1g/min, the carrier gas being argon at a flow rate of 3 SLPM, while the

plasma gas was a mixture of nitrogen and hydrogen, at a flow rate of 47.5 SLPM and 6.2 SLPM respectively. The temperature of the sprayed particles was measured using a DPV 200 pyrometer, and their velocity was evaluated using a Laser Doppler velocimeter.

The specimens were then characterized using a range of analytical techniques. A Hitachi S3400 scanning electron microscope (SEM) was used to image the overall morphology of the splats and the substrates. A FEI xP200 Focused Ion Beam microscope (FIB) was used to mill cross-sections of the splats using an energetic gallium ion beam, and to image them using secondary electrons induced by the ion beam. Details have been described elsewhere [51]. A FEI xT Nova Nanolab 200 dual beam microscope (that is a FIB and SEM combined into a single instrument) was used to prepare cross-sections of splats (100-200nm in thickness) suitable for TEM observation. These were prepared using the lift-out method as described elsewhere [51] and examined in a Philips CM200 transmission electron microscope (TEM) to which energy dispersive x-ray spectroscopy (EDS) facilities have been interfaced. Finally, the average surface roughness of the substrates was measured using a Digital Instruments DI3000 Atomic Force Microscope (AFM).

Several FIB and TEM cross-sections were prepared and studied for each particular feature and/or type of splat. However, for reasons of brevity only a small number of representative images will be presented here. The cross-section preparation process using FIB also involves the deposition of a layer of platinum on top of it prior to milling for protection purposes. This layer is present on the FIB and TEM images presented.

### III. Results and discussion

Observations concerning the morphology of the splats, their microstructure and the splat-substrate interface, as observed on FIB and TEM cross-sections, are detailed, and the splat formation discussed, firstly for the polished (SS\_P) and polished and thermally treated (SS\_PT) specimens, as they are quite similar, then secondly, for the substrates heated (SS\_PH) during spraying.

#### III.1. Study of the splats found on the SS\_P and SS\_PT substrates

##### III.1.a. *Description of the splat population*

SEM images of about 50-60 splats were recorded for both substrate types. For each splat, the diameter,  $D$ , was evaluated by measuring the smallest and largest values and taking the average,  $D_m$ . Splashed fingers were ignored. However, for splats presenting a dense ring of splashed fingers, the diameter,  $D_r$ , for this ring was also measured and expressed as a function of the diameter of the splat itself. See Fig. 1a for example.

Three types of splats were recognized:

- Splats presenting a large and dense ring of splashed fingers (see SEM image presented Fig. 1a). Such splats were denoted “RSF splats”.
- Splats with no splashed fingers (Fig. 1b). Such splats were denoted “NSF splats”.
- Very fragmented splats (Fig. 1c)

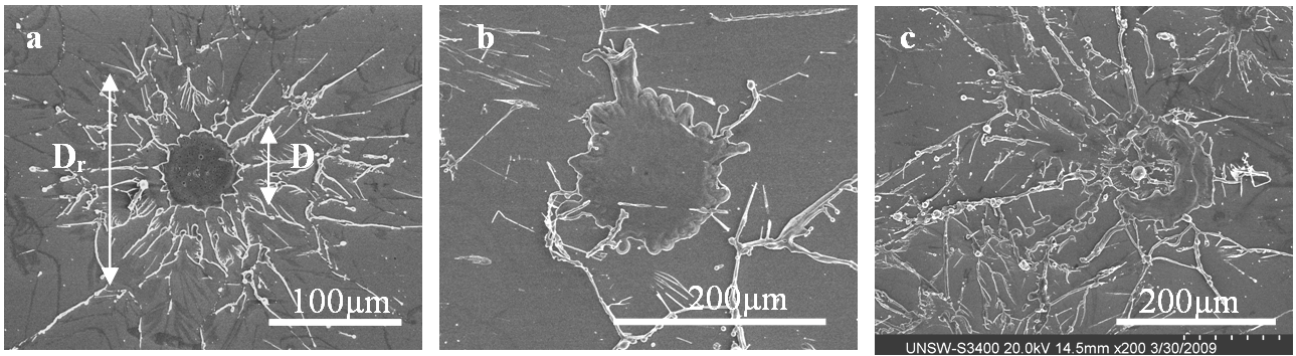


Figure 1. SEM images of different types of splats found on SS\_P and SS\_PT: (a) splat with a ring of splashed fingers, (b) splat with no splashed fingers, (c) very fragmented splat with splashed fingers.

The relative population and dimensions of the splats found on the SS\_P and SS\_PT specimens are summarized in Table 2.

**Table 2. Relative proportions and average diameter of the splats (and average diameter of the ring of splashed fingers if applicable) found on SS\_P and SS\_PT**

	SS_P	SS_PT
RSF splats	44% $D_m = [81 \pm 30] \mu\text{m}$ $D_r = [3.0 \pm 0.8] D$	60% $D_m = [135 \pm 45] \mu\text{m}$ $D_r = [2.2 \pm 0.6] D$
NSF splats	39% $D_m = [95 \pm 38] \mu\text{m}$	40% $D_m = [161 \pm 80] \mu\text{m}$
Very fragmented splats	17% $D_m = [104 \pm 30] \mu\text{m}$ $D_r = [2.3 \pm 0.8] D$	

It can be noted that the RSF splats represent the majority of the splats observed, but their diameter is smaller, possibly because of the material loss from the splashing. A detailed comparison between the values from the non-thermally treated and the thermally treated specimen is given later and provides an understanding of the effects of such a thermal treatment.

### III.1.b. *Structure and formation of the RSF splats*

Figure 2 shows a TEM cross-section made across the central part of such splat found on SS\_P (the inset secondary electron image shows both the splat and the location of the cross-section). Firstly, it can be observed that towards the centre of the splat, the splat-substrate interface (marked 1) is indistinct and the grains boundaries of the steel and NiCr phases are coincident across this interface (marked 2). The EDS elemental linescan, marked L1, (Fig. 2d) performed across this part of the interface shows that the variation of Ni and Fe concentrations is gradual (3): interdiffusion of both elements has occurred over a distance of about 200 nm. Electron diffraction studies, particularly the observation of Kikuchi maps, also showed that on each side of the interface the grains exhibit the same orientation. Both NiCr and austenitic stainless steel have the same crystal structure (face-centered cubic), with similar lattice parameter (0.352 nm for steel, 0.355 nm for NiCr). It can be concluded that, contrary to previous studies [35], localized melting of the substrate has occurred, allowing the interdiffusion of both phases over a significant depth, but no intermetallic phase was observed to be present. Furthermore, the Fe and Ni EDS elemental maps (Fig. 2b and 2c) show that the substrate has jetted within the NiCr splat (4) in a way that clearly indicates the steel substrate has been melted. The occurrence of

steel melting is consistent with modelling experiments which have shown that temperature at the splat-substrate interface may reach 1660°C, the melting point of steel being 1454°C [55]. This would, however, require intimate contact between the molten splat and the substrate.

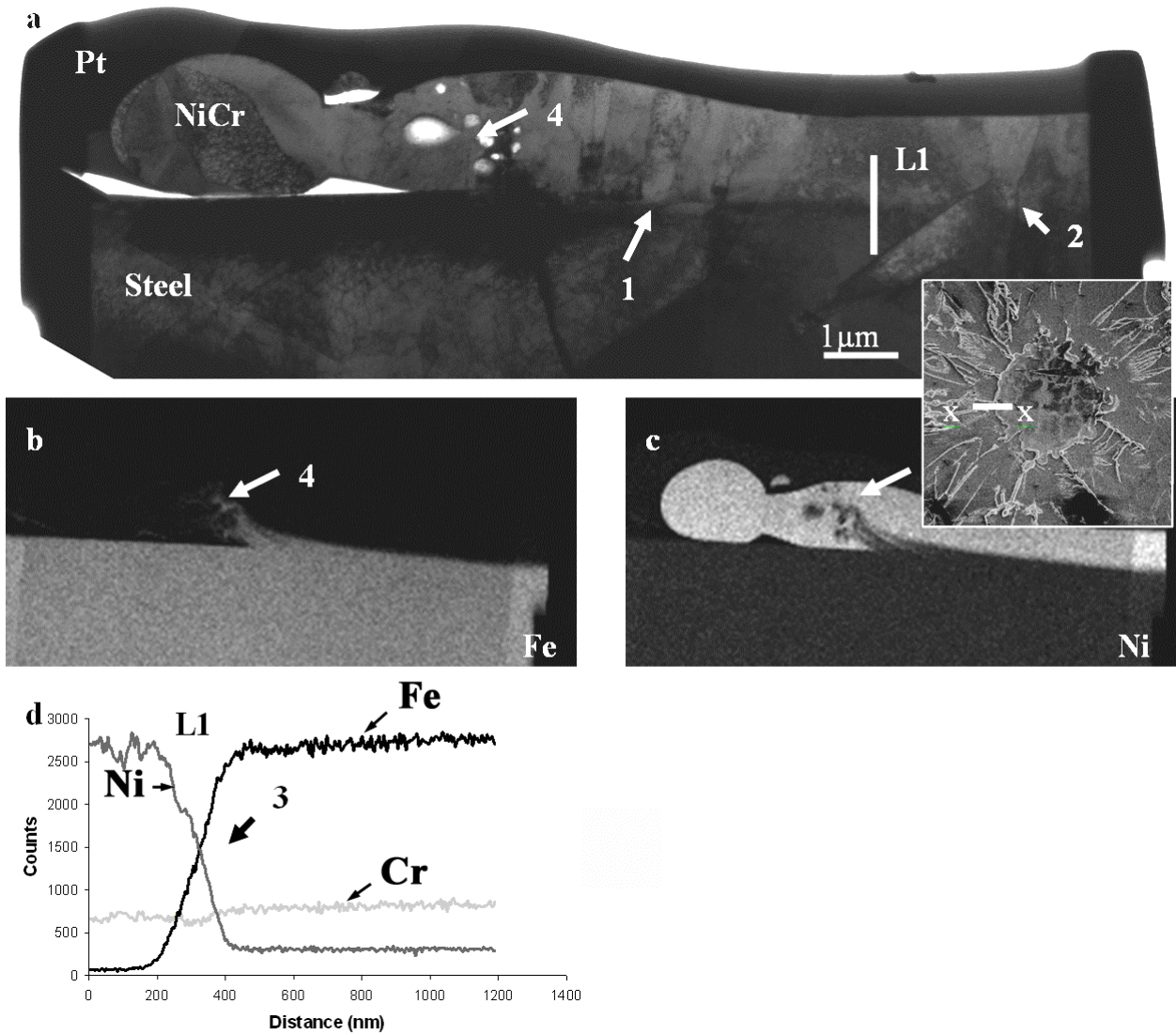


*Figure 2. TEM cross-section made across the rim of a RSF splat (see insert picture) found on SS\_P: (a) bright field image, EDS elemental maps for (b) Fe, (c) Ni, (d) EDS elemental linescan*

The grains of the splat, which here are columnar, have thus formed epitaxially on the pre-existing grains of the steel substrate. It was also observed that in such a location where very good contact between splat and substrate is achieved and substrate melting has occurred, that the grains are relatively large (up to 10  $\mu\text{m}$  in diameter, compared to 1-2  $\mu\text{m}$  in other regions where melting did not occur). This suggests that solidification in this region was relatively slow, which is unexpected considering that intimate contact between splat and substrate usually implies efficient heat removal from the splat through the interface with the substrate. The fact that the thermal diffusivity of steel ( $\sim 4 \times 10^{-5} \text{ m}^2 \cdot \text{s}^{-1}$ , as calculated from [84]) is relatively low compared to other metals may have played a role in retaining the heat and slowing the solidification process.

Some voids may also be found in the centre of such splats, as it can be seen on the FIB cross-section presented in Fig. 3a (region marked 1). It can be noted that they are not located at the splat-substrate interface, but rather within the splat itself. The splat-substrate interface (2) is also indistinct and irregular, evidence that melting of the substrate has occurred at this location, along with some mixing/interdiffusion between the NiCr and steel phases, while some grains boundaries (3) are coincident across the interface.

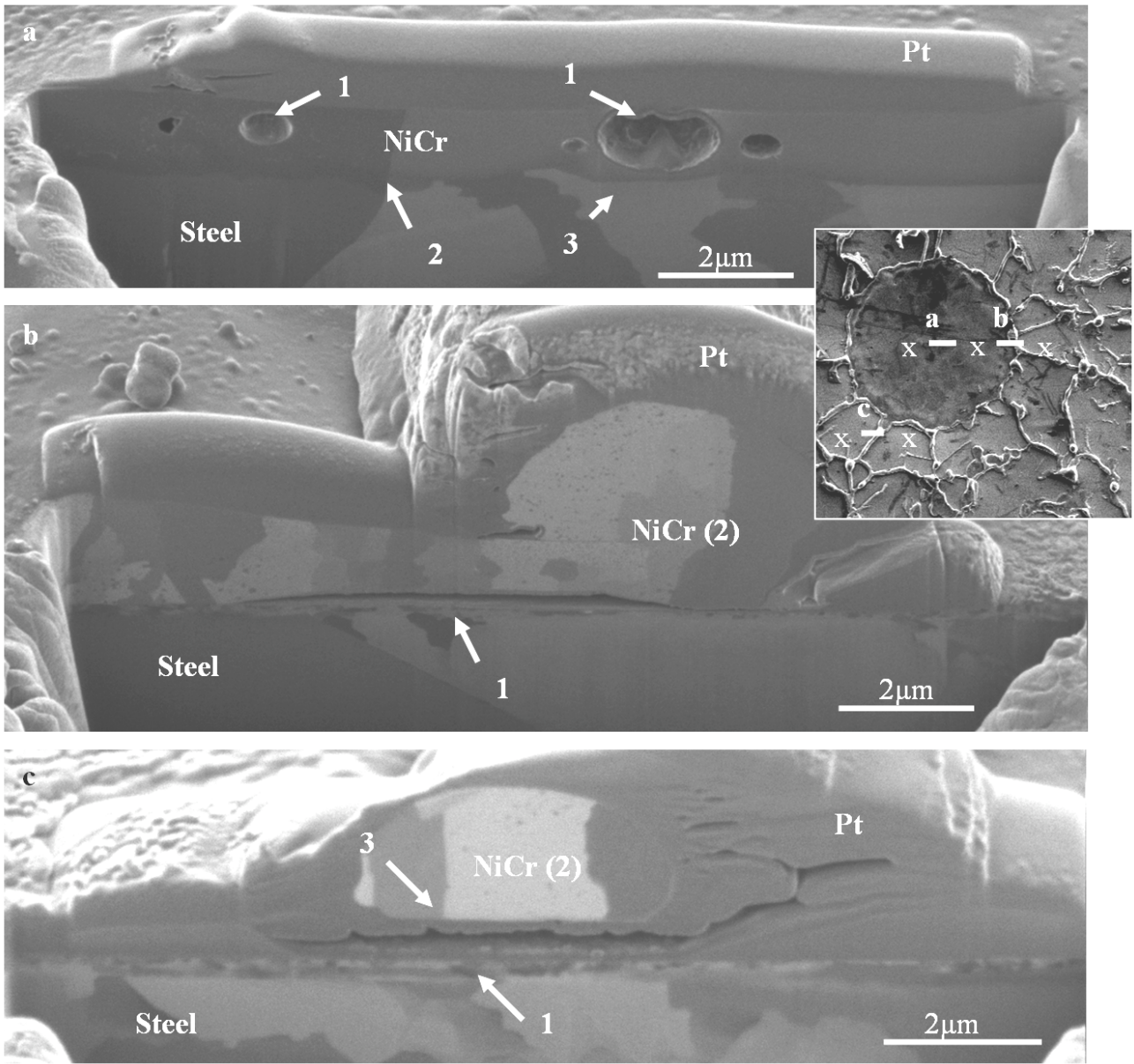


*Figure 3. FIB cross-section made across (a) the centre, (b) the rim, (c) a splashed finger of a RSF splat (see insert picture) found on SS\_P*

The intimate contact between the splat and substrate and the observation of substrate melting are not evident on all splats with this morphology or even all along a single splat. As it can be seen on the FIB cross-sections in Fig. 3, under the rim of the splats (Fig. 3b)

or under the splashed fingers of the splat (Fig. 3c), the contact between splat and substrate is always poor. Here, the outer surface of the substrate is clearly visible and flat (1), no evidence of substrate melting can be found, while the grains of the splat are coarse and irregular (2) rather than columnar (with diameters ranging from 1 to 5  $\mu\text{m}$ ). This is consistent with poor contact, as it shows that significant thermal contact resistance, induced by the gap present between the splat and the substrate, has prevented efficient heat removal from the splat through the substrate, inducing a relatively slow rate of solidification.

Iron oxide was often found to have formed on the lower surface of the splats where they have been lifted-up away from the substrate, notably under the rim or the splashed fingers of the splats, as it can be seen for instance on Fig. 3c (3). This phase has been identified by TEM as being wustite ( $\text{FeO}$ ). Such an oxide phase may have formed from iron that has deposited on the bottom surface of the splat and became oxidized by the hot oxidizing gases that may be present here (see paragraph II.1.d for more detail on their formation) when the splat becomes lifted-up. Wustite may have formed in preference to other forms of iron oxide possibly due to the limited supply of oxygen, as it is located in an enclosed space. Fig. 4 shows a TEM cross-section made across a splashed finger: EDS elemental maps (Figs. 4b, 4d and 4e) show that such a phase contains Fe, Cr and O (1), and the rings obtained from the diffraction pattern (presented Fig. 4f) are consistent with being from spinel  $\text{FeO}\cdot\text{Cr}_2\text{O}_3$ , which is another oxide form that can form, in a similar manner to  $\text{FeO}$  [61, 62].

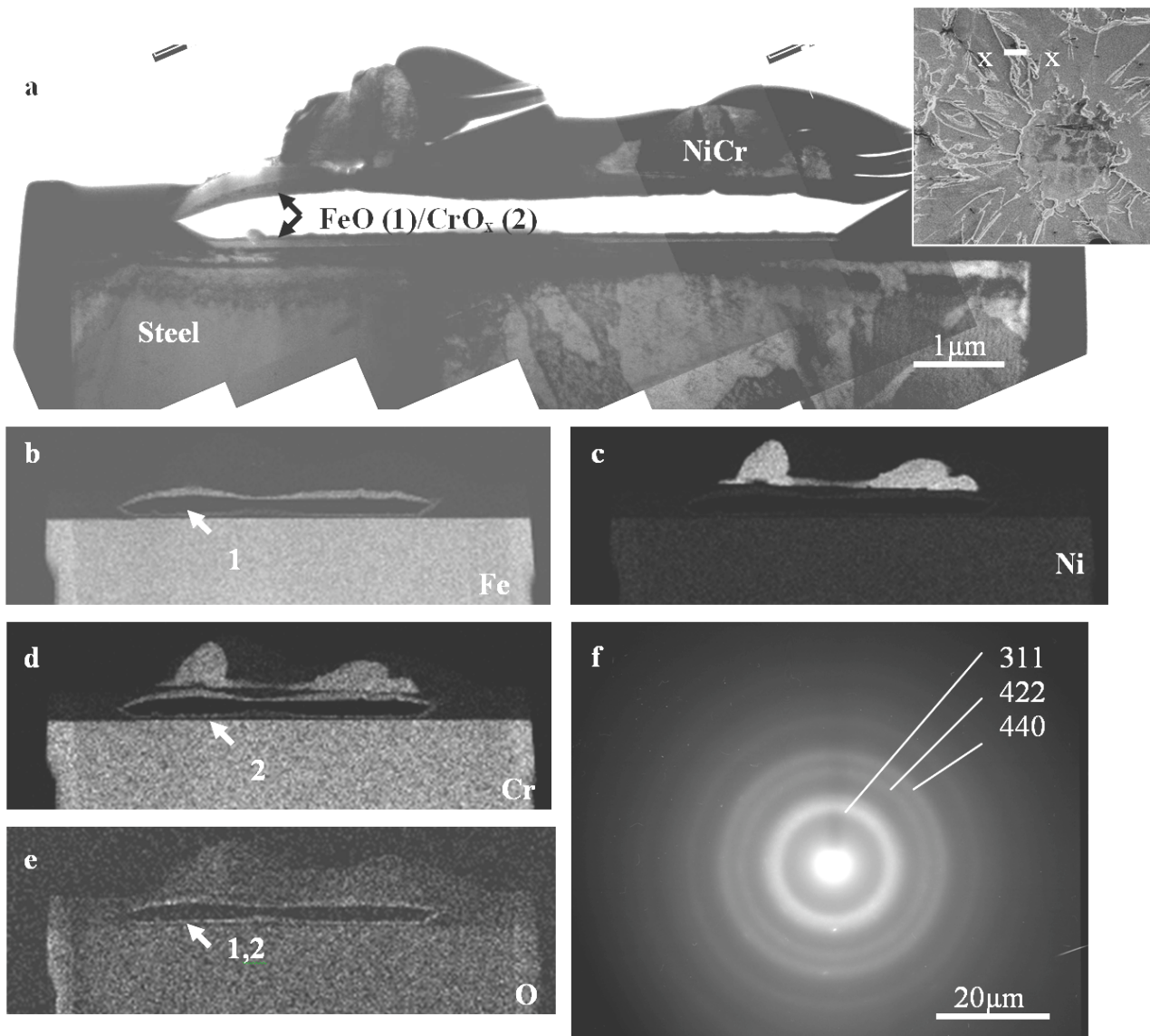


*Figure 4. TEM cross-section made across a splashed finger of a RSF splat (see insert picture) found on SS\_P: (a) bright field image, EDS elemental maps for (b) Fe, (c) Ni, (d) Cr, (e) O, (f) spinel  $FeO \cdot Cr_2O_3$  diffraction pattern.*

Some splats, found on the thermally treated substrate, SS\_PT, also display a distinct splat-substrate interface in their centre, such as that seen on the TEM cross-section presented Fig. 5a (1). The linescan L1 (Fig. 5) confirms the absence of interdiffusion

between Ni and Fe across the interface, as the variation of their concentrations is sharp at the interface (2). In such locations, grains are usually columnar and relatively large (5-10  $\mu\text{m}$ ) (3), similar to the splats where substrate melting has occurred, as described earlier.

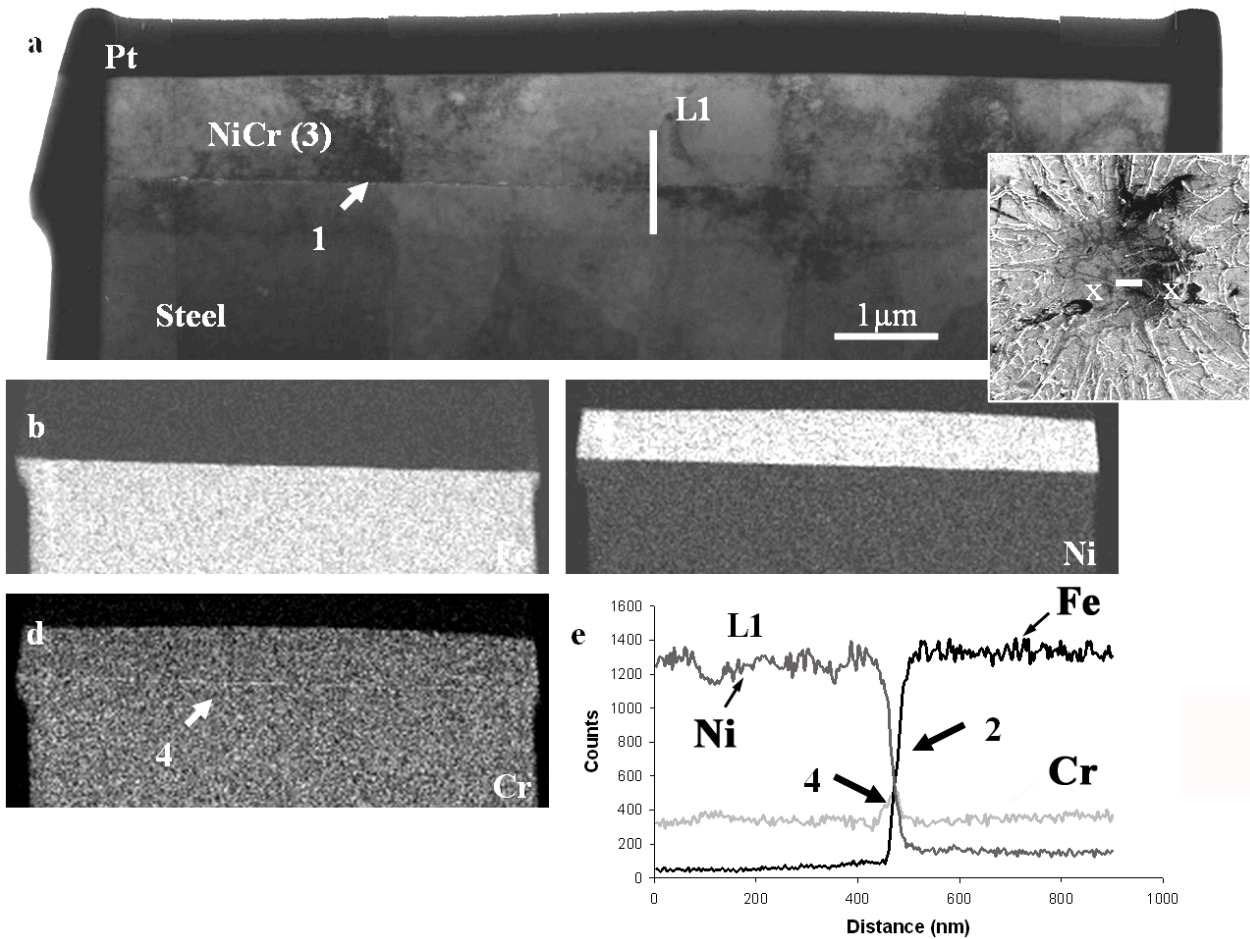


*Figure 5. TEM cross-section made across the centre of a RSF splat (see insert picture) found on SS\_PT: (a) bright field image, EDS elemental maps for (b) Fe, (c) Ni, (d) Cr, (e) EDS elemental linescan*

Furthermore, the Cr EDS elemental map (Fig. 5d) and the linescan (Fig. 5e) show that a thin layer of chromium has segregated to the splat-substrate interface (4), and it is most

probable that this phase is chromium oxide. Such an oxide may have formed from the oxidation of the chromium in the steel substrate, either from the heat treatment (as this is only found on the thermally treated specimen), or from the heat provided by the plasma flame. The layer of oxide is too thin to be unambiguously identified by electron diffraction, however previous studies of the oxidation of stainless steel showed that  $\text{Cr}_2\text{O}_3$  was the species most likely to form on stainless steels, such as the 304 type, along with  $\text{Fe}_2\text{O}_3$  and associated spinel oxides [61, 62].

### III.1.c. *Structure and formation of the NSF splats and very fragmented splats*

Despite their difference in shape, both categories of splats displayed the same general features regarding their interaction with the substrate. Indeed, it was frequently found that the contact between splat and substrate was poor, such as on the left side of the TEM cross-section shown Fig. 6 (1), where FeO is present on the underside of the splat (2) as a relatively thick (50-200 nm) and dense layer. In some zones, however, good contact between splat and substrate is achieved (3); the interface remains distinct in most cases, thus with no obvious evidence of substrate melting. However, as shown on the linescan L1 (Fig. 6f) performed across the interface, interdiffusion between Ni and Fe may occur, in this instance over a depth of about 100 nm (4).

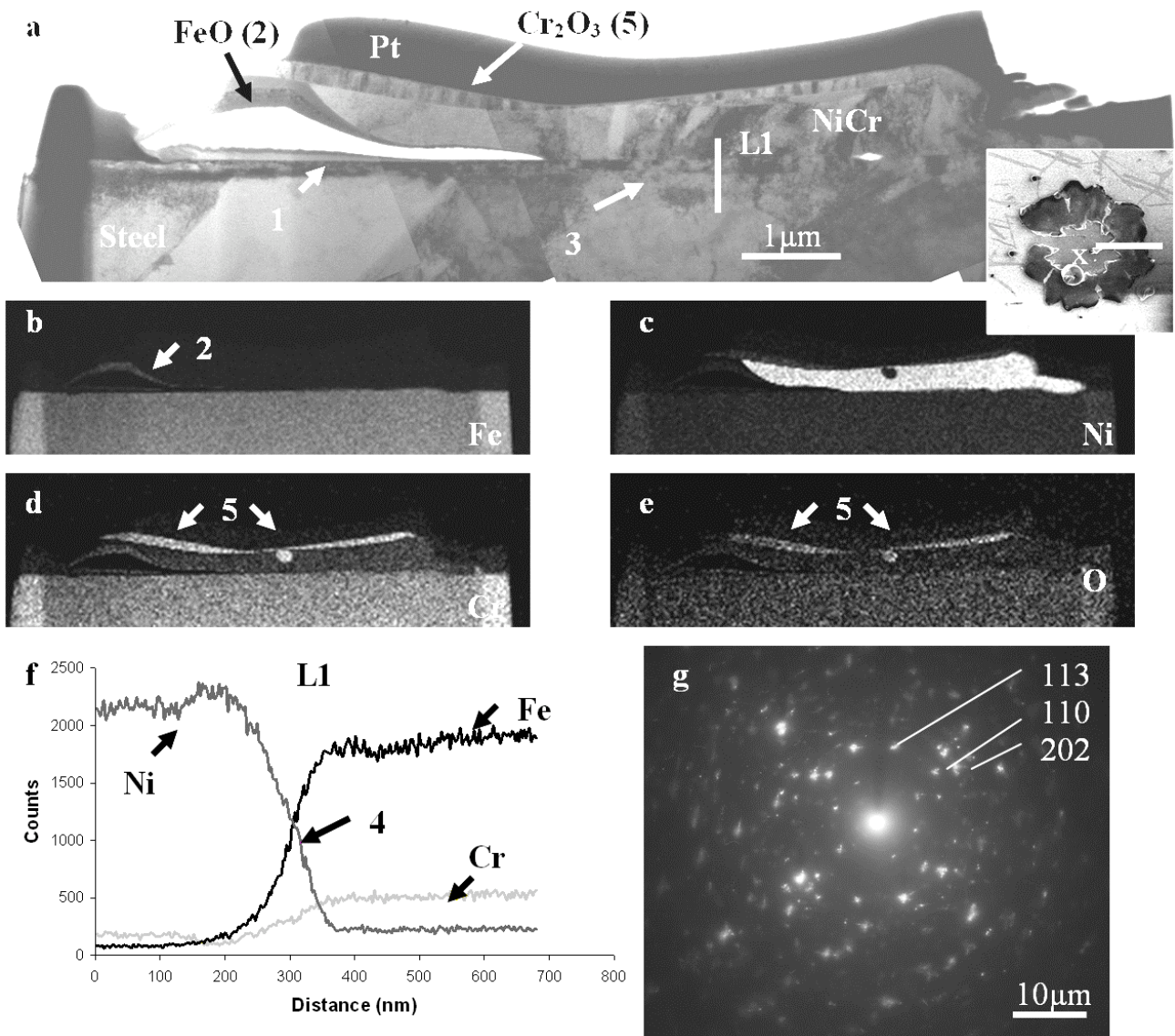


Figure 6. TEM cross-section made across a NSF splat (see insert picture) found on SS\_P: (a) bright field image, EDS elemental maps for (b) Fe, (c) Ni, (d) Cr, (e) O, (f) elemental linescan, (g)  $\text{Cr}_2\text{O}_3$  diffraction pattern

Substrate melting was not common, but it was observed in some instances, as shown for example on the TEM cross-section shown in Fig. 7: on the EDS elemental maps (Fig. 7b

and 7c) it can be seen that some steel has been jetted within the splat (1), while the splat-substrate interface is also indistinct (Fig. 7a, 2).

Oxide formation is, however, much more common for these splats. Apart from iron oxide, as described previously, chromium oxide was found in larger amounts compared to the RSF splats. Indeed, it may be observed as a dense layer on the outer surface of the splat, as seen in Fig. 6 (5) on the bright field image (Fig. 6a) and on the Cr and O EDS elemental maps (Fig. 6d and 6e). Where the layer was thick enough, electron diffraction allowed the identification of this phase as  $\text{Cr}_2\text{O}_3$ . An example of a diffraction pattern is shown in Fig. 6g. It can be seen that the pattern consists of poorly defined rings, due to the fine grained structure (a few 10 nm) of the oxide,  $\text{Cr}_2\text{O}_3$ . This oxide has been shown to be the most probable species of chromium oxide to form from the oxidation of NiCr alloys [70, 140].  $\text{Cr}_2\text{O}_3$  was also found at the splat-substrate interface, see Fig. 8, and present at the centre of a very fragmented splat. It is present here as a significantly thick layer, marked 1 on the bright field image (Fig. 8a) and the EDS elemental maps (Fig. 8d and 8e). However, while the formation of chromium oxide on the outer surface of the splat may be expected, the presence of such thick layer (100-200nm) of oxide at the splat-substrate interface is less obviously understood.

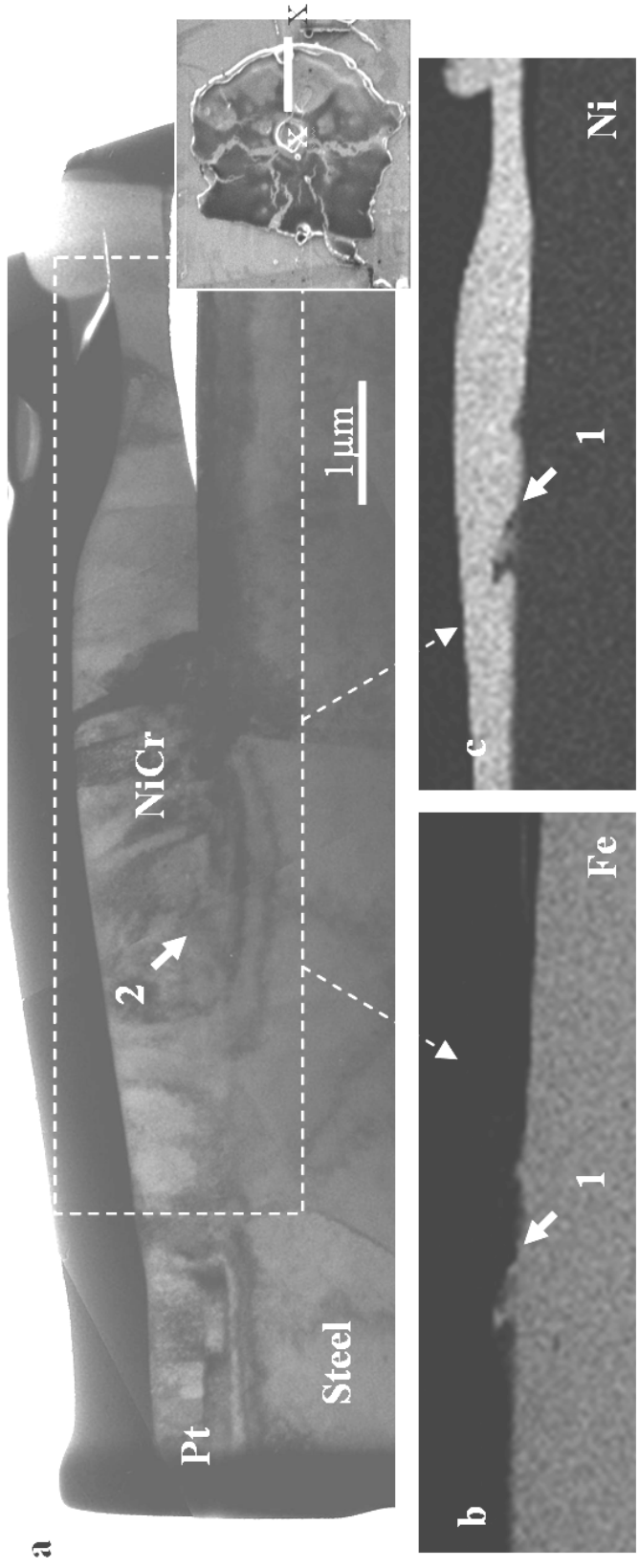


Figure 7. TEM cross-section made across a NSF splat (see insert picture) found on SS\_P:

(a) bright field image, EDS elemental maps for (b) Fe, (c) Ni

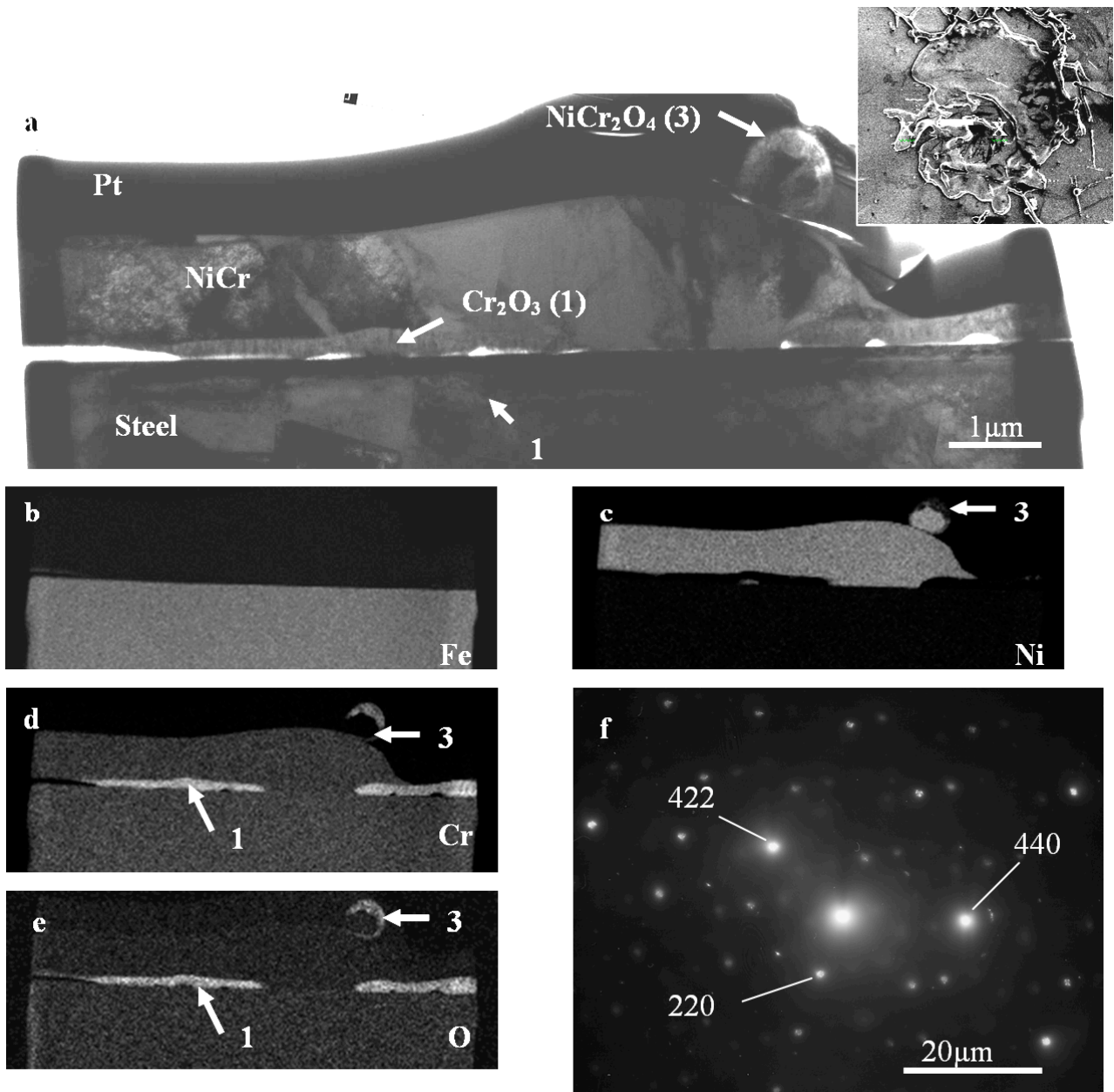


Figure 8. TEM cross-section made across the centre of a NSF splat (see insert picture) found on SS\_P: (a) bright field image, EDS elemental maps for (b) Fe, (c) Ni, (d) Cr, (e) O, (f) NiCr<sub>2</sub>O<sub>4</sub> diffraction pattern.

Indeed, the layer appears too thick to have formed from the oxidation of the stainless steel substrate only, as studies have shown that such layers are usually both uniform and only a few nanometres thick [61, 62]. It has presumably formed from oxidation of the splat. In-flight oxidation of the particle has been shown to lead to the formation of Cr oxide [6], and thus may be the cause of the layer of oxide observed here. Otherwise, such an oxide may have formed after impact due to the presence of significant amounts of hot oxidizing gases, as noted in previous studies of splat formation [6, 26, 32, 67] where there is evidence of gas release from the substrate upon impact and spreading of the particle.

On the same cross-section presented in Fig. 8, spinel  $\text{NiCr}_2\text{O}_4$  (2) was also identified by EDS elemental mapping (Fig. 8c to 8e) and electron diffraction (see corresponding diffraction pattern presented Fig. 8f). This phase, along with NiO (which was not observed on this section), is generally expected to form during the oxidation of NiCr alloys [70, 140], and was also found to form in previous microstructural studies of NiCr splats formed on steel [50, 67], but in those studies these phases were observed more frequently. Such differences may be linked to differences in the splat morphology (splats observed in the previous study did not display as many splashed fingers), possibly caused by variations in the spray conditions and substrate preparation conditions.

### III.1.d. *Summary of the splat formation processes*

In the plasma spray process, the particles impact the substrate in a fully molten state. Many previous studies have investigated how, upon particle impact, adsorbates/condensates become released from the substrate surface, creating instabilities leading to splashing [6, 26, 32, 67]. The numerous splashed fingers observed around the majority of the splats indicate this occurs here. Consequently, for the RSF splats, the formation process may be summarized as follows: upon impact and flattening of the molten NiCr particle, adsorbates/condensates are released from the substrate, and pushed outwards by the flowing NiCr (as no or few voids have been observed towards the centre of the splats previously described). Splashing occurs, possibly due to the instability created by the presence of the desorbed species, some molten material gets jetted away from the substrate, forming the fingers observed. Impact splashing, as described for example by Escure *et al.* [52] and Cedelle *et al.* [12], may also have occurred. Small NiCr droplets may then be splashed away and, when falling back on the substrate, form very small NiCr fragments (usually less than a few microns in size) that were not counted as splats.

In the central part of the splat, good contact with the substrate is achieved due to the pressure applied by the particle on impact on the substrate. This is where the heat transmitted from the molten splat to the substrate may cause local melting. Interdiffusion occurs between the splat and substrate and slow solidification of the molten material, then forming large columnar grains, takes place. However, in some cases melting of the

substrate may not be achieved. As will be discussed shortly, this is believed to be an effect of the thermal treatment applied to the substrate prior to spraying. Towards the periphery and the splashed fingers, the pressure applied by the splat on the substrate is insufficient to allow good adhesion between splat and substrate, or substrate melting. Consequently, when the splat solidifies and cools curling up of the splat take place as a means to accommodate thermal stress [54]. Some iron from the substrate may become attached to the bottom splat of the splat where it is lifted-up and this becomes oxidized, forming FeO layers.

For the very fragmented splats, an explanation of their shape would be that the species desorbed from the substrate are sufficient to create instabilities which are able to cause the breaking up of the flattening molten splat. Consequently, good contact between splat and substrate may not be achieved in the central part of the splat, and no substrate melting may occur.

Finally, for the NSF splats, it is not well understood why splashing was limited. Presumably, fewer adsorbates/condensates may have been released from the substrate, limiting the splashing. However, this would not explain why either no or limited substrate melting was observed, even on the non-heat treated specimen.

### III.1.e. *Effects of the thermal treatment prior to spraying*

As explained in the introduction, the effects of thermally treating stainless steel substrates before plasma spraying NiCr particles have been investigated in a previous study [67]. Overall, the trends observed were similar with the ones obtained here. Indeed, for both studies, splats on the heat treated substrates, compared to the non-heat-treated surfaces, display larger diameters. This can be seen here in Table 2. Possible explanations include the increase in the skewness of the surface of the substrate (because of the increase in the oxide content of the surface ( $\text{Fe}_2\text{O}_3$  and  $\text{Cr}_2\text{O}_3$ )) so it becomes positive, which improved the wettability of the molten splat on the substrate [11]. Also, evidence of substrate melting was less common for the thermally treated substrates, possibly because the splats were flatter, thus transmitting less heating per unit of area to the substrate, or the increase in oxide content increased the thermal resistance.

It should be noted that the effects of pre-heat treatment (increase in splat flattening and decrease in the occurrence of substrate melting) are similar between both studies despite the significant difference in the splats shapes.

It should also be noted that the relative proportion of NSF splats remained unchanged on heat-treatment of the substrate. On the other hand, after such treatment, there are no fragmented splats, rather larger, more regularly shaped RSF splats. As discussed previously, the heat treatment may, at least partially, dehydrate the substrate surface layers, thus limiting the amount of species which get desorbed upon splat formation,

which would then be insufficient to cause the break-up of the sprayed particle. The better wetting induced by the heat-treatment may also play a role.

To conclude, the occurrence of substrate melting is beneficial as it means that the bonding between splat and substrate is metallurgical in these areas. However, it occurs only in limited areas of only a portion of the splats. Elsewhere some voids, including those formed from splat curl-up, and oxides may be detrimental to the properties of the full deposited coating. Heat-treatment of the substrate before spraying, results in a reduction of the occurrence of substrate melting, which may be subsequently unfavourable to the coating's adhesion strength.

### III.2. Study of the splats found on the SS\_PH substrate

#### III.2.a. *Description of the microstructure and formation of the splats*

As it can be seen on the SEM images displayed in Fig. 9, the splats found on the SS\_PH substrate exhibited a very different morphology compared to the substrates held at room temperature during spraying (thus, they are described separately). Indeed, the large majority of splats are disc-shaped, with a smooth rim (see Fig. 9a and 9b). However, a bimodal distribution was observed and the splats can be divided into two different types: large circular splats (~ 45% of the total splat population with an average diameter  $D_m = [210 \pm 78] \mu\text{m}$ , see Fig. 9a), and small circular splats (~ 46%,  $D_m = [37 \pm 13] \mu\text{m}$ , Fig. 9b). In addition to this, some large splats were also found to exhibit a relatively

irregularly shaped rim with short splashed fingers, as seen in Fig. 9c ( $\sim 9\%$ ,  $D_m = [256 \pm 74] \mu\text{m}$ ).

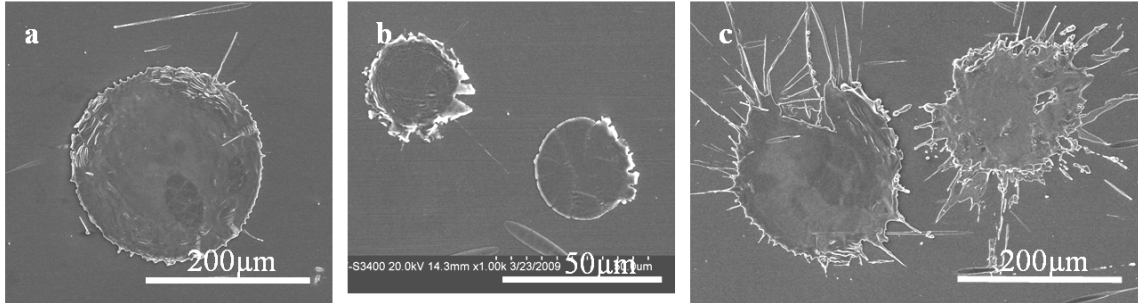


*Figure 9. SEM images of the different types of splats found on SS\_PH: (a) large circular splat, (b) small circular splat, (c) irregularly shaped splat.*

Figure 10 shows a TEM cross-section located in the centre of a large circular splat (similar to that shown in Fig. 9a). On the bright field image (Fig. 10a), the two arrows placed on each side of the cross-section and marked with an “I” indicate the actual position of the NiCr/steel interface, since the contrast between these two phases is not distinct in the TEM image. The splat-substrate interface is more clearly distinguished on the EDS elemental maps (Fig. 10b and 10c). Consequently, the interface marked 1 is not the splat-substrate interface, rather grain boundaries within the steel substrate. The splat-substrate interface, indistinct on the bright field image (2), can be more clearly seen on the EDS elemental maps (Fig. 10b and 10c), and is slightly irregular in shape (3). The linescan L1 (Fig. 10f) shows that interdiffusion between Ni and Fe has occurred across the interface over a distance of  $\sim 250 \text{ nm}$  (4). Consequently, localized substrate melting took place, followed by mixing or interdiffusion between the steel and the NiCr phase. The grains that have nucleated are relatively large (up to  $10 \mu\text{m}$  in diameter) and appear

to span the interface (5). This is consistent with a very slow cooling rate, and hence a low nucleation rate.

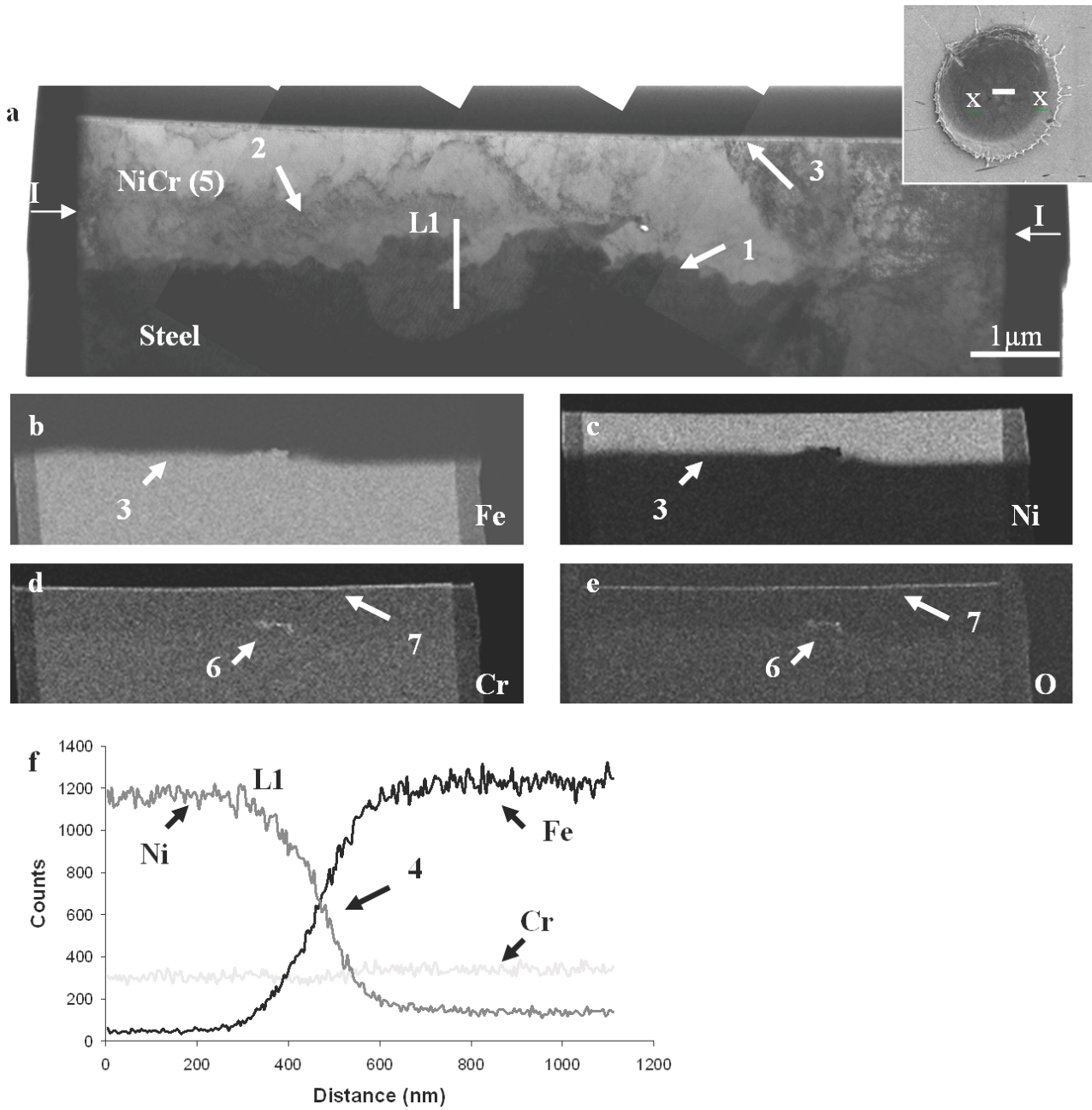
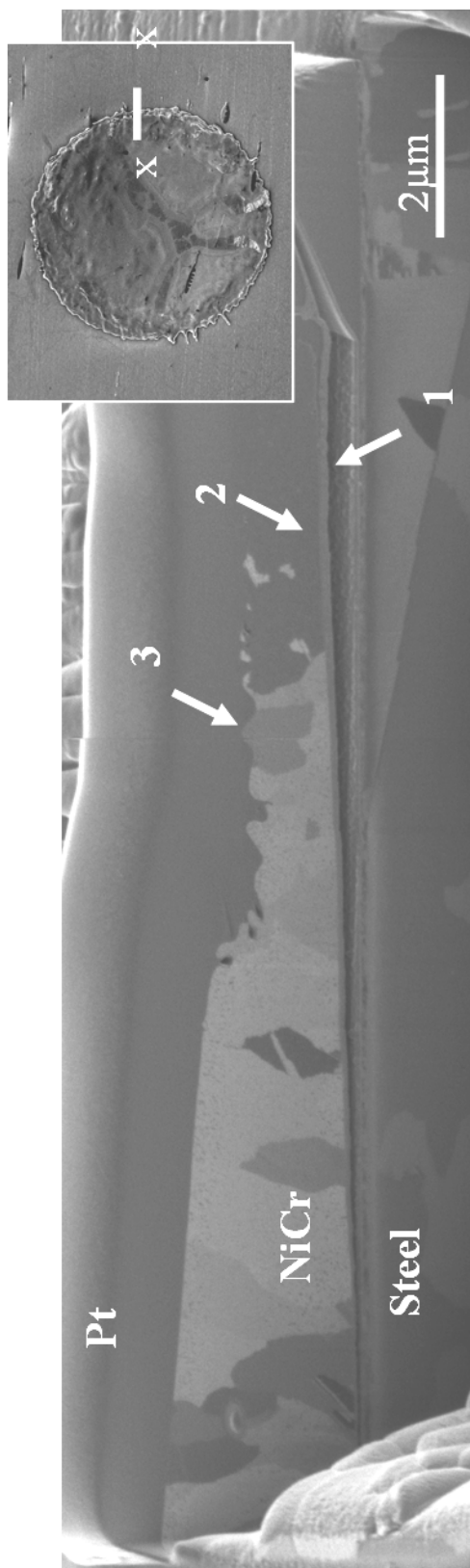


Figure 10. TEM cross-section made across the centre of a large circular splat (see insert picture) found on SS<sub>PH</sub>: (a) bright field image, EDS elemental maps for (b) Fe, (c) Ni, (d) Cr, (e) O, (f) EDS elemental linescan

On the EDS elemental maps (Fig 10d and 10e), chromium oxide can be observed at the splat-substrate interface (6): it appears as if it was present at this location upon splat formation, either from the oxidation of the substrate or the in-flight oxidation of the particle, and prevented substrate melting at this particular location, causing the irregularity observed in the interface shape. Chromium oxide is also observed on the outer surface of the splat as a thin, dense layer (7). This layer was too thin to be identified unambiguously by electron diffraction. However, as it has been discussed previously,  $\text{Cr}_2\text{O}_3$  is the most likely oxide to have formed in such conditions.

Such interfacial features of intimate contact between splat and substrate, localized substrate melting, Ni-Fe interdiffusion and large grains having grown across the interface, were found all along the main central sections of the large circular splats. This shows that strong metallurgical bonding can be achieved on most of the splat-substrate interfacial surface.

However, at the rim of the splat, curling up of the splat is observed. Figure 11 shows a FIB cross-section prepared across the rim of a large circular splat. Poor contact between splat and substrate can be seen towards the splat periphery (1), as the splat has been lifted up above the substrate. This curling up phenomenon also occurred for the RSF splats (see paragraph III.1.d). A thin dense layer can be observed on the bottom surface of the splat in this area (2), which was identified using TEM as FeO.



*Figure 11. FIB cross-section made across the rim of a large circular splat (see insert picture)  
found on SS\_PH*

The formation of this phase is expected to be similar as for the oxides observed on the substrates sprayed at room temperature. Furthermore, the outer surface of the splat at its periphery displays an undulated morphology (3): it appears as if the flow of the NiCr was inhibited due to surface tension effects associated with the splat being in contact of the substrate.

The very good contact between splat and substrate and metallurgical bonding described for the large circular splats was less commonly found, however, for the irregularly shaped splats. Indeed, for instance, as shown in the TEM cross-section presented in Fig. 12, located in the centre of such a splat, the interface is, here, straight and distinct (1). The contact between splat and substrate may also be poor in some areas (2), with the presence of a thin chromium oxide layer (3) (possibly  $\text{Cr}_2\text{O}_3$ , however the layer is too thin to obtain a clear electron diffraction pattern for unambiguous identification).

The small circular splats also displayed no evidence of substrate melting. Figure 13 displays a TEM cross-section of such a splat, where the splat-substrate interface appears straight and distinct, with some fine voids (1) (Fig. 13a). Through EDS mapping a dense layer of chromium oxide can be observed on the outer surface of the splat (2, Fig. 13d and e), and is most probably  $\text{Cr}_2\text{O}_3$ . It can be noted that these small splats are very thin (usually  $\sim 0.5 \mu\text{m}$  or less). Since their average diameter is  $\sim 37 \mu\text{m}$ , it can be calculated that the volume of NiCr in this splat is equivalent to a spherical particle of  $\sim 10 \mu\text{m}$  in diameter. By contrast, the diameters of the sprayed particles range from 5 to  $45 \mu\text{m}$ , thus these small splats were formed from the smallest particles of the feedstock powder.

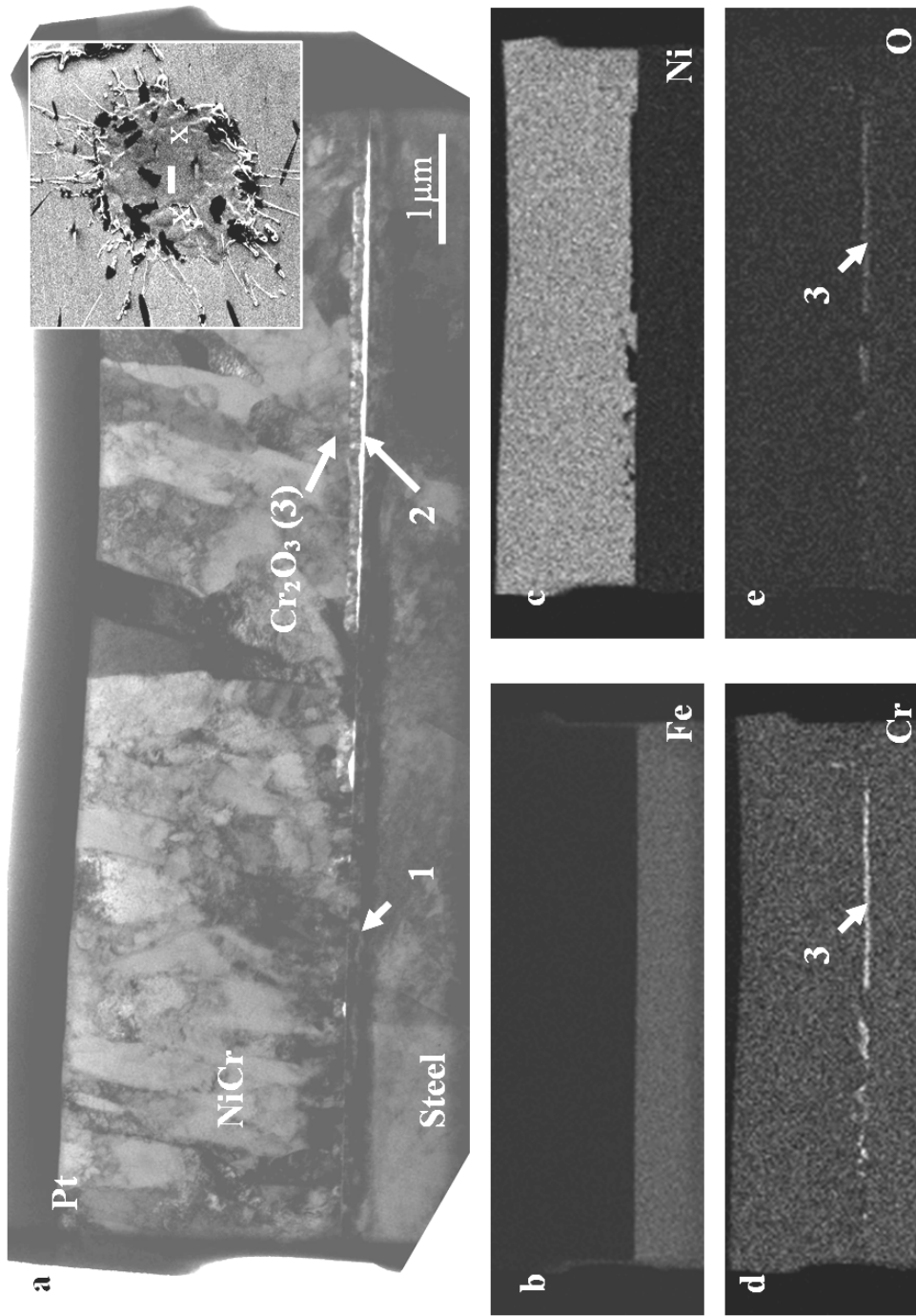


Figure 12. TEM cross-section made across the centre of an irregularly shaped splat (see insert picture) found on SS PH: (a) bright field image, EDS elemental maps for (b) Fe, (c) Ni, (d) Cr, (e) O.

Possibly because of their small size, their limited momentum (compared to the larger particles) and/or the thinner nature of the splats that formed may be responsible for the absence of signs of substrate melting. Indeed, limited momentum may translate to poorer contact upon impact between the particle and the substrate, limiting the heat transfer, and the thinner splats may transmit less heat to the substrate per unit of surface area. Some small splats may also arise from fragments splashed away from larger splats, as shown elsewhere [12, 52] such that, in the plasma spraying process, upon particle impact, vertical splashing occurred.

Finally, a few thick irregularly shaped splats were found on the specimen (the very few occurrences of these was such that they were not taken into account when statistically evaluating the splat population) such as shown in the inset image of Fig. 14: such splats appears to have formed from a NiCr particle that was only very partially molten. The FIB cross-section made on this splat reveals a structure of almost equiaxed grains (1), finer than the expected grain structure of the NiCr particle (usually 3-8  $\mu\text{m}$ ), which may then originated from the partial melting and/or recrystallization of a NiCr particle from the feedstock powder upon heating and deformation upon impact. Other FIB cross-sections of similar splats also showed the presence of fragments presenting a very similar grain structure reminiscent of the NiCr feedstock. Here, it can also be observed that the contact between the splat and the substrate is very poor (2). Moreover, a very finely grained layer can be seen on the under surface of the splat (3), possibly FeO as it is very commonly observed in such location (it should be noted that no TEM cross-section could be made due to the excessive thickness of these splat to assist in identification of this phase).

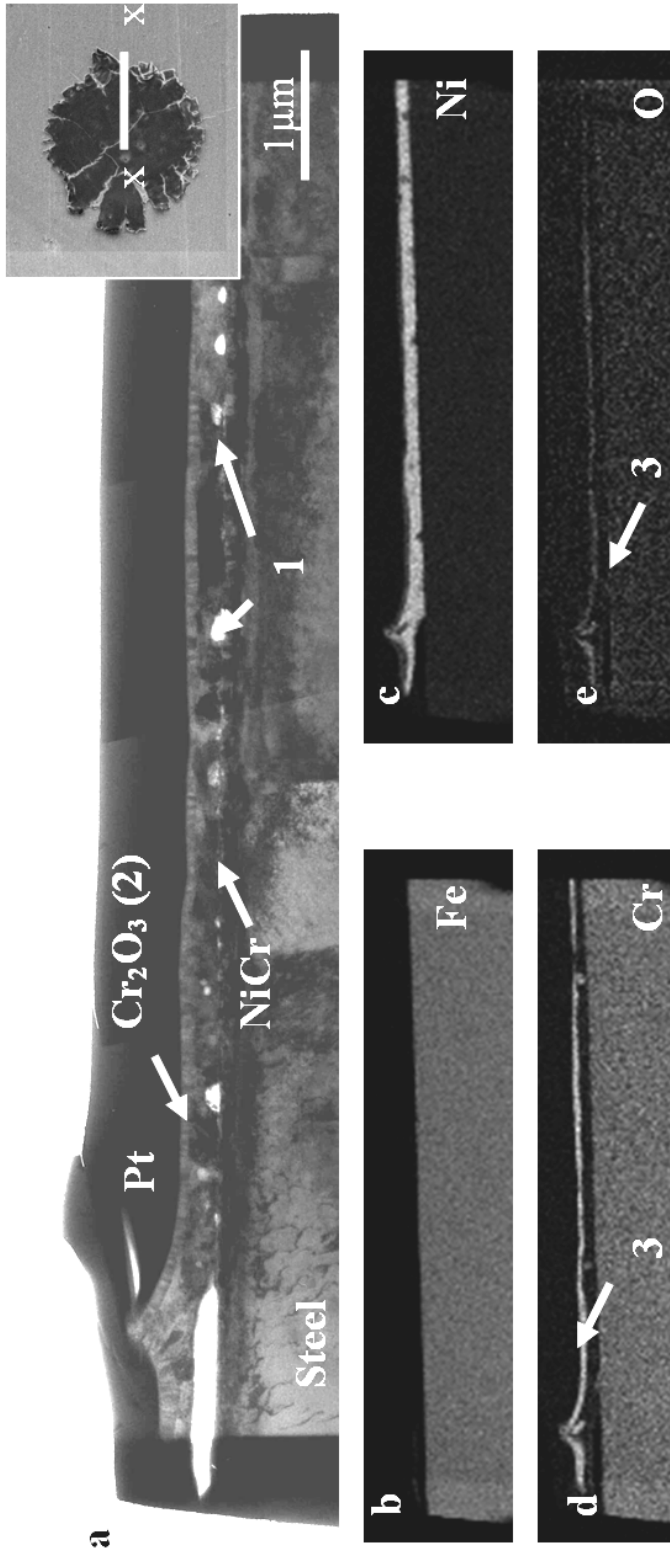


Figure 13. TEM cross-section across a small circular splat (see insert picture) found on SS\_PH:

(a) bright field image, EDS elemental maps for (b) Fe, (c) Ni, (d) Cr, (e) O.

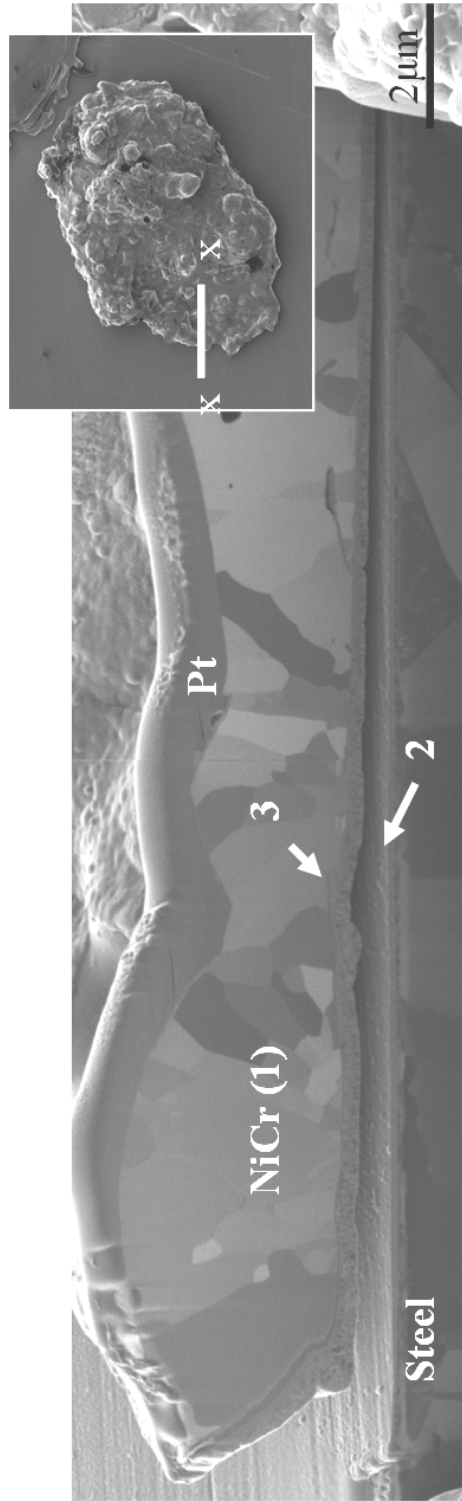


Figure 14. FIB cross-section of a partially melted splat found on SS\_PH

### III.2.b. *Effects of heating of the substrate during spraying on the splat morphology and formation*

Many studies have shown that heating a substrate during plasma spraying at a temperature above the transition temperature resulted in disc-shaped splats rather than irregularly shaped ones with many splashed fingers [6, 20, 21, 26-28]. In the case observed here, the steel specimen was heated at the temperature of 350°C during spraying, thus above the transition temperature of 337°C that was determined by Fukumoto *et al.* [6]. Consequently, the change observed in the shape of the splats, from very irregular with splashed fingers for the SS\_P specimen to disc-shaped for the SS\_PH specimen, was expected and the phenomena involved in such shift have already been widely discussed [6, 20, 21, 26-28].

On the other hand, additional phenomena were observed in the present study. Indeed, it was observed that substrate melting and interdiffusion between the splat and substrate occurred at a greater extent than for the non-heated specimen. Indeed, the observed depth of interdiffusion is usually ~ 150-250 nm for non-heated substrates, and ~200-300 nm for the heated substrates. Moreover, it appears that interdiffusion occurs on a larger proportion of the splat-substrate interface for the heated substrate. Indeed, the splats on these specimens present a much better contact with the substrate, as poor contact is observed only under the rim, compared to the many cases of poor contact observed for the non-heated substrates (under the rim and the splashed fingers of the RSF splats,

almost all over the splat-substrate interface for the NSF splats, ...). This may be explained, on one hand, by the absence (or limited amount) of gas released from the substrate. The heating of the substrate may also mean that the difference between the substrate temperature and the impacting splat is lower, and so the rate of heat removal across the interface will be slower. That is, the substrate is kept at a high temperature for longer. Also, it was observed that the splats formed tended to be relatively thicker than for the ones on the non-heated specimen. This suggests that the heating may affect the wetting of the molten splat, causing it to spread less. The presence of undulations of the splat surface at the periphery also may come from the flow of the molten NiCr which was inhibited by the surface tension effects from the substrate. Alternatively, it may originate from the solidification of the bottom layers of the splat starting while the splat is still spreading, and thus slowing down the flow of NiCr on the top.

Concerning the more irregularly shaped splats, their formation was expected as the concept of transition temperature does not represent a precisely-defined point above which all splats will be disc-shaped, but is rather an inflexion point representing the proportion of disc-shaped splats versus irregular ones [6]. Thus, irregularly shaped splats will form, especially when heating the substrate at a temperature close to the transition one. Their process of formation should be similar to the irregularly shaped splats found on the non-heated specimens, for those splats not presenting evidence of substrate melting.

Furthermore, contrary to the non-heated specimens, the presence of many small splats, presumably formed from the smallest particle of the feedstock powder, was observed. A possible explanation may be that due to the improved wetting, these smaller particles, which do not adhere on the non-heated specimens may, because of their limited momentum, adhere in this instance. Furthermore, the fact that a few partially melted splats were found only on the SS\_PH specimen may be explained by the improved adhesion induced by the heating of the substrate, as on the non-heated specimen they may just have not adhered to the substrate.

Finally, larger amounts of chromium oxide were found to form on the outer surface of the splat at this substrate temperature. A reason for this may be that splats, due to the heating, are kept a higher temperature longer and thus oxidation leading to the formation of  $\text{Cr}_2\text{O}_3$  is more likely to occur. While more oxide may adversely affect some properties of the fully deposited, it is clear that heating of the substrate during spraying, by significantly reducing the splashing and increasing the occurrence and depth of substrate melting and mixing with the sprayed material, would then have a positive effect on the adhesion on the coating.

#### **IV. Conclusion**

To conclude, the microstructural study of NiCr splats plasma sprayed on stainless steel led to the following observations:

- On both polished and polished and thermally treated substrates, sprayed at room temperature, a large proportion of the splats displayed a ring of splashed fingers. Towards their centre, evidence of substrate melting and interdiffusion between NiCr and steel phases was found, showing metallurgical bonding. This was not found for the other types of splats.
- Heat treatment of the substrate prior to spraying led not only to a better wetting of NiCr on steel, thus thinner splats with a larger diameter, but also to a reduction of the occurrence of substrate melting.
- Heating the substrate during spraying resulted in the formation of a very large majority of disc-shaped splats with no, or very limited, splashing, and also substrate melting on a larger scale, thus a likelihood of improved adhesive strength of the fully deposited coating.

## CHAPTER 10

# EXAMINATION OF THE SPLAT MICROSTRUCTURE, SPLAT-SUBSTRATE INTERFACE AND THE EFFECTS OF SUBSTRATE HEATING ON THE SPLAT FORMATION FOR NI-CR PARTICLES PLASMA SPRAYED ON TO ALUMINUM SUBSTRATES

---

*S. Brossard, P.R. Munroe, A.T.T Tran, M.M. Hyland, Journal of thermal Spray Technology, 2010, DOI: 10.1007/s11666-010-9511-2*

### Abstract

The present study investigates the mechanisms of formation of plasma sprayed coatings, crucial for improving the performances of such coatings. Splat morphology and the splat-substrate interface of NiCr single splats sprayed onto aluminum substrates, at a micro- and nano-scale level, were performed using a range of electron microscopy techniques. Two aluminum alloys (with and without Mg additions) and three different sets of substrate surface conditions (polished, heat treated prior spraying and during spraying) were investigated. Evidence of substrate melting and mixing with the splat material was found along with the formation of voids and a range of oxides phases. Mechanisms of

formation of these features were then discussed, along with the variations in splat morphologies induced by the different preparation conditions. It was also found that substrate heating during spraying significantly reduced splashing.

## I. Introduction

In the last few decades, a number of methods have been developed to modify the surface characteristics of materials. This includes thermal spray processing, which is based on the projection of particles, most usually melted, onto a substrate, to build a surface coating. In the case of plasma spraying, a plasma flame is used to melt the sprayed particles. Its large range of temperatures (500 to 25,000°C), along with the variability in the particle velocity (80 to 300m.s<sup>-1</sup>), material (any with a congruent melting point) and size distribution (from 5 to 50 µm for ceramics, 20 to 120 µm for metals), gives to the process significant flexibility and versatility. [1, 4, 141]

The study of the formation of the plasma sprayed coatings is critical for improving their performance. Indeed, properties, such as thermal and electrical conductivity, density, wear resistance or adhesion strength may be significantly influenced by factors such as the oxide content (which can form in-flight or during the coating formation), void content (usually ~ 1 to 5 vol %), or the bonding between the coating and the substrate [1, 4]. Furthermore, coatings are built-up by the accumulation of the sprayed particles which flatten upon impact, forming “splats”. Consequently, studying coating formation implies studying splat formation, especially, the splats which impact directly on to the substrate.

Therefore, the formation of single splats has often been studied through the observation of their morphology [19, 20] or the characteristics of the substrate (especially surface chemistry and topography [11, 21-25]). Notably, it was found that splashing of splats upon impact with the substrate and spreading was an important phenomenon that was significantly reduced by heating the substrate above a certain temperature (called transition temperature) during the spray process [6, 20, 21, 26-28]. This, in turn, may be associated with the desorption of adsorbates/condensates present on the substrate surface [6, 21, 26, 32] or by the splat solidification starting before flattening was complete [20, 28, 33, 34]. Adhesion of the coatings was also found to increase when heating the substrate during spraying [81]. The mechanisms of splat formation have also been studied using in-situ experiments with millimeter-sized droplets [11-15] or by modeling [13, 17, 18].

However, studies on the direct interaction between splat and substrate and of the splat microstructure at a high resolution are limited due to the difficulty in preparing specimens from local regions of the splat-substrate interface. Kitahara *et al.* studied the coating-substrate interface for various sprayed material/substrate combinations, including Ni particles sprayed onto an Al substrate, and found in that case, using X-ray diffraction, that an intermetallic phase, identified as  $\text{Al}_3\text{Ni}$ , was present at the interface. This was then interpreted as evidence of local substrate melting [35]. The occurrence of local substrate melting and formation of an intermetallic phase was also found in a small number of other cases; for example, Mo sprayed on steel, with the formation of  $\text{Fe}_2\text{Mo}$ , which was

observed by transmission electron microscopy (TEM) [20, 36]. However, in a prior study by the authors, no evidence of substrate melting or mixing between splat and substrate materials was observed for plasma-spray of NiCr on aluminium [131]. However, the spray conditions in that study were different to those used by Kitahara *et al.* The occurrence of substrate melting and intermixing between splat and substrate are of critical importance as they show the incidence of metallurgical, rather than mechanical, bonding, which may lead to improved adhesion of the coating.

Consequently, the aim of the present work is to observe the microstructural features of single splats, with a particular emphasis on the splat-substrate interface. The sprayed material was NiCr, which is commonly used in plasma spray coatings for applications such as wear resistant coatings or bond coats, including on aluminum substrates. Substrates were made of two aluminum alloys (5052 and 1005, alloys differing most notably by their Mg content) and submitted to various treatments: polished, thermally treated prior to spraying or heated during spraying. Our previous studies [49, 55, 131] found that thermal treatment of the aluminum substrate caused significant changes in the surface chemistry in two aspects. Firstly, thermal treatment lead to dehydration, and thus released water from the surface. The release occurred from the conversion of hydroxide to oxide between 250°C and 350°C. Secondly, thermal treatment induced surface segregation of magnesium, in particular in aluminum alloys containing high magnesium concentrations, such as aluminum 5052. The presence of magnesium oxide at high levels on the surface reduces the alumina proportion and may promote the wettability of the liquid metal on the aluminum substrates. The considerable differences in terms of

surface hydroxide (between the non-heated and heated substrate samples) and magnesium concentration (between the Al 5052 and Al 1005 samples) allowed the studies of the effects of surface chemistry on splat morphology and microstructure. The formation of oxides and voids along the splat-substrate interface, and the occurrence of substrate melting were examined using a range of electron microscopy techniques. The observations made were then used to study the effects of thermal treatment of the substrate on the splat formation process and splat morphology.

## II. Experimental procedure

Five different substrates were used, prepared from two aluminum alloys 5052 and 1005. Al 5052 contains Mg (2.2-2.8wt%), which is expected to become oxidized to form a very thin layer of MgO on top of the substrate surface and modify the surface chemistry [74, 131], while Al 1005 contains very limited amounts of Mg ( $\leq 0.05\%$ ). The different substrates and their pre-treatments are listed in Table 1.

**Table 1. Substrate Nomenclature and Condition**

<b>Specimen</b>	<b>Substrate</b>	<b>Pre-treatment</b>
Al5052_P	Aluminum 5052	Polished (to nanoscale smoothness)
Al5052_PT	Aluminum 5052	Polished and thermally treated
Al5052_PH	Aluminum 5052	Polished and heated during spraying
Al1005_P	Aluminum 1005	Polished (to nanoscale smoothness)
Al1005_PT	Aluminum 1005	Polished and thermally treated

All substrates were initially in a mirror polished state with a nano-scale roughness. The thermally treated substrate was heated at 350°C for 90 minutes in air. The substrate heated during spraying was held at a temperature of 350°C for 30 minutes and kept at this temperature during spraying. The aim of these thermal treatments is to alter the surface chemistry, particularly the oxyhydroxide concentration and oxide thickness, and/or to induce some level of surface roughness [49].

The sprayed material was a commercial NiCr alloy powder (Ni80-Cr20, Sulzer Metco 43 VF-NS, Switzerland, (-105+45)  $\mu\text{m}$ ). Plasma spraying was carried out with a Sulzer Metco (Switzerland) 7MB gun (with a nozzle diameter of 8 mm), operating at a current of 550A and at a voltage of 62V, with a spraying distance of 100mm. The feeding rate of the powder was of 1g/min, the carrier gas being argon at a flow rate of 3 SLPM, while the plasma gas was a mixture of nitrogen and hydrogen, at a flow rate of 47.5 SLPM and 6.2 SLPM respectively.

The specimens were then characterized using a range of analytical techniques. A scanning electron microscope (SEM) (Hitachi, S3400-X, Mito, Japan) was used to image the overall morphology of the splats and the substrates. A focused ion beam microscope (FIB) (FEI, xP200, Hillsboro, USA) was used to mill cross-sections of the splats using an energetic gallium ion beam, and to image them using secondary electrons induced by the ion beam. Details have been described elsewhere [51]. A dual beam microscope (that is a FIB and SEM combined into a single instrument) (FEI, xT Nova Nanolab 200, Hillsboro,

USA) was used to prepare cross-sections of splats (100-200nm in thickness) suitable for TEM observation. These were prepared using the lift-out method as described elsewhere [51] and examined in a transmission electron microscope (TEM) (Philips, CM200, Eindhoven, The Netherlands) to which energy dispersive x-ray spectroscopy (EDS) facilities have been interfaced. Finally, the average surface roughness of the substrates was measured using an Atomic Force Microscope (AFM) (Digital Instruments DI3000, Santa Barbara, USA).

Several FIB and TEM cross-sections were prepared and studied for each particular feature and/or type of splat. However, for reasons of brevity only a small number of representative images will be presented here. The cross-section preparation process using FIB also involves the deposition of a layer of platinum on top of it prior to milling for protection purposes. This layer is present on the FIB and TEM images presented.

### **III. Results and discussion**

The splats, and their formation, are described from electron microscopy observations.

Because of their overall similarity, the splats on the polished and polished and thermally treated substrates are detailed in a first part, then, in the second part, splats formed on the substrate heated during spraying are described and discussed.

### III.1. Description of the splats found on the polished and polished and thermally treated specimens

#### III.1.a. *Various splats morphologies found on the different specimens*

SEM images of 50-60 splats were taken for each specimen. Figure 1 displays some SEM images of typical splats. Different types of morphology were observed and are described below:

- Some splats, as presented in Fig. 1a, present an almost circular shape (although sometimes with deviation from circular), surrounded by a “halo” of splashed materials, for instance marked 1 on Fig. 1a. Such splats represented around 30% of the total splat population and will be denoted as “halo splats”.
- Many of the splats (~ 60%), such as on Fig. 1b, displayed a similar shape as the previous splats, but with a ring of splashed fingers (marked 2 on Fig. 1b) around the central core of the splat (marked 3). They will be denoted as “halo fingered splats”.
- Other splats (~ 10%), as seen in Fig 1c, have again a similar morphology to the halo splats but display a large central hole (marked 4 on Fig. 1c). They will be called “halo doughnut splats”.
- On both polished substrates (Al5052\_P and Al1005\_P), a very small number of splats were also found which displayed a ring of splashed fingers, but the central core of the splat was also very fragmented (Fig. 1d). These were denoted “fragmented splats”.

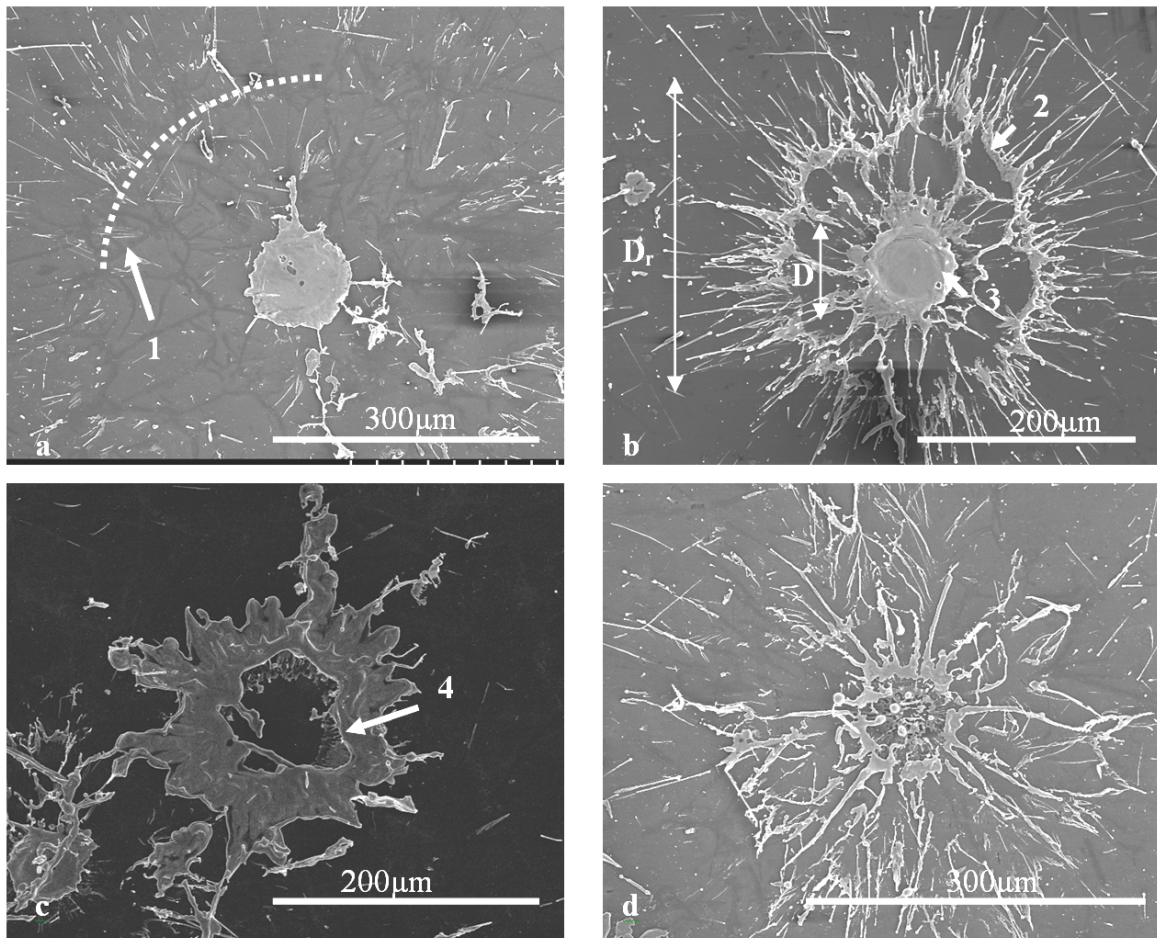


*Figure 1. SEM images of the different types of splats found on all of the substrates sprayed at room temperature: (a) halo splat, (b) halo fingered splat, (c) halo doughnut splat, (d) fragmented splat*

The diameter  $D$  was evaluated for each splat by measuring the smallest and largest values and taking the average, ignoring the splashed fingers. However, for splats with a ring of splashed fingers, the diameter  $D_r$  for this ring was also measured and expressed as a function of the diameter of the splat itself (see Fig. 1b for example). The average diameters for each category of splats for each specimen are presented in Table 2. The very few fragmented splats were not taken into account due to their very low frequency

of observation. The results presented in Table 2 are given mainly as an indication, considering the errors resulting from the fact that the values presented were calculated for only a relatively limited amount of splats (a more thorough statistical analysis will be the subject of a separate publication). Also, the large standard deviation for the diameter of the halo splats is partly due to the presence of significantly smaller splat (diameter around 30  $\mu\text{m}$ ). This may be explained by the large range in particle diameter for the feedstock powder.

**Table 2. Average diameters of the splats (and average diameter of the ring of splashed fingers if applicable) found on, Al5052\_P, Al1005\_P, Al5052\_PT and Al1005\_PT**

		Al5052_P	Al1005_P	Al5052_PT	Al1005_PT
Halo splats	$D_m$	$[80 \pm 44] \mu\text{m}$	$[99 \pm 45] \mu\text{m}$	$[80 \pm 60] \mu\text{m}$	$[76 \pm 56] \mu\text{m}$
Halo fingered splats	$D_m$	$[93 \pm 29] \mu\text{m}$	$[89 \pm 26] \mu\text{m}$	$[110 \pm 47] \mu\text{m}$	$[117 \pm 51] \mu\text{m}$
	$D_r$	$[2.7 \pm 1.0] D$	$[3.4 \pm 1.7] D$	$[2.6 \pm 0.9] D$	$[1.9 \pm 0.8] D$
Halo doughnut splats	$D_m$	$[112 \pm 57] \mu\text{m}$	$[100 \pm 28] \mu\text{m}$	$[160 \pm 57] \mu\text{m}$	$[160 \pm 49] \mu\text{m}$

### III.1.b. *Microstructure and formation process of the halo fingered splats*

Figure 2 displays three FIB cross-sections made across a halo fingered splat. The inset image shows the location of each cross-section on the splat. It can be observed that all along the central part of the splat (see the zones marked 1 on Figs. 2a and 2b), contact

between the splat and the substrate is very good. Towards the periphery of the splat, jetting of the Al substrate within the splat, and mixing of both splat and substrate can be seen (for example marked 2 on Fig. 2b). This shows that substrate melting has occurred.

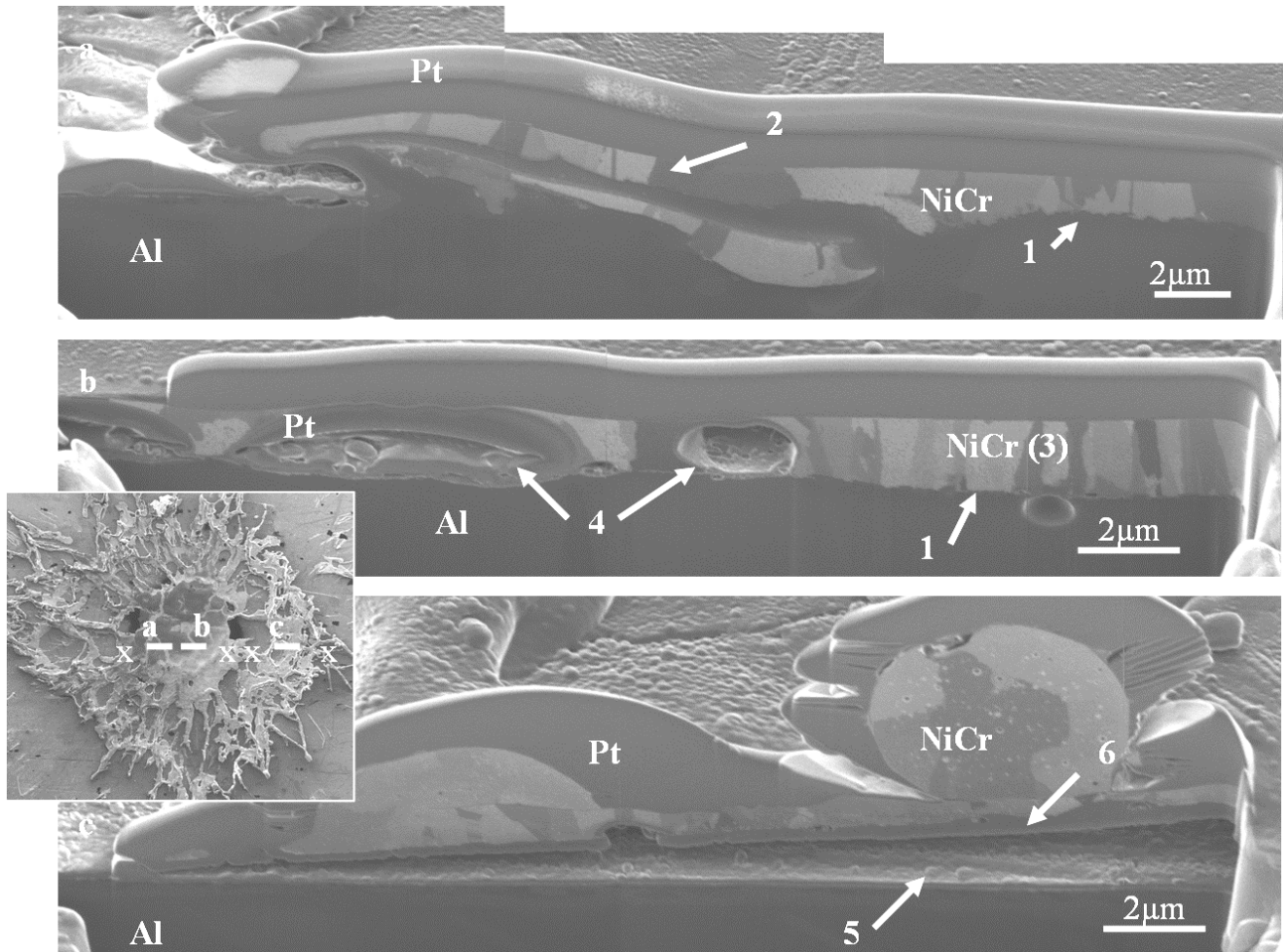


*Figure 2. FIB cross-sections of a halo fingered splat (see insert picture) found on Al1005\_P*

When examining the splat-substrate interface by TEM, such as the cross-section presented in Fig. 3, the interface appears irregularly shaped and indistinct (1), as seen on the bright field image (Fig. 3a) and on the elemental EDS maps (Figs. 3b and 3c).

However, a very distinct structure can be observed at the interface. On the bright field image (Fig. 3a), a layer exhibiting a darker contrast than the Al substrate can be seen just under the splat interface (1), which is also very irregularly shaped. On the higher magnification bright field image (Fig. 3e), it can be seen this is actually two layers. The layer adjacent to the NiCr splat appears amorphous (2), as no grain structure can be observed. Moreover the electron diffraction pattern obtained for this area only displayed a very diffuse ring, consistent with being a glassy phase. The second layer appears to be composed of very fine grains, firstly equiaxed (3), then, closer to the Al substrate, more needle-like grains can be observed (4). The electron diffraction pattern obtained from the finely grained layers exhibits an irregular array of reflections. Thus, it was not possible to obtain an unambiguous identification of an interfacial phase. However, on the elemental linescan, L1, performed across the interface (Fig. 3d), one can note that the variations in the Al and Ni concentrations are not sharp, but gradual (5), showing interdiffusion has occurred over a distance of more than 500 nm. Moreover, there is no step-like change in composition, but an almost uniform change, thus ruling out the presence of a stoichiometrically defined intermetallic phase. The most possible explanation would be these are metastable phases, with a layer of metallic glass and a layer made of non-equilibrium Ni-Al crystalline phases. Hung *et al.*, when studying glass formation in the Al/Ni system, found that intermetallic compounds, such as Ni<sub>3</sub>Al and NiAl<sub>3</sub>, were able to be amorphized, while NiAl would remain crystalline [142]. The presence of these glassy and metastable phases shows that solidification must have occurred at a very high rate, and as shown by the columnar shape of the grains composing the splat (see 3 on Fig. 2a and 6 on Fig. 3a), the heat is removed mainly through the substrate.

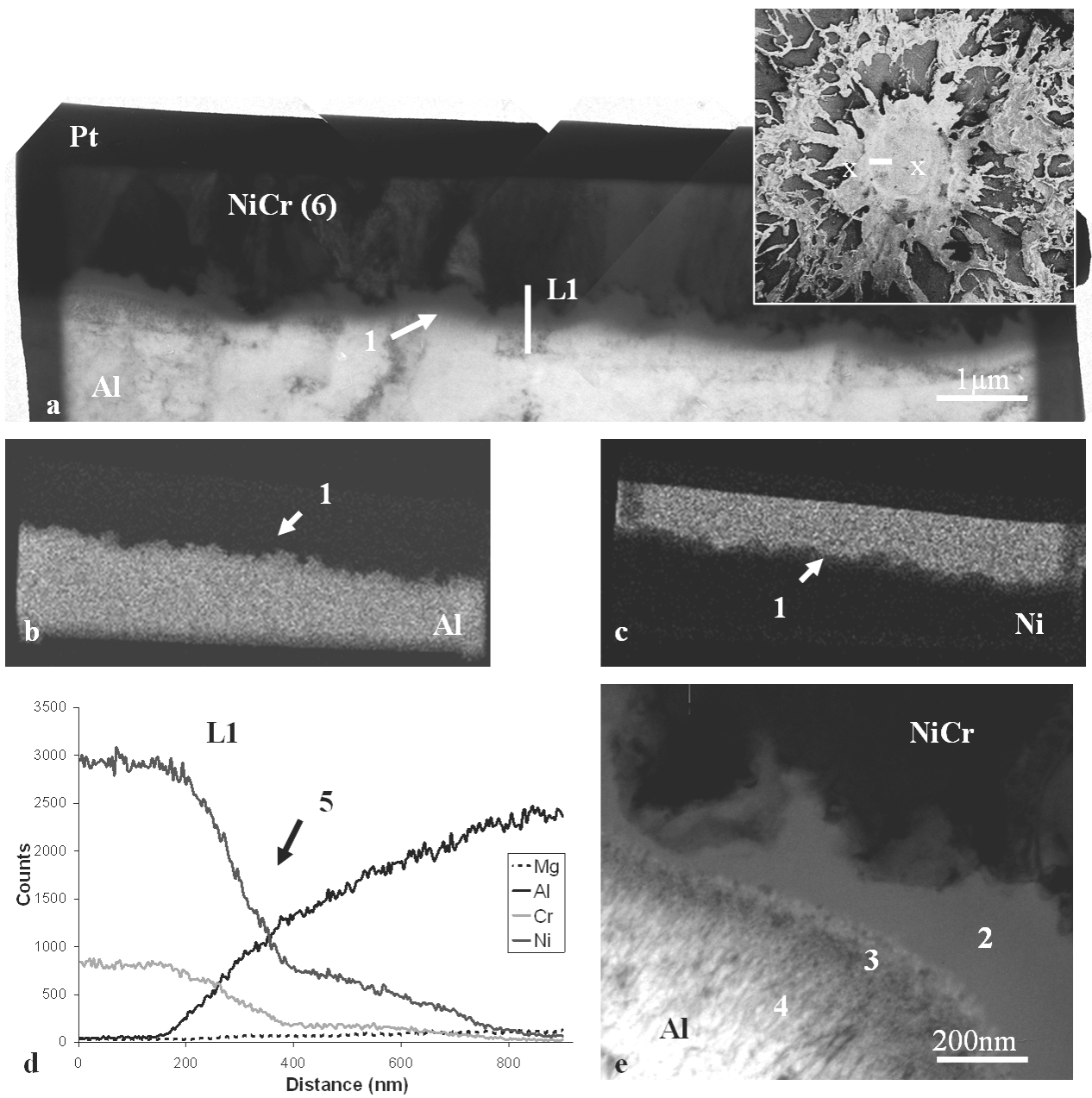


Figure 3. TEM cross-section made across a halo fingered splat (see insert picture) found on Al5052\_P: (a) bright field image, EDS elemental maps for (b) Al, (c) Ni, (d) EDS elemental linescan, (e) high magnification bright field image of the splat-substrate interface

The interfacial layers described are not uniform. As it can be seen on the TEM cross-section presented in Fig. 4, the splat-substrate interface may, in some areas, be straight and defined (1), with no evidence of substrate/splat mixing, juxtaposed to zones of substrate melting (2). The linescan, L1, performed across the interface in such zone show sharp variations in the concentration of Ni and Al (see 3 on Fig. 4f), in comparison with the linescan L2 (see 4 on Fig. 4g) acquired across the zone of substrate melting, denoting the absence of melting. On the EDS elemental maps (Figs. 4d and 4e), segregation of Cr in a thin layer may also be observed (5), which most likely occurred by the oxidation of Cr leading to the formation of an oxide, most probably  $\text{Cr}_2\text{O}_3$ . Such oxidation process may have occurred in-flight [6] or upon splat solidification and cooling down from the gases released either from the substrate or from the splat [129] (the gas release process is discussed in more detail later).

In the centre of the splat, some large voids (up to 10  $\mu\text{m}$  in diameter) were often noted to be present. These may be located either within the splat, such as on Fig. 2b (4) and Fig. 4a (6), or within the substrate, for example those present in the TEM cross-section presented Fig. 5. Dense and thick oxide layers are often found on the walls of such voids. EDS elemental maps (Figs. 5b and 5e) and electron diffraction studies (see diffraction pattern presented Fig. 5f) suggest that this layer may be alumina  $\gamma\text{-Al}_2\text{O}_3$  (1). On the bottom surface of the void however, the EDS elemental maps (Figs. 5c to 5e) show that the layers of oxide contain not only Al, but also Ni and Cr (2), it therefore may be a mix of spinel  $\text{NiAl}_2\text{O}_4$ , as identified by the electron diffraction pattern presented Fig. 5g (despite being made of poorly defined rings) and  $\text{Cr}_2\text{O}_3$ , or the spinel  $\text{NiCr}_2\text{O}_4$ , which has a

similar diffraction pattern to  $\text{NiAl}_2\text{O}_4$ . All these oxides species are expected to form on alloys containing Al, Ni and Cr [143].

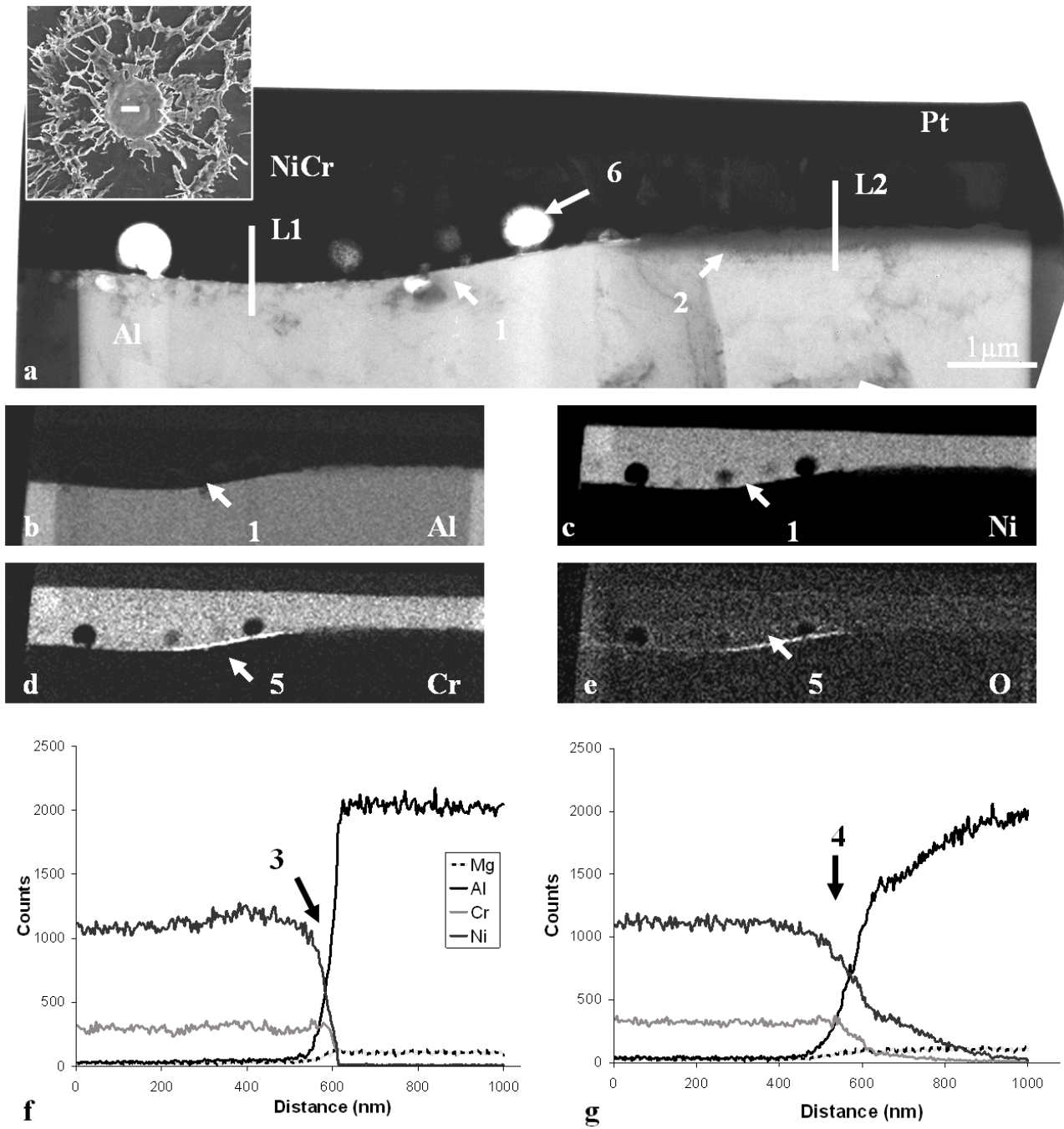


Figure 4. TEM cross-section made across a halo fingered splat (see insert picture) found on Al1005\_P: (a) bright field image, EDS elemental maps for (b) Al, (c) Ni, (d) Cr, (e) O, (f and g) EDS elemental line scans

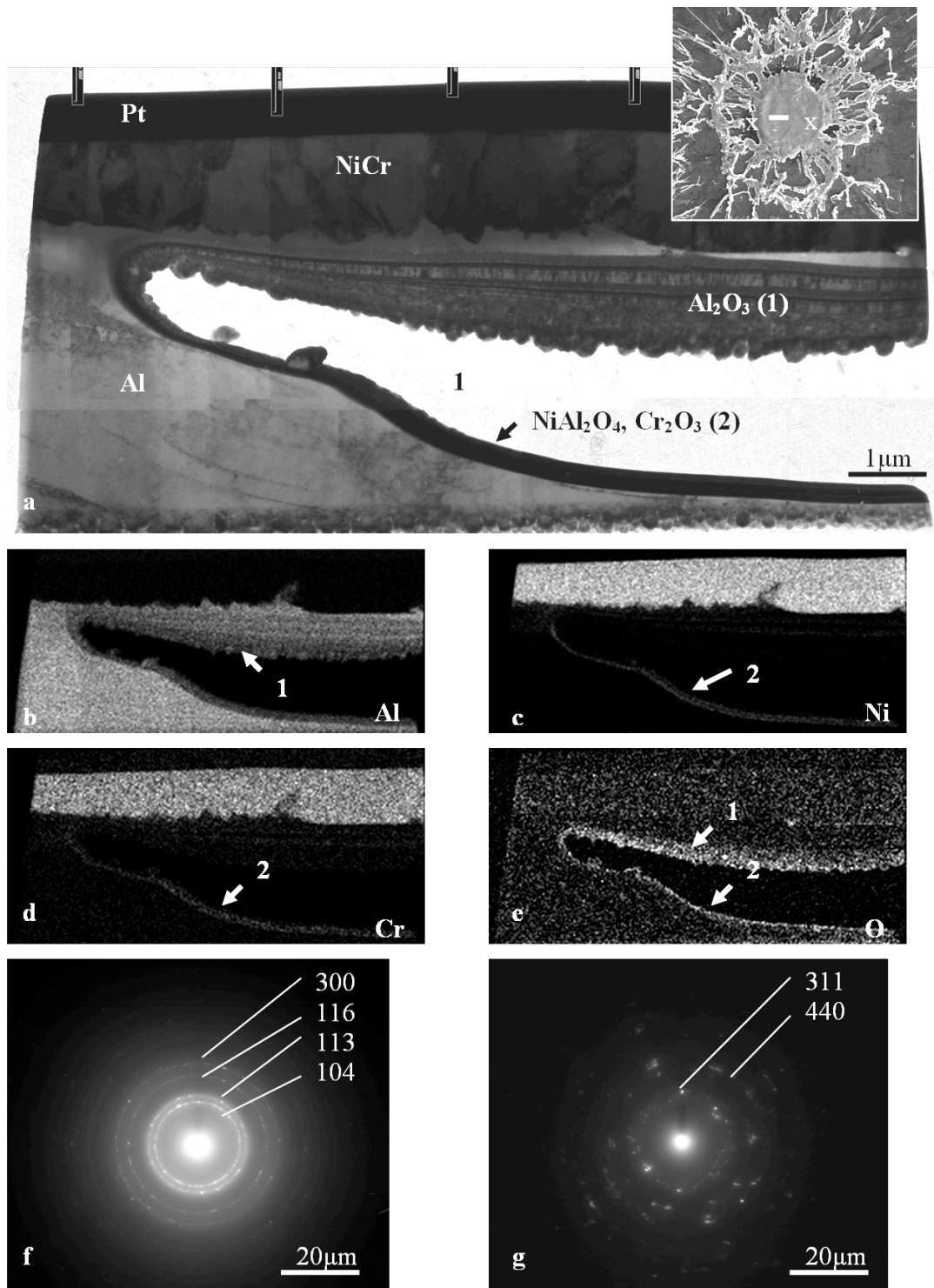


Figure 5. TEM cross-section made across a halo fingered splat (see insert picture) found on Al5052\_PT: (a) bright field image, EDS elemental maps for (b) Al, (c) Ni, (d) Cr, (e) O, electron diffraction pattern for (f)  $\gamma$ -Al<sub>2</sub>O<sub>3</sub>, (g) spinel NiAl<sub>2</sub>O<sub>4</sub>

Figure 2c shows a FIB cross-section prepared across a splashed finger at the periphery of the splat: it appears that here the contact between splat and substrate is very poor (5). The poor adhesion between these phases was possibly associated with the accommodation of stresses arising during the cooling of the splat, such that the splat gets lifted-up above the substrate. This phenomenon has often been observed elsewhere [54], and has been denoted as curling-up. An oxide, identified as  $\text{Al}_2\text{O}_3$ , was found to have formed on the bottom surface of the splat in these locations (6). Some Al may have adhered to the bottom surface on the splat when it was still in contact with the substrate, and upon lifting-up, have become oxidized to form alumina.

Previous studies attributed, at least partly, the occurrence of splashing to desorption of adsorbates/condensates present on the substrate surface, causing the formation of an unstable gas cushion [6, 21, 26, 32]. Qu *et al.* also suggested the release of gas from the splat itself during solidification and cooling, in which gas would have been dissolved upon impact due to the pressure build-up [129]. The presence of oxides in voids observed here, or on the bottom surface of the splat where curling-up has occurred, may be seen as an evidence of such gas release, as it shows that hot oxidizing gases were present, either entrapped in the voids formed, or pushed towards the periphery of the splat by the flowing molten NiCr. However, while the small voids ( $< 4 \mu\text{m}$ ) present within the substrate as shown in Fig. 2b (4) have most probably formed from gas bubbles [129], it should be noted that the size and location of the very large voids (4-12  $\mu\text{m}$ ) seen within the substrate, see Fig. 5, indicate that they may have been formed by a different process.

Modeling of the splat formation process, which usually does not take substrate melting into account, has shown that central voids are often formed because of the mechanics of the flow of the spreading splat, due to the change in curvature of the droplet upon impact [15, 55]. The mixing between Al and NiCr observed towards the periphery of the splat, such as seen Fig. 2a (2), suggests turbulence of the flow of such molten materials. Some voids may also be formed in this region, similar to the ones found towards the centre of the splat within the substrate. Mixing of the two phases also contributes to the splat displaying a raised ring close to the rim, which can be seen in the SEM images (see for instance the region marked 2 on Fig. 1a). The presence of such a ring may then allow prediction of those splats, which have undergone substrate melting, solely from inspection of a SEM image.

### III.1.c. *Microstructure and formation process of the other types of splats*

Figure 6 shows the FIB cross-section of a fragmented splat, similar to the one presented Fig. 1d. One can note the very poor contact between the splat and substrate (1), along with the thin, but dense layer present on the bottom surface on the splat (2), which from was identified using TEM as being  $\alpha$ -Al<sub>2</sub>O<sub>3</sub>, formed, most possibly, by the same process as described previously for the halo fingered splats. The splat is also very thin ( $< 1 \mu\text{m}$ ), and the grains are, in comparison, quite coarse ( $\sim 2 \mu\text{m}$ ) (3), which suggests a relatively slow solidification linked to the poor contact between splat and substrate and, consequently, the high thermal contact resistance hindering the heat removal through the splat-substrate interface [16, 28, 33]. The very poor adhesion, linked to the poor contact,

may explain why relatively few of these splats were observed, as they may be prone to delaminate from the substrate. Finally, the presence of the splashed fingers and oxide layers, along with the absence of substrate melting, shows that splashing of the splat probably arises from gas release from the substrate, rather than instabilities due to melting of the substrate.

Fig. 7 shows a FIB cross-section across a halo splat. The splat-substrate interface appears straight and distinct (1), while the contact between splat and substrate is mostly good. The splat grain structure is fine and columnar ( $< 1 \mu\text{m}$ ) (2), indicating a relatively fast rate of solidification with the heat removed mainly through the substrate [16], which is presumably linked to the good contact observed. Some fine voids were observed at the interface (3), probably formed from the gas released from the substrate. The rim of the splat has also been slightly lifted-up (4) due to the curling up process.



Figure 6. FIB cross-section of a fragmented splat with a ring of splashed fingers (see insert picture) found on Al5052\_P

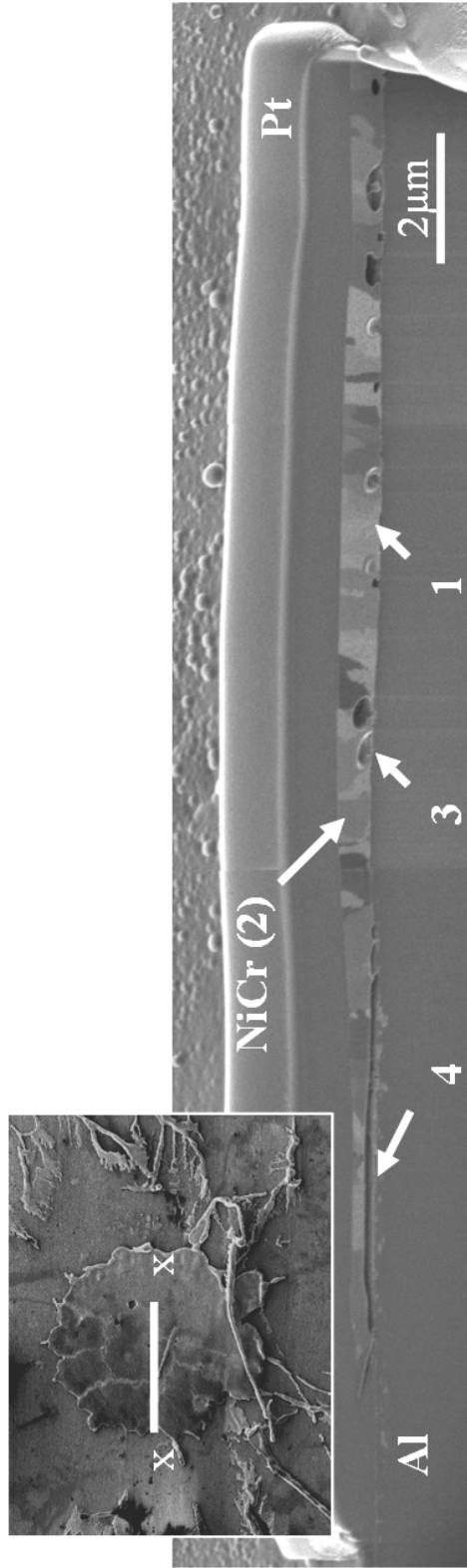


Figure 7. FIB cross-section of a halo splat (see insert picture) found on Al1005\_P

The various oxides phases present on halo and halo doughnut splats, and their typical locations, were similar between both splats and were identified using TEM, as shown in Fig. 8, presenting a TEM cross-section of a halo doughnut splat. In voids (1), like the halo fingered splats, alumina  $\gamma\text{-Al}_2\text{O}_3$  was found (2), identified by both EDS elemental maps (see Figs. 8b and 8e) and electron diffraction. A dense thin layer of  $\text{Cr}_2\text{O}_3$  was also observed on the outer surface of the splat (3), as seen on both Cr and O elemental maps (Figs. 8d and 8e). It was identified by electron diffraction as being  $\text{Cr}_2\text{O}_3$  (see Fig. 8f, which could be identified as  $\text{Cr}_2\text{O}_3$ ). Spinel  $\text{NiCr}_2\text{O}_4$  was also found to form at the base of one of the voids (4). Such phases were found to form often on sprayed NiCr splats in previous studies [56, 70].  $\text{Cr}_2\text{O}_3$  layers were also observed locally at the splat-substrate interface (5). While the formation process of Cr oxide on the outer surface of the splat is well understood and has been explained before [50], the manner in which the oxide may found at the interface is not clear. Indeed, it can not have formed from the oxidation of the substrate, thus it must have arisen from the oxidation of the NiCr particle. Fukumoto *et al.* previously reported Cr oxide ( $\text{CrO}_3$  and  $\text{Cr}_2\text{O}_3$ ) formed on the NiCr particle in-flight [6]. Consequently, this may be the origin the oxide observed here, however it is surprising that it is present in such a flat film shape. On Fig. 8a, it can finally be noted that the contact between the substrate and the halo doughnut splat is very poor (1).

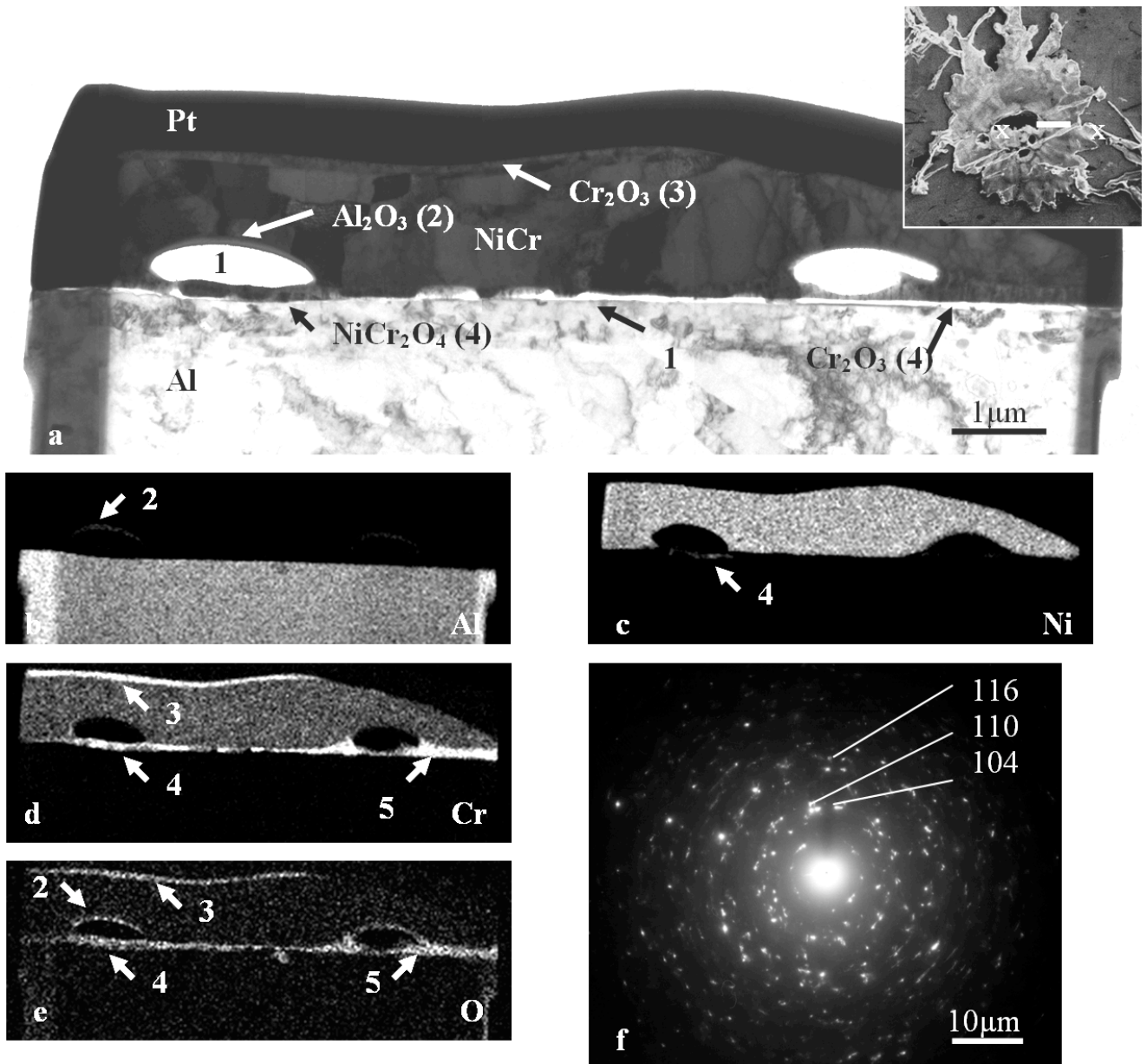


Figure 8. TEM cross-section made across a halo doughnut splat (see insert picture) found on Al5052\_P: (a) bright field image, EDS elemental maps for (b) Al, (c) Ni, (d) Cr, (e) O, (f) electron diffraction pattern for  $\text{Cr}_2\text{O}_3$

For halo doughnut and fragmented splats, neither substrate melting, nor mixing with the NiCr splat, was observed, while it was very rare and limited for the halo splats.

Moreover, as it can be seen on the SEM images (see Figs. 1a and 1c), the outer surface of the splat is usually smooth; the raised ring pattern observed previously for the halo fingered splats and due to the substrate melting, is absent.

#### III.1.d. *Summary of the splat formation process*

When the NiCr particles impact on the substrate, they are, mostly, in a fully molten state - the measured temperature of the splat at impact was 2400°C, which is significantly higher than the melting point of aluminum (649°C). Consequently, localized melting of the substrate may be expected, and this was clearly observed for the halo fingered splats. The depth of the substrate melting is up to several microns, as indicated by the depth of voids or zones of NiCr-Al mixing. It should also be noted that the occurrence of substrate melting was accompanied by the presence of a dense ring of splashed fingers. For the halo and the halo doughnut splats, there was only very limited splashed fingers, and they mostly are found far from the substrate as a “halo”. In a previous study, where NiCr particles were also plasma sprayed onto aluminum substrate, but where no substrate melting was observed, the splats also exhibited no, or limited, splashed fingers and very similar morphologies as the halo splats [131]. McDonald *et al.* photographed images of the spreading and fragmentation of plasma-sprayed nickel on a stainless steel substrate held at room temperature [144]. They observed that the splat spread out upon impact to a maximum extent and then broke up, leaving a small central core area surrounded by a ring of debris which is similar to halo splat type in our current study. They proposed that the formation of such a splat type was related to gas released from the substrate surface

upon impact of the droplet. The gas barrier inhibited the heat conduction from the splat to the substrate. As a result, the splat was in the liquid state for longer to undergo disintegration. In our study, we propose that the primary gas/adsorbate was, in fact, chemisorbed water in the form of hydroxide at the outermost surface. When a molten droplet at high temperature impacted the substrate, heat was conducted from the splat to the substrate, resulting in the increase of substrate surface temperature. This heat activated the conversion of surface hydroxide to oxide and released water vapor. This gaseous layer inhibited the contact between the splat and the substrate and provoked the splat splashing to form the central core as observed. The water released also resulted in the poor splat-substrate contact with separated interfaces and interfacial porosity, as in the case of halo splats, halo doughnut splats and fragmented splats. For these splats, substrate melting is limited.

Thermal treatment of the substrate prior to spraying removes surface hydroxide. This results a better contact between the splat and the substrate which sped up the onset of the splat solidification. The solidification was fast enough to inhibit a full disintegration of a satellite droplet out of the central core of the splat, as in the case of halo splat type. Some liquid ligaments were still attached to the central core of the splat, resulting in the formation of fingers radiating from it, which characterized for halo fingered splats. Details of splashing mechanism of the splat will be discussed in subsequent modeling paper. The better contact between the halo fingered splats and substrate promoted substrate melting, which may disturb the flow of the spreading molten particle. The

molten substrate jet within the flowing NiCr liquid towards the splat edge, resulting in the formation of a ring of splashed fingers as observed.

Due to the mechanics of the flowing splat forming, as described by some previous modeling studies [15, 55], large voids may form within the substrate either towards the centre of the splat or towards the periphery, when mixing between NiCr and Al takes place. The presence of gas at the interface of the substrate and the forming splat also plays a role, leading to potential smaller voids at the splat-substrate interface. Furthermore in many cases, towards the centre of the splat, this may lead to the formation of oxides such as  $\text{Al}_2\text{O}_3$  or  $\text{NiCr}_2\text{O}_4$ . The formation of such bubbles was studied by Qu *et al.*, who suggested that such gases may come from desorption of species adsorbed on the substrate surface, but also gas which becomes dissolved within the molten sprayed droplet upon impact, and released upon cooling down [129].

When the molten Al and NiCr solidify, they solidify to a very fine grain structure or a metallic glass. This suggests that solidification must occur very quickly: such fine grain structure means a very fast cooling, preventing the grains to coalesce, while metallic glasses require as well a very fast cooling to prevent the atoms to rearrange in a crystalline form [145]. Moreover, such phases are evidence of metallurgical bonding between splat and substrate in this zone. This may be seen as beneficial for the adhesion strength of the coating, provided that the interfacial layers are not brittle. It has been observed that compared to crystalline metals, metallic glasses are significantly more brittle (fracture may occurs at stress levels around 100 times less than the ones observed

for the corresponding crystalline metal) [145]. This, however, is not sufficient to determine the actual influence of the metallic glass layer on the adhesion properties of the coating.

Upon splat solidification and cooling down, curling up of the splat occurs, to accommodate the rise of thermal stresses, and the peripheral parts of the splat that have not strongly adhered to the substrate [53, 54]. This occurs at the rim of the splat or splashed fingers linked to the central part of the splat, get lifted-up. Some Al attached to the bottom surface of the splat in these zones then gets oxidized, forming thin, but dense layers of alumina. A similar phenomenon may occur in voids leading to the presence of alumina on the top wall of the void.

Finally, almost all very small splats ( $D \sim 30 \mu\text{m}$ ) belonged to the halo splat category. It can be expected that, because of their small size, the particles' momentum and temperature were not enough to produce substrate melting. Such small splats may originate from the spraying of the smaller particles of the feedstock powder. They may also possibly have formed from another phenomenon called "impact splashing" [12, 52]. It occurs upon impact of the molten droplets onto the substrate and may cause the rebound of small molten NiCr droplets which would fall back onto the substrate, forming small halo splats. In both cases, they may undergo significant oxidation due to the vicinity of hot gases from the flame for example, causing the formation of oxides such as  $\text{Cr}_2\text{O}_3$ .

### III.2. Description of the splats found on the specimen heated during spraying

Figure 9 displays SEM images of the different splat morphologies that were found on Al5052\_PH:

- The large majority of the splats (62%) found exhibited the morphology shown in Fig. 9a: a relatively irregular rim but essentially disc-shaped, and outer surface displaying a raised pattern (marked 1). A few splashed fingers could also be seen but they were usually made of Al and not NiCr. The average diameter  $D_m$  was evaluated to be  $D_m = [124 \pm 55] \mu\text{m}$ . These splats will be denoted almost disc-shaped splats.
- Some much smaller splats (24%,  $D_m = [30 \pm 10] \mu\text{m}$ ) were also found, with usually a very circular shape (see Fig. 9b). These splats will be denoted small circular splats
- Splat with a very irregular rim, and a smooth top surface, as shown Fig. 9c, were also found (11%,  $D_m = [196 \pm 46] \mu\text{m}$ ). They will be denoted irregularly shaped splats
- Finally, very few splats were observed displaying a granular morphology, as if they formed from partially molten NiCr particle (see Fig. 9d, 3%,  $D_m = [157 \pm 91] \mu\text{m}$ ). They will be denoted partially melted splats.

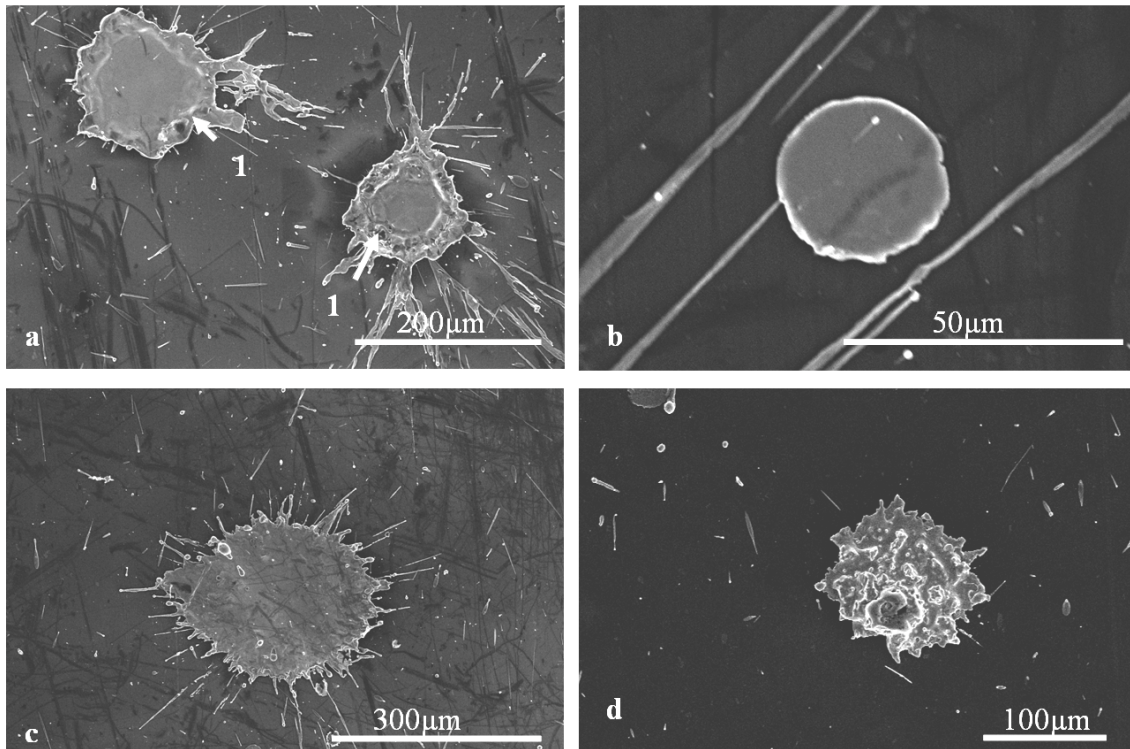


*Figure 9. SEM images of the different types of splats found on Al5052\_PH*

These splat morphologies are significantly different compared to the ones found on the polished/polished and thermally treated specimens. Heating of the substrate during spraying thus significantly modifies the splat formation process.

### *III.2.a. Microstructure and formation process of the almost disc-shaped splats*

Figure 10 displays a FIB cross-section made across such a splat. It can be seen that towards its centre, the splat is relatively thin ( $< 1 \mu\text{m}$ ) and flat, with a fine and columnar grain structure. However, towards the splat periphery, the structure is more complex.

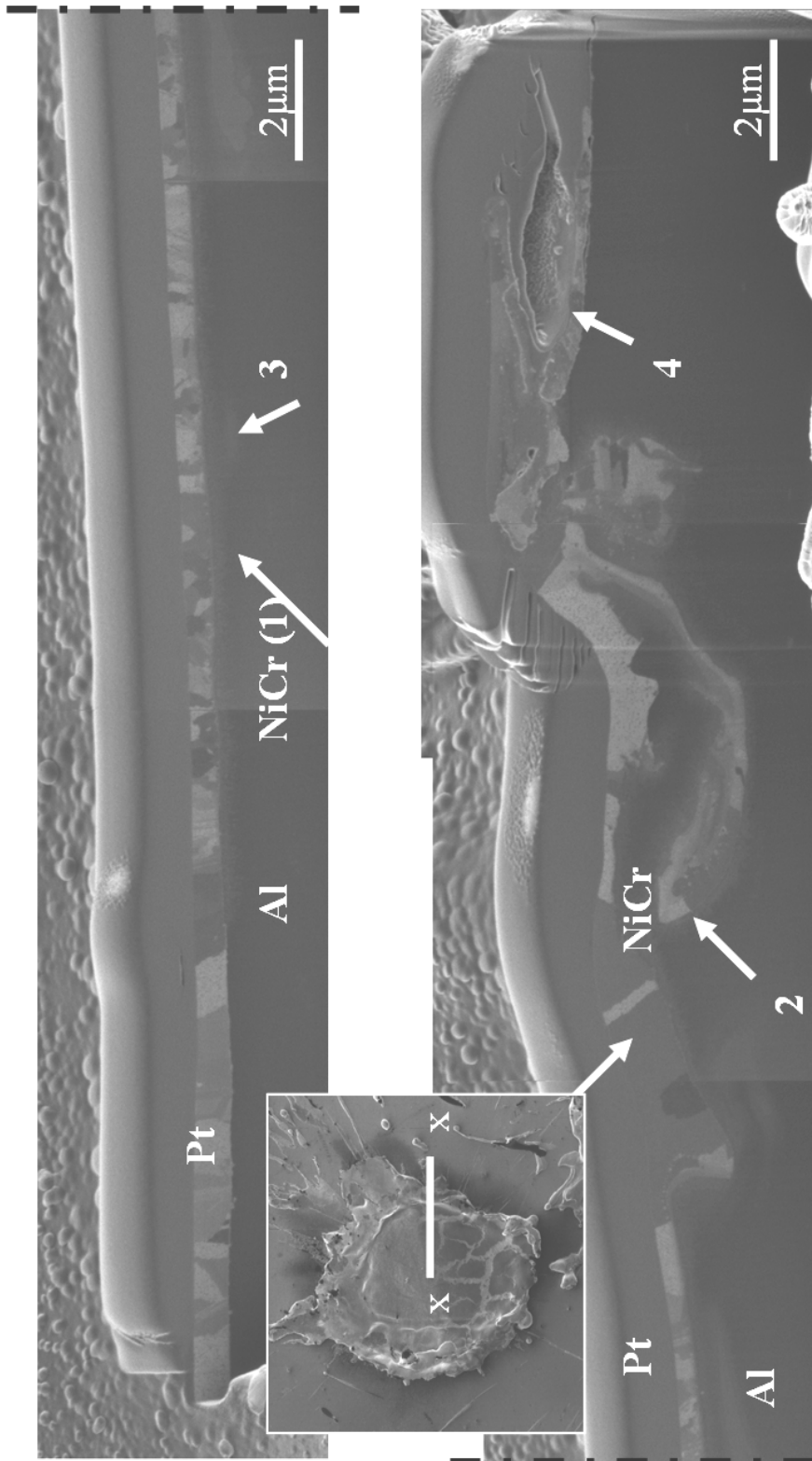


Figure 10. FIB cross-section of an almost disc-shaped splat (see insert picture) found on Al5052 PH

Mixing of the Al substrate and the NiCr splat has occurred, causing the lift-up of the splat and consequently the raised pattern observed on the SEM image. This shows that localized melting of the substrate has occurred to a significant degree.

On the TEM cross-section shown in Fig. 11, prepared in a similar location on an almost disc-shaped splat, mixing between splat and substrate can also be observed. On the bright field image (Fig. 11a) and on the EDS elemental maps (Figs. 11b and 11c), it can be observed how the splat-substrate interface is irregularly shaped and indistinct (1). Some Al is present even on the outer surface of the splat (2). The linescan L1 (see Fig. 11d) made across the interface confirmed the mixing between these phases (3). However, the equilibrium solubility of Ni in Al is negligible and the solubility of Al in Ni is also very limited (< 6w%) [132]. Thus, interdiffusion is very less likely compared, for example, to the case of NiCr on stainless steel [50].

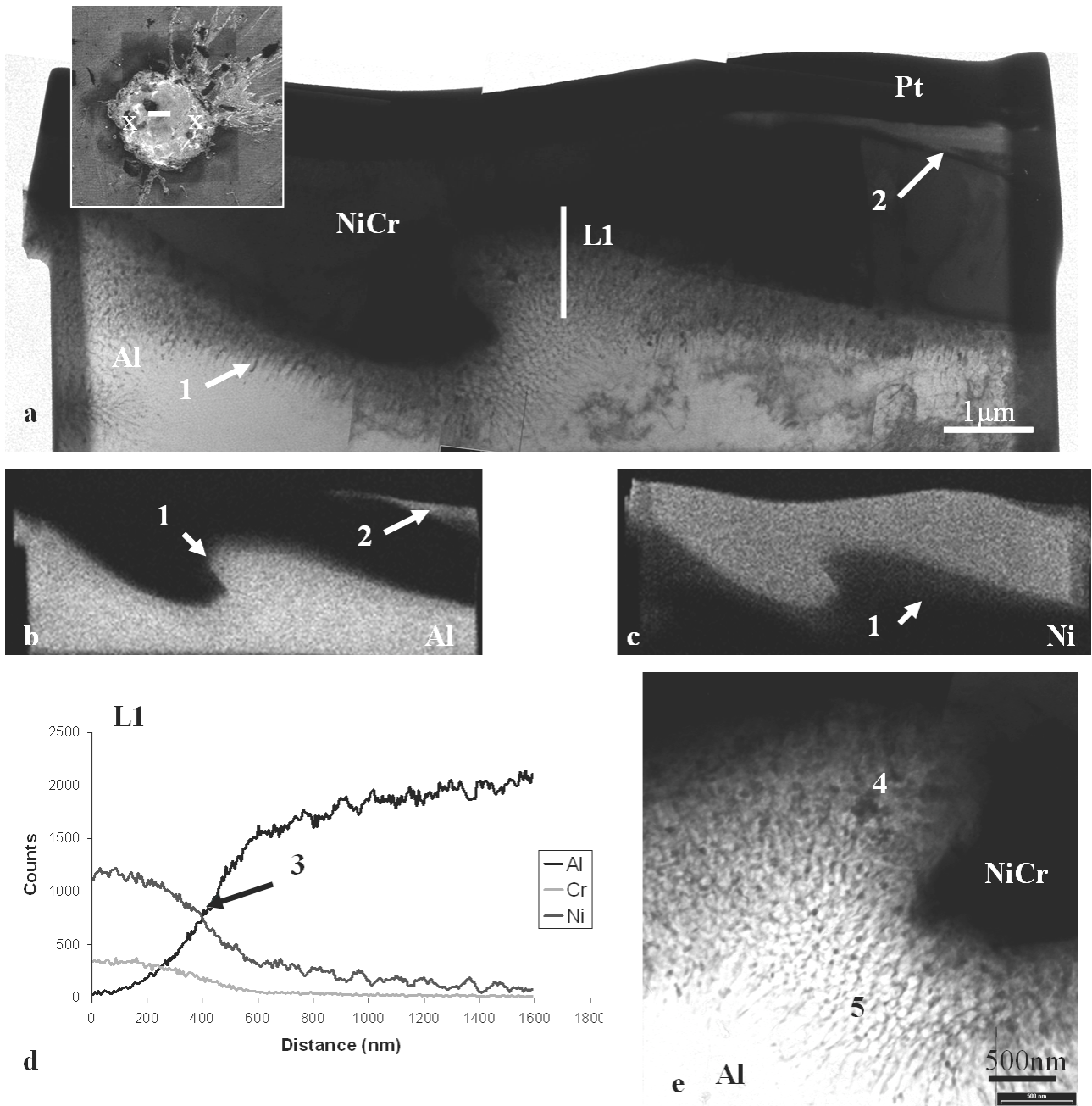


Figure 11. TEM cross-section made across an almost disc-shaped splat (see insert picture) found on Al5052\_PH: (a) bright field image, EDS elemental maps for (b) Al, (c) Ni, (d) EDS elemental linescan, (e) high magnification bright field image of the splat-substrate interface

On the higher magnification bright field image of the interface (Fig. 11e), a distinct microstructure can be observed, comprising nano-sized grains (4) that become needle-like and normal to the interface on the substrate side (5). Consequently, it is possible that both molten phases, NiCr and Al, intermixed and solidified into a non-equilibrium metastable phase made of a mixture of NiCr and Al nano-sized grains.

Furthermore, the few splashed fingers observed were made of Al, not NiCr. Consequently, they most probably originate from the jetting of the molten substrate caused by the spreading of the splat. The absence of pores and voids should finally be noted.

### III.2.b. *Microstructure and formation process of the other types of splats*

While for the almost disc-shaped splats, substrate melting was found to occur, for all the other types of splats formed, no evidence of this phenomenon was observed.

Figure 12 shows a TEM cross-section of a small circular splat. It appears very thin ( $\sim 0.5 \mu\text{m}$ ) (1), with the splat-substrate interface straight and distinct (2). A splat of such dimension (diameter of  $30 \mu\text{m}$  and thickness of  $0.5 \mu\text{m}$ ) has a volume which corresponds to a spherical particle of  $4.5 \mu\text{m}$  in diameter, which is thus too small to directly originate from the feedstock powder, especially as there are a relatively large number of small circular splats. As a result, such a splat more probably originates from NiCr fragment splashed away upon impact of a primary NiCr particle, also called “impact splashing” [12, 52].

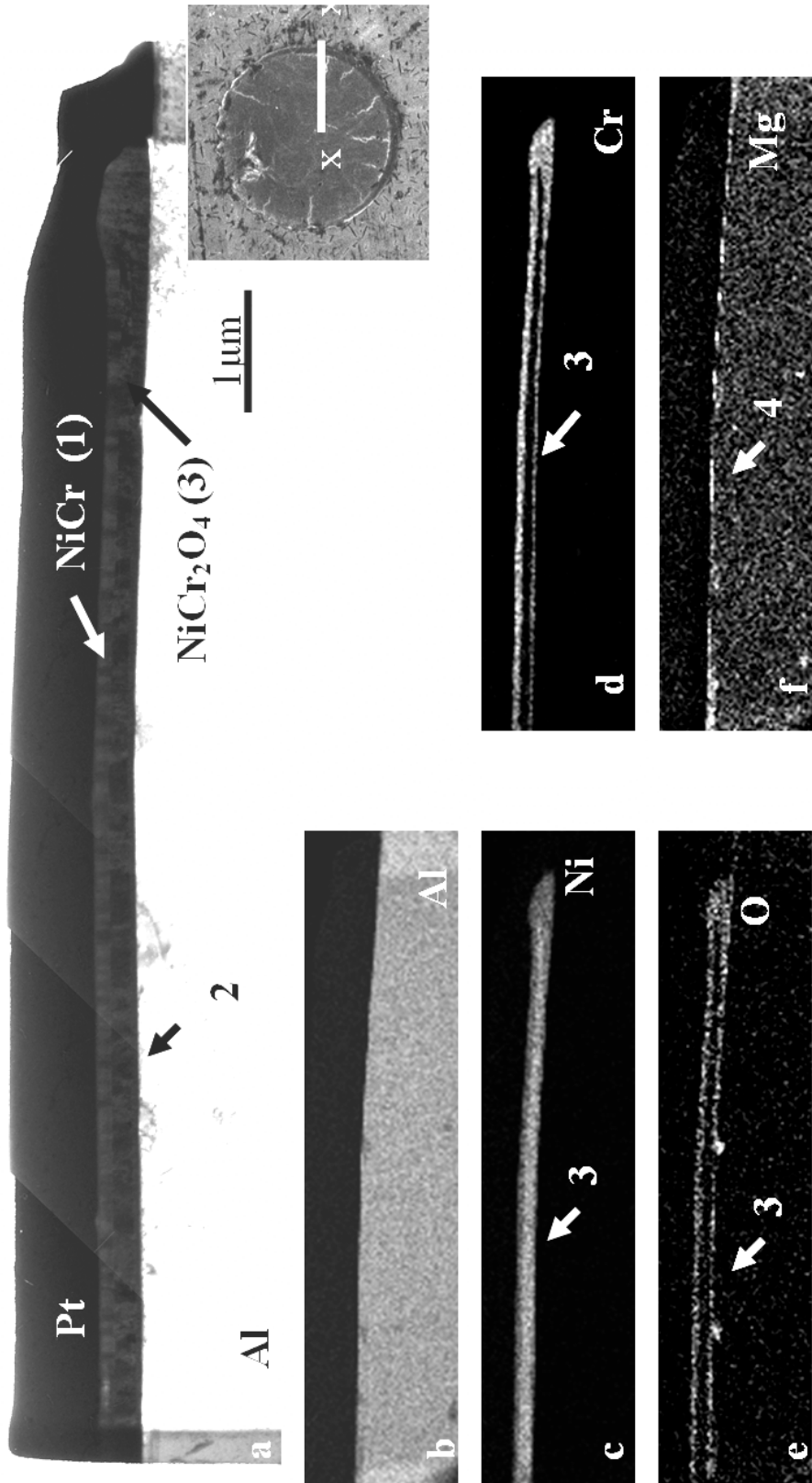


Figure 12. TEM cross-section made across small circular splat (see insert picture) found on

Al5052\_PH: (a) bright field image, EDS elemental maps for (b) Al, (c) Ni, (d) Cr, (e) O, (f) Mg

On the EDS elemental maps (Figs. 12c to 12e), it can be observed that a dense layer of oxide containing Ni and Cr is present around the entire periphery of the splat (3), and was identified by electron diffraction as being spinel  $\text{NiCr}_2\text{O}_4$ . It should be noted that such layers may not be present for all the small circular splats, or to such extent in terms of location and thickness, or sometimes it may be  $\text{Cr}_2\text{O}_3$  rather than spinel. As discussed for Fig. 8 (see III.1.c), the formation process of the oxide present at the splat-substrate interface is not clear. The shape of the spinel layers, fitting closely the splat, and the formation process of such splat, made from splashed NiCr, make the hypothesis of in-flight oxidation improbable. Since the substrate is heated during this time of formation, oxide may have formed after the splat formation. Such hypothesis still leaves the question of the origin of the oxygen for the oxide present under the splat, maybe from gases released from the substrate or from the cooling splat [129]. Finally, for the splats formed on the 5052 substrates, on the Mg EDS elemental maps (Fig. 12f), formation of MgO as a thin layer on top of the substrate (4), as discussed earlier, can be observed.

Figure 13 presents a TEM cross-section prepared across the centre of an irregularly shaped splat. It can be seen that the splat is quite thick ( $\sim 4\text{-}5\ \mu\text{m}$ ) (1) and that the splat-substrate interface is straight and distinct (2). On the EDS elemental maps (Figs. 13d to 13f) and also on the linescan L1 (Fig. 13g), thin layers of Cr oxide can be observed not only on the top (3), but also the bottom surface of the splat (4), possibly formed because of the heating of the substrate. In addition, a thin MgO layer on top of the substrate (5) can be observed.

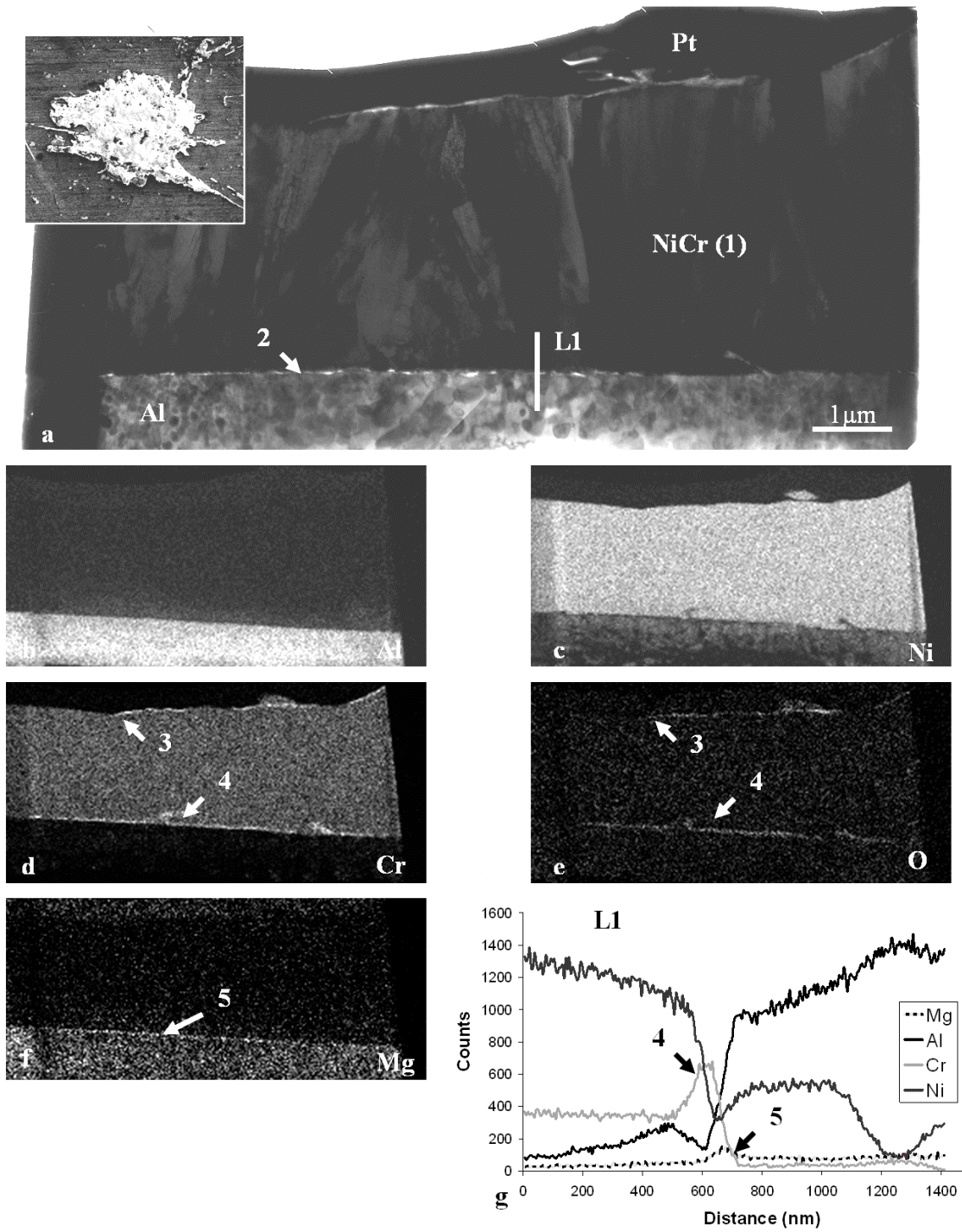
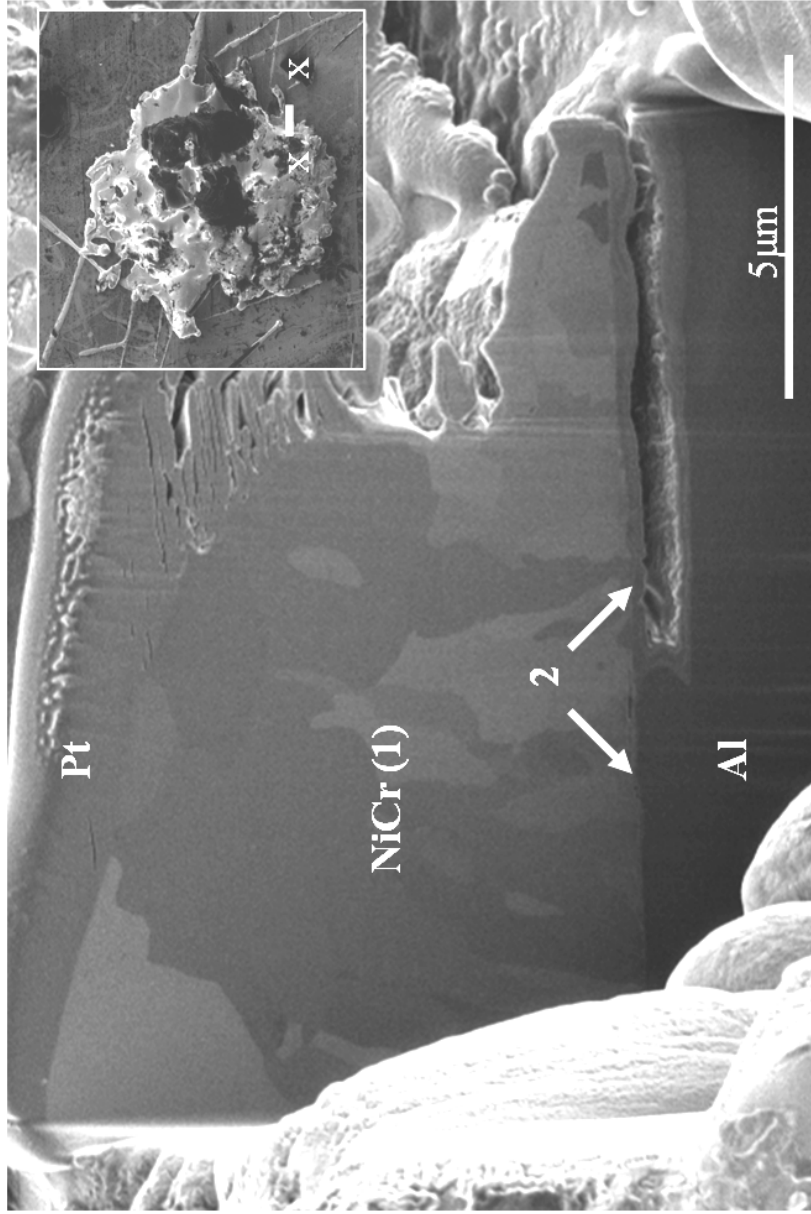


Figure 13. TEM cross-section made across an irregularly shaped splat (see insert picture) found on Al5052\_PH: (a) bright field image, EDS elemental maps for (b) Al, (c) Ni, (d) Cr, (e) O, (f) Mg, (g) EDS elemental linescan

For both the small circular splats and the irregularly shaped splats, substrate melting has been inhibited, possibly by the limited temperature and momentum in the case of the small circular splats, or for the other splats a poor contact between the NiCr particle and the substrate.

Finally, on Fig. 14 is displayed a FIB cross-section made across the rim of a partially melted splat. The coarse (2-5  $\mu\text{m}$ ) and irregular grain structure (1) is a sign of slow solidification, while some other FIB cross-sections showed the presence of zones with still very large (2-7  $\mu\text{m}$ ), but equiaxed grains, originating from the initial feedstock powder particles which were found to exhibit such a grain structure [137]. Such splats are, as a result, possibly made of a mixture of non-melted fragments and melted zones, solidifying slowly, possibly due to the thickness of such splats (5-10  $\mu\text{m}$ ) and the contact with the substrate that may not be uniform, as it can be seen on Fig. 14 as well (2).



*Figure 14. FIB cross-section made across the rim of a partially melted splat (see insert picture) found on Al5052\_PH*

III.2.c. *Summary of the splat formation process and the effects of heating during spraying*

Upon impact of molten NiCr droplets, vertical splashing occurs causing the formation of the small circular splats, in the same way as the other Al substrates. Heating the substrate at 350°C during spraying can completely remove the water released from the dehydration of surface hydroxide to oxide. This results in very good contact between the substrate and the splat, leading to localized melting of the latter to possibly a slightly greater extent compared to the specimens sprayed at room temperature (due to the better contact and the heat provided by the heating treatment). No, or very limited, splashing of the splat occurs, nor void formation either. However, the molten substrate does get jetted within the flowing NiCr, forming a disordered structure observed at the splat-substrate interface towards the splat periphery, and the raised pattern observed on the top surface of the splat in addition to the few splashed fingers. Solidification of the splat and the molten substrate occurs in the same way for the halo fingered splats but without formation of a metallic glass phase.

For the irregularly shaped splats, their formation process is expected to be very similar to the one of the irregularly shaped splats found on the non-heated specimens.

A few partially melted splats were found on the heated specimen. They have formed from sprayed NiCr particles that were only partially molten upon impact. Their lower

temperature and the presence of non-melted fragments limited the possibility of substrate melting.

#### **IV. Effects of substrate heating before and during spraying**

##### **IV.1. Effects of the Mg content in the substrate Al alloy**

From the values presented in Table 2, no significant difference can be noted between the splats formed on the Al 5052 substrates, which contain Mg as a major alloying addition, and Al 1005 substrate, without Mg. The proportions between the different categories of the splats were also very similar. Furthermore, the various FIB and TEM cross-sections did not show any noticeable difference in structure either. Upon heat treatment of the Al 5052 substrate, Mg is expected to segregate to the surface, forming mainly the oxide MgO (spinel  $\text{MgAl}_2\text{O}_4$  was sometimes found by usually at higher temperature than  $350^\circ\text{C}$ ) [74, 131, 146, 147], and, indeed, this was observed on several cross-sections (see results presented in a previous study [131] or for example on Fig. 12 (4) and Fig. 13 (5), as described in a latter section). If such layer has an influence on splat morphology and formation, by modifying the wetting of molten NiCr on the substrate for instance, this effect was too limited to be noticeable in the splats behavior examined here.

#### IV.2. Effects of heat treatment before and during spraying

As discussed in our previous study [131], there was a thin layer of 3.5 nm thick of native oxide/ hydroxide on the polished aluminum substrate. Thermal treatment of the substrates at 350°C caused a small increase in the oxide thickness to ~ 5 nm. Thermal treatment also led to the dehydration of surface hydroxide to oxide and induced the segregation of Mg from the bulk to the surface. Thus, thermal treatment of the substrate prior to spraying can eliminate the effect of water released from the conversion of surface hydroxide under impact of the splat on the splat morphology.

In a previous work, the authors studied the effects of pre-heat treating Al substrates on the morphology of plasma-sprayed NiCr splats [131]. It was found, in agreement to other works on stainless steel substrates [11, 67], that this tended to increase splat diameters, possibly because the thermal treatment modified the surface chemistry in a way that induced a better wetting of the splats. For the present study, the diameters measured, as presented Table 2, and despite the significant error intervals, do not contradict this trend. The slight decrease in the diameter of the halo splats, after thermal treatment, may be explained partly because of the error intervals but also possibly by the fact that the halo splat category includes very small splats ( $D \sim 30 \mu\text{m}$ ). Indeed the relative amount of these may have increased with the thermal treatment. Indeed, an increase in the wetting of NiCr on aluminum may signify that the adhesion of particles impacting with relatively low momentum/temperature would increase too, leading to a larger proportion of small splats and a smaller average diameter for the halo splats.

The effects of heat treating before spraying are, however, relatively limited compared to the effects of heat treating during spraying. Indeed, as seen Figs 1 and 9, the morphology of the splats is very different. Heating during spraying above the transition temperature has been known to significantly reduce splat splashing by preventing gas release from the substrate upon splat formation [6, 20, 21, 26-28]. Indeed here compared to the non heated specimens, most splats found on the substrate heated during spraying were disc-shaped with significantly reduced splashing. The very limited splashing that was observed comes from the jetting of the molten substrate, not from the presence of gas at the splat-substrate interface. The absence of pores for the Al5052\_PH splats also shows this important reduction in the amount of gas release from the substrate.

The presence of partially melted splats on Al5052\_PH, knowing that partially molten particles must have impacted as well on the non heated substrate even if similar splats could not be found, also shows that heating during spraying improve the adhesion of such splats.

Other differences can be noted as well: for Al5052\_PH, when substrate melting occurred there was never formation of a layer of metallic glass at the splat-substrate interface, as observed for the halo fingered splats on the non heated substrates. Splats on Al5052\_PH also displayed no large voids. Reasons for these absences are not fully understood yet. McDonalds *et al.* found that heating during spraying reduced the thermal contact resistance [28], this would means here a higher solidification rate for Al5052\_PH splats, compared to the non heated specimens, and consequently should promotes the formation

of a glassy phase, which requires a very fast solidification, and the freezing of large voids that may form. Possibly the change, with heating of the substrate, in the way the molten NiCr spreads into a splat may be accounted for the observed absence of glassy phase and large voids. Further study would be required to fully understand how the mechanics of the flow of the molten NiCr create the splats structures observed.

In conclusion, heating the substrate during spraying may be very beneficial as it significantly reduces splashing along with oxide and voids formation, but also increases the overall adhesion: firstly substrate melting occurs to a greater and deeper extent, without the occurrence of the formation of a potentially brittle phase such as a glassy layer, leading to a stronger metallurgical bonding, and secondly the limitation of voids and splashing means limitation of regions of poor adhesion. Consequently, properties of the complete coatings, such as density, strength, adhesion, etc. will be improved.

## **V. Conclusion**

To summarize, the observation of NiCr splats, sprayed on Al substrates, by electron microscopy, led to the following conclusions:

- On the substrates sprayed at room temperature, substrate melting, on a depth up to a few microns, and mixing with melted NiCr was observed for splats with a ring of splashed fingers, but not for the one without splashed fingers. Significant concentrations of oxides and voids were also observed, and where substrate melting occurred interfacial layers were found, some amorphous and some

composed of nano-sized grains, probably formed from the mixing between NiCr and Al and a rapid solidification.

- Either using an alloy with Mg or heating the substrate before spraying were not found to have a significant effect on splat formation.
- Heating the substrate during spraying was found to result in reduced splashing and potentially slower solidification, leading to the absence of interfacial amorphous layers, and very limited amounts of voids and oxides.

**CHAPTER 11**

**EFFECTS OF SUBSTRATE ROUGHNESS ON SPLAT FORMATION**

**FOR NiCr PARTICLES PLASMA SPRAYED ON TO ALUMINUM**

**SUBSTRATES**

---

*S. Brossard, P.R. Munroe, A.T.T Tran, M.M. Hyland, Journal of thermal Spray Technology, 2010, DOI: 10.1007/s11666-010-9508-x*

**Abstract**

Roughening of the substrate, for instance by grit-blasting or etching, is often used before plasma spraying in order to provide a high degree of roughness that promotes mechanical interlocking of the sprayed coating and consequently improved adhesion. The present work investigates the morphology and microstructure of NiCr splats formed on such rough Al substrates, where roughness was generated by a number of methods including grinding and etching. Cross-sections of the splats and the splat-substrate interface were examined using a range of electron microscopy techniques. Localized substrate melting and chemical mixing with the splat material was observed, forming very particular structures. The formation of various oxides phases and voids was also noted and found to increase, along with the degree of the substrate melting, with increasing substrate

roughness. The structures observed were related to the spray conditions and substrate morphology.

## I. Introduction

Thermal spraying processes encompass a number of coating manufacturing techniques aimed at enhancing the performance of components or increasing their durability, whilst conserving the properties of the bulk substrate material. Amongst them, conventional plasma spraying makes use of a plasma flame to melt the particles, which are then sprayed, usually in a fully molten state, on to the substrate, flattening upon impact in lamellae often termed “splats”, which by accumulation end up creating a coating of a thickness up to 250  $\mu\text{m}$  [1, 4, 141].

The mechanical properties of the coatings depend heavily on the adhesion mechanisms between the first splats to form and the substrate. Many studies have investigated these mechanisms by studying single splats sprayed on to smooth substrates [20, 35, 36, 50]. In particular, it was noted that localized melting of the substrate from the heat provided by the sprayed particle may occur, which may then lead to the formation of intermetallic compounds or the generation of non-equilibrium microstructures [35, 148]. In such cases, metallurgical bonding is achieved, and assuming that the interfacial phase is not brittle, this is then beneficial for adhesion strength [1, 4]. When substrate melting does not occur, as limited to certain spray conditions and combinations of materials, adhesion between splat and substrate may occur by either diffusion between the splat and substrate [67, 81, 149] or chemical-metallurgical interactions [82]. Although it should be noted that this

only occurs in zones where good contact is achieved, which are then often present in local regions of the substrate-coating interface due, for instance, to the presence of voids. However, in many cases, bonding is mechanical, occurring by interlocking between the splat and substrate [1]. To obtain effective bonding plasma spraying is often performed on to rougher substrates, usually prepared by processes such as grit-blasting to promote such mechanical interlocking [1, 4, 23].

When discussing the effect of roughness on splat formation and adhesion to the substrate, Fauchais *et al.* made a distinction between cases of low roughness ( $R_a < 2 \mu\text{m}$ ) and high roughness ( $R_a > 2 \mu\text{m}$ ) [2]. Some models and experiments showed that increasing substrate roughness, but keeping the roughness level below 2 microns, resulted in decreasing the contact angle of the splat on the substrate, thus increasing splat thickness, decreasing flattening time and increasing the solidification time [24, 150]. Other studies, on the other hand, found that wetting of the substrate was often improved [2], which may result in larger and flatter splats [12, 67, 151]. These effects may also depend on the manner by which the increased roughness is achieved, notably if it is by preheating the substrate to oxidize its surface [2].

In the cases of higher roughness (i.e.  $> 2\mu\text{m}$ ), however, the spreading of the splat may be hindered by irregularities present on the substrate surface [2, 22], especially if the wavelength (i.e. the distance between two consecutive peaks) of these irregularities is smaller than the particle diameter [152]. If it becomes greater than the particle diameter, Liu *et al.*'s model showed that spreading of the liquid droplet ends up in “violent” break

up of the splat [152]. Inducing such high roughness was then usually found to cause extensive finger formation in the splats [153, 154], but the adhesive strength may also be improved due to increased mechanical interlocking [23, 154]. Furthermore, a reduction in the number of voids in the formed splat may occur, as found by Qu *et al.* who observed that micron-scale roughness may decrease the driving force for bubble nucleation and also prevent splat curling-up [129], a phenomenon often observed for splats formed on flatter substrates [54].

Wroblewski *et al.* and Basu *et al.* studied by both experiments and modelling the influence of roughness on substrate melting upon spraying yttria stabilized zirconia (YSZ) splats on to a YSZ substrate [155, 156]. They found that such melting occurred at a lower substrate heating temperature or, to a greater extent, for a lower roughness ( $R_a = 50\text{-}100\text{ nm}$ ) than for a higher roughness levels (several microns). Both roughness levels were noted to be more prone to substrate melting than a smoother substrate.

It can be noted that for almost all the studies on the effects of surface roughness on splat formation, only the exterior morphology of the splats was observed. In other studies, properties, such as the adhesion strength, were measured. However, no work has been published on the observation of cross-sections of splats made on rough substrates ( $R_a > 2\text{ }\mu\text{m}$ ), which could reveal, in detail, the structural and chemical interaction between the splat and substrate. The present study, on the other hand, proposes to study the microstructure of splats, formed on substrates presenting various level of roughness, at a nano-scale level, using a range of electron microscopy techniques. NiCr particles, a

material commonly used in plasma spray coating for applications such as bond coats or wear-resistant coatings [1], were then plasma sprayed onto aluminium substrates having undergone various pre-treatments to generate different levels of surface roughness. The results are compared with studies obtained for smoother substrates, which are described in more detail in an associated study [148].

## II. Experimental procedure

Five different substrates were used; prepared from either aluminium 1005 or 5052. (Details on both alloys, which differ in their Mg content (2.2-2.8wt% in Al5052, close to nil in Al1005), can be found in the associated paper [148]). However, it was found that the difference in composition between both alloys did not have any significant influence on splat formation). The different substrates and their methods of preparation are listed in Table 1.

**Table 1. Substrates Nomenclature and Condition**

<b>Specimen</b>	<b>Substrate</b>	<b>Pre-treatment</b>
Al5052_P	Aluminium 5052	Polished to a nano-scale roughness
Al1005_R	Aluminium 1005	Roughened with sand paper
Al1005_GB	Aluminium 1005	Grit blasted
Al5052_E	Aluminium 5052	Etched in HF
Al5052_ET	Aluminium 5052	Etched in HF and heat treated in air (350°C, 90 min)

The polished substrates were mechanically ground and mirror polished with diamond paste, to a nano-scale roughness. The roughened substrate was ground using sand paper P120 (average particle diameter of 125  $\mu\text{m}$ ). The grit blasted substrate was grit blasted with ICMAD-A BlastAB 14ED using a pressure of 50 psi. Finally, the etched substrates were immersed at room temperature for 10 minutes in a solution made of 10%HF and 15% $\text{H}_2\text{SO}_4$ . One of them was then heat treated in air for 90 min at 350°C.

The sprayed material was a commercial NiCr alloy powder (Ni80-Cr20, Sulzer Metco 43 VF-NS, Switzerland, (-45+5)  $\mu\text{m}$ ). Plasma spraying was carried out with a Sulzer Metco (Switzerland) 7MB gun (with a nozzle diameter of 8 mm), operating at a current of 550A and at a voltage of 62V, with a spraying distance of 100mm. The feeding rate of the powder was of 1g/min, the carrier gas being argon at a flow rate of 3 SLPM, while the plasma gas was a mixture of nitrogen and hydrogen, at a flow rate of 47.5 SLPM and 6.2 SLPM respectively.

The specimens were then characterized using a range of analytical techniques. A Hitachi S3400 scanning electron microscope (SEM) was used to image the overall morphology of the splats and the substrates. A FEI xP200 Focused Ion Beam microscope (FIB) was used to mill cross-sections of the splats using an energetic gallium ion beam, and to image them using secondary electrons induced by the ion beam. Details have been described elsewhere [51]. A FEI xT Nova Nanolab 200 dual beam microscope (that is a FIB and SEM combined into a single instrument) was used to prepare cross-sections of splats (100-200nm in thickness) suitable for TEM observation. These were prepared using the

lift-out method as described elsewhere [51] and examined in a Philips CM200 transmission electron microscope (TEM) to which energy dispersive x-ray spectroscopy (EDS) facilities have been interfaced. Finally, the average surface roughness of the substrates was assessed using a Digital Instruments DI3000 Atomic Force Microscope (AFM), except for the very rough substrates (Al1005\_R and Al1005\_GB), whose roughness was evaluated using a profilometer (Mitutoyo Surfpak-SV 600).

Several FIB and TEM cross-sections were prepared and studied for each particular feature and/or type of splat. However, for reasons of brevity only a small number of representative images will be presented here. The cross-section preparation process using FIB also involves the deposition of a layer of platinum on top of it prior to milling for protection purposes. This layer is present on the FIB and TEM images presented.

### **III. Results and discussion**

The morphology and microstructure of the typical splats found on the different substrates will be described from the observations made from the electron microscope images and cross-sections. Once they are described, the formation of the various features observed will be discussed.

### III.1. Splat microstructure and formation on the polished substrates

In an associated paper by the same authors [148] the morphology, microstructure and formation process of NiCr splats plasma sprayed on to aluminium substrates was described. This includes both Al5052 and Al1005 alloys, having first undergone polishing to nano-scale levels of roughness, and in some cases, thermal pre-treatments aimed at modifying the substrate surface chemistry. The observations made are briefly summarized here to allow comparison with the rougher substrates described in more detail in this paper.

Figure 1 presents two SEM images of the most typical splat morphologies found on polished Al5052 (roughness  $R_a = [ 7.3 \pm 2.3 ]$  nm) . For the larger splat with a ring of splashed fingers (Fig. 1a), evidence of localized substrate melting was found at the splat-substrate interface towards the centre of the splat, along with chemical mixing between the NiCr and Al phases, forming some interfacial layers of both a metastable metallic glass and a very fine mixture of Ni and Al non-equilibrium phases, associated with the rapid solidification of the melted phases. This structure was also found to form on substrates with a higher roughness, as will be described later in detail. Towards the periphery of the fingered splats and for the splat with no splashed fingers, the splat-substrate interface was typically found to be straight and distinct, often with a poor contact between splat and substrate. Voids and various oxides phases, such as alumina  $\gamma$ - $Al_2O_3$ ,  $Cr_2O_3$  or spinel like  $NiAl_2O_4$ , were found to form in typical locations around the splat. It was also found that effects of heat treating the substrate prior spraying, or using

an alloy containing or not containing Mg (Al5052 compared to Al1005), had negligible effects on the splat morphology. As noted earlier, more details of these structures can be found elsewhere [148].

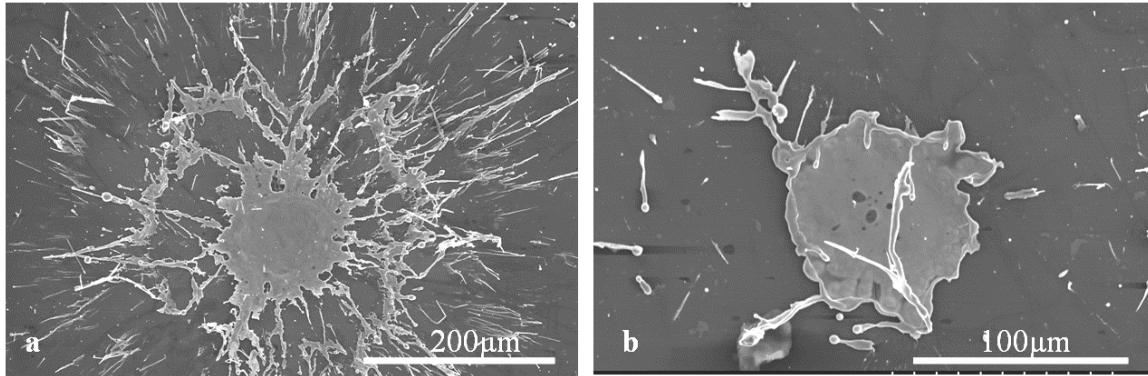


*Figure 1. SEM images of typical splats found on Al5052\_P*

In addition, other types of splats were observed, such as the splats without a ring of splashed fingers, as shown in Fig. 1b, and presented a similar structure as the one described above, except no evidence of substrate melting was usually found: the splat-substrate interface was mostly distinct and straight. Evidence of a slower solidification rate (poorer contact at the interface, coarser grain structure) and larger concentration of oxides were also observed.

### III.2. Splat microstructure and formation for the roughened and grit-blasted substrates

As it can be observed in Fig. 2a, when examining the substrate surface around the splat, the roughened substrate displays many scratches from the grinding process. The surface roughness was measured to be  $Ra = [ 1.2 \pm 0.2 ] \mu\text{m}$ . On the other hand, the grit-blasted substrate (Fig. 2b) displays cavities and peaks which are less linear compared to the elongated scratches on the ground substrate. The average roughness is also significantly higher ( $Ra = [ 6.9 \pm 0.2 ] \mu\text{m}$ ).

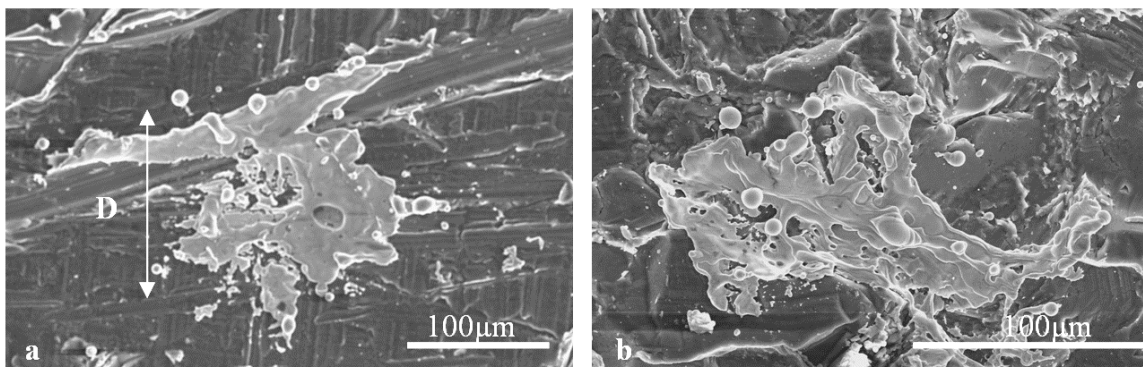


*Figure 2. SEM images of typical splats found on (a) Al1005\_R, (b) Al1005\_GB*

Figure 2 shows SEM images of splats found on Al1005\_R (Fig. 2a) and Al1005\_GB (Fig. 2b): both appear irregularly shaped, with some spherical particles distributed around the splat. As it can be seen on the FIB cross-sections presented in Fig. 3, made on various locations across a splat on Al1005\_GB, the microstructure of such a splat is very irregular. In some zones, such as the ones marked 1 on Fig. 3a and 3c, the contact between the splat and substrate is poor, and the splat-substrate interface is irregularly

shaped, as seen for instance on Fig 3b (marked 2). In contrast, in some regions the contact between both phases is excellent and evidence of localized substrate melting can be observed. Indeed, jetting of Al within the NiCr phase can be seen (marked 3), which can only have formed from the melting of the substrate and mixing of the latter with the flowing molten splat. Finally, in other locations the contact between splat and substrate interface appears good (marked 4 on Fig. 3a), but as it is not clear if the irregular shape of the interface arises from the original substrate topography or from localized melting and mixing of the substrate, it can not be definitely concluded whether substrate melting has occurred or not.

However, when substrate melting does occur, a distinctive interfacial structure may form, as it can be observed on the TEM cross-section presented in Fig. 4. Towards the right side of the section, the contact between splat and substrate is good and the interface appears indistinct on the bright field image (see 1 on Fig. 4a) The EDS elemental linescan L1, performed across the interface, reveals a gradual variation of the concentrations in Ni and Al (2), showing that mixing between both phases has occurred over a depth of about 400 nm. The fact that these variations do not exhibit a step-function shows that there is no defined stoichiometric intermetallic compound present at the interface. However, on the higher magnification bright field image of the interface, two layers can be seen: a first layer close to the splat which appears featureless (3), and a second layer of nano-sized grains with needle-like shape normal to the interface (4).

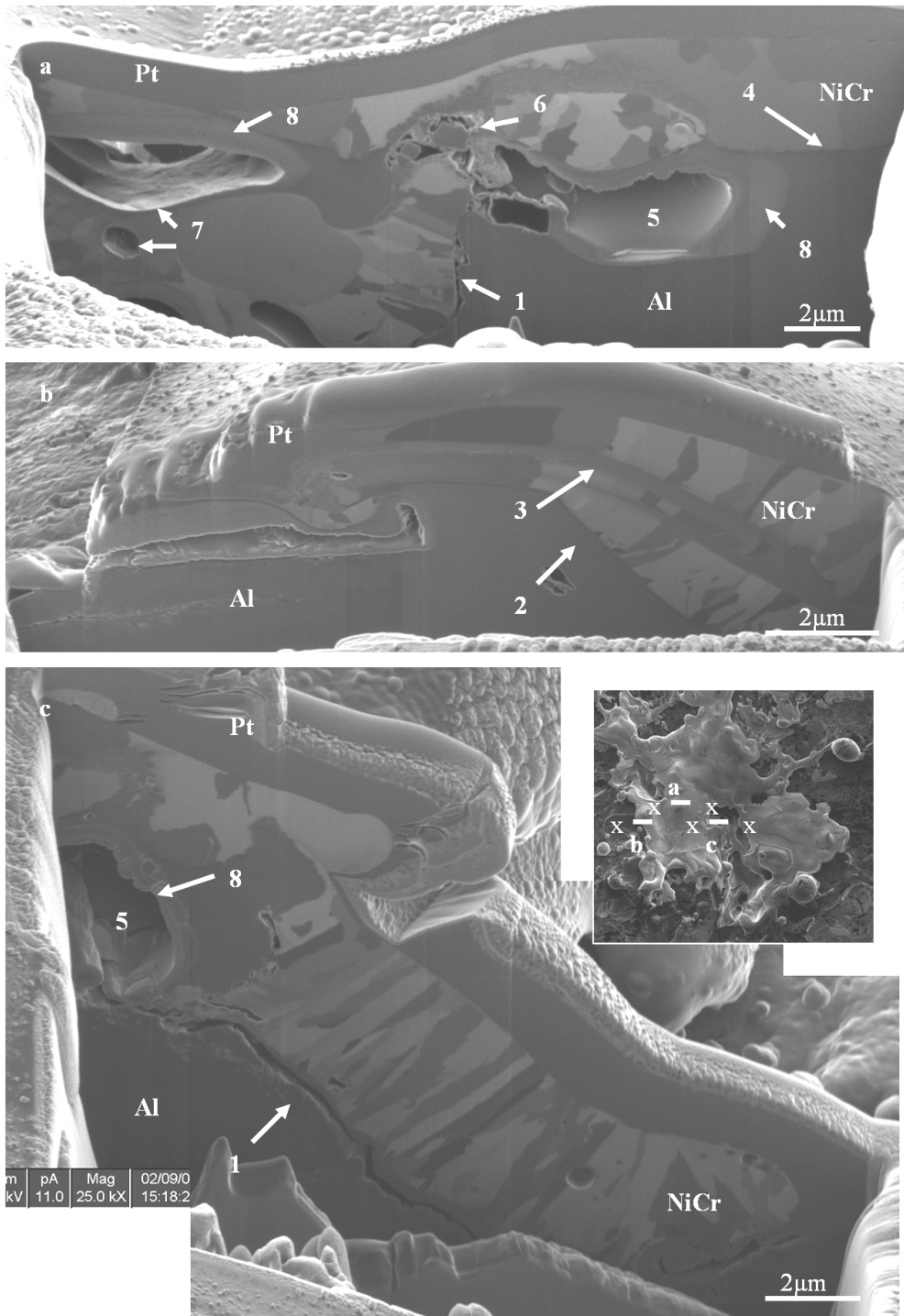


*Figure 3. FIB cross-sections made across various locations on a splat (see insert image) found on Al1005\_GB*

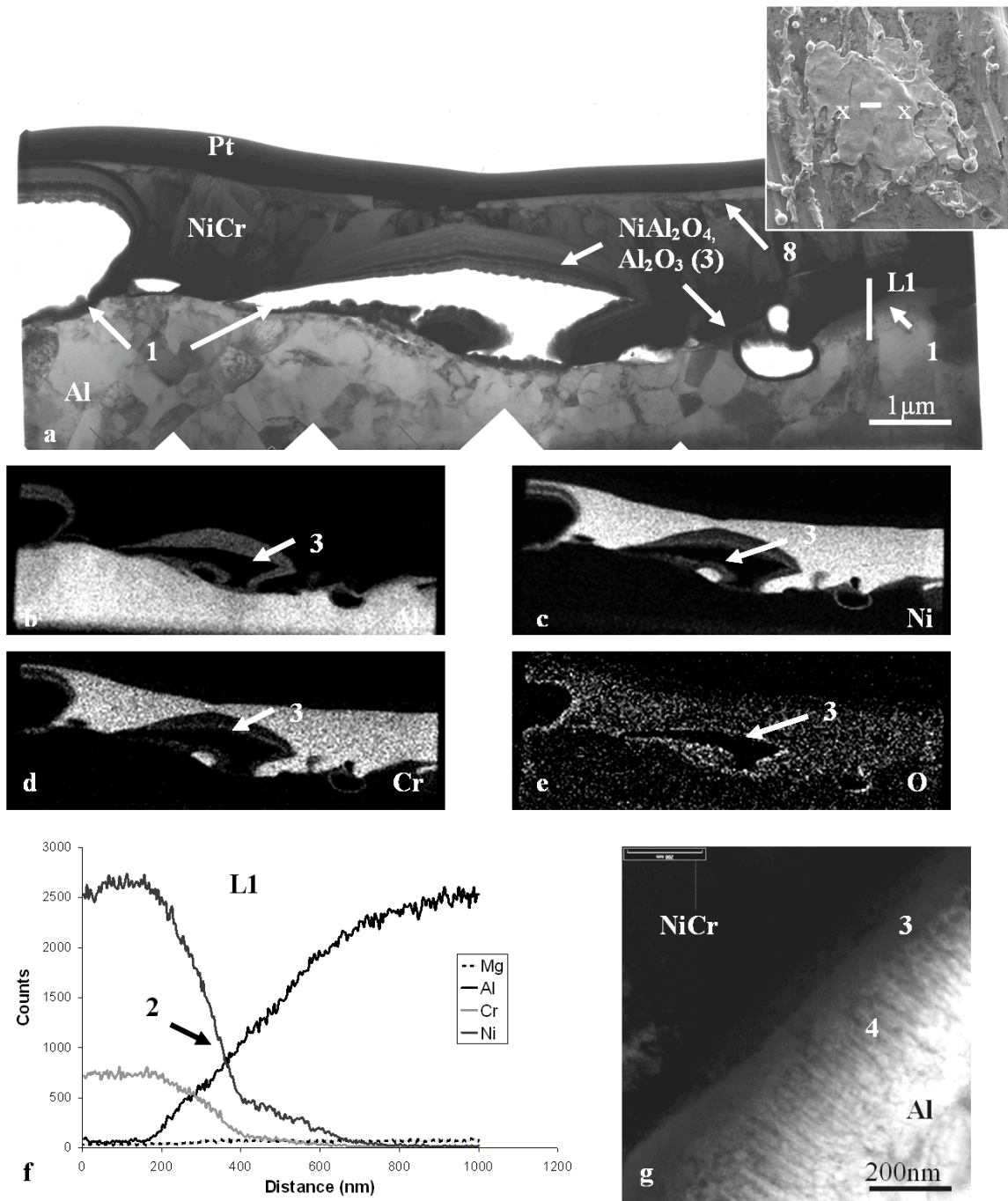


Figure 4. TEM cross-section across a splat (see insert image) found on Al1005\_R: (a) bright field image, EDS elemental maps for (b) Al, (c) Ni, (d) Cr, (e) O, (f) EDS elemental linescan, (g) high magnification bright field image of the splat-substrate interface

This particular interfacial structure was observed for the polished substrates and described in more detail in the associated paper [148]. It was concluded that the first layer was a metastable metallic glass composed of a mixture of Al and NiCr, while the second layer was a mixture of nano-sized Ni-rich and Al-rich metastable phases.

Large voids (several microns in size) can be found to have formed near the splat-substrate interface (see 5 on Figs. 3a and 3c), along with some much smaller ( $< 1 \mu\text{m}$  in size) voids (for instance 6 on Fig. 3b), also within the splat itself (see 7 on Fig. 3a). Especially visible for the larger voids are thick and dense oxide layers that can be observed on the walls of most voids (for instance 8 on Figs. 3a and 3c). Studies of the oxidation of alloys containing Al, Ni and Cr showed that alumina  $\gamma\text{-Al}_2\text{O}_3$ , chromium oxide  $\text{Cr}_2\text{O}_3$ , NiO and spinel species such as  $\text{NiAl}_2\text{O}_4$  and  $\text{NiCr}_2\text{O}_4$  were the most probable oxides to form [143]. On the TEM cross-section shown Fig. 4, it can be seen from the EDS elemental maps (Figs. 4b to 4e) that on the walls of the large void present at the splat-substrate interface are oxide layers containing mainly Al, but also containing some Cr and Ni. The diffraction patterns of phases such as  $\gamma\text{-Al}_2\text{O}_3$ , NiO and spinels  $\text{NiAl}_2\text{O}_4$  and  $\text{NiCr}_2\text{O}_4$  are all quite similar to each other (these phases have similar d-spacings) and are consistent with the patterns obtained from this area. However, from the EDS maps (3), it can be concluded that such layers may be composed mainly of alumina and a mixture of spinel ( $\text{NiAl}_2\text{O}_4$  and/or  $\text{NiCr}_2\text{O}_4$ ). Chromium oxide, notably  $\text{Cr}_2\text{O}_3$ , was often reported to form as a thin dense layer on top of NiCr splats in previous studies [50, 148]. Here, it was not observed on the TEM cross-sections prepared; however the possibility of its formation on other splats should not be ruled out.

Structural features, such as the presence of layers of Al folded within the splat (as seen in Fig. 3b) and voids located for instance within the splat, denote the turbulent spreading of the splat upon its formation. Many studies have reported that the presence of high scale roughness-induced instabilities in the spreading of plasma sprayed splat, causing the formation of features such as splashed fingers or voids [2, 152-154]. The presence of hot oxidizing gases is also evident by the presence of layers of oxides observed on the walls on the voids. Such gases may come from desorption of adsorbates/condensates initially present on the surface of the substrate [6, 26, 32], or may have been entrapped in the cavities on the substrate surface upon particle impact and spreading[22], or finally, as suggested by Qu *et al.*, they may come from gases that get dissolved within the molten particle due to the pressure upon impact, and which get released by the forming void due to the nucleation sites provided by the irregularities of the substrate's surface [129]. However, it can be noted that some voids are significantly large (several microns in diameter), apparently too large to be formed solely from bubble formation. Several modelling studies of splat formation on flat surfaces have shown that large central voids may form due to the mechanics of the flow of the molten splat, because of the change in the curvature of the droplet [15, 55].

Localized melting of the aluminium substrate from the heat provided by the impacting molten NiCr particle was observed and was discussed in detail for polished substrates [148]. Here, the presence of a large scale roughness means that the molten flowing NiCr encounters peaks on the aluminium substrate, which are then prone to melting from both

the heat and the pressure applied by the spreading splat. Previous studies showed that melting was more prominent for substrates with a large scale roughness compared to smooth substrates. In addition to the mechanical interlocking induced by the irregularities of the substrate's surface, the metallurgical bonding that results from the melting of the substrate and intermixing with the splat material may be another factor contributing to the significant improvement in the adhesion strength usually observed for the coatings sprayed on to rougher specimens [23, 154]. This is true, however, only if the interfacial phases formed are not brittle, which may not be the case for the glassy layer observed here (metallic glasses are well known to be brittle [145]). Finally, a remark can be made about how the grit-blasted substrate Al1005\_GB may present a higher adhesion strength compared to the rough substrate, Al1005\_R, as the latter presents long scratches on its surface, while Al1005\_GB exhibits more equiaxed anchorage points.

### III.3. Splat microstructure and formation on the etched and etched and thermally treated substrates

The etching treatment of the aluminium substrates produced many relatively small surface cavities (usually less than a few microns in size), as it can be observed when examining at the substrate surface around the splats in Figs. 5a and 5b. The roughness levels measured were  $R_a = [444 \pm 100]$  nm for the non heat-treated substrate, and  $R_a = [626 \pm 88]$  nm for the heat-treated substrate.

On Fig. 5 are displayed SEM images of typical splats found on both etched substrates, Al5052\_E and Al5052\_ET. In many instances splats were found to be very fragmented as shown for example in Fig. 5a, which suggests that the sprayed particle did not adhere to the substrate, leaving only some small droplets many of which are spherical in morphology. This splat shape probably arises from surface tension effects [2].

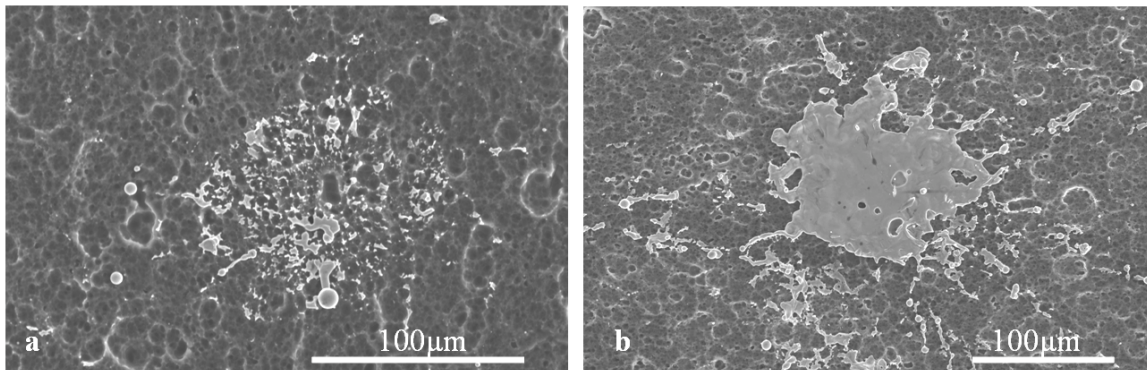


*Figure 5. SEM images of typical splats found on (a) Al5052\_E and (b) Al5052\_ET*

Figure 6 displays a FIB cross-section performed across such a droplet. The very rounded splat shape can be noted (1), the grains are elongated in a direction normal to the interface (2), suggesting a slow solidification which can be linked to poor contact with the substrate (3).

As shown on the SEM image (Fig. 5b), the other splats were found to have a relatively irregular shape, although to a lesser extent compared to the splats found on the rough and grit-blasted substrates. Figure 7 displays FIB cross-sections made across such a splat on the Al5052\_ET substrate.

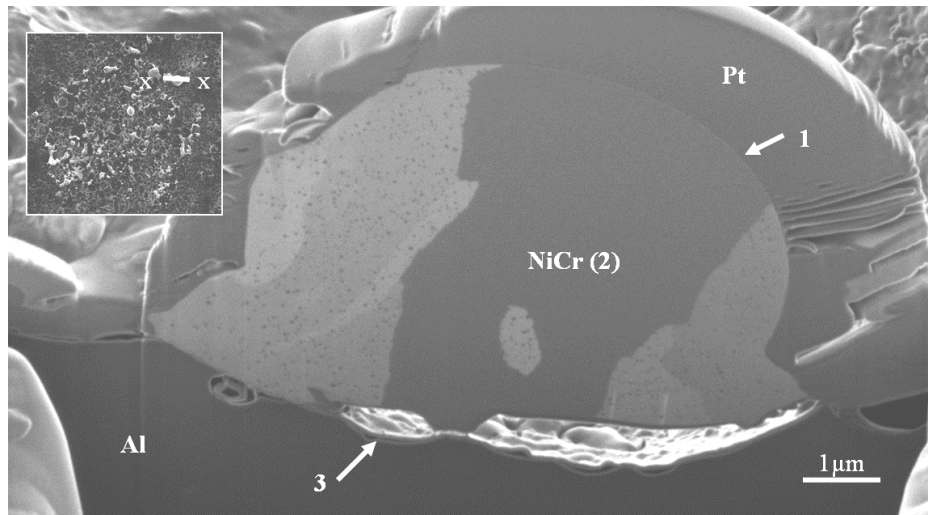


Figure 6. FIB cross-section of a NiCr droplet from a non-adhered splat (see insert image) found on Al5052\_E

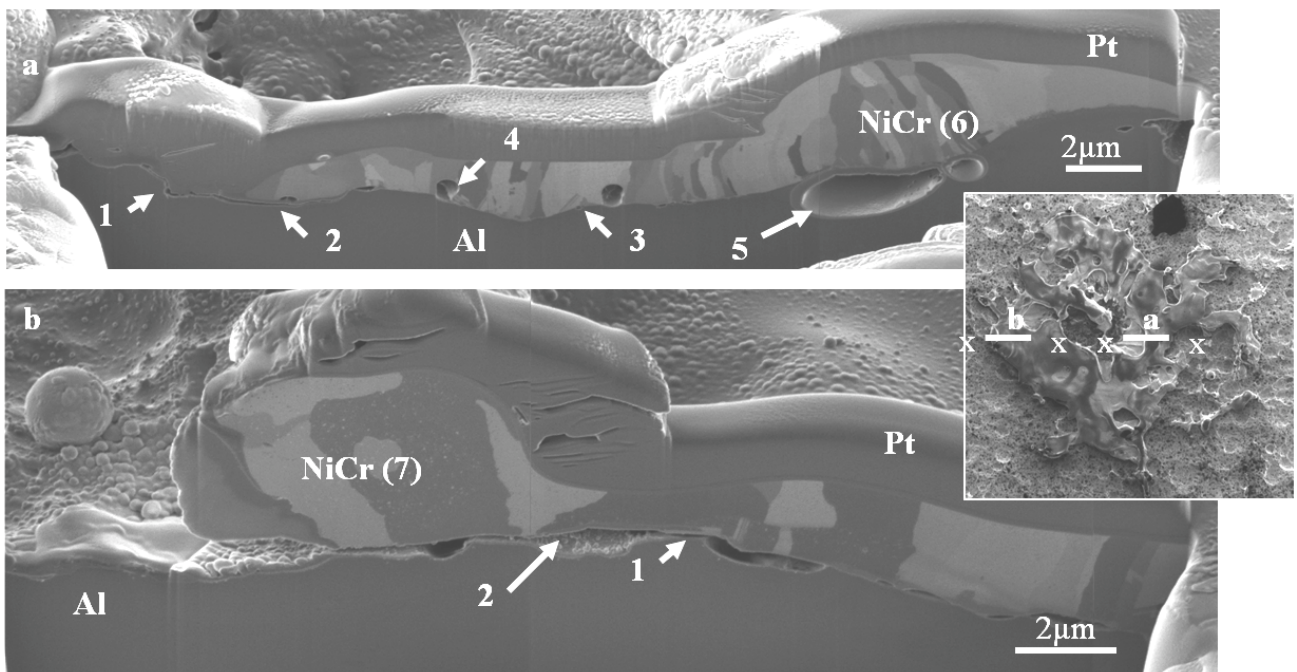


Figure 7. FIB cross-sections made across a splat (see insert image) found on Al5052\_ET

The substrate surface is quite irregularly shaped (1) and the contact between splat and substrate is poor in some regions (2), while good in others (3). Voids can also be noted close to the interface, some within the splat (4) and some within the substrate (5). The voids, along with the irregularities of the substrate's surface, may have formed either from localized substrate melting, as it has been observed for the rough and grit-blasted specimens, or also may be due to the etching treatment. NiCr grains are quite irregularly shaped, often elongated in a normal direction to the interface in zones where there is good contact (6), showing the direction of solidification as the heat is efficiently removed through the interface. Where the contact is poor the grains are coarser (7) as the heat removal and solidification were slower and not as unidirectional because of the interfacial thermal contact resistance.

However, evidence of substrate melting was found, as for instance on the TEM cross-section presented Fig. 8. As it can be seen, the same distinct structure, as observed previously in zones of substrate melting for the polished and roughened specimen, is present here: the splat-substrate surface is quite indistinct (1); the EDS elemental linescan L1 performed across this interface (Fig. 8e) confirms the mixing between the NiCr and Al phases (2); on the higher magnification bright field image (Fig. 8f) the glassy layer (3) and the nano-sized grained layer (4), discussed earlier, can be seen. Consequently, localized substrate melting, mixing with the splat material and rapid solidification resulting in the formation of metastable phases [148] occurs on the etched substrates. The darker zone present within the substrate that can be observed on the bright field

image (Fig. 8a) was identified by EDS as being a Mg-rich intermetallic particle (5 on Fig. 8d).

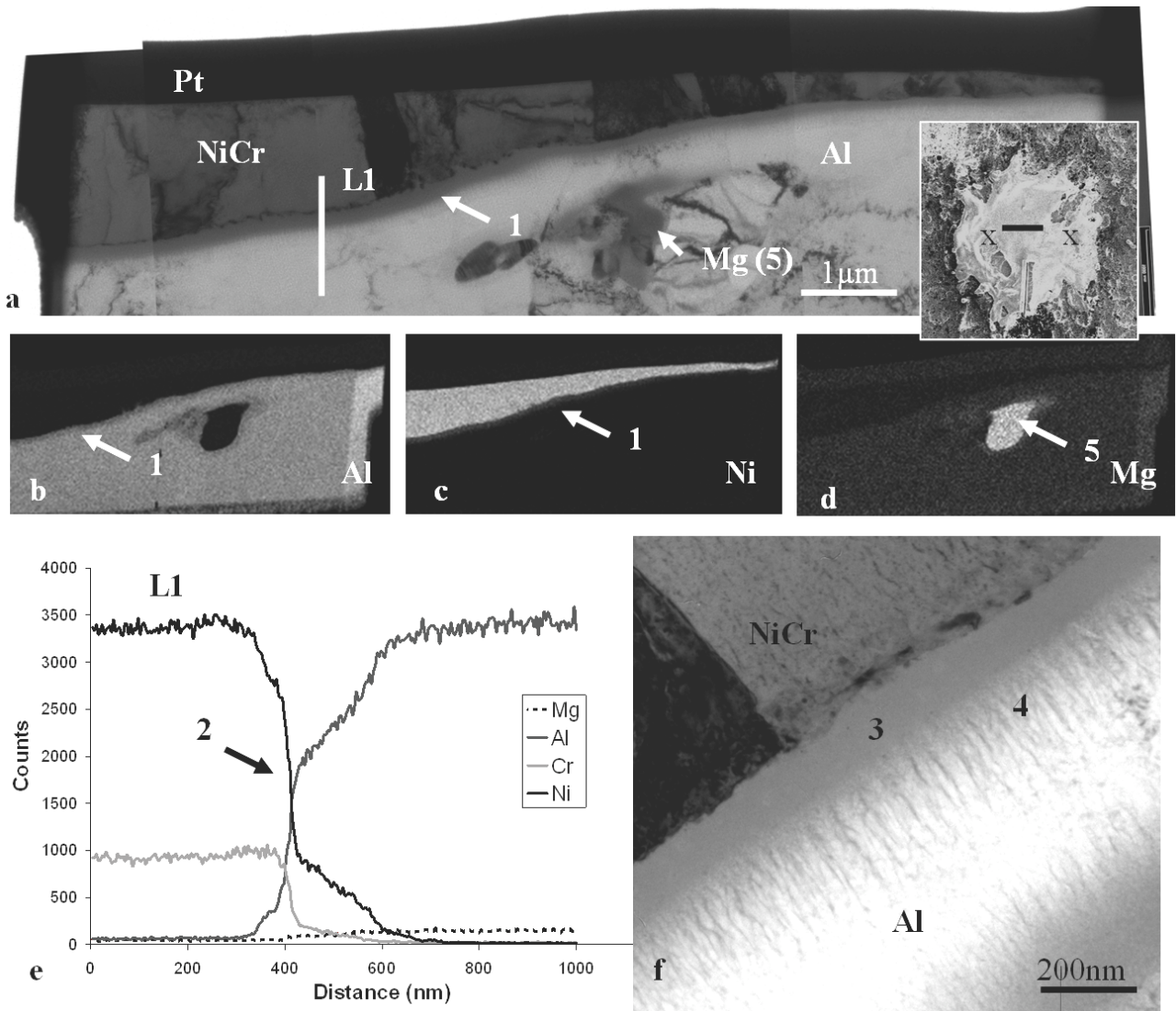


Figure 8. TEM cross-section across a splat (see insert image) found on Al5052\_E: (a) bright field image, EDS elemental maps for (b) Al, (c) Ni, (d) Mg, (e) EDS elemental linescan, (f) high magnification bright field image of the splat-substrate interface

The same range of oxides phases, as described earlier, was also present. For example, several oxide species were identified on the TEM cross-section presented in Fig. 9. On the wall of the large voids, a thick and dense layer of alumina  $\gamma\text{-Al}_2\text{O}_3$  can be seen (1) which was identified by elemental EDS mapping and electron diffraction (more details can be found on the identification of such phases in an associated paper [148]).

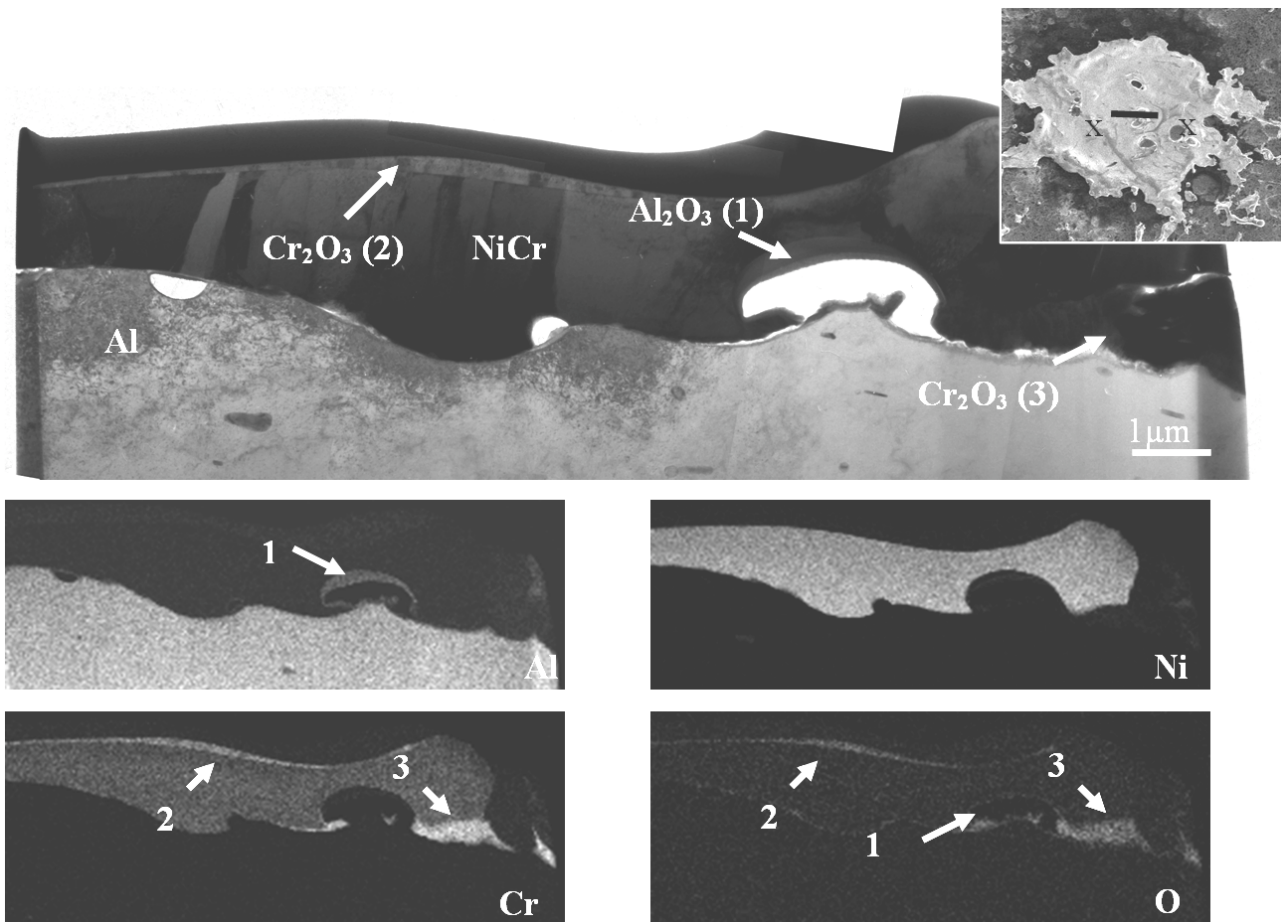


Figure 9. TEM cross-section across a splat (see insert image) found on Al5052\_ET: (a) bright field image, EDS elemental maps for (b) Al, (c) Ni, (d) Cr, (e) O

A thin and dense layer of Cr oxide is present on top of the splat (2) which was identified as being  $\text{Cr}_2\text{O}_3$ . Towards the right side of the section,  $\text{Cr}_2\text{O}_3$  is also found as a thicker, but less dense layer (3). Such a layer, which was also found to form similarly in irregularly shaped splats found on the polished substrates (see associated paper [148]), may come from in-flight oxidation of the NiCr particle, a phenomenon that has been reported before in plasma spraying [6], or from oxidation occurring upon splat formation similarly as for the oxides formed in voids, which is, however, less likely [148].

Effects of a thermal treatment prior to plasma spraying on the substrate surface chemistry, roughness and splat formation, were discussed in previous papers [107, 148]. In summary, it was found that such heat treatment increased the  $\gamma\text{-Al}_2\text{O}_3$  content of the oxide layers already present on the surface, partially dehydrating them (reducing the hydroxide content), and increasing the thickness (a few nanometres) and roughness (slightly from about 7 nm to 8 nm). Such changes had, however, limited effects on splat morphology and formation. However, in the case here of etched specimens, it was found that the proportion of “normal” splats, such as those seen Fig. 5b, compared to ensemble of small droplets resulting from the non-adhesion of the sprayed NiCr particle, such as seen Fig. 5a, was significantly increased by the heat treatment. That is, on Al5052\_E there was around 3/4 of non-adhered splats and 1/4 of fully adhered splats, whilst on Al5052\_ET all the splats found had fully adhered. The non-adhesion of sprayed particles on the etched substrate may itself be related to the etching treatment, which is performed by immersing the substrate in an acidic solution, since, even if it may be expected that the substrate would fully dry prior to spraying, it is likely that some chemical residues remain

adsorbed on to the substrate surface, particularly considering the many cavities induced by the etching treatment. These are then likely to evaporate upon heating. This would then result in the release of a large amount of gas upon impact and spreading of the sprayed NiCr particle because of the heat, forming a gas cushion hindering the adhesion of the forming splat. On the other hand, heat treatment of the substrate would allow most of these adsorbed species to evaporate from the substrate surface, allowing a good adhesion of the sprayed particles on the substrate.

#### III.4. Effects of the substrate roughness on the splat formation process

In Table 2 are detailed the average surface roughness measured for the different specimens studied, as well as the average diameters of the splats. Diameters,  $D$ , were evaluated for each splat by measuring the smallest and largest values and taking the average (see for instance Fig. 2a), ignoring possible splashed fingers. Considering the very irregular shape of the splats, such measurements are approximate.

The roughness criteria used by Fauchais *et al.* stated that for  $R_a < 2 \mu\text{m}$  the roughness is defined as “low”, and for  $R_a > 2 \mu\text{m}$ , it is defined as being “high” [2] With such a criteria, only the grit-blasted specimen would be considered high roughness. However, the microstructure of the splats observed for all four rough specimens (Al1005\_R, Al1005\_GB, Al5052\_E, Al5052\_ET) appears to correspond to the effects described for surfaces which exhibit a high roughness, that is disturbance of the flow of the spreading molten splat by the irregularities of the interface [2, 22], creating very irregularly shaped

splats [152-154], occurrence of substrate melting [155, 156], especially the peaks, etc. Accurate quantification of the effects is difficult because of the relatively limited number of FIB and TEM cross-sections that were prepared for each specimen. However, it can be noted that the etched specimens, in addition to presenting a relatively low roughness compared to the rough and grit-blasted ones, presented the most “regularly” shaped splats. However, less substrate melting was observed, which is in agreement with the observations made by Basu *et al.* and Wroblewski *et al.* [155, 156], together with less mixing with NiCr, and fewer and smaller voids.

Roughening of the substrates is very often used in plasma spray to increase the adhesion strength of the coatings. Nevertheless, such a process may result in the formation of many large voids and significant concentrations of oxides compared to smoother substrates, which can be subsequently detrimental for some properties of the coating such as density, strength, thermal and electrical conductivity. Moreover, while the adhesion strength increase observed is accounted to mechanical interlocking, here it was shown that on both smooth and rough substrates, the occurrence of substrate melting allowed metallurgical bonding to occur. On the other hand, there is the possibility that the glassy phase, associated with rapid solidification of the molten zone, found at the splat-substrate interface is brittle, which would then be detrimental to the quality of the metallurgical bonding. When intending to perform roughening of the substrate prior to spraying, it may be interesting to aim for an intermediate value for the roughness ( $R_a = 0.5\text{-}1\ \mu\text{m}$ ), where mechanical interlocking would occur, but without resultant large voids and/or oxide formation.

#### IV. Conclusion

In summary, the following observations and conclusions can be drawn from the study by electron microscopy of the NiCr splats plasma sprayed onto Al substrates with various levels of roughness:

- The peaks and cavities present on the rough substrates hindered the spreading of the molten splats, leading to very irregular splat morphologies and the formation of many voids, including some very large voids (several microns in diameter).
- Localized substrate melting was observed for all smooth and rough substrates, notably for the peaks present on the rough ones. This led to mixing with the molten NiCr and the formation of metastable interfacial layers, including a metallic glass one which could potentially be detrimental to the adhesion strength of the coating.
- The formation of various oxide phases was observed. Their presence in some of the voids near the splat-substrate interface accounted for the release of gas from the substrate and/or the splat.
- Finally, it was noted that increasing the roughness resulted in an increase in the degree of substrate melting and the concentration of oxides and voids.

## CHAPTER 12

### GENERAL DISCUSSION AND SUMMARY

---

In summary, the microstructural study of a range of thermally sprayed specimens, varied in terms of substrate type, substrate pre-treatment and spray conditions, using a range of electron microscopy techniques such as SEM, FIB and TEM, has led to important results regarding splat microstructure and formation, together with the influence of substrate and spraying conditions on splat morphology. The principal findings can be summarized as follows:

#### I. Splat microstructure and formation

##### I.1. Splat-substrate interaction and interface

As explained throughout this thesis, there have been very few prior studies which have investigated the occurrence of substrate melting during splat formation [20, 35, 157]. Most models and theories of splat formation are based on the notion that the substrate remains solid upon splat formation [23, 25, 82, 138, 139]. Consequently, the recurrent observation of evidences of localized substrate melting, notably for plasma sprayed specimens and both Al and stainless steel substrates, was a new and important finding.

For substrate melting to occur, a certain number of conditions are required:

- The temperature of the sprayed particles should be higher than the melting point of the substrate. This explains why for the HVOF sprayed specimens, where the range of temperature with which the particles impact on the substrate is lower than for the plasma spray process, evidence of substrate melting could not always be found. If this condition is not fulfilled, localized substrate melting may still occur upon particle impact by the dissipation of its kinetic energy into heat and deformation of the substrate. This was observed for HVOF-sprayed Al substrates, where the relatively low substrate hardness (compared to the steel substrate for instance) means that both extensive deformation, from the impacting particle, and localized substrate melting was observed. However, the structure observed at the splat-substrate interface could also possibly arise from adiabatic shear instability [45], which is usually observed in cold spraying: that is, jetting of the substrate and mixing between splat and substrate occurs due to the extensive deformation of the substrate.
- The hot impacting particle ideally must make intimate contact with the substrate. Such contact may be hindered by the presence of gas species released from the substrate or, possibly, from the sprayed particle itself, causing splashing of the splat. Consequently, substrate melting tends to be more extended for disc shaped splats, such as those obtained on the substrates heated during spraying, and where relatively smaller volumes of gas were present at the splat-substrate interface, compared to the splats on the non-heated substrates which exhibit extensive splashing. A higher spraying

velocity, meaning that the particle impact on the substrate occurs with a higher momentum and, thus, applies a higher pressure, can also promote substrate melting. This is apparent here as the splats on the Al substrate for the first sprayed set did not show evidence of substrate melting, whilst the splats of the second set, sprayed at a higher velocity, did show evidence of substrate melting

- The combination of material used may also play an important role. Indeed, Zhang *et al.* found that, for instance, while substrate melting is easy to obtain for Mo particles plasma sprayed onto stainless steel, the temperature of the particles and substrate need to be much higher in the case of YSZ particles sprayed on the same substrate [158]. The hypothesis proposed was that the heat of chemical mixing between the splat and substrate materials may have a significant contribution in the substrate melting process.

The interfacial structure that forms when substrate melting has occurred depends on both the substrate and feedstock powder physical characteristics, such as their crystalline structure and also their cooling rate:

- In the case of the stainless steel substrates and NiCr sprayed particles, both materials have the same crystalline structure (f.c.c.) with similar lattice parameters. Moreover, examination of the Fe-Ni binary phase diagram shows that at high temperatures these elements are intersoluble [132]. As a result, a continuous structure often forms across the splat-substrate interface, with,

usually, interdiffusion between both materials, and grains growing across the interface into both phases.

- For Al substrates, Ni has only a limited solubility in Al and vice-versa [132], and their crystalline structures have different lattice parameters. Upon substrate melting and mixing with NiCr, a fine phase of non-equilibrium nanoparticles forms at the interface, and a layer of metallic glass can also be sometimes found. These non-equilibrium structures arise from the very rapid cooling and solidification of the splat and substrate.

In some cases, notably for HVOF sprayed splats formed on steel substrates, interdiffusion across the interface may be observed without evidence of any substrate melting. This is presumably due to the heat provided by the hot splat to the substrate on impact.

Evidence of substrate melting or interdiffusion at the splat-substrate interface signifies metallurgical bonding, which is regarded as very beneficial for the adhesion of the coating. Areas of poor contact between splat and substrate were, however, very often observed. These areas are detrimental to the adhesion of the coatings; however, their occurrence may be limited by adjusting spraying and substrate conditions.

## I.2. Splat formation

Chapters 2, 6, 7 and 8 propose models describing the splat formation for HVOF and plasma sprayed NiCr particles on Al and steel specimens based on the observations made

from electron microscopy studies. It should be noted that the model reported in Chapter 6 is based on modelling performed by A.T.T. Tran, a postgraduate student from the University of Auckland, NZ, who collaborated on part of this project.

Apart from observing the occurrence of phenomena such as substrate melting or pore and oxide formation, electron microscopy also allowed the observation of the grain microstructure of the splat, which can be very useful in understanding the solidification process of the splat. Indeed, the shape of the grain can indicate how the heat was removed from the splat, notably columnar grains show that the heat was efficiently removed through conduction to the substrate, while their size may indicate the solidification rate (finer grains are a sign of a faster solidification) [16].

## **II. Influence of the substrate and spraying conditions**

Thermal spray processes involve many parameters (materials and spraying process used, spray parameters, substrate preparation, etc.). In order to obtain a coating with optimum properties, understanding how these parameters affect splat formation is necessary.

## II.1. Effects of spraying conditions

### II.1.a. *Effect of spraying temperature and velocity for plasma spraying*

As explained in the introduction, the first set of plasma sprayed specimens was prepared prior to the commencement of this thesis. Subsequently, a second set of plasma sprayed specimens was made. Both sets were prepared at Stony Brook University, New York. For the first set of plasma sprayed specimens, the temperature and velocity of the NiCr particles were not provided. For the second set, these were measured to be around 2,450°C and 115 m.s<sup>-1</sup> respectively (the temperature of the sprayed particles was measured using a DPV 200 pyrometer, and their velocity was evaluated using a Laser Doppler velocimeter). While a strict comparison is, thus, not possible between both sets of conditions, it would seem that the first set was sprayed at a lower velocity than the second set, and, possibly, a lower temperature. Splats from the second set displayed significantly more splashing than the splats of the first set, and more substrate melting. The increase in substrate melting is consistent with an increase in velocity and temperature, as it means a higher momentum of the particle upon impact, thus a better contact with the substrate, and a more extended heating of the substrate. An increased particle velocity was also found in previous work to promote splashing of the splat [52, 58], as it affects splat formation through the Sommerfeld parameter,  $K$ :  $K$  is indeed proportional to the velocity, and the higher the parameter the more splashing is likely to occur [2].

### II.1.b. *Comparison between HVOF and plasma spraying*

HVOF spraying, compared to plasma spraying, is characterized by higher particle velocities (400-800 m.s<sup>-1</sup> compared to 80-400 m.s<sup>-1</sup> for plasma spraying) and lower particles temperature (the temperature in the torch is around 3000°C, while it ranges from 8,700 to 12,000°C for the plasma torch) (see the introductory sections of Chapters 2 and 7) [1]. The lower temperature means that, while in the plasma spray process, most particles are fully molten upon impact on the substrate, for the HVOF process many are only partially molten, with a solid core, and some are even completely solid. As a result, the process of splat formation is significantly different (see Chapters 7 and 8), and so the splat morphology and, subsequently, the characteristics of the coatings are different. HVOF splats undergo much less splashing, and have a lower oxide content. The higher velocity also means a higher particle momentum upon impact for HVOF, leading to a higher pressure applied by the particle on the substrate, and also a denser coating.

Some of the main differences observed between plasma and HVOF splats are summarized in Table 1.

**Table 1: Principal differences between plasma and HVOF splats sprayed at room temperature**

<b>Spray Method</b>	<b>Plasma</b>	<b>HVOF</b>
Splashing	Very frequent	Relatively limited
Porosity	Pores mainly formed from gas released from the substrate, thus often globular and fine	Pores formed mainly from the mechanics of the flow of the molten NiCr, thus often large and lamellar shaped.
Oxide content	More oxide	Less oxide
Interaction with substrate	Substrate melting and inter-mixing	Deformation of the substrate. Possibility of substrate melting from this deformation. Interdiffusion occurs across the interface.

As a result, HVOF coatings tend to be denser, with a lower oxide content, but also with a bimodal structure, due to the unmelted portions of the sprayed particles, and their mechanical properties (adhesion to the substrate, hardness, Young modulus, tensile/compressive strength, etc.) are usually higher than plasma sprayed coatings [38, 159].

## II.2. Effects of substrate surface conditions

### II.2.a. *Effects of the surface chemistry*

The surface chemistry of the substrates was modified by various treatments: e.g. pre-heat treating and/or boiling, or heating during spraying. The effects of these treatments for the plasma sprayed specimens are summarized in Table 2.

**Table 2: Summary of the effects of the substrates treatments for the plasma sprayed specimens**

<b>Treatment</b>	<b>Effect on substrate surface</b>	<b>Effect on splat formation/morphology</b>
Heat-treatment prior to spraying	Increase oxide content/thickness and reduce the amount of hydroxide and chemisorbed water, leading to less gas released upon splat formation. Slight increase in substrate surface roughness (and possibly skewness)	Increase wetting on NiCr, resulting in flatter splats with larger diameter. Reduce occurrence of substrate melting
Boiling	Steel: increase hydroxide content (to some extent) Al: Create 300nm thick hydroxide layer	Steel: more irregular splats (to some extent) Al: prevents adhesion of splats

Heating during spraying	Evaporate most of the adsorbates/condensates before splat formation, thus significantly reducing the amount of gas present at the splat-substrate interface when the splat forms.	Significantly reduces splashing, giving disc-shaped splats. Increases the extent of substrate melting.
-------------------------	---	---

The presence of adsorbates/condensates on the substrate surface is a key parameter in splat formation. Extensively studied elsewhere [6, 20, 21, 26-28], it has been shown that these are gas species, mainly water, adsorbed on the surface and, because of the heat from the spraying process, they evaporate upon splat formation causing instabilities leading to splashing. In the case of boiled aluminium substrates, the amount of gas released from the thick hydroxide layer prevents splats adhering to the substrate. Heating the substrate during spraying above the transition temperature, [6, 20, 21, 26-28] at which the adsorbates/condensates evaporate, prevents this gas release and, thus, reduces splashing. It may also delay solidification of the splat, which can lead to splashing (see Chapter 9 and 10) by disrupting spreading of the splat, or even interrupting it [160]. However, some studies have found that other parameters may influence droplet splashing, notably the pressure applied by the impacting droplet on the substrate: for instance, McDonalds *et al.* developed a model showing that a higher pressure can reduce the fragmentation of the droplets upon impact [79]. This could also explain the reduced splashing in the case of HVOF splats.

The desorbed gas species can also promote pore formation, along with the formation of oxide within these pores. However, according to Qu *et al.*, interfacial porosity may also arise from the formation of bubbles arising from the release of gas primarily dissolved within the molten droplet, such release occurring from the pressure increase upon impact and from the cooling down of the droplet resulting in a decrease in the solubility [129].

In comparison with heating the substrate during spraying, heating the substrate prior to spraying, and spraying at room temperature, has only a limited action on the adsorbates/condensates, because once the substrate cools down and is exposed to air, these compounds become reabsorbed on the surface. Although, for the etched specimens, this treatment promoted removal of any chemicals remaining from the etching treatment, which significantly improved splat adhesion, (see Chapter 11). Finally, heat-treatment created oxide layers that increased NiCr wetting, but hindered substrate melting.

In the case of HVOF spraying, surface chemistry has much less effect on splat formation. Moreover HVOF particles impact on the substrate with a much higher velocity, thus applying a higher pressure to the substrate, as shown by the substrate deformation. The high pressure applied by the splat would then push away the gas released from the substrate and partly destroy potential oxide/hydroxide layers (see, for instance, the HVOF splats formed on a boiled Al substrate in Chapter 8).

### II.2.b. *Effects of the substrate material*

Splat morphologies and characteristics were often found to significantly differ between steel and Al substrates, even when sprayed under similar conditions. Indeed, the substrate material can influence splat formation through its thermal properties: depending on its melting point and its thermal diffusivity, substrate melting may, or not, occur. Also, these thermal properties have a significant influence on the rate by which the heat is removed from the splat and thus on its solidification. If substrate melting occurs, depending on the substrate's physical properties (solubility or crystalline structure) various interfacial phases may form. The hardness of the substrate will also influence splat formation in the case of HVOF sprayed splats [39]. Finally, surface chemistry is heavily dependant on the substrate material. For instance, Al reacts more strongly with water and releases more gas upon splat formation than stainless steel.

### II.2.c. *Effects of the substrate surface roughness*

Increasing the substrate roughness, while maintaining it on a scale of a few nanometres, which, for example, occurs when heat treating the substrate because of the increased thickness of the oxide layers, can increase the degree of wetting of the splats, but the changes in splat morphology are negligible compared to the changes obtained from generating much higher levels of roughness. For very rough specimens (roughness levels of at least a few 100 nm), the asperities present on the substrate surface disrupt the flow of the spreading splat, leading to very irregularly shaped splats, with the formation of large pores.

Plasma spraying is often performed on an industrial scale on grit-blasted substrates which promote mechanical interlocking leading to effective adhesion of the coating. Under these circumstances substrate melting is not expected. However, as shown in Chapter 11 of this thesis, localized substrate melting may occur (especially near substrate asperities), and the presence of the large pores around the splats may be detrimental to the global adhesion of the coating. One can expect that splats generated when the substrates are heated during spraying, where extensive substrate melting, and hence metallurgical bonding, occurs, would display a superior adhesion. It is also suggested that the removal of adsorbates/condensates following substrate heating will allow the liquid splat to flow more effectively around the irregularities on a rough surface [23].

### **III. Implications of findings for thermal spray processing**

The approach proposed in the present thesis to investigate the splat microstructure, and splat/substrate interface at a nano-scale, using electron microscopy techniques, is novel in the field of thermal spraying. It led to important observations such as:

- Evidence of substrate melting, very rarely observed prior to this study, was commonly seen. Most models that have been proposed have been built on the hypothesis that melting did not occur.
- The observations of oxides in pores, indicating the presence of gas at the interface, and of improved substrate melting/reduced splashing when heating the

substrate during spraying, are consistent with previous theories on gas release upon splat formation [6, 20, 21, 26-28].

- The observation of HVOF splat microstructure, and the study of their formation process, has received little attention, although HVOF spraying is a growing and increasingly popular technique in the thermal spraying industry. Notably, the observation of substrate melting, interdiffusion and/or mixing between splat and substrate materials provides some explanation of the strong adhesion properties of HVOF coatings.
- Similarly, the microstructure of splats plasma sprayed on to very rough surface has been rarely studied, although it is a common method of coating preparation. The evidence of localized substrate melting and the observation of the large pores are important in the understanding the behaviour of coatings sprayed on to rough substrates.
- The observed characteristics of the splat sprayed on heated substrates (disc shape, extended substrate melting and mixing with NiCr, absence of porosity) helped understanding the improved properties of coatings sprayed in such conditions.

From these results, improved models predicting splat formation, and improved spraying conditions, can be developed. However, further study is required to clarify some of the findings from this thesis. For instance:

- Studying splat formation when the particle impacts on already deposited splats, as coatings' properties are also significantly dependant of the subsequent splat characteristics. For plasma sprayed splats this could focus on splat remelting. For

HVOF sprayed splats further studies would investigate how the impacting particle may deform and interact with already deposited splats.

- Studying other combinations of materials, notably ceramics, to investigate the extent of deformation or substrate melting in these systems. Indeed, the observations made in this thesis were strongly linked to the particular combination of materials used (NiCr on stainless steel or aluminium). Other combinations of materials, presenting different thermal, physical and chemical properties, would be expected to behave differently. This also could allow studying the influence of these various properties on splat formation and characteristics.

To conclude, the present work has used electron microscopy to investigate in detail the structure of thermally spray materials. Hitherto, this technique has not been applied in detail to materials processed in this way. It is hoped that the observations in this thesis, and the publications which stem from it, are of value to those working in the thermal spray community.

## REFERENCES

---

- [1] R.F. Bunshah, Handbook of hard coatings. Deposition technologies, properties and applications, Norwich, N.Y., 2001.
- [2] P. Fauchais, M. Fukumoto, A. Vardelle, M. Vardelle, Knowledge concerning splat formation: an invited review, *J. Therm. Spray Technol.*, 2004, 13 (3), p. 337-360.
- [3] H. Herman, S. Sampath, R.C. McCune, Thermal spray: current status and future trends, *MRS Bulletin*, 2000, 25 (7), p. 17-25.
- [4] M. Dorfman, Thermal spray basics, *Adv. Mater. Process.*, 2002, (7), p. 47-50.
- [5] <http://www.plasmacoat.co.uk/technologies.htm>.
- [6] M. Fukumoto, M. Shiiba, H. Kaji, T. Yasui, Three-dimensional transition map of flattening behavior in the thermal spray process, *Pure Appl. Chem.*, 2005, 77 (2), p. 429-442.
- [7] F. Otsubo, H. Era, K. Kishitake, Interface reaction between Nickel-base self-fluxing alloy coating and steel substrate, *J. Therm. Spray Technol.*, 2000, 9 (2), p. 259-263.
- [8] H. Du, J.H. Shin, S.W. Lee, Study on porosity of plasma-sprayed coatings by digital image analysis method, *J. Therm. Spray Technol.*, 2005, 14 (4), p. 453-461.
- [9] J.M. Guilemany, J. Nutting, M.J. Dougan, A transmission electron microscopy study of the microstructures present in alumina coatings produced by plasma spraying, *J. Therm. Spray Technol.*, 1997, 6 (4), p. 425-429.
- [10] S. Chandra, P. Fauchais, Formation of solid splats during thermal spray deposition, *J. Therm. Spray Technol.*, 2009, 18, p. 148-180.

- [11] J. Cedelle, M. Vardelle, P. Fauchais, Influence of stainless steel substrate preheating on surface topography and on millimeter- and micrometer-sized splat formation, *Surf. Coat. Technol.*, 2006, 201, p. 1373-1382.
- [12] J. Cedelle, M. Vardelle, B. Pateyron, P. Fauchais, Investigation of Plasma Sprayed coatings formation by visualization of droplet impact and splashing on a smooth substrate, *Trans. Plasm. Sci.*, 2005, 33 (2), p. 414-415.
- [13] R. Dhiman, A.G. McDonald, S. Chandra, Predicting splat morphology in a thermal spray process, *Surf. Coat. Technol.*, 2007, 201, p. 7789-7801.
- [14] R. Ghafouri-Azar, S. Shakeri, S. Chandra, J. Mostaghimi, Interactions between molten metal droplets impinging on a solid surface, *Int. J. Heat Mass Transf.*, 2003, 46, p. 1395-1407.
- [15] S. Goutier, M. Vardelle, J.C. Labbe, P. Fauchais, Alumina splat investigation: visualization of impact and splat/substrate interface for millimetre sized drops, *J. Therm. Spray Technol.*, 2010, 19 (1-2), p. 49-55.
- [16] L. Bianchi, A. Denoirjean, F. Blein, P. Fauchais, Microstructural investigation of plasma-sprayed ceramic splats, *Thin Solid Films*, 1997, 299, p. 125-135.
- [17] J. Mostaghimi, S. Chandra, Splat formation in plasma-spray coating process, *Pure Appl. Chem.*, 2002, 74 (3), p. 441-445.
- [18] M. Pasandideh-Fard, S. Chandra, J. Mostaghimi, A three-dimensional model of droplet impact and solidification, *Int. J. Heat Mass Transf.*, 2002, 45, p. 2229-2242.
- [19] S. Sampath, X. Jiang, Splat formation and microstructure development during plasma spraying: deposition temperature effect, *Mater. Sci. Eng.*, 2001, A304-306, p. 144-150.

- [20] H. Zhang, X.Y. Wang, L.L. Zheng, X.Y. Jiang, Studies of splat morphology and rapid solidification during thermal spraying, *Int. J. Heat Mass Transf.*, 2001, 44, p. 4579-4592.
- [21] H. Li, S. Costil, H.-L. Liao, C.-J. Li, M. Planche, C. Coddet, Effects of surface conditions on the flattening behavior of plasma sprayed Cu splats, *Surf. Coat. Technol.*, 2006, 200, p. 5435-5446.
- [22] L. Bianchi, A.C. Leger, M. Vardelle, A. Vardelle, P. Fauchais, Splat formation and cooling of plasma-sprayed zirconia, *Thin Solid Films*, 1997, 305, p. 35-47.
- [23] T. Chraska, A.H. King, Effect of different substrate conditions upon interface with plasma sprayed zirconie - a TEM study, *Surf. Coat. Technol.*, 2002, 157, p. 238-246.
- [24] Z.G. Feng, M. Domaszewski, G. Montavon, C. Coddet, Finite element analysis of effect of substrate surface roughness on liquid droplet impact and flattening process, *J. Therm. Spray Technol.*, 2002, 11 (1), p. 62-68.
- [25] A.A. Syed, A. Denoirjean, B. Hannyoy, P. Fauchais, P. Denoirjean, A.A. Khan, J.C. Labbe, Influence of surbstrate surface conditions on the plasma sprayed ceramic and metallic particles flattening, *Surf. Coat. Technol.*, 2005, 200, p. 2317-2331.
- [26] C.-L. Li, J.-L. Li, Evaporated-gas-induced splashing model for splat formation during plasma spraying, *Surf. Coat. Technol.*, 2004, 184, p. 13-23.
- [27] M. Fukumoto, E. Nishioka, T. Matsubara, Flattening solidification behavior of a metal droplet on a flat substrate surface held at various temperatures, *Surf. Coat. Technol.*, 1999, 120-121, p. 131-137.
- [28] A. McDonald, C. Moreau, S. Chandra, Thermal contact resistance between plasma-sprayed particles and flat surfaces, *Int. J. Heat Mass Transf.*, 2007, 50, p. 1737-1749.

- [29] M. Fukumoto, H. Nagai, T. Yasui, Influence of surface character change of substrate due to heating on flattening behavior of thermal sprayed particles, *J. Therm. Spray Technol.*, 2006, 15 (4), p. 759-764.
- [30] S. Sampath, X.Y. Jiang, J. Matejicek, A.C. Leger, A. Vardelle, Substrate temperature effects on splat formation, microstructure development and properties of plasma sprayed coatings Part I: Case study for partially stabilized Zirconia, *Mater. Sci. Eng.*, 1999, A272, p. 181-188.
- [31] Y. Tanaka, M. Fukumoto, Investigation of dominating factors on flattening behavior of plasma sprayed ceramic particles, *Surf. Coat. Technol.*, 1999, 120-121, p. 124-130.
- [32] X.Y. Jiang, Y. Wan, H. Herman, S. Sampath, Role of condensate and adsorbates on substrate surface on fragmentation of impinging molten droplets during thermal spray, *Thin Solid Films*, 2001, 385, p. 132-141.
- [33] M. Fukumoto, Y. Huang, Flattening mechanism in thermal sprayed nickel particle impinging on flat substrate surface, *J. Therm. Spray Technol.*, 1999, 8 (3), p. 427-432.
- [34] M. Pasandideh-Fard, V. Pershin, S. Chandra, J. Mostaghimi, Splat shapes in a thermal spray coating process: simulations and experiments, *J. Therm. Spray Technol.*, 2002, 11 (2), p. 206-217.
- [35] S. Kitahara, A. Hasui, A study of the bonding mechanism of sprayed coatings, *J. Vac. Sci. Technol.*, 1974, 11 (4), p. 747-753.
- [36] L. Li, X.Y. Wang, G. Wei, A. Vaidya, H. Zhang, S. Sampath, Substrate melting during thermal splat quenching, *Thin Solid Films*, 2004, 468, p. 113-119.
- [37] J.A. Browning, Hypervelocity impact fusion - A technical note, *J. Therm. Spray Technol.*, 1992, 1 (4), p. 289-292.

- [38] E. Turunen, T. Varis, S.-P. Hannula, A. Vaidya, A. Kulkarni, J. Gutleber, S. Sampath, H. Herman, On the role of the particle state and deposition procedure on mechanical, tribological and dielectric response of high velocity oxy-fuel sprayed alumina coatings, *Mater. Sci. Eng.*, 2006, A415, p. 1-11.
- [39] W.J. Trompetter, M. Hyland, D. McGrouther, P. Munroe, A. Markwitz, Effect of substrate hardness on splat morphology in high-velocity thermal spray coatings, *J. Therm. Spray Technol.*, 2006, 15 (4), p. 663-669.
- [40] P. Bansal, P.H. Shipway, S.B. Leen, Effect of particle impact on residual stress development in HVOF sprayed coatings, *J. Therm. Spray Technol.*, 2006, 15 (4), p. 570-575.
- [41] C.J. Kong, P.D. Brown, S.J. Harris, D.G. McCartney, The microstructure of a thermally sprayed and heat treated Al-20 wt.%Sn-3 wt.%Si alloy, *Mater. Sci. Eng.*, 2005, A403, p. 205-214.
- [42] T. Marrocco, L.C. Driver, S.J. Harris, D.G. McCartney, Microstructure and properties of thermally sprayed Al-Sn-based alloys for plain bearing applications, *J. Therm. Spray Technol.*, 2006, 15 (4), p. 634-639.
- [43] J.M. Guilemany, J. Nutting, J.R. Miguel, Z. Dong, Microstructure characterization of WC-Ni coatings obtained by HVOF thermal spraying, *Scr. Met. Mater.*, 1995, 33 (1), p. 55-61.
- [44] S.V. Klinkov, V.F. Kosarev, M. Rein, Cold spray deposition: significance of particle impact phenomena *Aerosp. Sci. Technol.*, 2005, 9, p. 582-591.

- [45] R.C. Dykhuizen, M.F. Smith, D.L. Gilmore, R.A. Neiser, X. Jiang, S. Sampath, Impact of high velocity cold spray particles, *J. Therm. Spray Technol.*, 1999, 8 (4), p. 559-564.
- [46] L. Ajdelsztajn, A. Zúñiga, B. Jodoin, E.J. Lavernia, Cold gas spraying of a high temperature Al alloy, *Surf. Coat. Technol.*, 2006, 201, p. 2109-2116.
- [47] B.S. Sidhu, S. Prakash, Nickel-chromium plasma spray coatings: a way to enhance degradation resistance of boiler tube steels in boiler environment, *Journal of thermal spray technology*, 2006, 15 (1), p. 131-140.
- [48] V. Higuera, J. Belzunce, A. Carriles, S. Poveda, Influence of the thermal-spray procedure on the properties of a nickel-chromium coating, *Journal of materials science*, 2002, 37, p. 649-654.
- [49] A.T.T. Tran, M.M. Hyland, Q. T., W. B., B.J. James, Effect of surface chemistry on splat formation during plasma spraying, *J. Therm. Spray Technol.*, 2008, 17 (5-6), p. 637-645.
- [50] S. Brossard, P.R. Munroe, A.T.T. Tran, M.M. Hyland, Study of the microstructure of NiCr splats plasma sprayed on stainless steel by TEM, *Surf. Coat. Technol.*, 2010, 204 (9-10), p. 1608-1615.
- [51] P.R. Munroe, The application of focused ion beam microscopy in the material sciences, *Mater. Charact.*, 2009, 60, p. 2-13.
- [52] C. Escure, M. Vardelle, P. Fauchais, Experimental and theoretical study of the impact of alumina droplets on cold and hot substrates, *Plasma Chem. Plasma Process.*, 2003, 23 (2), p. 185-221.

- [53] A.T.T. Tran, S. Brossard, M.M. Hyland, P.R. Munroe, Evidence of Substrate Melting of NiCr Particles on Stainless Steel Substrate by Experimental Observation and Simulations, *Plasma Chem. Plasma Process.*, 2009, 29 (6), p. 475-495.
- [54] M. Xue, S. Chandra, J. Mostaghimi, Investigation of splat curling up in thermal spray coatings, *J. Therm. Spray Technol.*, 2006, 15 (4), p. 531-536.
- [55] A.T.T. Tran, M.M. Hyland, The role of substrate surface chemistry on splat formation during plasma spray deposition by experiments and simulations, *J. Therm. Spray Technol.*, 2010, 19 (1-2), p. 11-23.
- [56] J. Stringer, B.A. Wilcox, R.I. Jaffee, The high-temperature oxidation of nickel - 20wt% chromium alloys containing dispersed oxide phases, *Oxidation of metals*, 1972, 5 (1), p. 11-47.
- [57] S. Inada, W.-J. Yang, Solidification of molten metal droplets impinging on a cold surface, *Exp Heat Transf.*, 1994, 7, p. 93-100.
- [58] M. Vardelle, A. Vardelle, A.C. Leger, P. Fauchais, D. Gobin, Influence of particle parameters at impact on splat formation and solidification in plasma spraying processes *J. Therm. Spray Technol.*, 1994, 4 (1), p. 50-58.
- [59] A.P. Grosvenor, B.A. Kobe, N.S. McIntyre, Examination of the oxidation of iron by oxygen using X-ray photoelectron spectroscopy and QUASES, *Surf. Sci.*, 2004, 565, p. 151-162.
- [60] A.P. Grosvenor, B.A. Kobe, N.S. McIntyre, Studies of the oxidation of iron by water vapour using X-ray photoelectron spectroscopy and QUASES, *Surf. Sci.*, 2004, 572, p. 217-227.

- [61] S.B. Newcomb, A microstructural study of the oxidation of Ni-Cr steels in air and in CO-CO<sub>2</sub>, PhD thesis, University of Cambridge, 1982.
- [62] G.C. Allen, J.M. Dyke, S.J. Harris, A. Morries, A surface study of the oxidation of type 304L stainless steel at 600K in air, *Oxid. Met.*, 1988, 29 (5/6), p. 391-408.
- [63] J. Dünwald, A. Otto, An investigation of phase transitions in rust layers using Raman spectroscopy, *Corros. Sci.*, 1989, 29 (9), p. 1167-1176.
- [64] L.L. Shaw, D. Goberman, R. Ren, M. Gell, S. Jiang, Y. Wang, T.D. Xiao, P.R. Strutt, The dependency of microstructure and properties of nanostructured coatings on plasma spray conditions, *Surf. Coat. Technol.*, 2000, 130, p. 1-8.
- [65] K.A. Khor, Z.L. Dong, C.H. Quek, P. Cheang, Microstructure investigation of plasma sprayed HA/Ti6Al4V composites by TEM, *Mater. Sci. Eng.*, 2000, A281, p. 221-228.
- [66] S. Sampath, H. Herman, Rapid solidification and microstructure development during plasma spray deposition, *J. Therm. Spray Technol.*, 1996, 5 (4), p. 445-456.
- [67] S. Brossard, P.R. Munroe, A.T.T. Tran, M.M. Hyland, Study of the effects of surface chemistry on splat formation for plasma sprayed NiCr onto stainless steel substrates, *Surf. Coat. Technol.*, 2010, 204 (9-10), p. 1599-1607.
- [68] D.B. Williams, C. Barry Carter, *Transmission electron microscopy: a textbook for materials science*, Plenum Press, New York and London, 1996.
- [69] P. Nash, The Cr-Ni (Chromium-Nickel) system, *Bull. Alloy Ph. Diagr.*, 1986, 7 (5), p. 466-476.

- [70] N.S. McIntyre, T.C. Chan, C. Chen, Characterization of oxide structures formed on nickel-chromium alloy during low pressure oxidation at 500-600°C, *Oxidation of metals*, 1990, 33 (5/6), p. 457-479.
- [71] A.A. Syed, A. Denoirjean, P. Denoirjean, J.C. Labbe, P. Fauchais, In-flight oxidation of stainless steel particles in plasma spraying, *J. Therm. Spray Technol.*, 2005, 14 (1), p. 117-124.
- [72] R. McPherson, Formation of metastable phases in flame and plasma-prepared alumina, *J. Mater. Sci.*, 1973, 8, p. 851-858.
- [73] V.V. Sobolev, J.M. Guilemany, A.J. Martin, Influence of surface roughness on the flattening of powder particles during thermal spraying, *J. Therm. Spray Technol.*, 1996, 5 (2), p. 207-214.
- [74] R.H. Jones, *Environmental effects on engineered materials*, Marcel Dekker, New York, 2001.
- [75] R.S. Alwitt, Aluminium-water system, *Oxid. Oxid Films*, 1976, 4, p. 169-254.
- [76] W.J. Trompetter, M.M. Hyland, D. McGrouther, P.R. Munroe, A. Markwitz, The effect of substrate surface oxides on the bonding of NiCr alloy particles HVAF thermally sprayed onto aluminium substrates, 2010, *J. Therm. Spray Technol.* (*in publication*)
- [77] J.R. Davis, *Aluminum and aluminum alloys*, ASM International, Materials park, OH, 1993.
- [78] M.S. Hunter, P. Fowle, Natural and thermally formed oxide films on aluminum, *J. Electrochem. Soc.*, 1956, 103 (9), p. 482-485.

- [79] A. McDonald, M. Xue, S. Chandra, J. Mostaghimi, C. Moreau, Modeling fragmentation of plasma-sprayed particles impacting on a solid surface at room temperature, *C. R. Mec.*, 2007, 335, p. 351-356.
- [80] S. Kitahara, A. Hasui, A study of the bonding mechanism of sprayed coatings, *Journal of Vacuum Science and Technology*, 1975, 11 (4), p. 747-753.
- [81] V. Pershin, M. Lufitha, S. Chandra, J. Mostaghimi, Effect of substrate temperature on adhesion strength of plasma-sprayed nickel coatings, *J. Therm. Spray Technol.*, 2003, 12 (3), p. 370-376.
- [82] H.-D. Steffens, B. Wielage, J. Drozak, Interface phenomena and bonding mechanism of thermally-sprayed metal and ceramic composites, *Surf. Coat. Technol.*, 1991, 45, p. 299-308.
- [83] C. Lea, C. Molinari, Magnesium diffusion, surface segregation and oxidation in Al-Mg alloys, *Journal of materials science*, 1984, p. 2336-2352.
- [84] MatWeb. *Material property data*. 2008 11/11/2008; Available from: <http://www.matweb.com/>.
- [85] H. Zhang, X.Y. Wang, L.L. Zheng, S. Sampath, Numerical simulation of nucleation, solidification and microstructure formation in thermal spraying, *Int. J. Heat Mass Transf.*, 2004, 47, p. 2191-2203.
- [86] R. McPherson, The relationship between the mechanism of formation, microstructure and properties of plasma-sprayed coatings, *Thin Solid Films*, 1981, 83, p. 297-310.

- [87] W. Zhang, G.H. Wei, H. Zhang, L.L. Zheng, D.O. Welch, S. Sampath, Toward the achievement of substrate melting and controlled solidification in thermal spraying, *Plasma Chem. Plasma Process.*, 2007, 27, p. 717-736.
- [88] S. Dallaire, Influence of temperature on the bonding mechanism of plasma-sprayed coatings, *Thin Solid Films*, 1982, 95, p. 237-244.
- [89] S.-P. Wang, G.-X. Wang, E.F. Matthys, Melting and resolidification of a substrate in contact with a molten metal: operational maps, *Int. J. Heat Mass Transf.*, 1998, 41, p. 1177-1188.
- [90] M. Bussmann, S. Chandra, J. Mostaghimi, Modeling the splashing of a droplet impacting a solid surface, *Phys. Fluids*, 2000, 12, p. 3121-3132.
- [91] M. Bussmann, J. Mostaghimi, S. Chandra, On a three-dimensional volume tracking model of droplet impact, *Phys. Fluids*, 1999, 11, p. 1406-1417.
- [92] V. Medhi-Nejad, J. Mostaghimi, S. Chandra, Air bubble entrapment under an impacting droplet, *Phys. Fluids*, 2003, 15 (1), p. 173-183.
- [93] H.B. Parizi, L. Rosenzweig, J. Mostaghimi, S. Chandra, T. Coyle, H. Salimi, L. Pershin, A. McDonald, C. Moreau, Numerical simulation of droplet impact on patterned surfaces, *J. Therm. Spray Technol.*, 2007, 16, p. 713-721.
- [94] J.M. Cairney, R.D. Smith, P.R. Munroe, Transmission electron microscope specimen preparation of metal matrix composites using the focused ion beam miller, *Microstruct. Microanal.*, 2000, 6, p. 452-462.
- [95] N. Rowlands, P.R. Munroe, FIB for the evaluation of non-semiconductor materials, *Microstruct. Sci.*, 1998, 26, p. 233-242.

- [96] A.P. Grosvenor, B.A. Kobe, N.S. McIntyre, Studies of the oxidation of iron by air after being exposed to water vapour using angled-resolved X-ray photoelectron spectroscopy and QUASES, *Surf. Interface Anal.*, 2004, 36, p. 1637-1641.
- [97] J.U. Brackbill, D.B. Kothe, C. Zemach, A continuum method for modelling surface tension, *J. Comput. Phys.*, 1992, 100, p. 335-354.
- [98] C. Prakash, V. Voller, On the numerical solution of continuum mixture model equations describing binary solid-liquid phase change, *Numer. Heat Transf., Part B Fundam.*, 1989, 15, p. 171-189.
- [99] W.D. Bennon, F.P. Incropera, A continuum model for momentum, heat and species transport in binary solid-liquid phase change systems - I. Model formulation, *Int. J. Heat Mass Transf.*, 1987, 30, p. 2161-2170.
- [100] C.W. Hirt, B.D. Nichols, Volume of fluid (VOF) methods for the dynamics of free boundaries, *J. Comput. Phys.*, 1981, 39, p. 201-225.
- [101] H.K. Versteeg, W. Malalasekera, *An introduction to computational fluid dynamics: the finite volume method*, 2nd Ed., Prentice Halls, Englewood Cliffs, 2007.
- [102] AnsysInc, *Ansys CFX Documentation*, USA, 2007.
- [103] ASM-International, *Metals handbook*, vol. 2, 10th Ed., ASM International, Materials Park, 1990.
- [104] E.A. Brandes, C.J. Smithells, *Metals reference book*, 6th Ed., Butterworths, London, 1983.
- [105] U.R. Evans, *The corrosion and oxidation of metals. Scientific principles and practical applications*, Edward Arnold, London, 1960.

- [106] R.M. Cornell, U. Schwertmann, The iron oxides: structure, properties, reactions, occurrence and uses, Wiley-VCH, Weinheim, 2003.
- [107] S. Brossard, A.T.T. Tran, P.R. Munroe, M.M. Hyland, Study of the splat-substrate interface for a NiCr coating plasma sprayed on to polished aluminum and stainless steel substrates, *J. Therm. Spray Technol.*, 2010, 19 (1), p. 24-30.
- [108] R. Dhiman, S. Chandra, Freezing-induced splashing during impact of molten metal droplets with high Weber numbers, *Int. J. Heat Fluid Flow*, 2005, 48, p. 5625-5638.
- [109] H. Fujimoto, Y. Shiotani, A.Y. Tong, T. Hama, H. Takuda, Three-dimensionnal numerical analysis of the deformation behavior of droplets impinging onto solid substrate, *Int. J. Multiph. Flow*, 2007, 33, p. 317-332.
- [110] S. Duhr, D. Braun, Why molecules move along a temperature gradient, *Proc. Natl. Acad. Sci.*, 2006, 103, p. 19678-19682.
- [111] S. Chandra, C. Avedisian, On the collision of a droplet with a solid surface *Proc. R. Soc. Lond. Ser. A. Math. Phys. Eng.*, 1991, 432, p. 13-41.
- [112] L. Li, B. Kharas, H. Zhang, S. Sampath, Suppression of the crystallization during high velocity impact quenching of alumina droplets observations and characterization, *Mater. Sci. Eng.*, 2007, A 456, p. 35-42.
- [113] Y.M. Qiao, S. Chandra, Experiments on adding a surfactant to water drops boiling on a hot surface, *Proc. R. Soc. Lond. Ser. A. Math. Phys. Eng.*, 1997, 453, p. 673-689.
- [114] S. Deshpande, S. Sampath, H. Zhang, Mechanisms of oxidation and its role in microstructural evolution of the metallic thermal spray coatings - case study for Ni-Al, *Surf. Coat. Technol.*, 2006, 200, p. 5395-5406.

- [115] N. Birks, G.H. Meier, F.S. Pettit, Introduction to the high-temperature oxidations of metals, Cambridge University Press, Cambridge, 2006.
- [116] S. Taniguchi, N. Hongawara, T. Shibata, Influence of water vapour on the isothermal oxidation behaviour of TiAl at high temperatures, Mater. Sci. Eng., 2001, A 307, p. 107-112.
- [117] K. Volenik, F. Hanousek, P. Chraska, J. Ilavsky, K. Neufuss, In-flight oxidation of high-alloy steels during plasma spraying, Mater. Sci. Eng., 1999, A 272, p. 199-206.
- [118] C. Zhou, J. Yu, S. Gong, H. Xu, Influence of water vapor on the isothermal oxidation behavior of low-pressure plasma sprayed NiCrAlY coating at high temperature, Surf. Coat. Technol., 2002, 161, p. 86-91.
- [119] C.-J. Li, W.-Y. Li, Effect of sprayed powder particle size on the oxidation behavior of NiCrAlY materials during high velocity oxygen-fuel deposition Surf. Coat. Technol., 2002, 162, p. 31-41.
- [120] K. Volenik, V. Novak, J. Dubsky, P. Chraska, K. Neufuss, Properties of alloy steel coatings oxidized during plasma spraying, Mater. Sci. Eng., 1997, A 234-236 493-496.
- [121] V.V. Sobolev, J.M. Guilemany, Effect of oxidation on droplet flattening and splat-substrate interaction in thermal spraying, J. Therm. Spray Technol., 1999, 8 (4), p. 523-530.
- [122] M.E. Aalamialeagha, S.J. Harris, M. Emamighomi, Influence of the HVOF spraying process on the microstructure and corrosion behaviour of Ni-20%Cr coatings, J. Mater. Sci., 2003, 38, p. 4587-4596.
- [123] O. Madelung, U. Rössler, M. Schulz, Non-tetrahedrally bonded binary compounds II, Springer-Verlag, 2006.

- [124] C.-J. Li, Y.-Y. Wang, Effect of particle state on the adhesive strength of HVOF sprayed metallic coating, *J. Therm. Spray Technol.*, 2001, 11 (4), p. 523-529.
- [125] T.C. Totemeier, R.N. Wright, W.D. Swank, Microstructure and stresses in HVOF sprayed iron aluminide coatings, *J. Therm. Spray Technol.*, 2002, 11 (3), p. 400-408.
- [126] S. Kuroda, Y. Tashiro, H. Yumoto, S. Taira, H. Fukanuma, S. Tobe, Peening action and residual stresses in High-velocity oxygen fuel thermal spraying of 316L stainless steel, *J. Therm. Spray Technol.*, 2001, 10 (2), p. 367-374.
- [127] D. Zhang, S.J. Harris, D.G. McCartney, Microstructure formation and corrosion behaviour in HVOF-sprayed Inconel 625 coatings, *Mater. Sci. Eng.*, 2003, A344, p. 45-56.
- [128] A.P. Alkhimov, V.F. Kosarev, A.N. Papyrch, A method of cold gas dynamic deposition, *Dokl. Akad. Nauk. USSR*, 1990, 318, p. 1062-1065
- [129] M. Qu, A. Gouldstone, On the role of bubbles in metallic splat nanopores and adhesion, *J. Therm. Spray Technol.*, 2008, 17 (4), p. 486-494.
- [130] V.V. Sobolev, J.M. Guilemany, Investigation of coating porosity formation during high velocity oxy-fuel (HVOF) spraying, *Mater. Lett.*, 1994, 18, p. 304-308.
- [131] S. Brossard, A.T.T. Tran, P.R. Munroe, M.M. Hyland, Study of the splat formation for plasma sprayed NiCr on an aluminum substrate as a function of substrate condition, *Surf. Coat. Technol.*, 2010, 204 (16), p.2647-2656.
- [132] T.B. Massalski, H. Okamoto, P.R. Subramanian, L. Kacprzak, Binary alloy phase diagrams, 2nd, ASM International, Materials park, Ohio, 1990.

- [133] B. Wielage, A. Wank, H. Pokhmurska, T. Grund, C. Rupprecht, G. Reisel, E. Friesen, Development and trends in HVOF spraying technology, *Surf. Coat. Technol.*, 2006, 201, p. 2032-2037.
- [134] R.S. Lima, B.R. Marple, Optimized HVOF titania coatings, *J. Therm. Spray Technol.*, 2003, 12 (3), p. 360-369.
- [135] N.Z. Mehdizadeh, M. Lamontagne, C. Moreau, S. Chandra, J. Mostaghimi, Photographing impact of molten molybdenum particles in a plasma spray, *J. Therm. Spray Technol.*, 2005, 14 (3), p. 354-361.
- [136] K. Shinoda, H. Murakami, S. Kuroda, S. Oki, K. Takehara, T.G. Etoh, High-speed thermal imaging of yttria-stabilized zirconia droplet impinging on substrate in plasma spraying, *Appl. Phys. Lett.*, 2007, 90, p. 194103-1-194103-3.
- [137] W.J. Trompetter, M. Hyland, P. Munroe, A. Markwitz, Evidence of mechanical interlocking of NiCr particles thermally sprayed onto Al substrates, *J. Therm. Spray Technol.*, 2005, 14 (4), p. 524-529.
- [138] C.-J. Li, J.-L. Li, Transient contact pressure during flattening of thermal spray droplet and its effect on splat formation, *J. Therm. Spray Technol.*, 2004, 13 (2), p. 229-238.
- [139] L. Li, A. Vaidya, S. Sampath, H. Xiong, L. Zheng, Particle characterization and splat formation of plasma sprayed zirconia, *J. Therm. Spray Technol.*, 2006, 15 (1), p. 97-105.
- [140] J. Stringer, B.A. Wilcox, R.I. Jaffee, The high- temperature oxidation of nickel-20 wt.% chromium alloys containing dispersed oxide phases, *Oxid. Met.*, 1972, 5 (1), p. 11-47.

- [141] M. Dorfman, Thermal spray processes, *Adv. Mater. Process.*, 2002, (8), p. 47-49.
- [142] L.S. Hung, M. Nastasi, J. Gyulai, J.W. Mayer, Ion-induced amorphous and crystalline phase formation in Al/Ni, Al/Pd, and Al/Pt thin films, *Appl. Phys. Lett.*, 1983, 42 (8), p. 672-674.
- [143] C.S. Giggins, F.S. Pettit, Oxidation of Ni-Cr-Al alloys between 1000° and 1200°C, *J. Electrochem. Soc.*, 1971, 118 (11), p. 1782-1790.
- [144] A. McDonald, M. Lamontagne, S. Chandra, C. Moreau, Photographing impact of plasma-sprayed particles on metal substrates, *J. Therm. Spray Technol.*, 2006, 15 (4), p. 708-716.
- [145] H. Beck, H.-J. Güntherodt, *Glassy Metals*, Springer-Verlag, Berlin, Heidelberg, New York, Tokyo, 1983.
- [146] C. Lea, J. Ball, The oxidation of rolled and heat treated Al-Mg alloys, *Appl. Surf. Sci.*, 1984, 17, p. 344-362.
- [147] J.M. Ritchie, J.V. Sanders, P.L. Weickhardt, Oxidation of a dilute Aluminum Magnesium Alloy, *Oxid. Met.*, 1971, 3 (1), p. 91-101.
- [148] S. Brossard, P.R. Munroe, A.T.T. Tran, M.M. Hyland, Examination of the splat microstructure, splat-substrate interface and the effects of substrate heating on the splat formation for Ni-Cr particles plasma sprayed on to aluminum substrates, *J. Therm. Spray Technol.*, 2010, DOI: 10.1007/s11666-010-9511-2
- [149] S. Brossard, P.R. Munroe, M.M. Hyland, Study of the splat formation for HVOF sprayed NiCr on stainless steel substrates and the effects of heating and boiling pre-treatments, 2010, DOI: 10.1007/s11666-010-9502-3

- [150] C. Moreau, P. Gougeon, M. Lamontagne, Influence of substrate preparation on the flattening and cooling of plasma-sprayed particles, *J. Therm. Spray Technol.*, 1995, 4 (1), p. 25-33.
- [151] M. Raessi, J. Mostaghimi, M. Bussmann, Effect of surface roughness on splat shapes in the plasma coating process, *Thin Solid Films*, 2006, 506-507, p. 133-135.
- [152] H. Liu, E.J. Lavernia, R.H. Rangel, Modeling of molten droplet impingement on non-flat surface, *Acta Met. Mater.*, 1995, 43 (5), p. 2053-2072.
- [153] M. Ivosevic, V. Gupta, J.A. Baldoni, R.A. Cairncross, T.E. Twardowski, R. Knight, Effect of substrate roughness on splatting behavior of HVOF sprayed polymer particles: modelling and experiments, *J. Therm. Spray Technol.*, 2006, 15 (4), p. 725-730.
- [154] N. Ferguen, P. Fauchais, A. Vardelle, D. Gobin, Numerical investigation of impact and solidification of YSZ droplets plasma-sprayed onto a substrate: effect of thermal properties and roughness, 32nd International Conference on Advanced Ceramics and Composites, Daytona Beach, Florida, USA, January 27 - February 1, H.-T. Lin and D. Zhu, 2008, p. 159-170.
- [155] D.E. Wroblewski, R. Khare, M. Gevelber, Solidification modeling plasma sprayed TBC: analysis of remelt and multiple length scales of rough substrates, *J. Therm. Spray Technol.*, 2002, 11 (2), p. 266-275.
- [156] S.N. Basu, G. Ye, R. Khare, B. McCandless, M. Gevelber, D.E. Wroblewski, Dependence of splat remelt and stress evolution on surface roughness length scales in plasma sprayed thermal barrier coatings, *Int. J. Refract. Met. Hard Mater.*, 2009, 27, p. 479-484.

- [157] C.-L. Li, C.-X. Li, G.-J. Yang, Y.-Y. Wang, Examination of substrate surface melting-induced splashing during splat formation in plasma spraying, *J. Therm. Spray Technol.*, 2006, 15 (4), p. 717-724.
- [158] W. Zhang, G.H. Wei, H. Zhang, L.L. Zheng, D.O. Welch, S. Sampath, Toward the achievement of substrate melting and controlled solidification in thermal spraying, *Plasma Chem. Plasma Process.*, 2007, 27 (6), p. 717-736.
- [159] Y. Liu, T.E. Fischer, A. Dent, Comparison of HVOF and plasma-sprayed alumina/titania coatings - microstructure, mechanical properties and abrasion behavior, *Surf. Coat. Technol.*, 2003, 167, p. 68-76.
- [160] Y.P. Wan, V. Prasad, G.-X. Wang, S. Sampath, J.R. Fincke, Model and powder particle heating, melting, resolidification, and evaporation in plasma spraying processes, *J. Heat Transf.*, 1999, 121 (3), p. 691-699.